NASA CR-114504
Available to the Public

THE DEVELOPMENT OF AN AUGMENTOR WING JET STOL RESEARCH AIRCRAFT (MODIFIED C-8A)

Volume II: Analysis of Contractor's Flight Test

By H. Skavdahl and D. H. Patterson

August 1972

D6-40720-2

Prepared under contract NAS2-6025 by
BOEING COMMERCIAL AIRPLANE COMPANY
P.O. Box 3707
Seattle, Washington 98124

for

Ames Research Center
NATIONAL AERONAUTICS AND SPACE ADMINISTRATION

This report presents the results of the initial phase of Flight Testing on the Augmentor Wing Jet STOL Research Aircraft that was conducted between May 1 and July 28, 1972. STOL Take-offs and Landings were not scheduled for this phase of testing. The results of STOL operations with the aircraft will be published in subsequent NASA publications.

CONTENTS

SUMMARY

The contractor's flight testing of the Modified C-8A airplane was conducted during May of 1972. The primary objective of the testing was to establish the basic airworthiness of the research vehicle. This included verification of the structural design and evaluation of the aircraft's systems. The Modified C-8A research aircraft was demonstrated to be airworthy.

The first flight was made on May 1, 1972. The flight program was completed in eight flights with a total flight time of 9 hours and 8 minutes. The testing was conducted from Boeing Field International and Snohomish County Airport (Paine Field).

The flight envelope was investigated from a minimum airspeed of 50 KEAS to the design dive speed of 180 KEAS. Flap placards were reached at flaps 65° (90 KEAS) and flaps 30° (120 KEAS). Approaches to stall were made at three primary flap settings: up, 30° and 65°. The full ranges of flap setting, conical nozzle deflection, and power setting were evaluated.

Angles of attack from -3° to 24° were investigated. Variations in load factor from 0.3 to 1.8 g were obtained during pushover/pull-up maneuvers. Sideslip angles of 15° were tested and bank angles exceeding 45° were flown. The flight envelope was sufficiently explored to clear the airplane for the augmentor wing research flight test program.

The airplane exhibited positive static lateral and directional stability throughout the flight envelope. Satisfactory lateral control power was demonstrated down to the 60 KEAS condition, where full wheel produced a roll acceleration of $\ddot{\phi} = 0.5$ rad/sec^2. Directional control power was adequate for sideslips and engine-out control. With the lateral-directional stability augmentation system (SAS) the airplane exhibited good turn entry characteristics, positive spiral stability, and well-damped Dutch roll for large-amplitude disturbances. With the SAS turned off the airplane characteristics were judged acceptable for safe flight to a landing. The one undesirable lateral-directional characteristic found in the test program was a low-amplitude directional "snaking" tendency at speeds below 90 KEAS.

Longitudinal trim was maintained for most flight conditions at elevator deflections within ±5° of neutral. Trim changes for changes in speed, flaps, nozzle, and power were small. The airplane exhibited positive static longitudinal stability at speeds above 80 KEAS. Static longitudinal stability was neutral or negative at lower speeds. The airplane felt as if without close attention it would diverge into a stall. Stable maneuvering characteristics were demonstrated throughout the flight envelope. Taxi tests revealed that tab stall limited trailing-edge-up elevator to two-thirds of

maximum using one-hand stick force. Existing data indicate that minimum distance takeoffs and landing flare from the 60-KEAS STOL approach will be restricted. Stall recovery may also be hindered.

Although the specific purpose of the contractor's flight test program was to verify the structural design and evaluate the aircraft's systems, a significant amount of performance information was extracted from the relatively short airworthiness testing. This information provides a basis for future flight test planning and investigations.

Minimum test speeds were demonstrated within 0 to 7 kt of the predicted 1 g stall speeds. Full stalls were not scheduled. The approach-to-stall conditions were stopped at a predetermined angle-of-attack limit and not continued into full stall. However, no significant increase in buffet was noted during the stall approach to indicate pending stall. For all conditions, the minimum test speeds were to the angle-of-attack limit and the aircraft does not appear to have any minimum control speed restrictions within the speed range flown.

The lowest speed attained during the test program was 50 KEAS, corresponding to an equivalent lift coefficient (W/qs) of 5.4. The configuration was representative of a STOL approach with the flaps at 65° and the conical nozzles deflected down to 58°.

Takeoff distances less than 2000 ft were demonstrated although high-power STOL takeoffs were not conducted. The takeoff power setting used during the contractor's test program ranged from 95% to 97% N_H, which corresponds to 75% to 85% of the maximum takeoff thrust available.

Several single-engine climb checks were made to verify the takeoff flap settings being used. Sufficient emergency climb capability exists to permit takeoffs over a reasonable range of gross weights and ambient conditions.

Descent and climb capability from -2000 to +3000 ft/min were demonstrated during the flight test program. Flap setting was varied from up (5.6°) to full down (73°). Thrust levels 10% to 20% higher than predicted were required to maintain a given rate of climb. It was not possible to determine the reasons for the higher thrust because of the limited amount of performance testing. Possible explanations include local separated regions as indicated by a buffet level noted in flight, a lower augmentation ratio, and the inability to resolve drag and thrust to the necessary accuracies. The measured angle of attack (not corrected for position error) was 1° to 2° higher than predicted for all flap settings.

Vectoring the conical nozzles down required an additional 2% to 3% higher power setting (N_H) than predicted from wind tunnel data.

All the landings during the test program were conducted with conventional approaches, 3° glide slope, and the conical nozzles aft at 6°. The landing flap setting varied from 25° to 54°. Single-engine landings were made without difficulty with flaps at 30°.

No landings from a STOL approach were attempted. A trim condition closely representing the design approach of 60 KEAS, 800 ft/min rate of descent, and 40 000 lb gross weight was tested at an altitude of 7670 ft. Extrapolating the test data to represent a standard day landing at sea level, the STOL approach characteristics would be 11° to 12° fuselage angle of attack and 93% N_H with the conical nozzles at 58°. Rotating the conical nozzles to 90° would decrease the angle of attack to 3° and increase the power to 96% or 97% N_H.

Since the original objectives of the Modified C-8A program were to prove the augmentor wing concept with respect to aerodynamics, performance, and handling qualities and to contribute to the development of jet STOL transport design and operating criteria, it is recommended that NASA extend the flight test program into the following areas:

- Conduct a test program exploring the STOL flight regime in further depth. Particular emphasis should be placed on landing maneuvers, including the following specific items:

  - Steep approach flare techniques related to simulator findings.
  - Evaluation and, possibly, measurement of ground effects.
  - Simulation of engine failure at critical conditions.

  Caution is urged in approaching flight conditions having low margins. Give particular attention to the type of longitudinal stability augmentation needed on the airplane.

- Conduct a flight test investigation to determine accurate performance characteristics including a ground test to measure static thrust. With accurate data in hand, conduct an analysis of airplane performance. Static thrust data, flaps on and off, will allow identification of static augmentation. Tuft studies of suspected areas of poor flow during both flight and static tests will allow qualitative assessment of drag sources and will guide corrective action to improve performance. This work is recommended as essential to the proof of the augmentor wing concept.

- Install a powered elevator system on the airplane to permit full and safe exploration of the airplane's high-lift and STOL operation capabilities.

- Use the variable-gain SAS to find the optimum lateral-directional handling qualities and reduce the "snaking" tendency, then modify the fixed-gain SAS to this configuration.

INTRODUCTION

The initial flight test phase of the Modified C-8A airplane was conducted during May of 1972. The primary objective of the testing was to establish the basic airworthiness of the research vehicle. This included verification of the structural design and evaluation of the aircraft's systems. Only a minimum amount of performance testing was scheduled; this has been used to provide a preliminary indication of the airplane's performance and flight characteristics for future flight planning.

The tests were conducted from Boeing Field International and Snohomish County Airport (Paine Field). Six taxi tests were made, with the initial test on April 18, 1972. The first flight, shown in figure 1, was made on May 1, 1972. A total of eight flights were conducted during the program, with a total flight time of 9 hours and 8 minutes.

The testing included flutter and loads investigations up to the maximum design speed. The operational characteristics of all systems were assessed including hydraulics, environmental control system, air ducts, the vectoring conical nozzles, and the stability augmentation system (SAS). Approaches to stall were made at three primary flap settings: up, 30° and 65°, but full stalls were not scheduled. Minimum control speeds and maneuver margins were checked. All takeoffs and landings were conventional, and STOL performance was not scheduled during this phase of the evaluation.

A description of the airplane and program summary is given in volume I of this report (NASA CR-114503).

FIGURE 1.—FIRST FLIGHT TAKEOFF

ABBREVIATIONS AND SYMBOLS

a	airplane longitudinal acceleration, ft/sec^2
b	wing span, 78.75 ft
C_c	chordwise force coefficient = chordwise force/qS (positive aft)
C_D	airplane drag coefficient = drag/qS (positive aft)
$C_{H_{ail}}$	aileron hinge moment coefficient = hinge moment/qS$\bar{c}$ (positive trailing edge up)
C_j	isentropic thrust coefficient = cold thrust/qS
C_L	airplane lift coefficient = lift/qS (positive up)
C_ℓ	rolling moment coefficient = rolling moment/qSb (positive right wing down)
$C_{M_{LE}}$	pitching moment coefficient about the leading edge = pitching moment/qS$\bar{c}$ (positive nose up)
C_N	normal force coefficient = normal force/qS (positive up)
C_n	yawing moment coefficient = yawing moment/qSb (positive nose right)
CG	center of gravity
$\bar{c}$	surface average chord length, ft
D_H, D_V	horizontal and vertical components of load applied by augmentor duct to flap support beam at wing station 158
EGT	exhaust gas temperature
F	engine fuel flow, lb/hr
$F/P_{T_1}\sqrt{T_1}$	corrected engine fuel flow where P_{T_1} is the inlet total pressure in $lb/in.^2$ and T_1 is the inlet total temperature in °K
F_S	stick force, lb (positive for pull)
F_w	wheel force, lb (positive for right wheel)
FOD	foreign object damage
FTE	flight test equipment
GW, W	airplane gross weight, lb
g	acceleration due to gravity, ft/sec^2
I_{XX}	airplane moment of inertia, $slug\text{-}ft^2$
IAS	indicated airspeed, kt
IRIG	standardized time, hr:min:sec

MAC	mean aerodynamic chord, 12.4 ft
N_H, N_L	high- and low-pressure engine shaft speed, RPM
$N_H/\sqrt{T_1}$, $N_L/\sqrt{T_1}$	corrected high- and low-pressure shaft speed, where T_1 is the inlet total temperature in °K
n, n_z	normal load factor, g
OEW	operating weight empty including pilot, copilot, trapped fuel, engine oil, and deliverable flight test equipment, lb
P	Dutch roll period, sec
P_T	total pressure, psi
P_S	static pressure, psi
PCM	data acquisition system termed "pulse code modulation"
PCU	power control unit
PLF	power setting for level flight
q	freestream dynamic pressure
R/C	rate of climb, ft/min
R/D	rate of descent, ft/min
S	wing reference area, 865 ft^2
SAS	stability augmentation system
T	total temperature, ° K
T_A	blowing thrust per aileron, lb
V_{app}	approach velocity in equivalent airspeed, kt
V_D	design dive airspeed, kt
V_{MCA}	minimum control airspeed, kt
V_{MO}	maximum operating airspeed, kt
V_R	takeoff rotation airspeed, kt
V_e	equivalent airspeed (EAS), kt
V_1	critical takeoff engine failure speed, kt
V_2	takeoff climb speed with engine out, kt
WS	wing station; distance measured outboard from and perpendicular to the airplane centerline
X_S	column position, in. (positive aft)
α, α_F	fuselage angle of attack as measured on the nose boom, deg (positive leading edge up)

α_{wing}	wing angle of attack = $\alpha_F + 2.5^\circ$
β	sideslip, deg (positive nose left)
β_{SS}	steady sideslip, deg
γ	flightpath angle, deg (positive up)
Δt	time increment, sec
δ_a	aileron deflection, deg (positive trailing edge down)
$\dot{\delta}_a$	aileron deflection rate, deg/sec
δ_{CH}	augmentor choke deflection, deg (positive up)
$\dot{\delta}_{CH}$	augmentor choke deflection rate, deg/sec
δ_{col}	column deflection, deg (positive aft)
δ_e	elevator deflection, deg (positive trailing edge down)
δ_F	flap deflection, deg (positive trailing edge down)
δ_{SP}	spoiler deflection, deg (positive trailing edge up)
$\dot{\delta}_{SP}$	spoiler deflection rate, deg/sec
δ_r	rudder deflection, deg (positive trailing edge left)
$\dot{\delta}_r$	rudder deflection rate, deg/sec
δ_t, $\delta_{t_{trim}}$	elevator trim tab deflection, deg (positive trailing edge down)
δ_{t_s}, $\delta_{t_{spring}}$	elevator spring tab deflection, deg (positive trailing edge down)
δ_w	wheel deflection, deg (positive right)
$\dot{\delta}_w$	wheel deflection rate, deg/sec
ζ	Dutch roll damping ratio
θ	pitch attitude, deg
$\dot{\theta}$	pitch rate, deg/sec
$\ddot{\theta}$	pitch acceleration, deg/sec^2
θ_1	elevator control system limits beyond which the control column is directly connected to the elevator
μ	braking coefficient of friction
ν	hot thrust nozzle angle measured relative to the fuselage datum; deg (positive down)
σ_A, σ_B, σ_C	individual longitudinal direct stresses measured on the outer surface of augmentor duct at wing station 178

σ_D	direct stress measured in the circumferential direction on the outer surface of the reinforcing ring on the augmentor duct at wing station 183
σ_{LES}, σ_{FSW}, σ_{WLS}	individual stresses measured in the wing structure
τ_R	roll mode time constant
ϕ	bank angle, deg
$\dot{\phi}$	roll rate, deg/sec
$\ddot{\phi}$	roll acceleration, deg/sec^2
ψ	yaw angle, deg
$\dot{\psi}$	yaw rate, deg/sec
$\ddot{\psi}$	yaw acceleration, deg/sec^2
ω	frequency

SUBSCRIPTS

B	engine station at bypass air outlet
E	engine station at exhaust nozzle outlet
LE, TE	leading edge and trailing edge
LH, RH	left-hand and right-hand locations as viewed from the pilot's station looking forward
LOF	liftoff
TF	trailing edge flaps
1	engine station at inlet
2	engine station at low-pressure compressor delivery
2.5	engine station at bypass duct reference station
3	engine station at high-pressure compressor delivery
4	engine station at high-pressure turbine entry
6	engine station at low-pressure turbine exit (upstream of colander)
8	engine station at exhaust nozzle hinge plate

FLIGHT ENVELOPE

Operation throughout most of Modified C-8A airplane flight envelope was demonstrated in the flight test program. Flight weights ranged from 46 600 lb at takeoff to a minimum of 37 200 lb at landing. Center of gravity varied between 29% and 31% MAC. Flight at flap settings from full up (5.6°) to full down (73°) was demonstrated. Power settings ranged from idle (61% N_H) to emergency (103% N_H). The conical nozzles were rotated in flight from fully up ($\nu = 6°$) to down ($\nu = 91°$).

Figure 2 summarizes the load factor, angle of attack, and airspeeds achieved in the flight test program. Flap placard speeds were reached at flaps 65° (90 kt) and flaps 30° (120 kt). Flaps up V_{MO} (160 kt) and V_D (180 kt) were flown and cleared for flutter. Minimum angle of attack was $\alpha_F = -4°$ and maximum angle of attack was $\alpha_F \approx 24°$. Angles of attack in excess of $\alpha_F \approx 22°$ were reached at all flap settings. Variations in load factor from 0.3 to 1.8g were attained during pushover/pull-up maneuvers.

In addition, the airplane was sideslipped to $\beta = 15°$ at speeds from 65 to 166 kt (all flap settings). Pitch attitudes ranged from $\theta = 20°$ nose up to $\theta = -15°$ nose down. Bank angles to $\phi \geqslant 45°$ were demonstrated.

The airplane was flown at altitudes ranging from sea level to almost 10 000 ft. Temperatures were near to standard day. Conventional takeoffs and landings were conducted with approach speeds down to 78 kt. All flying was conducted under visual flight rules in daylight.

It should be noted that the complete STOL operating envelope was not explored. In particular, high-power STOL takeoffs, fully developed stalls, and STOL landings from steep approach with nozzles down were not conducted. The calibration of the airspeed system and angle of attack indicator was not performed. Airplane performance was not fully assessed including engine cutback at takeoff, cruise performance, and determination of minimum field lengths.

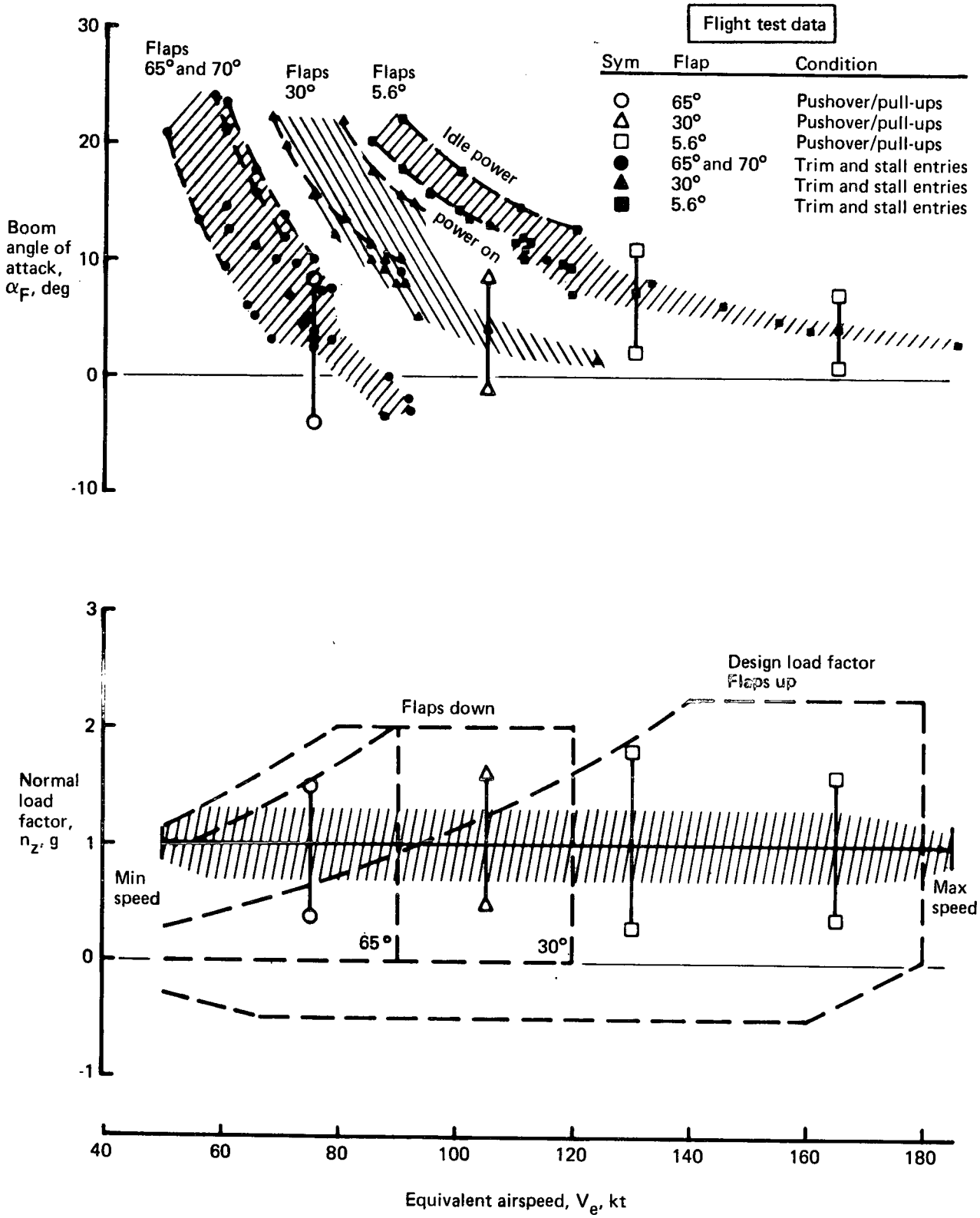

FIGURE 2.–FLIGHT TEST DEMONSTRATED ANGLE OF ATTACK, LOAD FACTOR, AND AIRSPEED ENVELOPE

PERFORMANCE AND FLIGHT CHARACTERISTICS

SCOPE OF PERFORMANCE TESTING

The specific purpose of the flight test program was to verify the structural design and evaluate the aircraft systems. A sufficient amount of data was derived from the relatively short flight time of 9 hours to give a preliminary indication of the aircraft's performance and flight characteristics. However, not enough data were obtained to separate the thrust and aerodynamics as required to evaluate the augmentor wing performance per se. It should also be noted that the airspeed and angle-of-attack calibrations have not yet been conducted to determine their position error during flight.

The minimum speed of the Modified C-8A is limited by wing stall and does not appear to have any minimum control speed restrictions. However, full stalls were not conducted. A speed of 50 kt was attained during the flight test program, which corresponds to a W/qS of 5.4.

STOL takeoffs at maximum power and STOL landings from steep approaches were not scheduled. Takeoff distances of less than 2000 ft were demonstrated.

Climbs of 3000 ft/min and descents exceeding 2000 ft/min were made during the test program. To maintain a given rate of climb, a higher power setting is required than was predicted. However, single-engine climb performance at emergency power is as predicted.

Nominal specific range during cruise will be about 0.025 nmi per pound of fuel. This corresponds to a range of approximately 235 nmi with the maximum fuel load of 13 500 lb with appropriate reserves.

TAKEOFF

Takeoff Performance

Eight takeoffs were made during the flight test program. The maximum takeoff gross weight at brake release was 46 600 lb, and the power setting ranged from 95% to 97% N_H. STOL takeoffs at maximum power were not made. All the takeoffs were conducted in a conservative manner appropriate for initial testing of a flight test vehicle.

The liftoff angle of attack is shown in figure 3. The predicted values do not include any estimation of ground effect. In addition to the takeoffs, data are included for flaps 30° and 65° from taxi tests where the Modified C-8A lifted off and remained airborne for approximately 5 seconds. Liftoff angle of attack is shown as a function of liftoff velocity on the upper portion of figure 3 where the flight test data have been normalized to 46 600 lb and 96% N_H. The comparison between measured and predicted angles gives an indication of the ground effect. Flaps 25° and 30° show a favorable ground effect, where flaps 65° is unfavorable. These trends are the expected results based on observations of wind tunnel data for the augmentor wing configuration.

Ground roll accelerations and flare times are presented in figure 4. Nominal accelerations of slightly less than 0.3 g and flare times of 3 seconds were demonstrated. Takeoffs where the flare time exceeded 4 seconds were cases when the pilot intentionally stopped the pitch rate during the flare.

Takeoff field length performance is shown in figure 5 for the nominal flight test conditions of 46 600 lb and 96% N_H. Except for the first flight, the flight test takeoff distances were estimated from velocity time histories and were not physically measured. No engine-out conditions were tested to check engine-out field lengths or rotation speeds. The predicted field lengths are actual distances and do not include FAR factors.

Second segment climb capability is given in figure 6. Discussion of the flight test data is contained in the section "Climb/Descent." Adequate climb capability exists at flaps up or 15° over an acceptable range of ambient conditions.

The takeoff for the first flight was the only one where distances were measured using the theodolite camera system. That takeoff time history is shown in figure 7. The takeoff gross weight was 43 500 lb with 25° flaps and the conical nozzles at 6°. The 96% N_H power setting represents a thrust which is approximately 80% of the maximum takeoff thrust available. The distance to liftoff was 1250 ft and the total distance to a 35-ft altitude was 2064 ft.

A tabular summary of all the takeoff conditions is presented in table I.

Takeoff Rotation and Trim

Minimum nosewheel liftoff speeds were determined in the taxi tests. Tab stall prevented achieving full trailing-edge-up elevator. The pilot was able to pull the column at $F_S \approx 75$ lb (maximum one-hand effort) and attain $\delta_e \approx -16°$. At flaps 30°, takeoff rotation could be initiated as low as 60 kt, slightly better than the prediction.

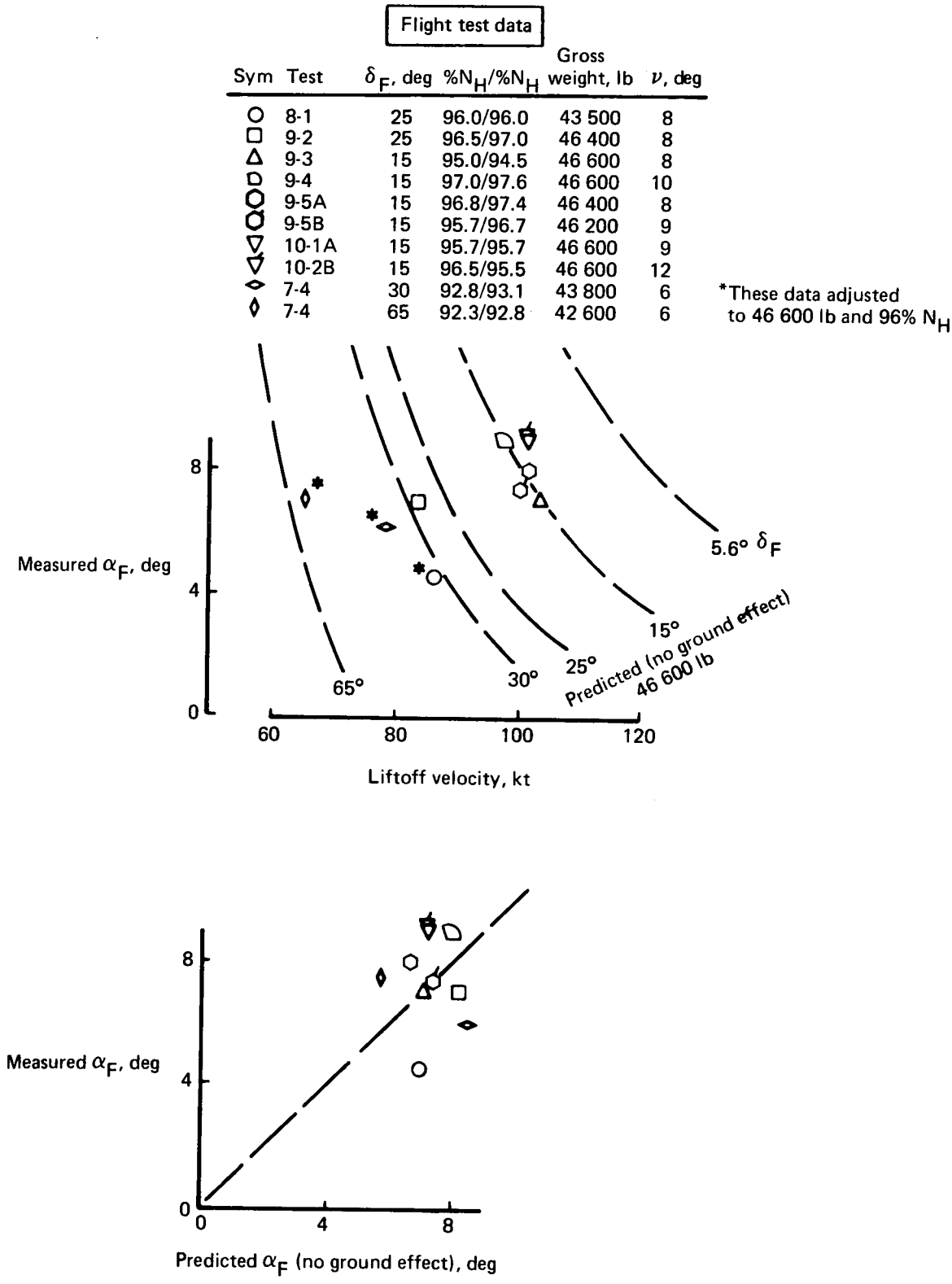

FIGURE 3.–LIFTOFF ANGLE OF ATTACK

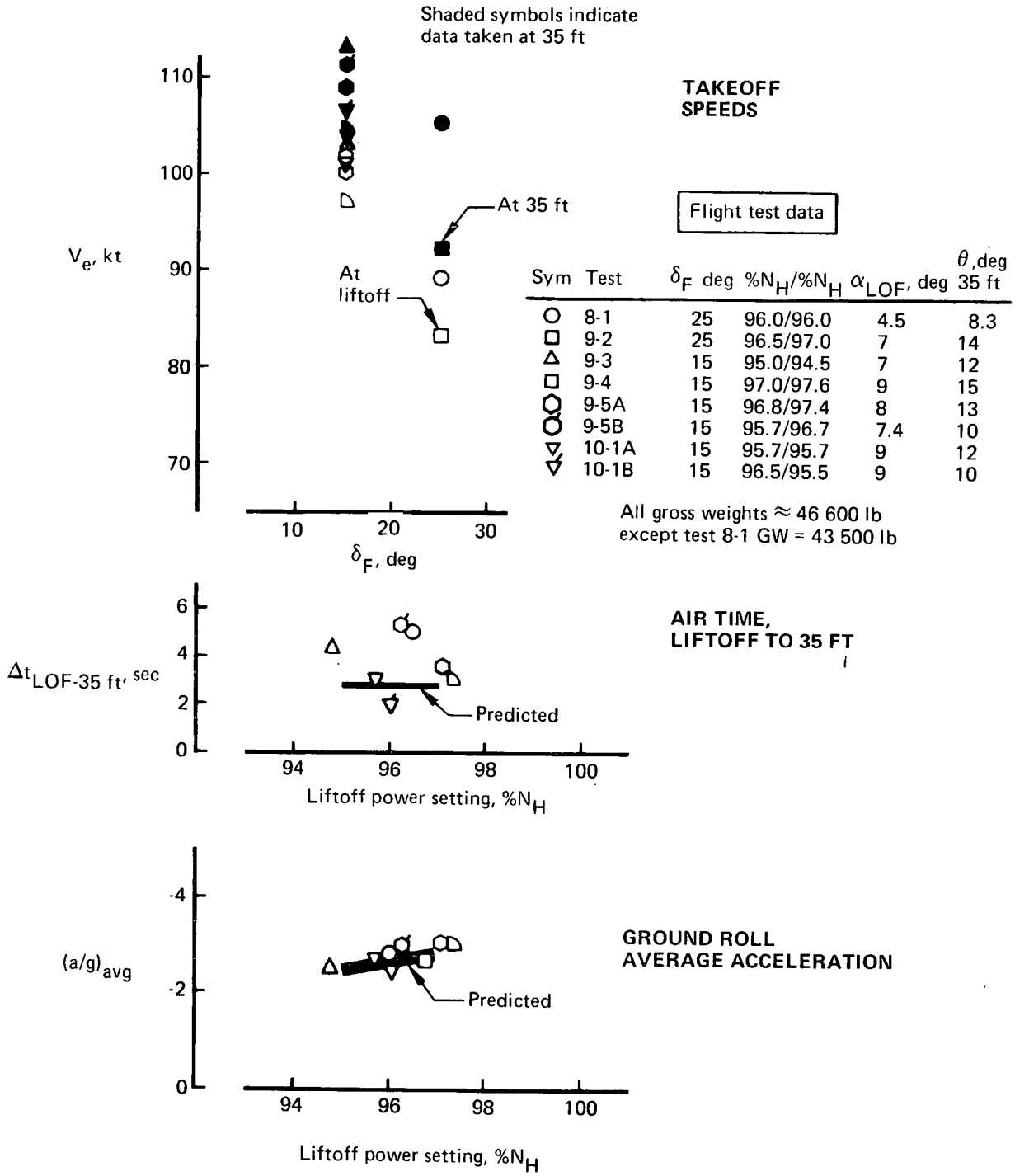

FIGURE 4.–TAKEOFF PERFORMANCE DATA

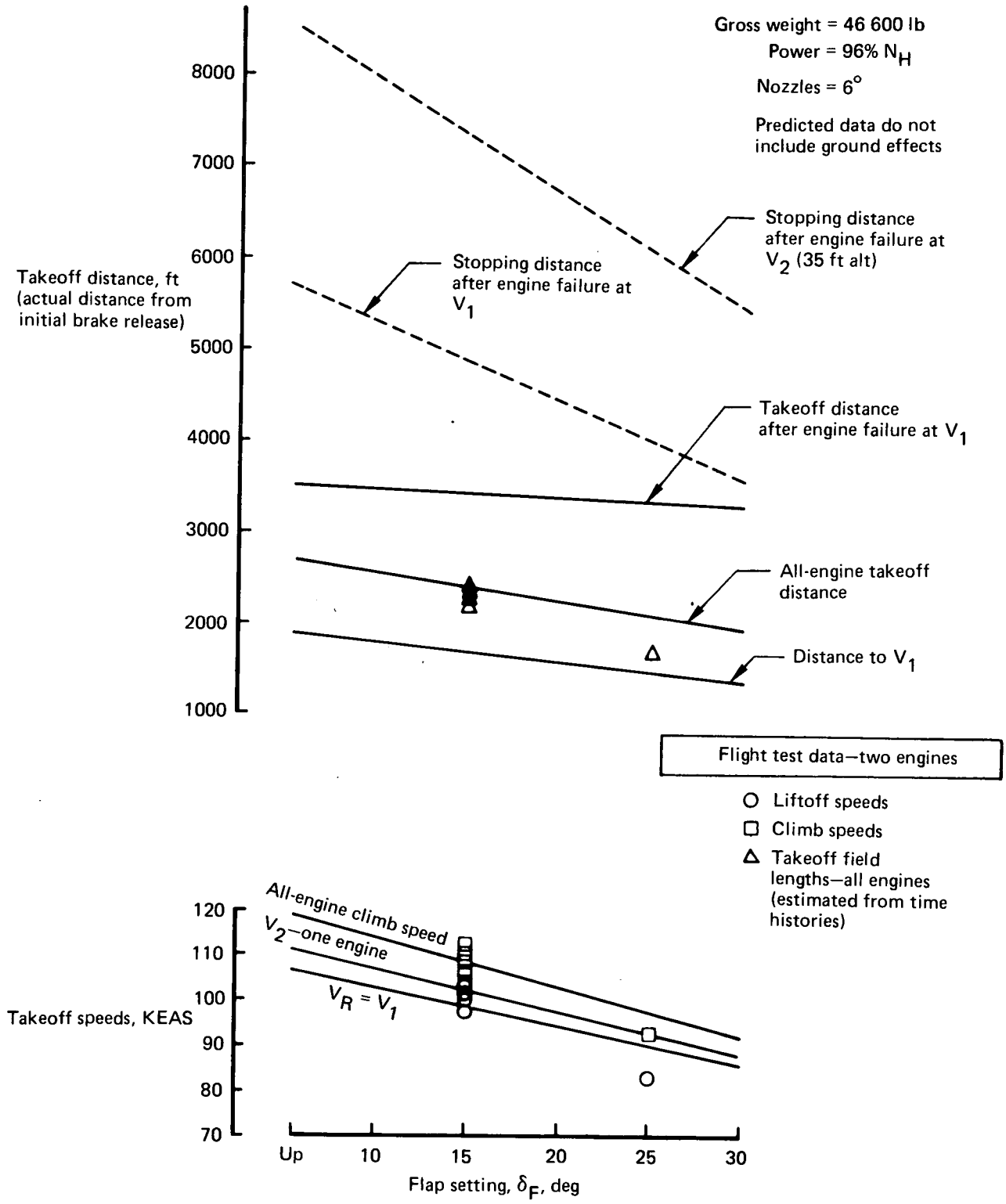

FIGURE 5.—TAKEOFF PERFORMANCE—SEA LEVEL, STANDARD DAY

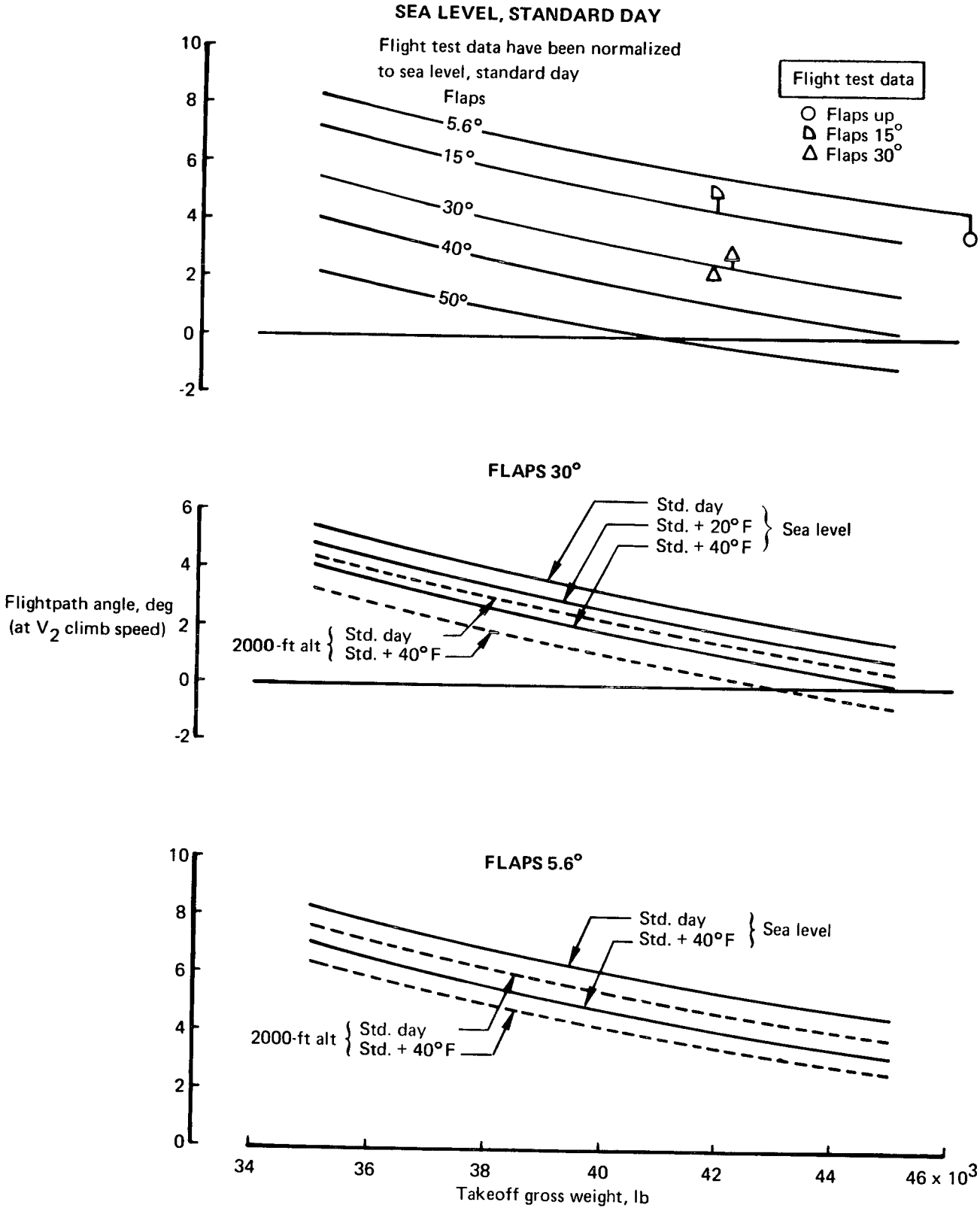

FIGURE 6.–SECOND SEGMENT CLIMB–ONE ENGINE AT EMERGENCY POWER, 6° NOZZLE ANGLE

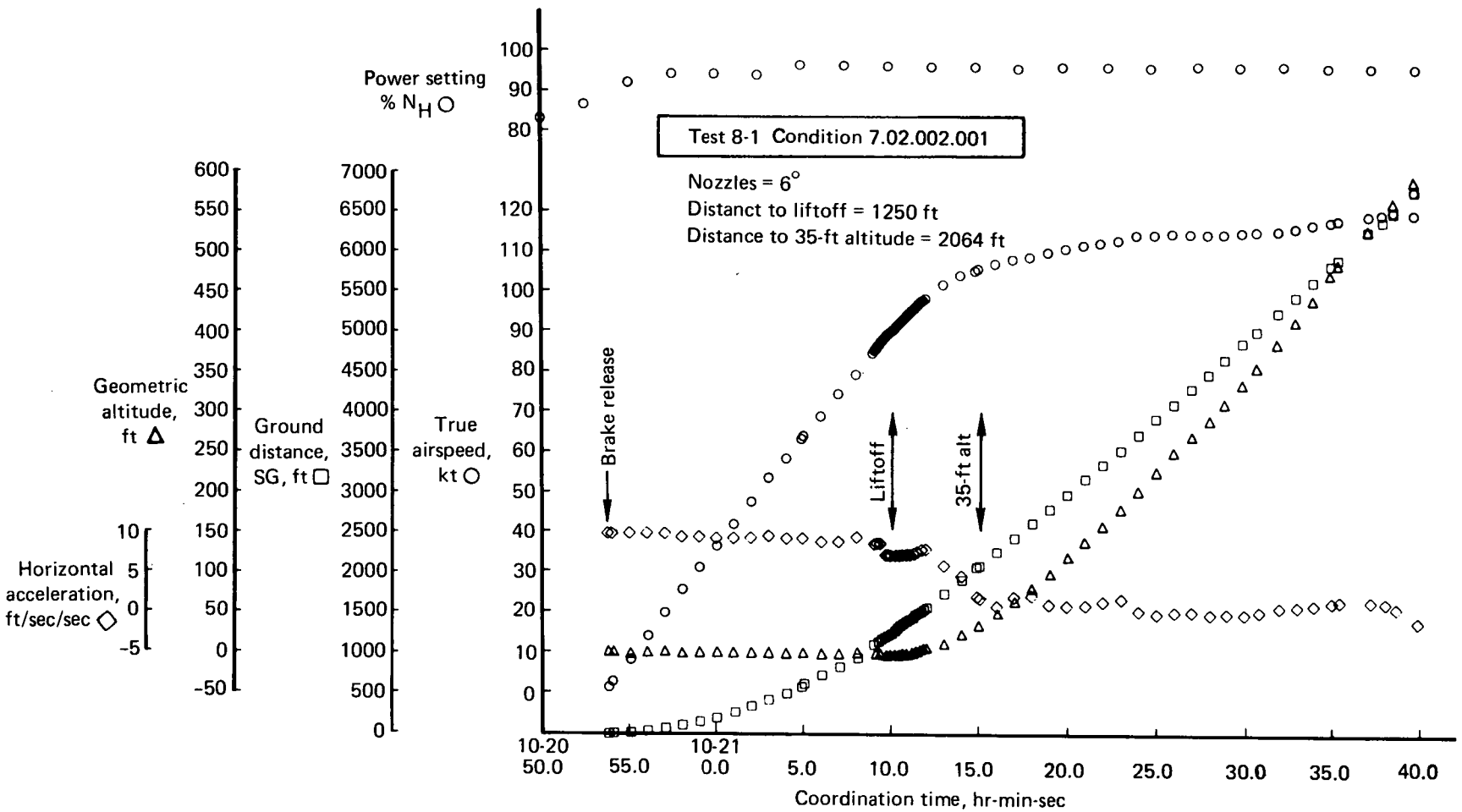

FIGURE 7.—TAKEOFF TIME HISTORY—FLAPS 25°, GW = 43 500 LB

TABLE I.–FLIGHT TEST DATA–TAKEOFF CONDITIONS

Test Condition	8-1 1.02.002.001	9-2 1.00.003.002	9-3 1.00.003.002	9-4 1.00.003.002	9-5A 1.00.003.002	9-5B 1.00.003.002-1	10-1A 1.00.003.002	10-1B 1.00.003.002-1
Flap position, $\delta_{F_{nom}}$, deg	25	25	15	15	15	15	15	15
Nozzle position, ν, deg	8	8	8	10	8	9	9	12
Power setting, % N_H								
Engine 1	96.0	96.5	95.0	97.0	96.8	95.7	95.7	96.5
Engine 2	96.0	97.0	94.5	97.6	97.4	96.7	95.7	95.5
Gross weight, lb	43,500	46,400	46,600	46,600	46,400	46,200	46,600	46,600
Temperature, OAT°C, at liftoff	11.2	12.6	15.5	21.0	14.4	15.4	11.3	12.4
Ground run, a/g	0.23 avg	0.27 avg	0.25 avg	0.3 avg	0.3 avg	0.3 avg	0.27 avg	0.25 avg
Rotation rate, $\dot{\theta}_{max}$, deg/sec	3.0	3.6	1.0	4.0	2.5	2.5	5.0	3.0
Lift-off, IRIG, hr-min-sec	10-21-10.0	11-39-01.5	14-49-54.2	15-12-10	14-05-57.5	16-18-11.7	13-20-27.7	15-34-40.5
Altitude, ft	389	505	270	260	600	620	380	360
V_e, kt	86	83.2	103	97	101.5	100	101	101
α_{boom}, deg	4.5	7.0	7.0	9.0	8.0	7.4	9.0	9.0
θ, deg	6.1	9.0	8.0	10.5	9.0	8.0	10.3	9.0
δ_e, deg	-6.4	-6.6	-5.0	-6.8	-7.0	-5.5	-7.0	-5.0
35 ft, IRIG, hr-min-sec	10-21-15.0	11-39-23	14-49-58.5	15-12-13	14-06-01	16-18-16.5	13-20-30.7	15-34-42.5
V_e, kt	103	92	113	104.5	108.7	111	103.3	106.3
α_{boom}, deg	2.8	6.0	7.0	10.0	6.0	7.2	7.0	6.5
θ, deg	8.3	14.0	12.0	15.0	12.8	10.1	12.0	10.0
δ_e, deg	-1.0	0	-3.5	-5.0	-2.5	-3.5	-2.5	-3.5

Nosewheel liftoff speeds for the actual flight test takeoffs are also plotted on figure 8. The pilot made only conventional takeoffs beginning rotation using $\delta_e \approx -10°$ ($F_S \approx 20$ lb). Nosewheel liftoff speeds were close to those predicted for the elevator angle used.

Elevator-to-trim at climbout ranged between $-2.5° < \delta_e < -5.0°$ at the recorded flaps 15° conditions. Trim tab setting was put in the "takeoff" range marked on the trim indicator ($\delta t_{trim} \approx 0°$). This setting was found satisfactory for takeoff trim.

CLIMB/DESCENT

Two-Engine Performance

A summary of the climb and descent performance is presented in figures 9 through 15 for the three primary flap settings: up, 30°, and 65°. The flight test data points shown were taken at a variety of gross weights, temperatures, altitudes, power settings, and conical nozzle positions. To present an overall indication of the flight test results, the test points have been normalized to the condition shown. It should be noted that the airspeed system had not been calibrated and, therefore, position error corrections have not been applied to the airspeed or angle-of-attack data. A complete summary of the specific flight conditions and results is presented in table II.

Comparisons of the flight test results to the predicted results are given in figures 16 through 23 for flaps up, 30°, 65°, and 73° at the altitude and temperature of the test conditions. The comparisons are made at both a constant rate of climb and a constant power setting. For the constant power setting case, the predicted rate of climb is estimated at the same power setting as that used for the flight test condition. The alternate case is also shown for a constant rate of climb. The power setting is predicted which gives the same rate of climb as was measured for the flight condition. Comparison of the predicted versus measured power settings indicates the amount of additional thrust required to maintain a given flight condition. Angle of attack and elevator position required for trim are also presented for each flap setting.

A relatively consistent trend is evident from the data. To maintain a given rate of climb with the nozzles aft, approximately 2.5% more N_H is required for flaps up, 1% for flaps 30°, and 1% to 1.5% more for flaps 65° and 73°. At a constant rate of climb the angle of attack measured on the nose boom is 1° to 2° higher than predicted for all flap settings. The higher angles are consistent with the expected upwash at the alpha measuring station on the nose boom.

The effect of deflecting the conical nozzles down to the 60° to 90° range is evident in figure 21. An additional 2% or 3% higher N_H is required with the nozzles deflected than with the

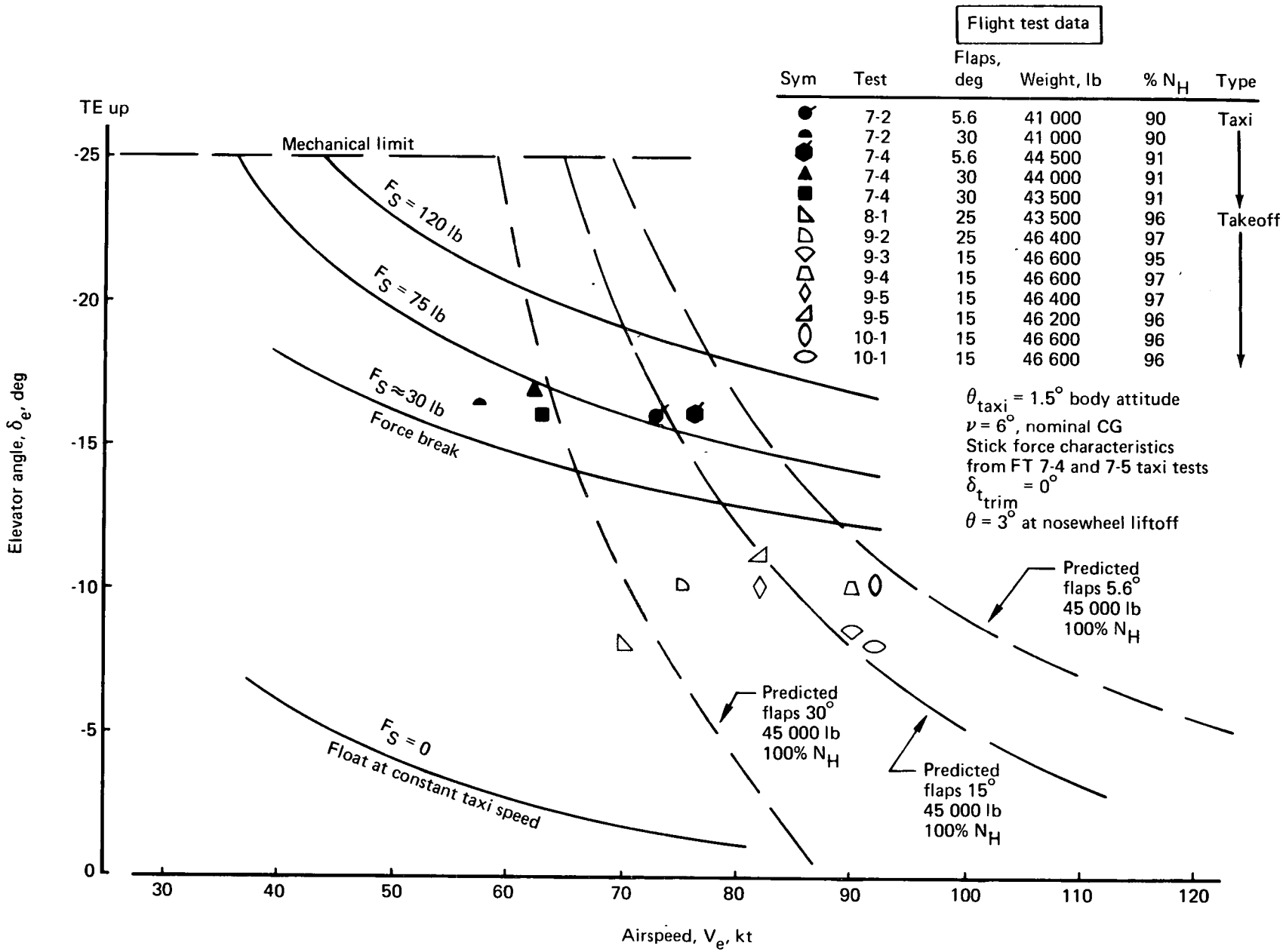

FIGURE 8.—NOSEWHEEL LIFTOFF FOR TAKEOFF ROTATION

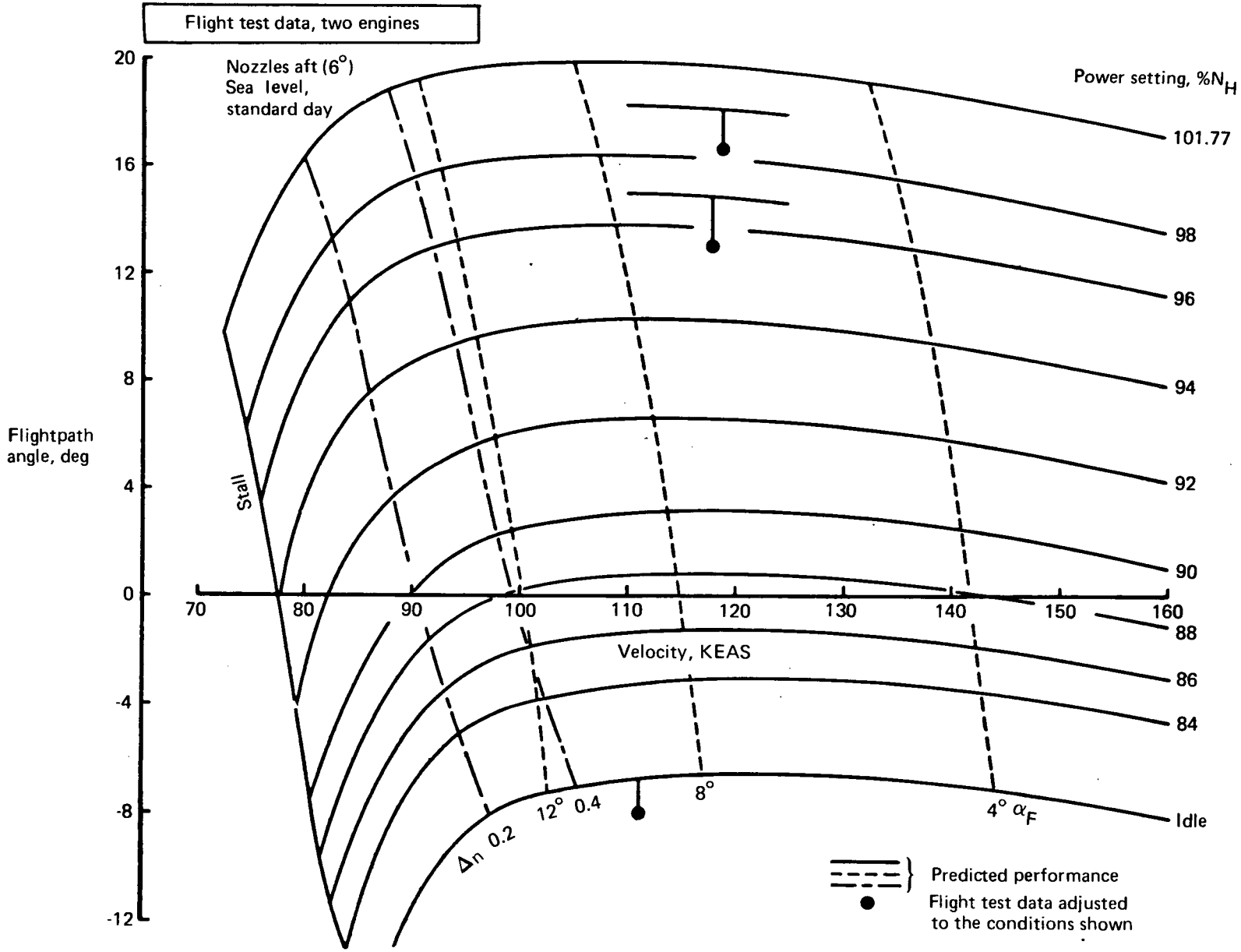

FIGURE 9.—FLAPS-UP CLIMB—GROSS WEIGHT = 40 000 LB

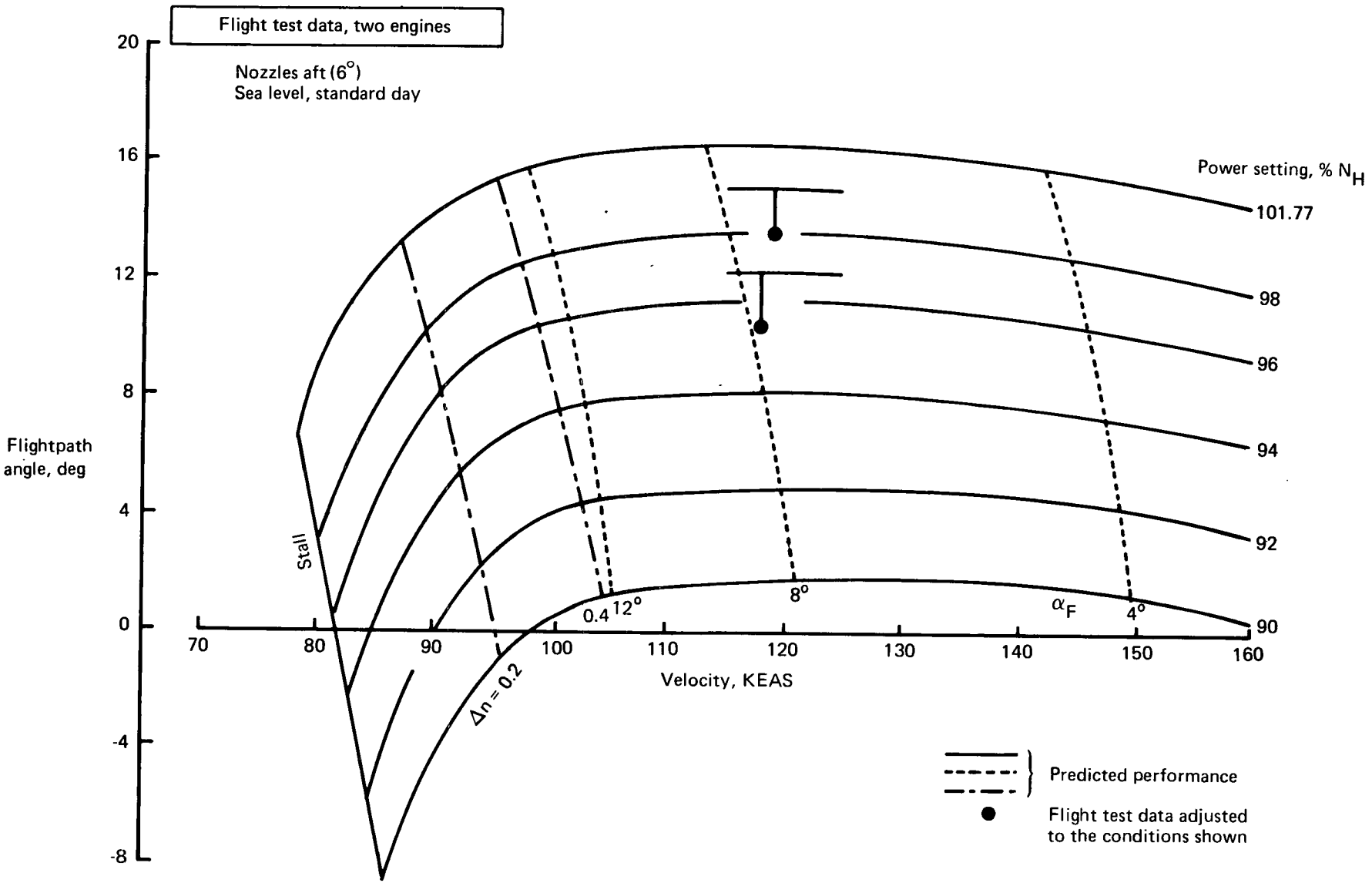

FIGURE 10.–FLAPS-UP CLIMB–GROSS WEIGHT = 45 000 LB

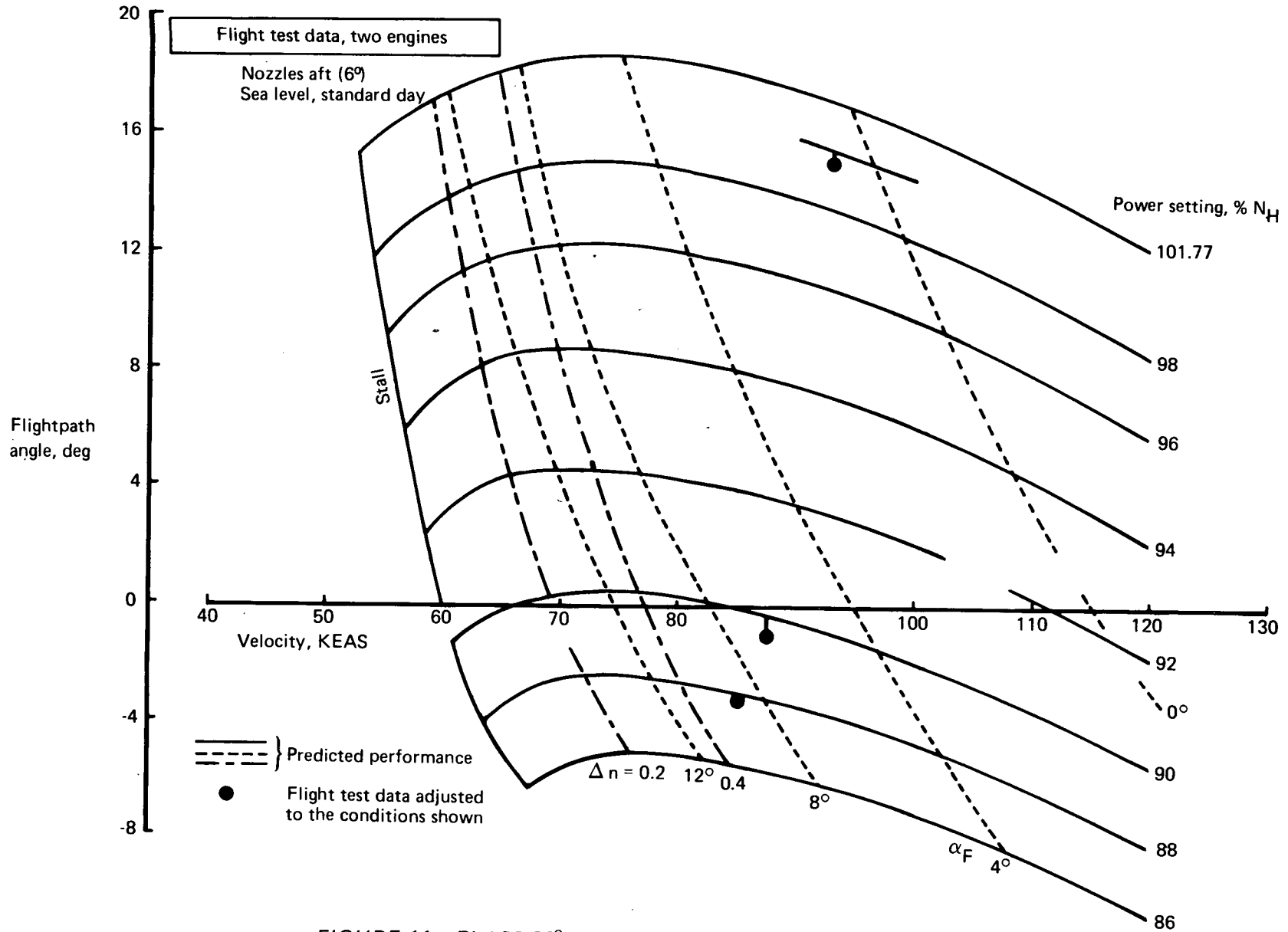

FIGURE 11.—FLAPS 30° CLIMB—GROSS WEIGHT = 40 000 LB

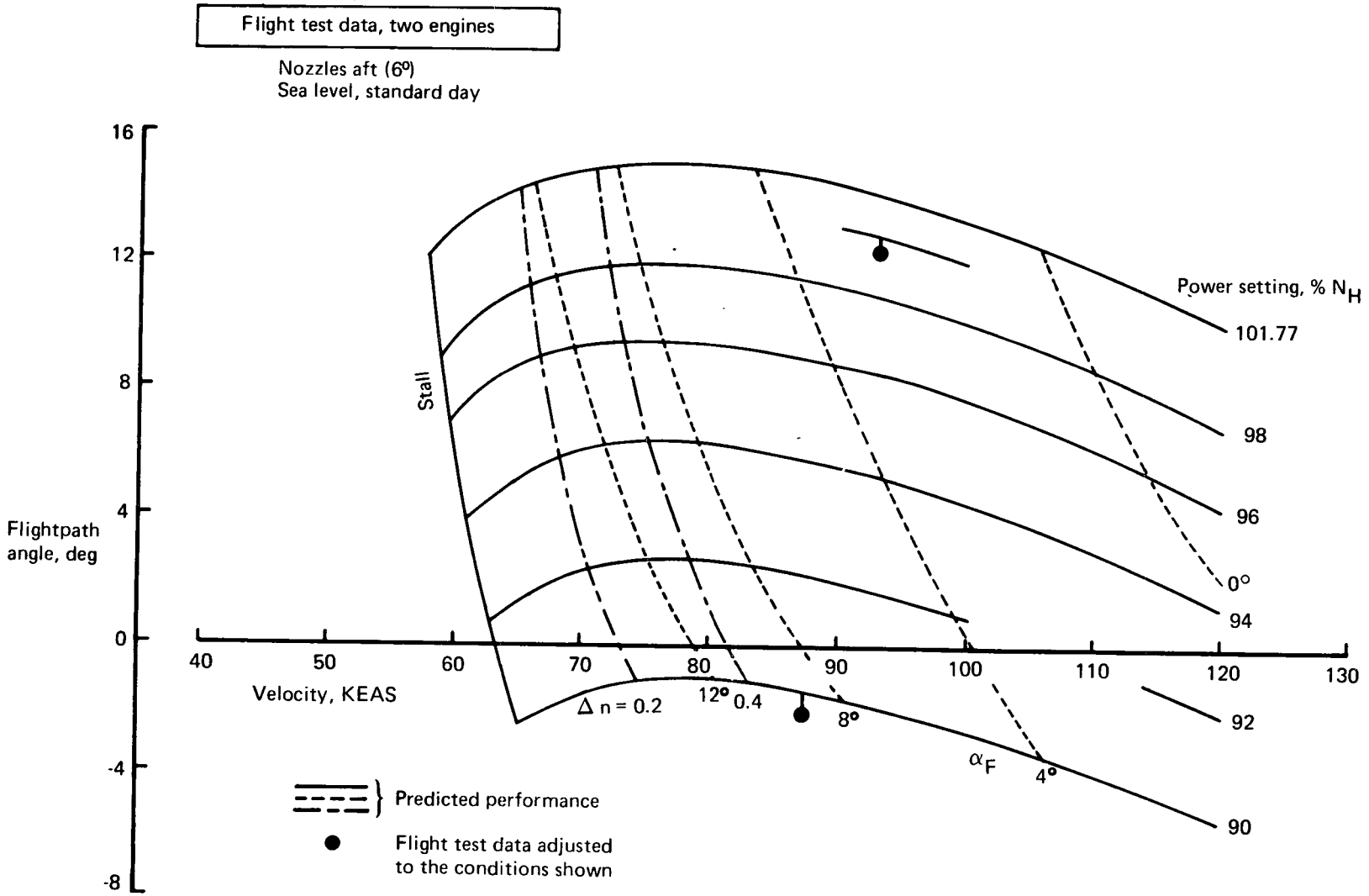

FIGURE 12.—FLAPS 30° CLIMB—GROSS WEIGHT = 45,000 LB

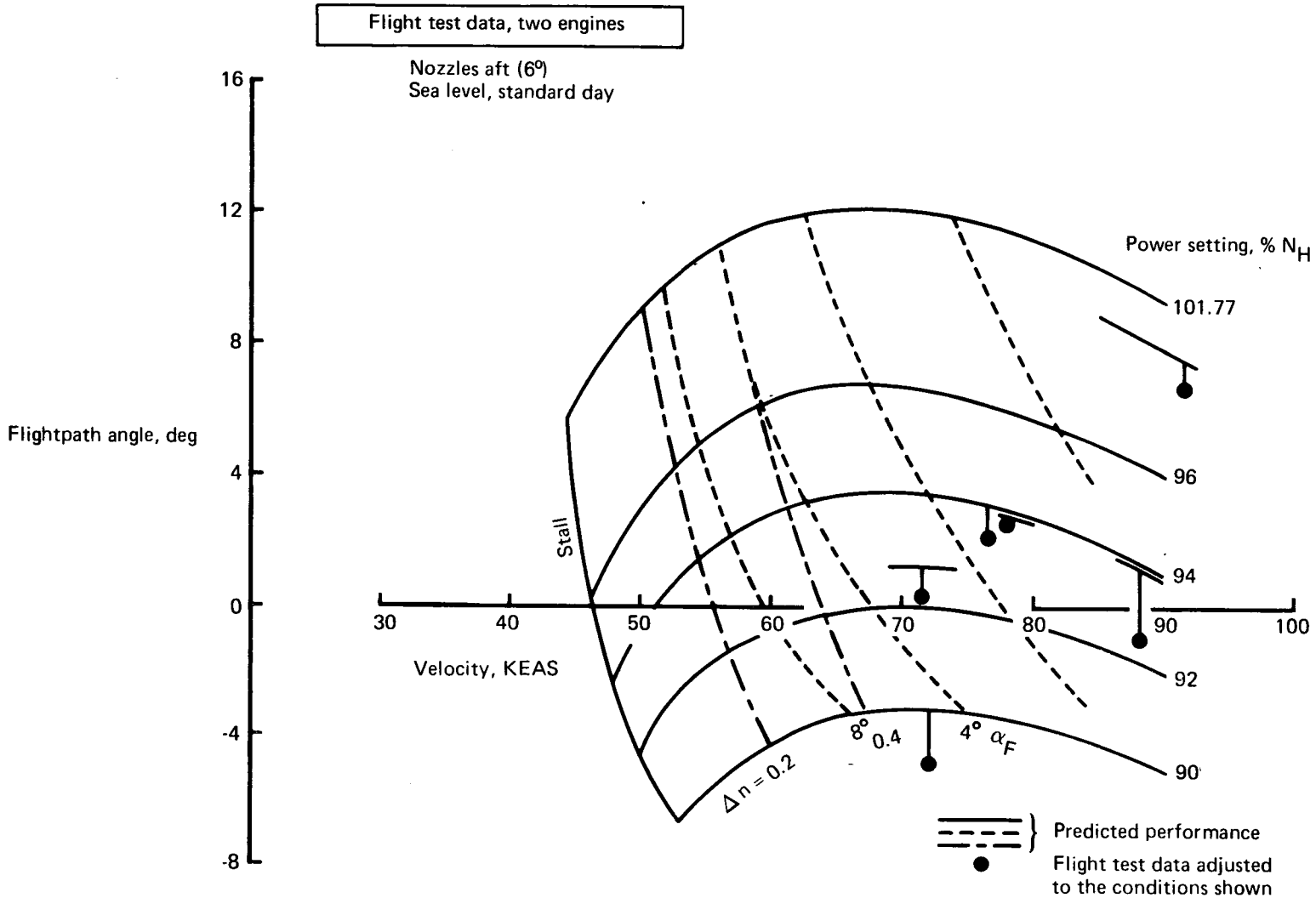

FIGURE 13.–FLAPS 65° CLIMB–GROSS WEIGHT = 40 000 LB

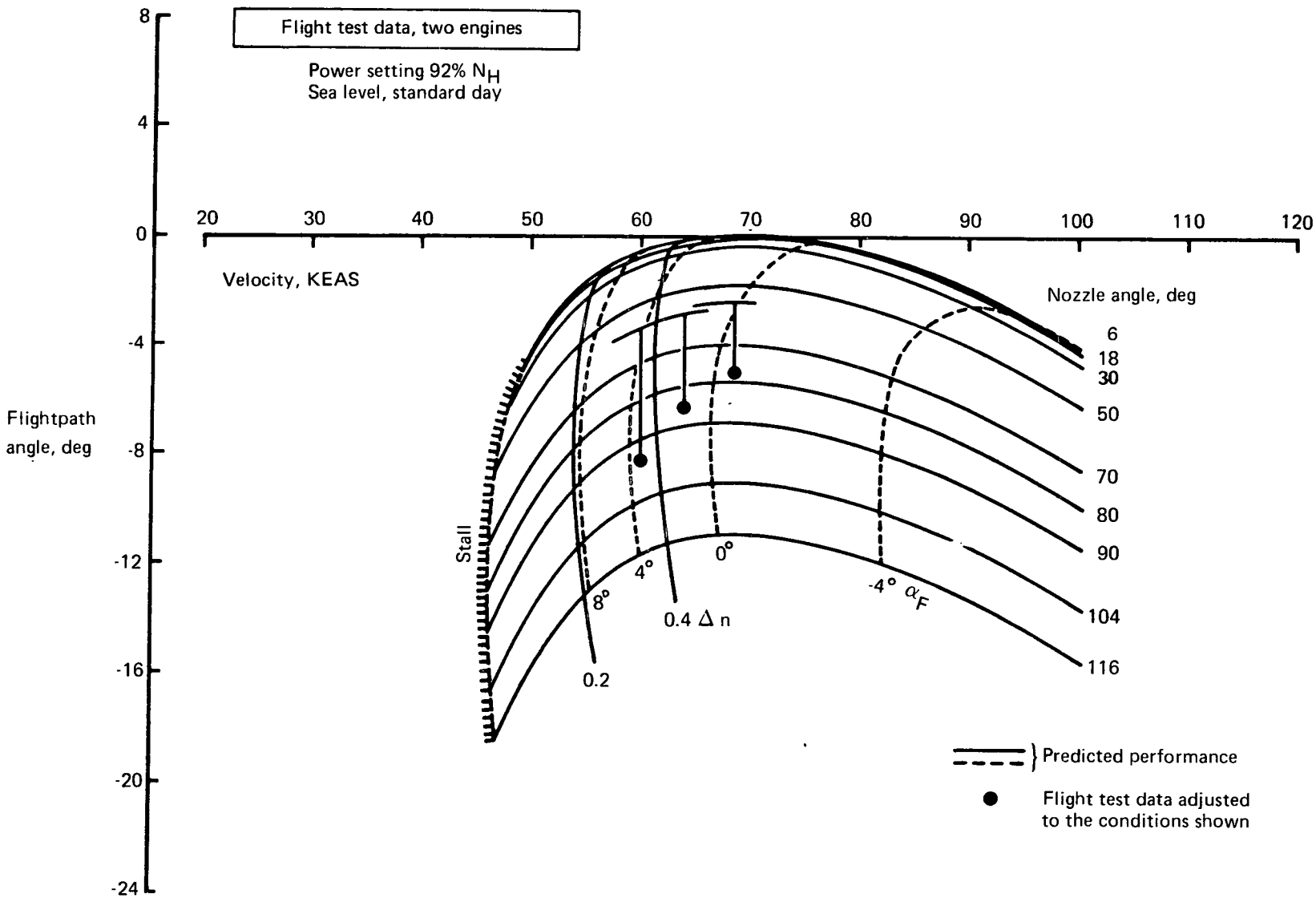

FIGURE 14.–FLIGHTPATH ANGLE–FLAPS 65°, GROSS WEIGHT = 40 000 LB

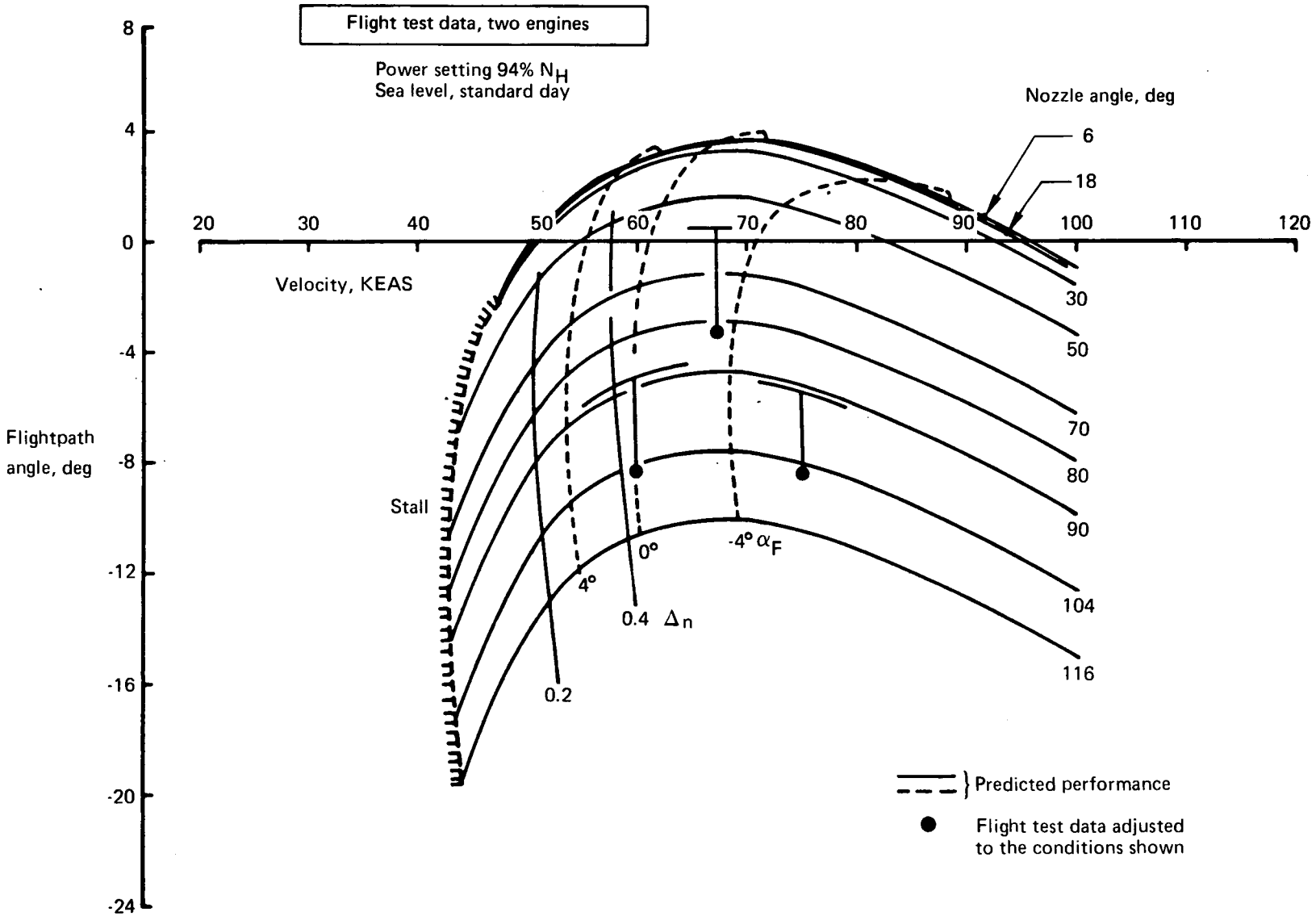

FIGURE 15.–FLIGHTPATH ANGLE–FLAPS 65°, GROSS WEIGHT = 40 000 LB

TABLE II.–FLIGHT TEST DATA–CLIMB AND DESCENT CONDITIONS–TWO ENGINES

Test Condition	9-2 1.00.002.003	9-2 1.00.002.008	9-2 1.00.002.007-1	9-2 1.00.002.009-1	9-2 1.00.002.009-2	9-2 1.00.002.011	9-2 1.00.002.004-1	9-2 1.00.002.004-2	9-2 1.00.003.008
IRIG time, hr-min-sec	11-48-23 to 11-48-48	12-08-0 to 12-09-0	12-11-50 to 12-12-10	12-40-45 to 12-40-55	12-41-15 to 12-41-25	12-44-0 to 12-44-30	12-54-15 to 12-54-45	12-55-30 to 12-55-58	13-08-10 to 13-08-40
Flap pos, $\delta_{F_{nom}}$, deg	Up	30	30	65	65	65	Up	Up	30
Nozzle pos, ν, deg	10	10.5	10.5	10.5	10.2	9.5	8	8	7.9
Power setting, % N_H									
Engine 1	97	100	61	91.9	91.9	61.7	100	61	88
Engine 2	96.8	100	61	91.9	91.9	61.7	100	61	88
Velocity, V_e, KEAS	118	93	92	78	88	90	119	111	85
Gross weight, lb	46,200	43,800	43,400	40,200	40,100	39,800	38,500	38,300	37,200
Altitude, ft	5,700	8,800	6,000	7,100	6,800	4,500	6,200	6,400	1,360
Temperature, std +°C	3.1	1.6	2.2	2.6	2.9	3.2	3.1	2.7	2.2
Rate of climb, ft/min	1,650	1,280	-1,900	-200	-800	-2,100	3,000	-1,600	-480
Angle of attack, α_{boom}, deg	9.5	5	15	3	0	9	7	11.5	10
Pitch angle, θ, deg	17.0	12.5	3.8	1	-3	-3	20	3.7	6.3
Elevator pos, δ_e, deg	-4.8	-1	9.4	3	4	-3.2	-4.2	-7.8	-5.9
Elevator spring tab, deg	3	1	1.8	1.5	-2	0.7	1.2	1.5	1.4
Elevator trim tab, deg	0	-0.5	0.7	-3	-3	0.7	1.8	6	2.6

TABLE II.—Continued

Test Condition	9-3 4.06.002.017	9-3 4.08.001.010	9-4 1.00.001.002	9-4 1.00.001.002-1	9-4 1.00.003.009	9-5 1.00.003.009	9-5 1.00.003.002.2-1	9-5 1.00.003.002.2-2	9-5 1.28.001.006
IRIG time, hr-min-sec	14-57-0	15-58-20 to 15-58-50	16-00-50 to 16-01-40	16-02-20 to 16-02-30	16-13-00 to 16-13-15	15-25-00	16-23-50 to 16-24-20	16-25-20 to 16-25-40	16-36-00 to 16-36-12.5
Flap pos, $\delta_{F_{nom}}$, deg	15	65	73	65	30	50	65	65	65
Nozzle pos, ν, deg	7	11	13	13	11	11	10	91	88.2
Power setting, % N_H									
Engine 1	93.5	100.4	92.3	92.4	90.3	90.6	94.1	94.0	93.3
Engine 2	93.4	100.1	92.9	93.0	89.7	89.8	94.0	93.9	93.9
Velocity, V_e, KEAS	141	91.5	73.2	71.5	87.5	79	76.5	75.2	60
Gross weight, lb	46,400	39,400	41,100	41,000	40,000	37,900	45,700	45,500	44,500
Altitude, ft	5,780	2,850	3,890	3,610	360	700	6,730	5,780	5,400
Temperature, std +°C	1.9	0.9	5.6	5.7	5.5	0.2	-0.7	-0.8	-1.1
Rate of climb, ft/min	620	960	-260	-200	-380	-380	-70	-1470	-1260
Angle of attack, α_{boom}, deg	3	-3	4.5	7.0	9.5	8	7.3	3.8	14.4
Pitch angle, θ, deg	6	3	2	3.5	7.5		5.2	-6.5	0
Elevator pos, δ_e, deg	-1.5	6.5	3.5	1.5	-5.5	-3	2.5	3	1.4
Elevator spring tab, deg	0.3	-3.0	-3.0	-2.0	1.5	-1.0	-1.0	-2.5	-2.3
Elevator trim tab, deg	0.5	-4.0	-2.0	-2.0	2.5	1.6	-2.5	-2.0	-2.0

Table II.—Concluded

Test Condition	9-5 4.08.001.016	9-5 4.08.001.017	9-5 1.28.001.009	10-1 1.21.002.002	10-1 1.21.002.003	10-1 1.21.002.004	10-1 4.08.001.045	10-1 3.08.001.005	10-1 1.13.001.004
IRIG time, hr-min-sec	16-58-10 to 16-58-40	16-59-15 to 16-59-50	17-08-15 to 17-08-45	14-17-30 to 14-18-10	14-21-00 to 14-21-30	14-22-10 to 14-22-20	14-38-50 to 14-39-35	15-39-30 to 15-40-00	14-28-50 to 14-29-40
Flap pos, $\delta_{F_{nom}}$, deg	73	73	73	65	65	65	54	65	65
Nozzle pos, ν, deg	11.5	11.5	60	7	58	58	10	56	58
Power setting, % N_H									
Engine 1	93.8	100.4	93.5	89.7	93.5	92.8	90.3	93.0	92.8
Engine 2	94.1	100.3	94.2	89.8	93.4	92.4	89.4	92.6	92.4
Velocity, V_e, KEAS	60.2	65.2	87.5	72	67.5	64	78	68.5	60
Gross weight, lb	41,700	41,500	40,400	41,000	40,700	40,400	38,900	46,200	39,600
Altitude, ft	5,310	5,400	4,200	7,900	6,950	6,550	620	7,020	7,670
Temperature, std + °C	-1.3	-1.2	-1.1	-3.3	-3.4	-3.5	-3.3	-3.6	-4.2
Rate of climb, ft/min	-160	640	-1050	-570	-620	-600	-520	-760	-750
Angle of attack, α_{boom}, deg	12.5	4.9	-3.5	9.7	3	6	7.5	10	10
Pitch angle, θ, deg	8.7	9	-9.5	3.5	-2	0	4	2	2.5
Elevator pos, δ_e, deg	4	6.5	8.5	0	5	4	-2	3	2.5
Elevator spring tab, deg	-2	-3.5	-4	-1	-3.5	-4	-1	-2.8	-2.5
Elevator trim tab, deg	-4	-4	-4	0	-2.6	-2.8	1.2	-2.5	-2.7

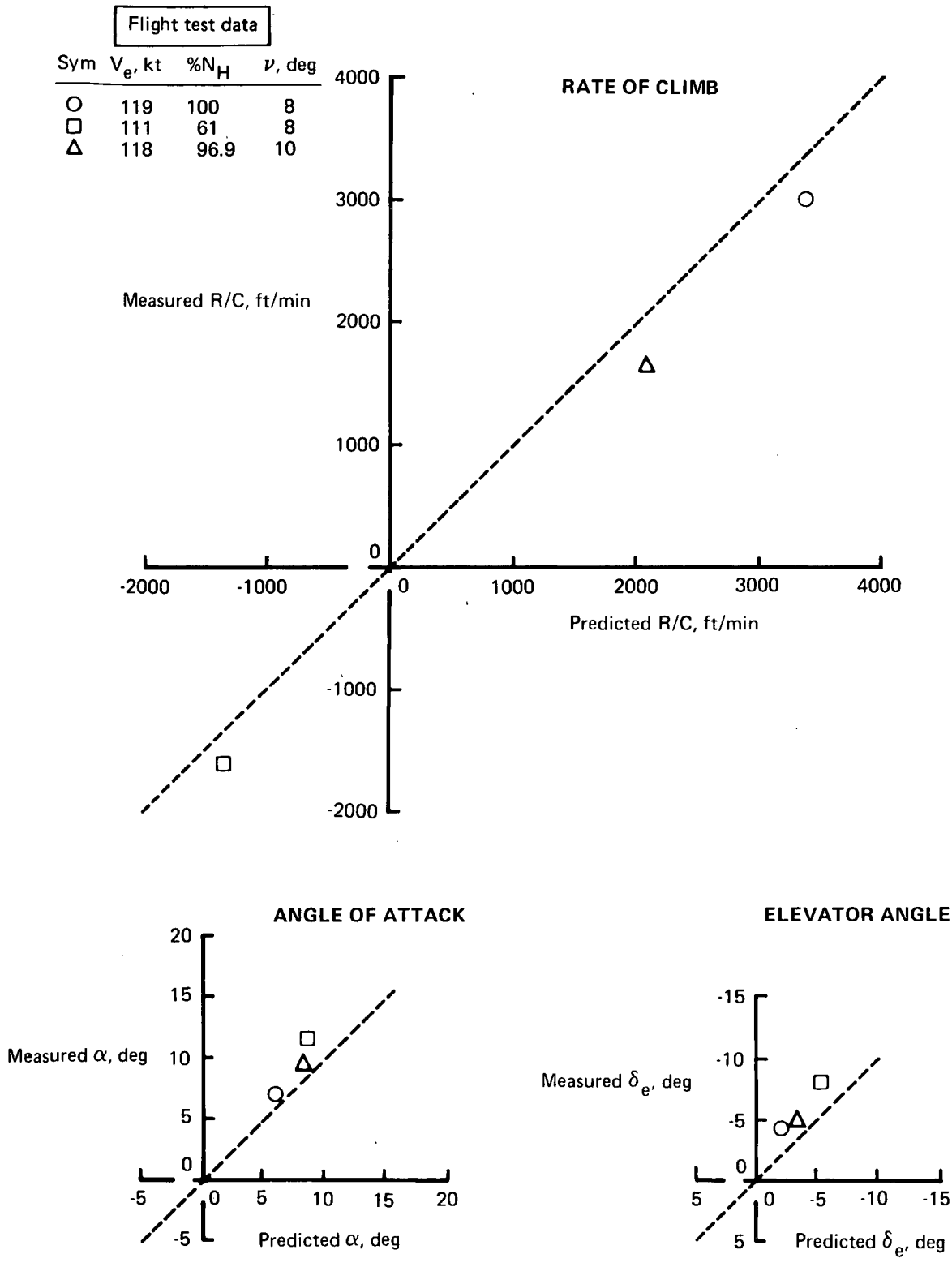

FIGURE 16.–COMPARISON OF MEASURED AND PREDICTED PERFORMANCE–FLAPS UP, CONSTANT POWER SETTING (TWO ENGINES)

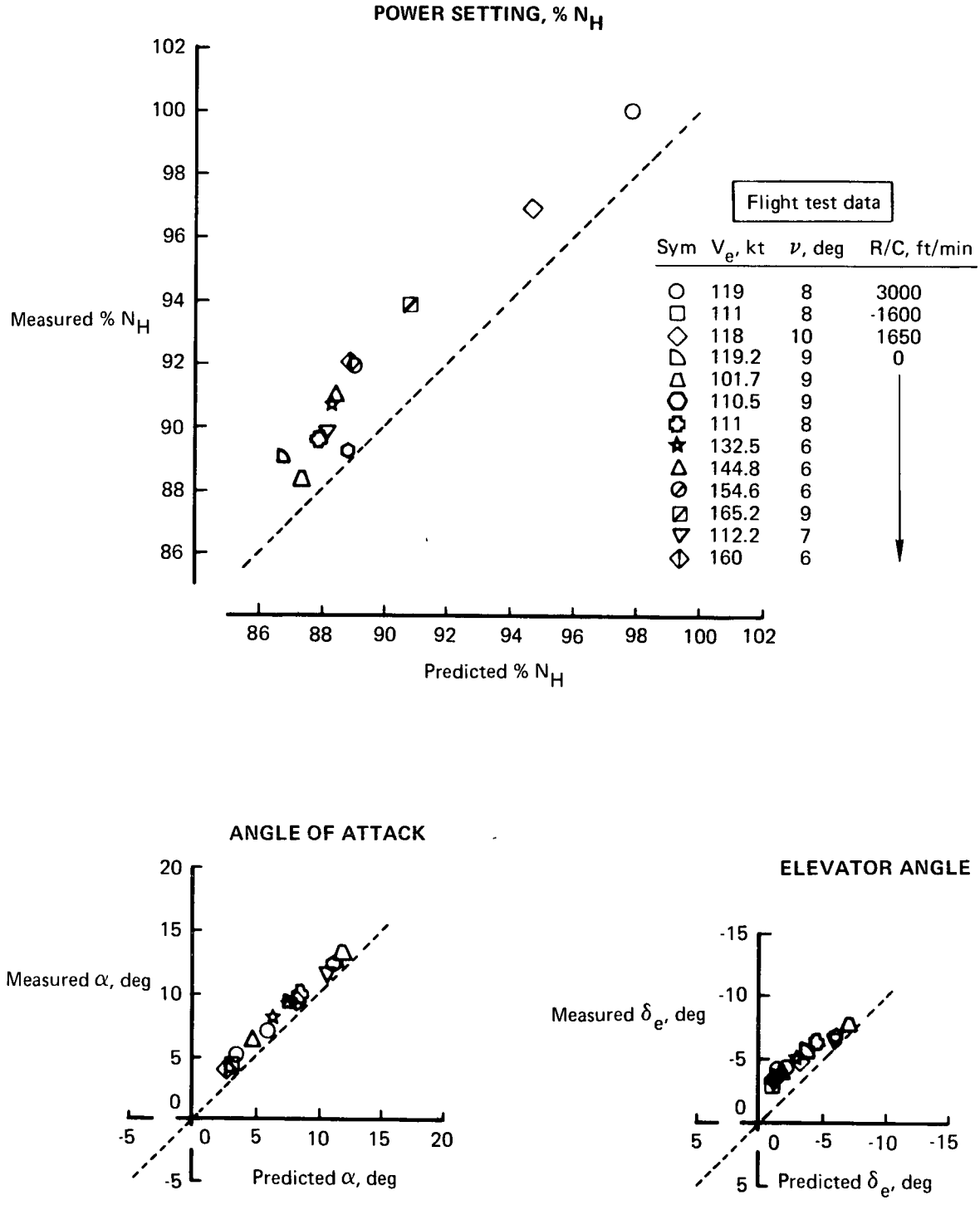

FIGURE 17.–COMPARISON OF MEASURED AND PREDICTED PERFORMANCE–FLAPS UP, CONSTANT RATE OF CLIMB (TWO ENGINES)

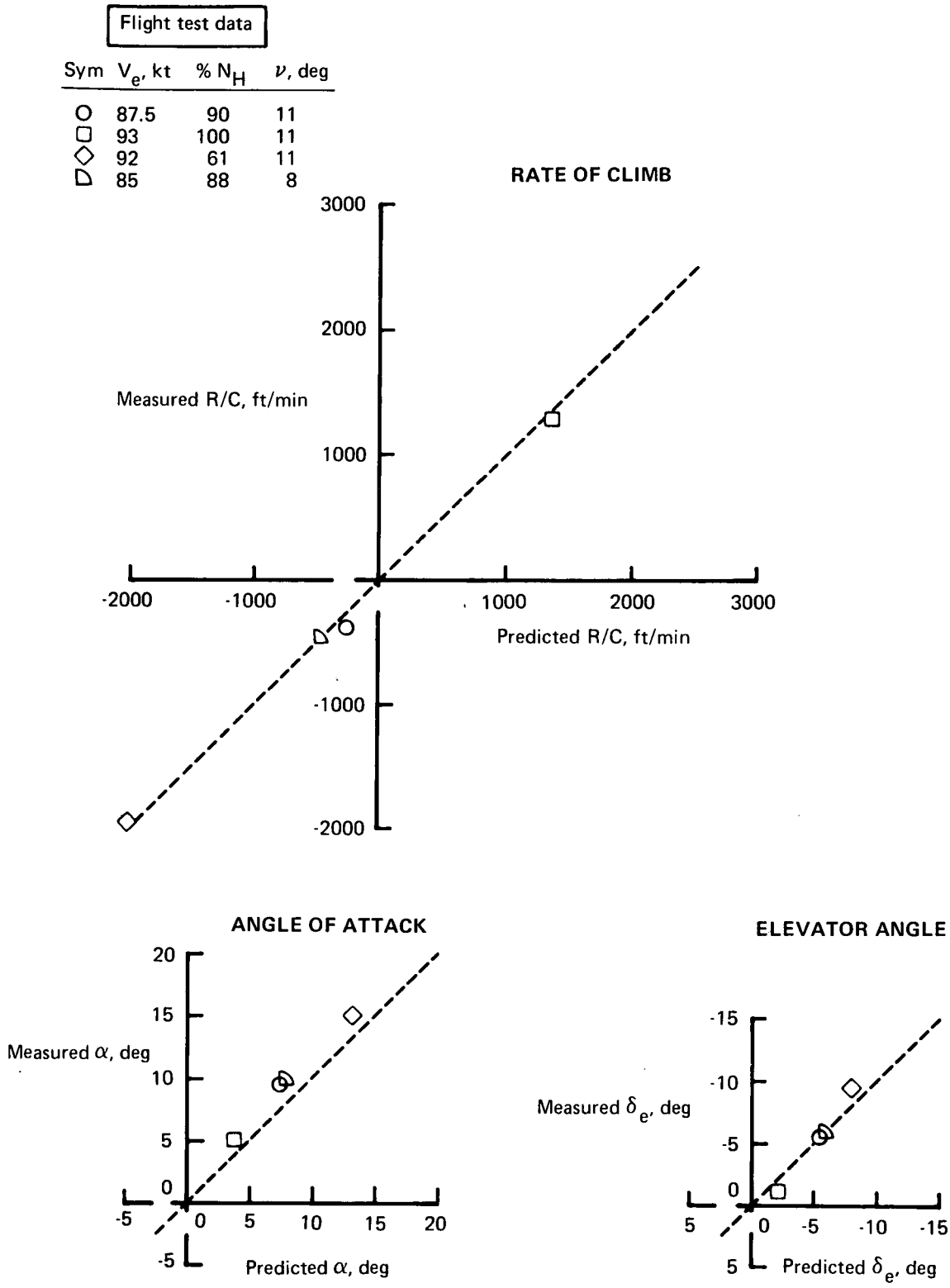

FIGURE 18.—COMPARISON OF MEASURED AND PREDICTED PERFORMANCE—FLAPS 30°, CONSTANT POWER SETTING (TWO ENGINES)

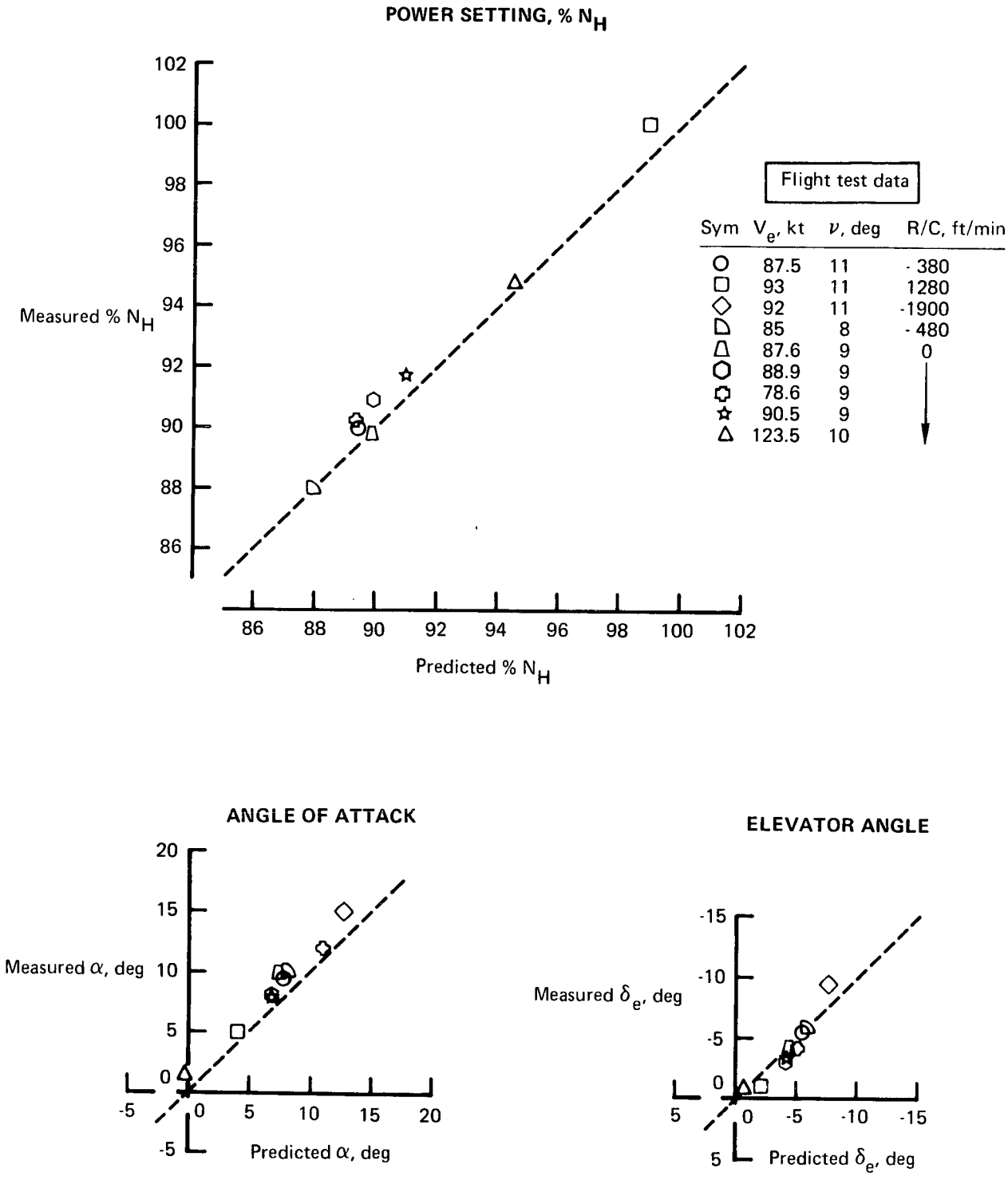

FIGURE 19.–COMPARISON OF MEASURED AND PREDICTED PERFORMANCE–FLAPS 30°, CONSTANT RATE OF CLIMB (TWO ENGINES)

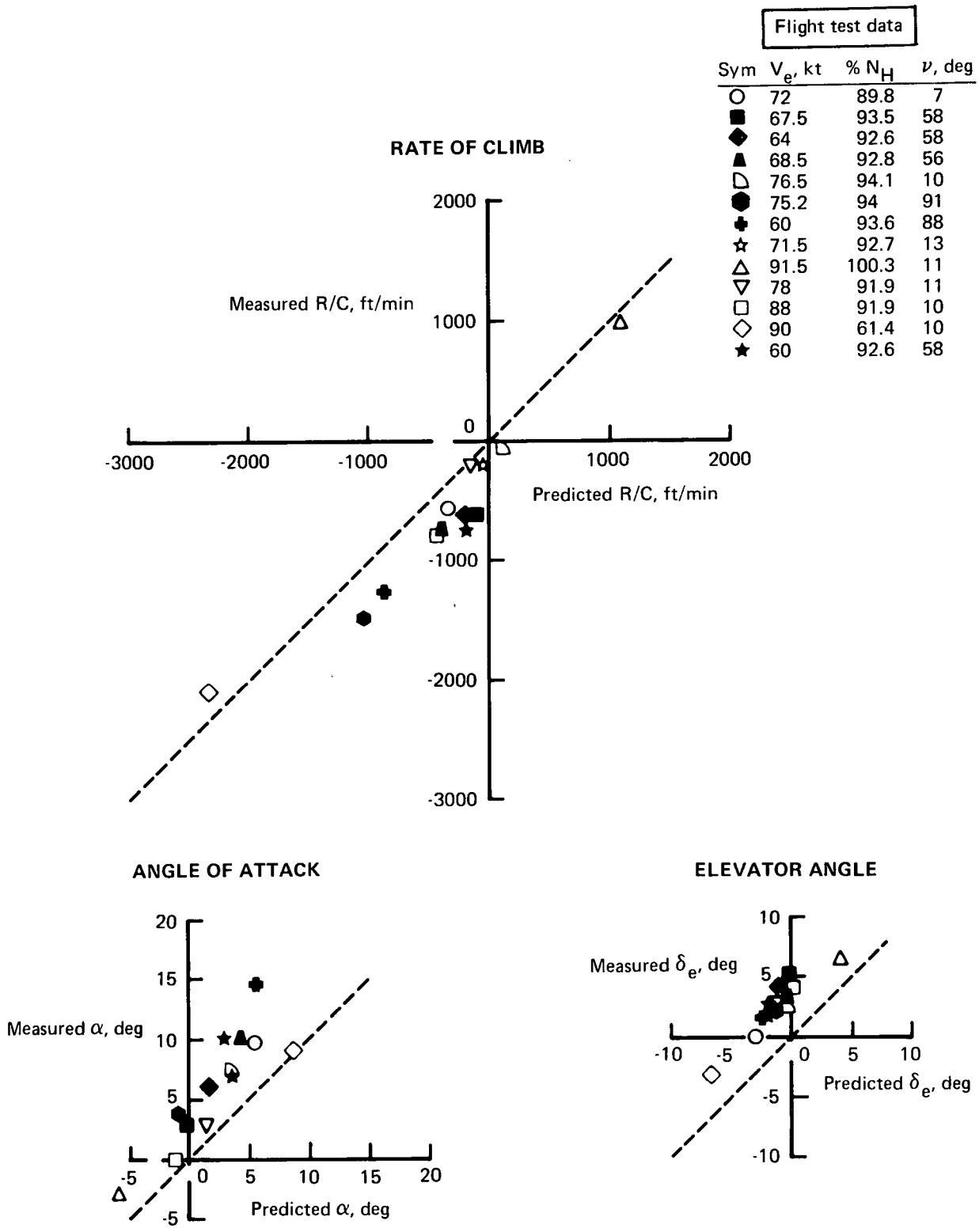

FIGURE 20.–COMPARISON OF MEASURED AND PREDICTED PERFORMANCE–FLAPS 65°, CONSTANT POWER SETTING (TWO ENGINES)

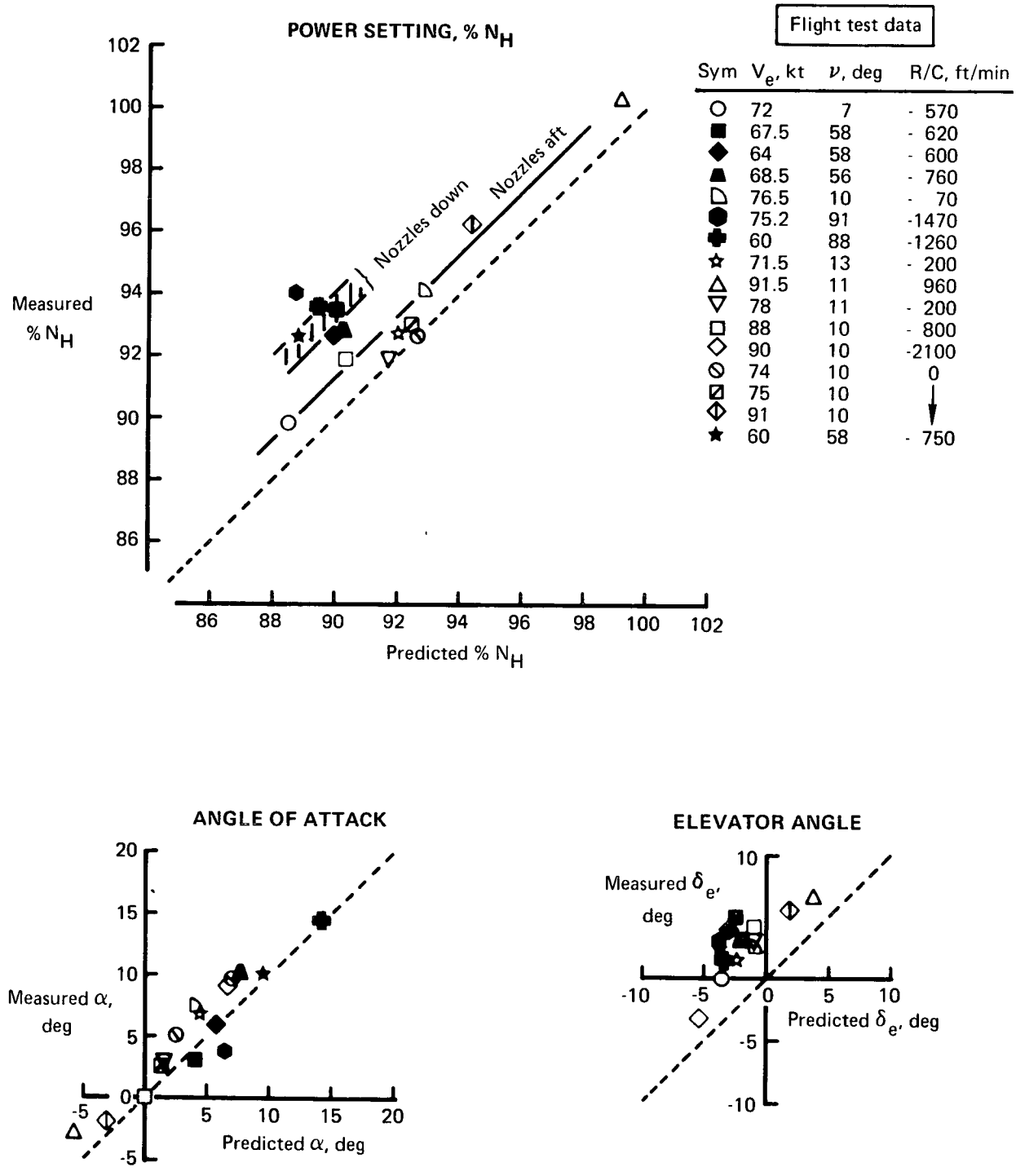

FIGURE 21.–COMPARISON OF MEASURED AND PREDICTED PERFORMANCE–FLAPS 65°, CONSTANT RATE OF CLIMB (TWO ENGINES)

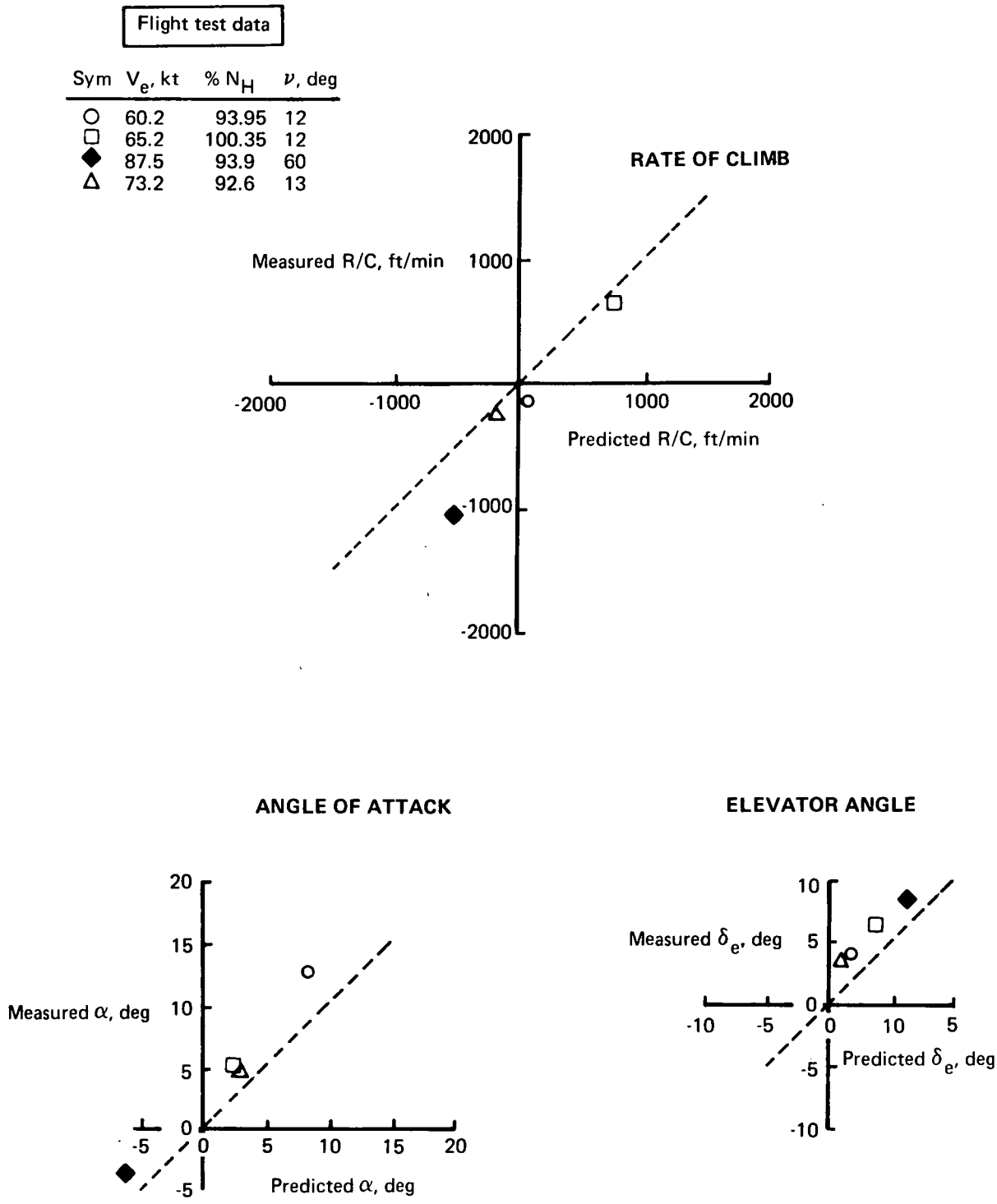

FIGURE 22.–COMPARISON OF MEASURED AND PREDICTED PERFORMANCE–FLAPS 73°, CONSTANT POWER SETTING (TWO ENGINES)

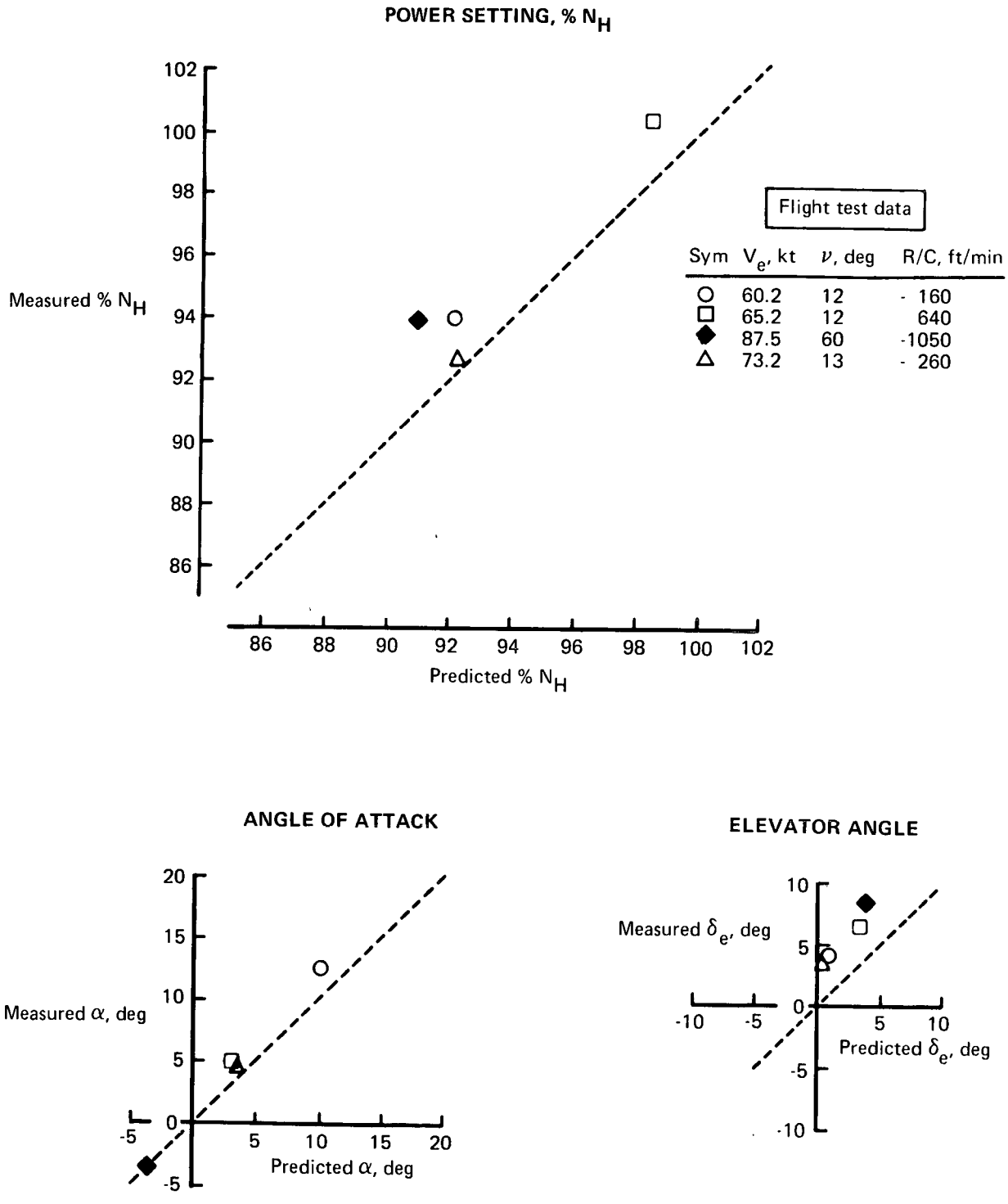

FIGURE 23.–COMPARISON OF MEASURED AND PREDICTED PERFORMANCE–FLAPS 73°, CONSTANT RATE OF CLIMB (TWO ENGINES)

nozzles aft as compared to the predicted N_H. The predicted effect for deflecting the nozzles was based on wind tunnel data which showed that the forces followed the vector components of the hot thrust with no adverse interference on lift and drag.

A review of the predicted performance was made to resolve the differences between the flight test results and the predicted data. Differences between the final configuration as flight tested and that assumed for the original prediction were noted. Items considered included (1) actual trailing edge flap setting of 5.6° compared to the 0° used for the flaps up prediction, (2) excrescences such as the nose boom, bluff rear nacelle fairing, flap and aileron beams, actuators, mass balance weights, and conical nozzle position indicators, and (3) revision of the fixed landing gear and leading edge slat drag. After accounting for the above items, the required thrust for flight test with the nozzles aft was 10%-15% higher than predicted for flaps up, and 5%-20% higher for flaps down.

It was not possible to determine the reasons for the higher thrust because of the limited amount of performance testing. One probable source is indicated by the continuous low to moderate buffet level noted on the aircraft during the flight program. The buffet appeared to be a function of power setting and conical nozzle position. The intensity decreased with power reduction and when the nozzles were rotated down to positions greater than approximately 20°. In addition to the drag of local separated regions as indicated by the buffet level, other possible explanations for the higher thrust levels include a lower augmentation ratio, the inability to resolve drag and thrust to the necessary accuracies, and the lack of a calibrated airspeed system.

Single-Engine Performance

Six single-engine climb checks were conducted during the flight test program. A comparison of the results with the predictions is given in figure 24. It should be noted that the power setting for several of the conditions was not at the emergency rating of 102.9% N_H for engine 1 and 102.0% for engine 2.

The test procedure was to set the simulated dead engine at idle. A correction has been made for the idle thrust and expected windmilling drag. The corrected emergency climb performance is presented in figure 25, where the data are normalized to 45 000 lb, standard day temperatures, and the velocity shown. A summary of the flight test conditions is given in table III.

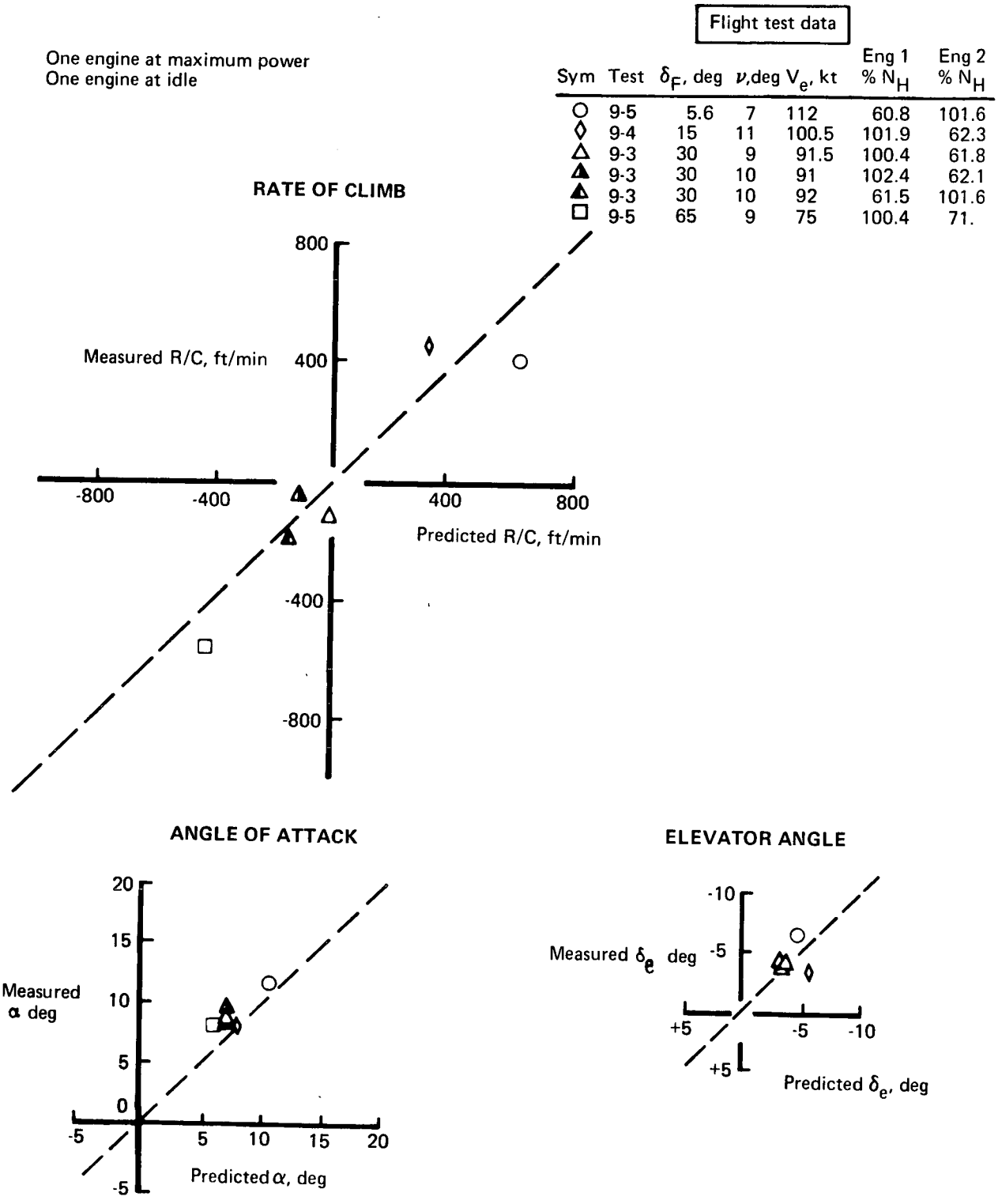

FIGURE 24.–SINGLE-ENGINE CLIMB CORRELATION

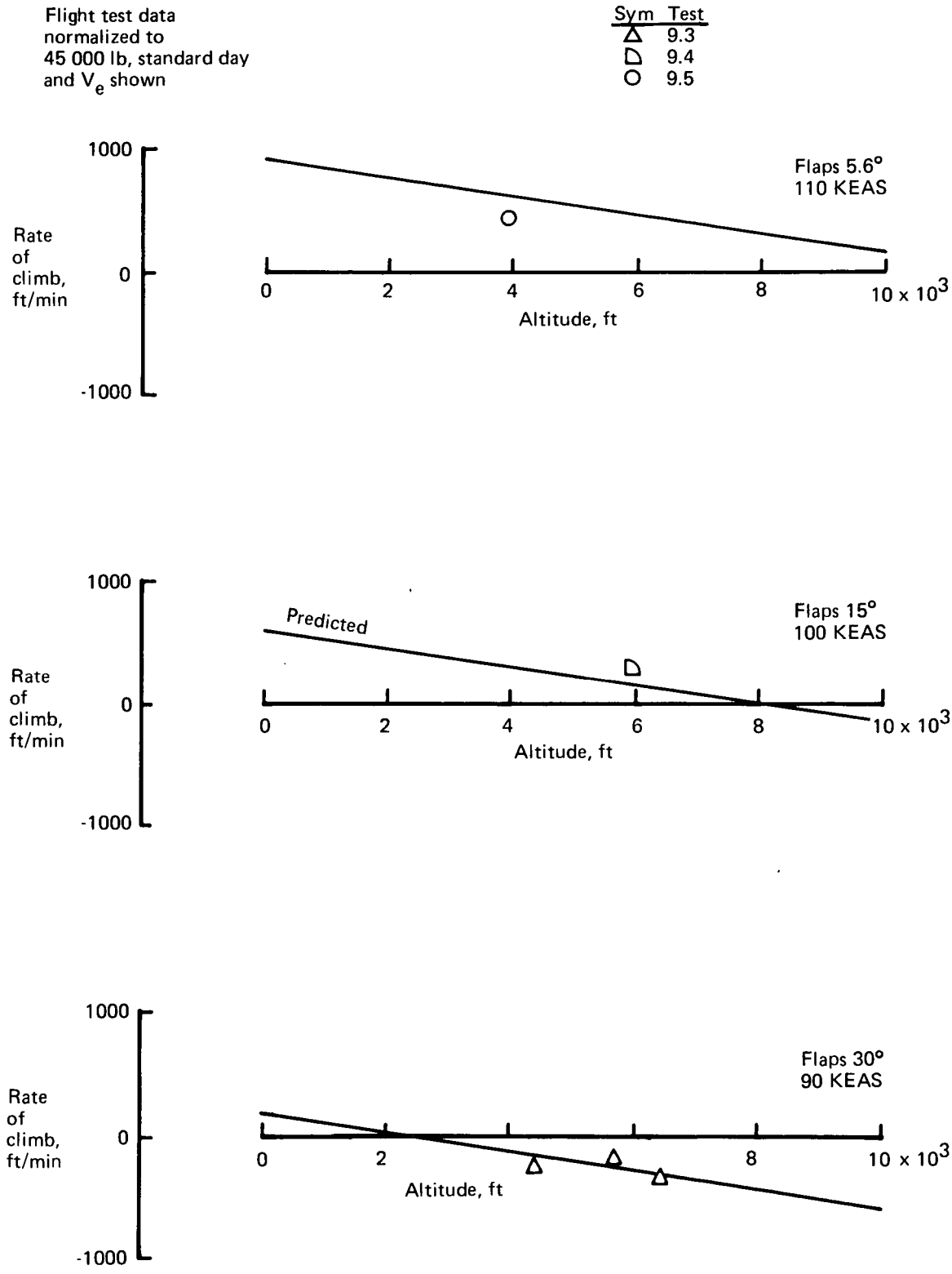

FIGURE 25.—ENGINE-OUT RATE OF CLIMB, GROSS WEIGHT = 45 000 LB

TABLE III.–FLIGHT TEST DATA–SINGLE-ENGINE CLIMB CONDITIONS

Test Condition	9-3 4.08.001.008	9-3 1.00.002.002	9-3 1.00.002.002.1	9-4 1.00.002.002	9-5 1.00.002.002	9-5 4.08.001.013
IRIG time, hr-min-sec	15-31-30 to 15-32-0	15-34-50 to 15-35-10	15-37-05 to 15-37-25	15-55-15 to 15-15-50	14-09-00 to 14-09-40	15-10-0 to 15-10-49
Flap pos, $\delta_{F_{nom}}$, deg	30	30	30	15	5.6	65
Nozzle pos, ν, deg	9	10	10	11	7	9
Power setting, % N_H						
Engine 1	100.4	102.4	61.5	101.9	60.8	100.4
Engine 2	61.8	62.1	101.6	62.3	101.6	71.0
Velocity, V_e, KEAS	91.5	91.0	92.0	100.5	112.0	75.0
Gross weight, lb	42,600	42,100	41,800	41,800	46,200	39,800
Altitude, ft	4,340	5,700	6,420	5,950	3,890	8,130
Temperature, std +°C	0.6	1.4	0.9	5.7	-1.0	-1.2
Rate of climb, ft/min	-114	-50	-195	450	400	-570
Angle of attack, α_{boom}, deg	8.5	9.0	8.5	7.8	11.5	8.0
Pitch angle, θ, deg	7.5	8.5	7.8	9.0	13.3	
Elevator pos, δ_e, deg	-4.0	-4.0	-4.0	-3.2	-6.3	0
Elevator spring tab, deg	1.0	1.0	1.0	-1.5	1.4	2.0
Elevator trim tab, deg	1.0	1.0	1.0	3.0	3.3	-4.0

CRUISE PERFORMANCE

Level Flight

The thrust required for level flight is presented in figure 26 for flaps up. All of the flight test data have been adjusted to the conditions shown: 40 000 lb gross weight, 5000-ft altitude, and standard day temperature. These conditions are representative of the majority of the testing. As noted from the figure, an approximate 2.5% higher power setting is required than was predicted consistent with the data presented in the previous section, "Climb/Descent." The corresponding specific range is 0.024 nautical air miles per pound of fuel at 5000-ft altitude.

The power setting required for level flight is shown in figure 27 for flaps 30°. Specific range will nominally be approximately 0.014 nmi/lb. The power required and specific range at the landing flap setting of 65° is given in figure 28.

The angle of attack and elevator required for level flight is presented in figures 29, 30, and 31 for flaps up, 30°, and 65°, respectively. A 1.5° to 2° higher alpha is required at all flap settings than was predicted.

A tabular summary of the level flight conditions taken during the test program is given in table IV.

Range

The nominal altitude used for the level flight testing was about 5000 ft. An altitude of 10 000 ft is more representative of the nominal cruise altitude for the Modified C-8A. A two-engine and single-engine fuel mileage check was made at the expected cruise altitude and speed to substantiate the data presented in "Level Flight." The results shown in figure 32 indicate a 32% to 34% reduction in specific range from that expected, giving about 0.024 nmi per pound of fuel for both two- and single-engine operation at the nominal airspeeds and weights tested.

The fuel flows for all the level flight trim conditions are shown in figure 33 as measured by the PCM flight test instrumentation. Fuel flows were approximately 7% higher than predicted. The cockpit fuel flow gages were also read during the ground testing and correlated with predicted as discussed in "Propulsion Systems Tests and Operation, Engine Operation." Based on the correlation of other engine parameters, it is considered that the cockpit gages are a better indication of the engine performance. Therefore, the range performance presented could be 7% to 8% conservative since all of the nautical miles per pound data are based on the PCM flight test instrumentation.

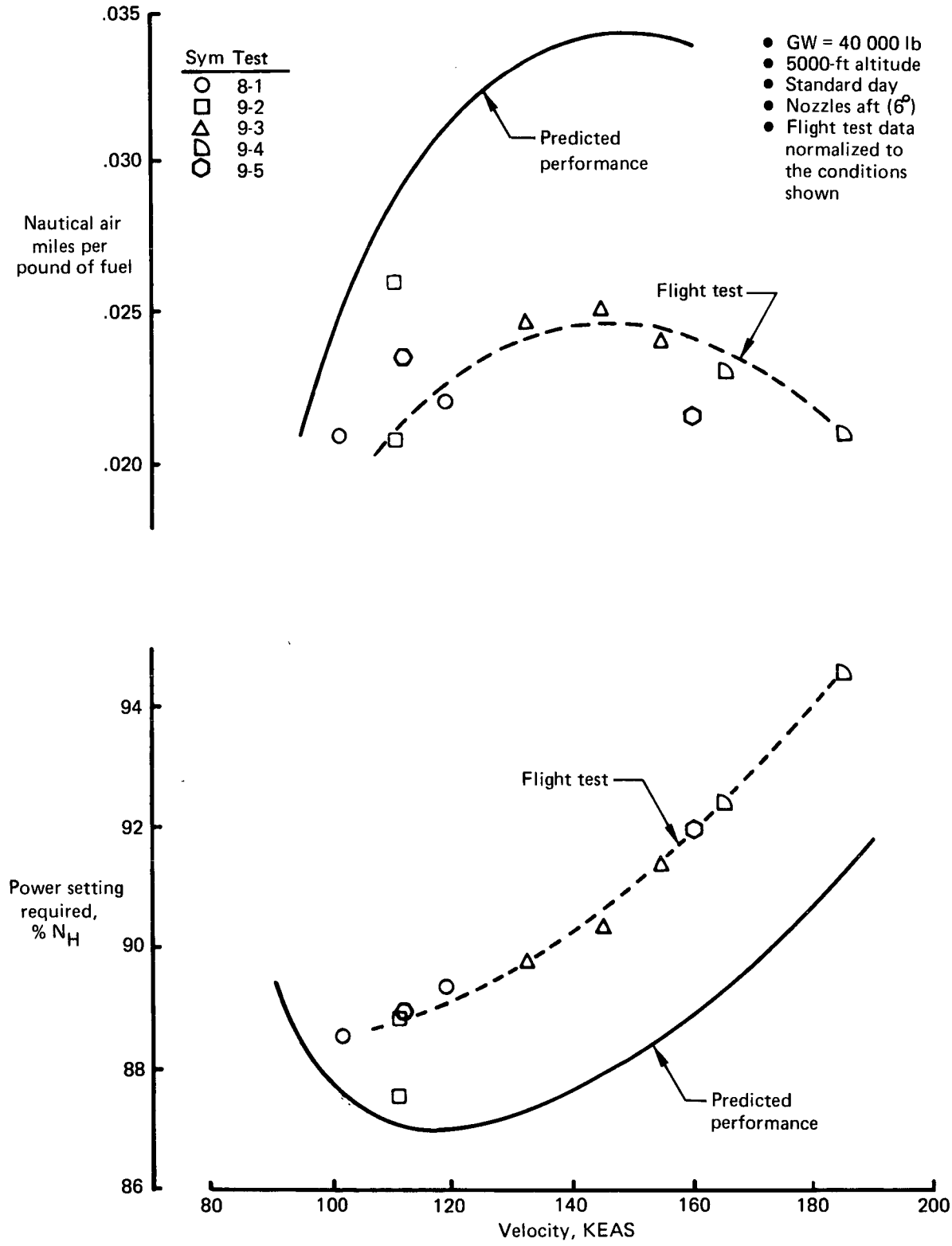

FIGURE 26.–LEVEL FLIGHT PERFORMANCE–FLAPS UP

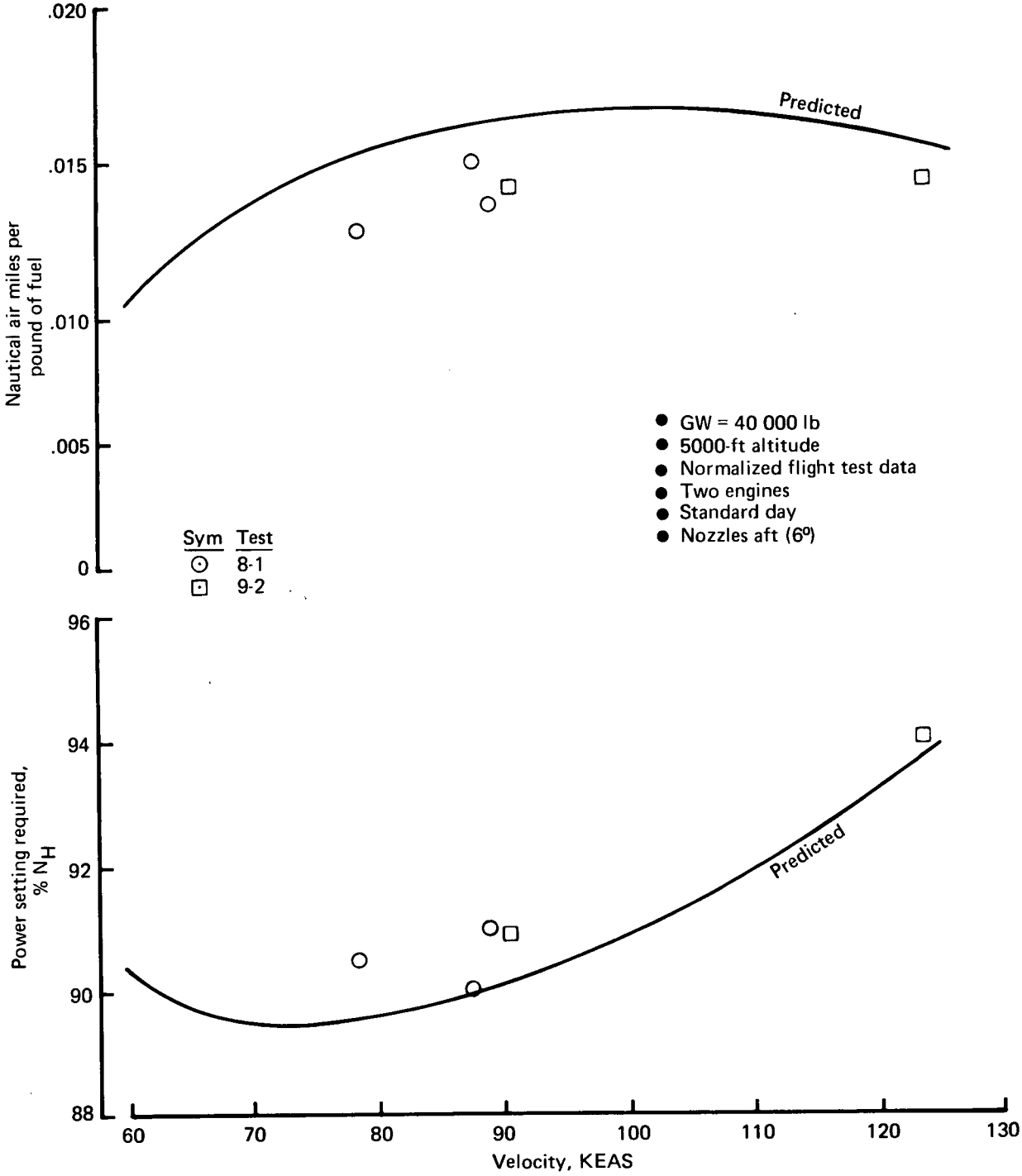

FIGURE 27.–LEVEL FLIGHT PERFORMANCE–FLAPS 30°

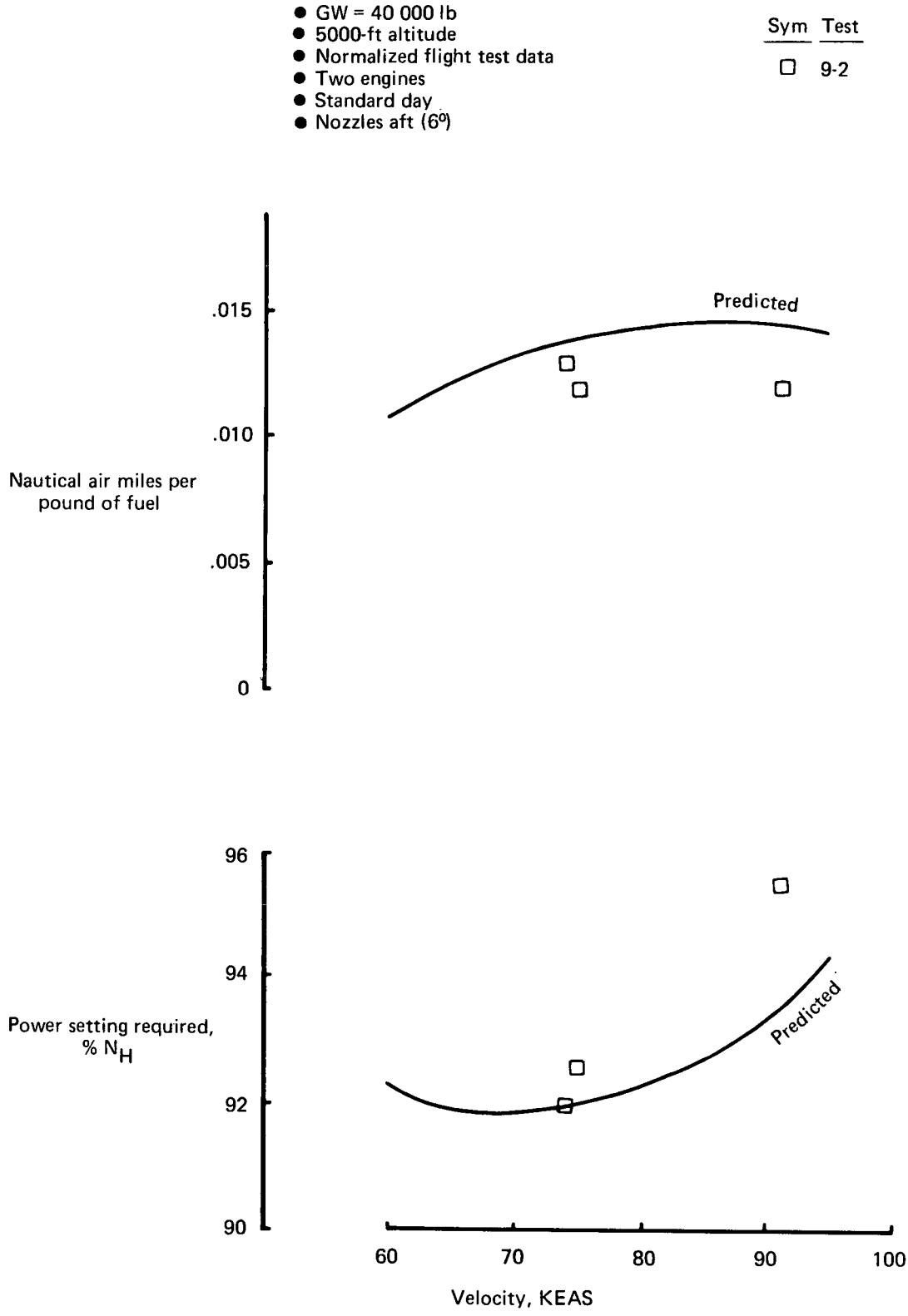

FIGURE 28.–LEVEL FLIGHT PERFORMANCE–FLAPS 65°

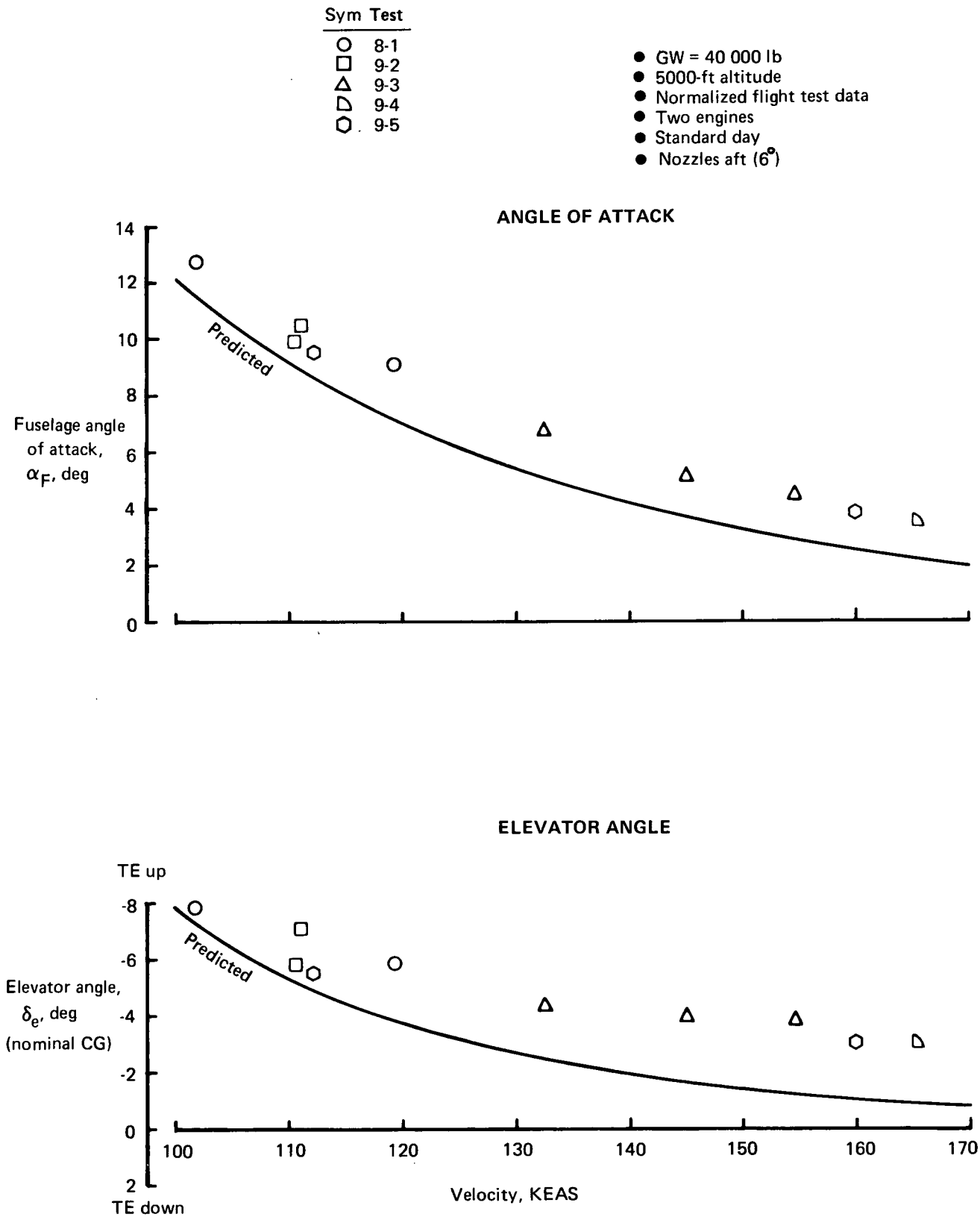

FIGURE 29.–ANGLE OF ATTACK AND ELEVATOR–LEVEL FLIGHT, FLAPS UP

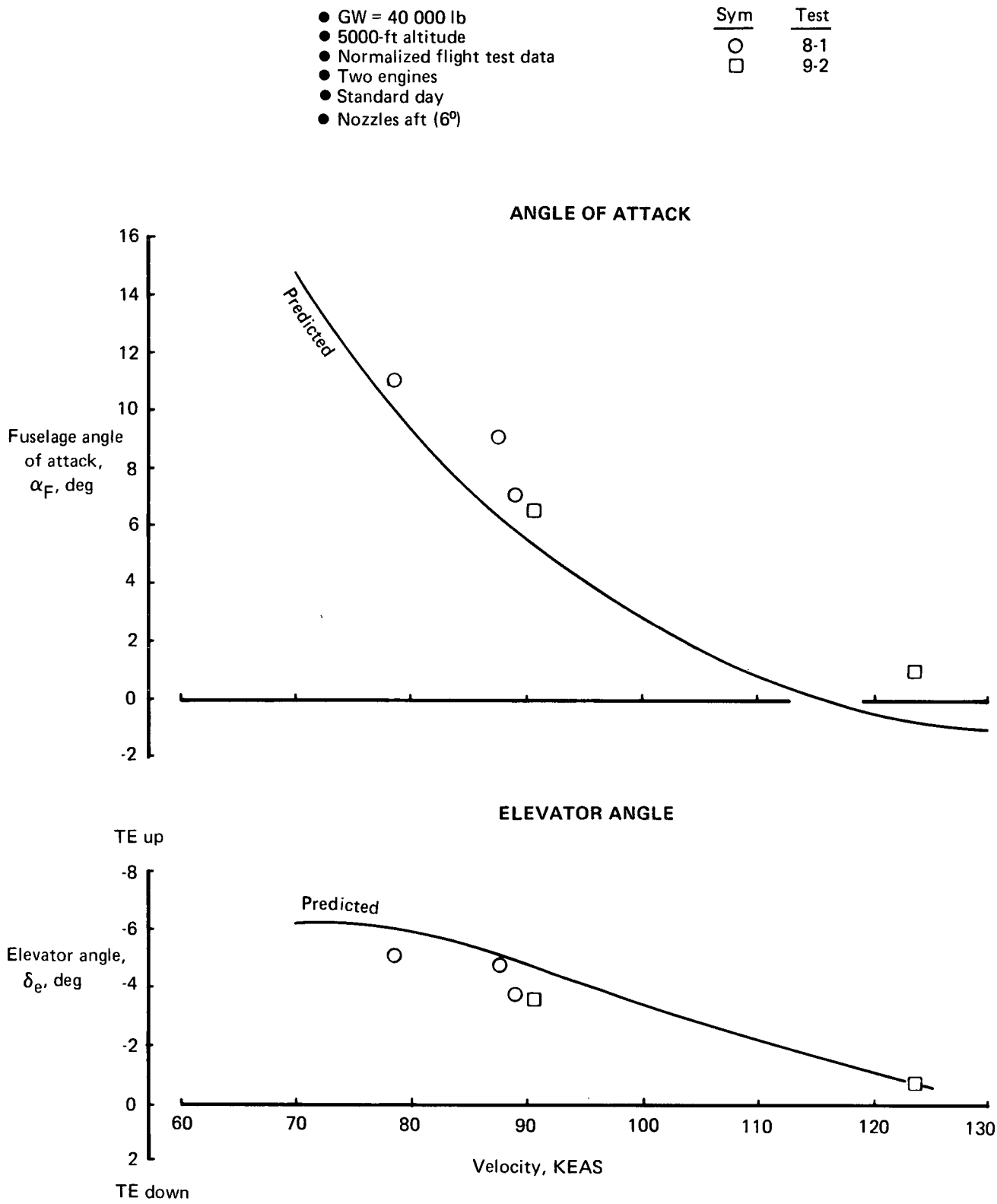

FIGURE 30.–ANGLE OF ATTACK AND ELEVATOR–LEVEL FLIGHT, FLAPS 30°

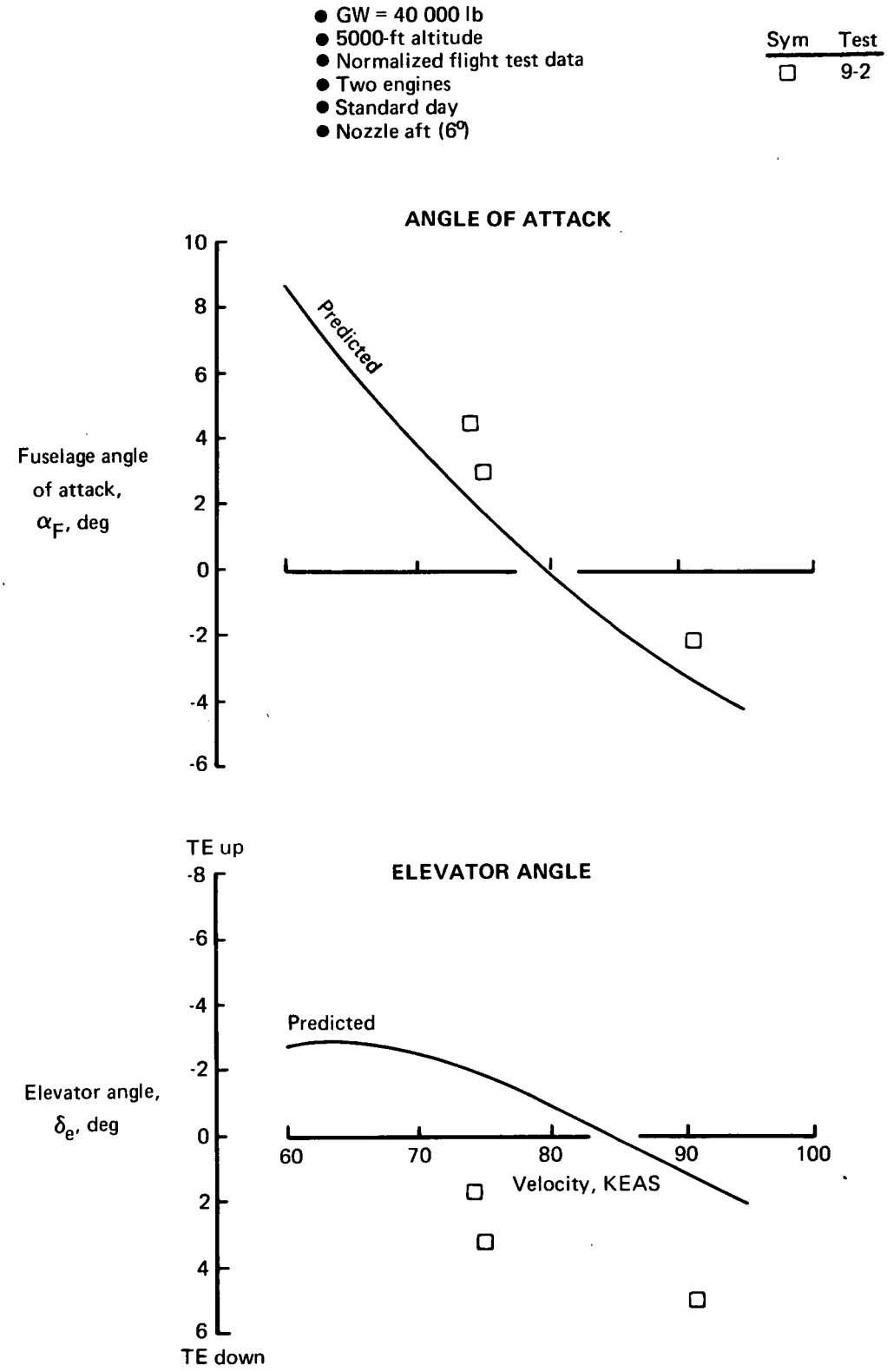

FIGURE 31.–ANGLE OF ATTACK AND ELEVATOR–LEVEL FLIGHT, FLAPS 65°

TABLE IV.–FLIGHT TEST DATA CONDITIONS–TWO ENGINES–LEVEL FLIGHT

Test Condition	8-1 7.02.002.018-1	8-1 7.02.002.018-2	8-1 7.02.002.021	8-1 7.02.002.002.2	8-1 7.02.002.002.3	9-2 4.06.002.010	9-2 1.00.002.007	9-2 1.00.002.006	9-2 1.00.002.002.1
IRIG time, hr-min-sec	10-37-52.5 to 10-37-55	10-38-15 to 10-38-20	10-42-10 to 10-42-15	10-51-30 to 10-51-35	10-52-45 to 10-52-50	11-45-30 to 11-45-38	12-06-10 to 12-06-37	12-10-15 to 12-19-35	12-37-15 to 12-37-35
Flap pos, $\delta_{F_{nom}}$, deg	30	30	30	Up	Up	Up	30	30	65
Nozzle pos, ν, deg	9	9	9	9	9	9	9	10	10
Power setting, % N_H									
Engine 1	90.1	91.1	90.5	88.7	88.3	89.3	91.6	94.6	92.3
Engine 2	89.6	90.7	90.0	89.3	88.2	89.1	91.8	94.9	92.9
Velocity, V_e, KEAS	87.6	88.9	78.6	119.2	101.7	110.5	90.5	123.5	74.0
V_T, KTAS	96.1	97.5	85.0	128.8	109.8	124.1	101.3	137.3	83.4
Gross weight, lb	42,200	42,200	41,800	40,800	40,700	45,900	44,000	42,600	40,600
Altitude, ft	6,540	6,560	5,710	5,630	5,550	7,450	7,300	9,400	7,575
Temperature, std + °C	-2.8	-2.7	-3.6	-3.4	-3.5	2.4	2.2	2.3	2.5
Total fuel flow, lb/hr	6,350	7,121	6,790	5,860	5,330	5,310	7,220	6,780	7,820
Angle of attack, α_{boom}, deg	10	8	12	9.3	13	11.9	8.1	1.4	5
Pitch angle, θ, deg	8	8	11.5	9	12	11.5	8.4	2.5	3.8
Elevator pos, δ_e, deg	-4	-3	-4	-5.6	-7.5	-6.7	-3.2	-0.7	2.4
Elevator spring tab, deg	0.2	0	0.5	1	2.7	1.4	0.5	0	-2
Elevator trim tab, deg	2	1	1.5	3.4	3.4	4	1	2	-2

TABLE IV.—Concluded

Test Condition	9-2 1.00.002.010	9-2 1.00.002.012	9-2 1.00.002.002.4	9-3 1.00.003.005	9-3 1.00.003.005.1	9-3 1.00.003.00521	9-4 1.00.003.005	9-4 4.08.001.001	9-5 1.28.001.001	9-5 1.19.001.001
IRIG time, hr-min-sec	12-42-30 to 12-42-45	12-46-30 to 12-46-59	12-53-15 to 12-53-45	15-04-00 to 15-04-10	15-07-30 to 15-08-30	15-17-45 to 15-18-05	15-17-35 to 15-18-05	15-28-22 to 15-28-40	14-11-10 to 14-11-20	14-52-30 to 14-53-55
Flap pos, $\delta_{F_{nom}}$, deg	65	65	Up	Up	Up	Up	Up	Up	Up	Up
Nozzle pos, ν, deg	10	10	8	6	6	6	9	6	7	6
Power setting, % N_H										
Engine 1	96	93	89.4	90.8	90.9	92.1	93.8	95.8	89.4	92.3
Engine 2	96.5	93	89.8	90.7	90.9	91.6	93.8	95.7	90.1	91.7
Velocity, V_e, KEAS	91	75	111	132.5	144.8	154.6	165.2	184.7	112.2	160
V_T, KTAS	100.4	79	118.9	138.6	151.3	162.6	181.1	199.7	120.0	183
Gross weight, lb	40,000	39,500	38,700	45,900	45,500	44,200	46,200	44,800	46,000	41,700
Altitude, ft	6,470	3,600	4,180	2,990	2,985	3,330	5,520	4,650	4,480	9,020
Temperature, std +°C	3.1	3.1	3.3	0.7	0.2	0.3	5.4	5.0	-1.4	1.5
Total fuel flow, lb/hr	6,470	8,575	5,625	6,860	6,970	7,620	8,535	10,420	6,230	7,560
Angle of attack, α_{boom}, deg	-2.0	+2.5	10	8	6	5	4.2	3	11.5	4
Pitch angle, θ, deg	-0.5	2	9.5	8	6	5.8	5	4	11.7	4.3
Elevator pos, δ_e, deg	5.5	4	-6.5	-5	-4.3	-4	-3	-2.7	-6.5	-3
Elevator spring tab, deg	-3	-1.8	1.5	1	0.8	0.8	0.5	0.5	1.5	1.0
Elevator trim tab, deg	-3	-3.8	0.4	3	2.4	2.0	1.5	1	4	1.5

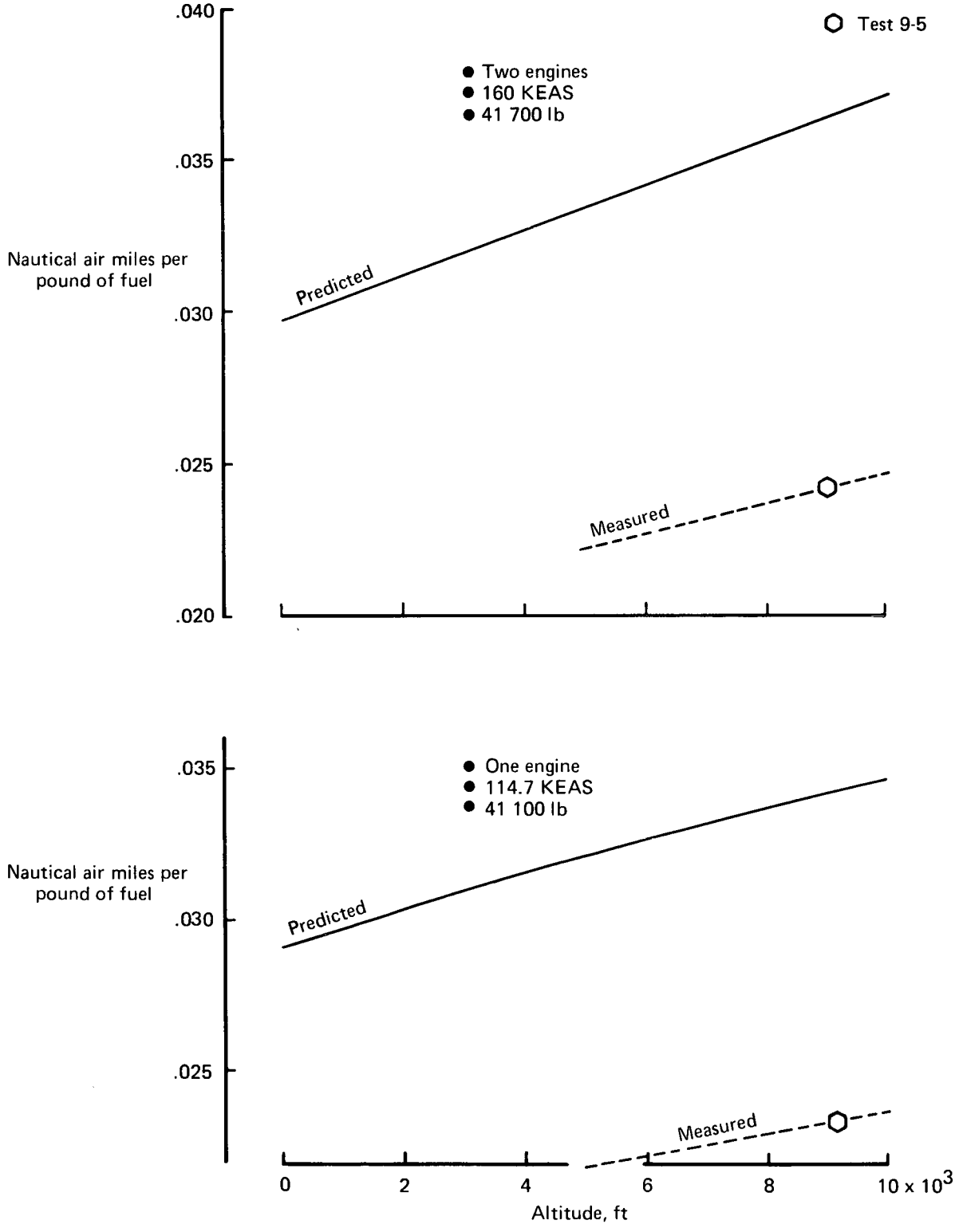

FIGURE 32.–SPECIFIC RANGE–FLAPS UP

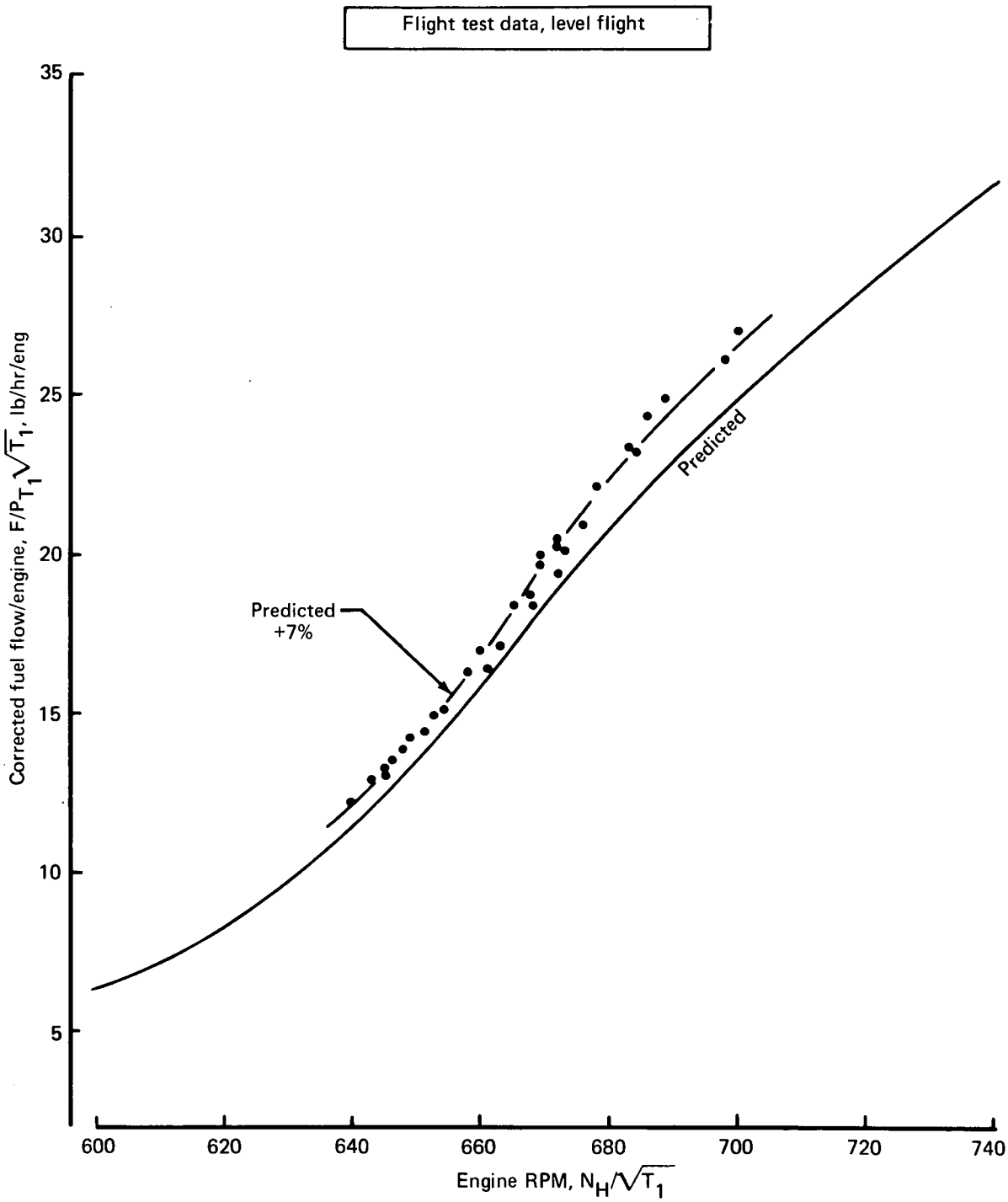

FIGURE 33.–CORRECTED ENGINE FUEL FLOW

The ferry range is given in figure 34. The maximum range is expected to be approximately 235 nmi at the fuel capacity limit of 13 500 lb and assuming 2000 lb for fuel reserves. A fuel density of 6.5 lb/gal was used in determining the gross weights.

APPROACH AND LANDING

Approach Performance

All of the landings made during the flight test program were conducted with conventional approaches: 3° glide slopes with the conical nozzles aft at 6°. Landing flap settings ranged from 25° to 54°. The test approach speeds followed the speed schedule with flap setting shown in figure 35, which was based on flight test minimum speeds and angle-of-attack data. Single-engine approaches at flaps 30° were conducted without difficulty.

A STOL approach and landing was not tested. However, a trim condition closely representing the design approach point was conducted at an altitude of 7670 ft. The design and test conditions are compared in table V.

The purpose in examining this flight test point in detail is to extrapolate from the altitude test data what characteristics can be expected for a sea level STOL approach at 60 kt. The significant parameters of power setting and angle of attack are compared at the 7670-ft test altitude in figure 36. The predicted data are estimated at the same rate of descent and ambient conditions as the test point. The flight test results are extrapolated to give a sea level approach case as shown using the altitude trends of the predicted data. At these conditions, the angle of attack would be 11.7° with 93.2% N_H power setting. The angle of attack could be reduced as much as 8° by rotating the conical nozzles to 85° or 90°. This would necessitate increasing the power 2% to 3% to maintain the rate of descent. Additional testing will be required to evaluate the Modified C-8A research vehicle in the STOL approach flight regime.

Landing Flare

Only eight landings were performed in the flight test program (two at $\delta_F \approx 50°$ and six at $\delta_F \approx 30°$). The liftoff in ground effect at flaps 65° during taxi tests also provided some useful data. The data permit only qualitative trends to be discerned about elevator-to-flare characteristics.

Figure 37 summarizes the available data on the landing flare characteristics. Several general points apply: only conventional landings at shallow glide slope were made, conical nozzles were always aft, average landing weight was just under 40 000 lb, average power setting was about 90%

- OEW = 32 600 lb
- Reserves = 2000 lb
- Unusable fuel = 740 lb at $\theta = 5°$
- Fuel capacity = 13 500 lb (fuel wt = 6.5 lb/gal)
- Sea level, standard day
- Zero winds
- Cruise: 160 KEAS at 10 000-ft altitude

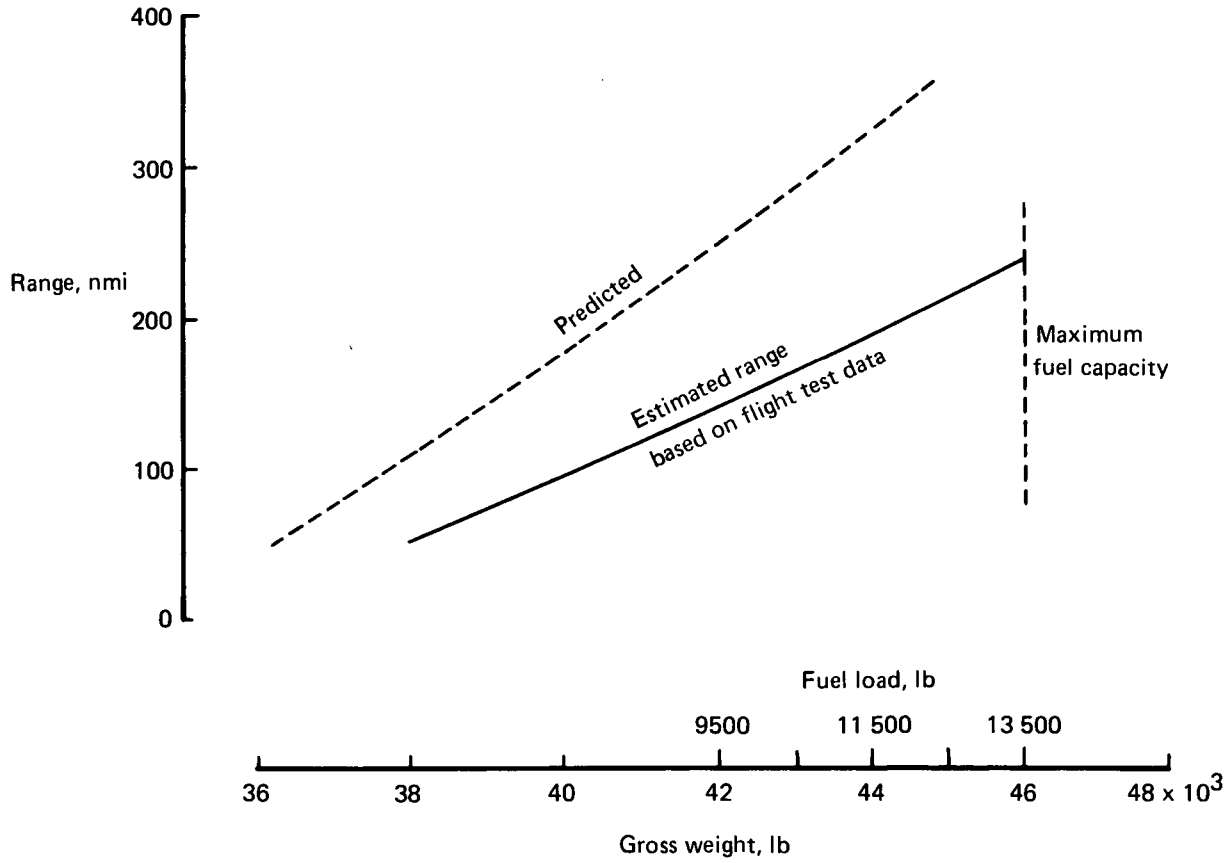

FIGURE 34.—FERRY MISSION

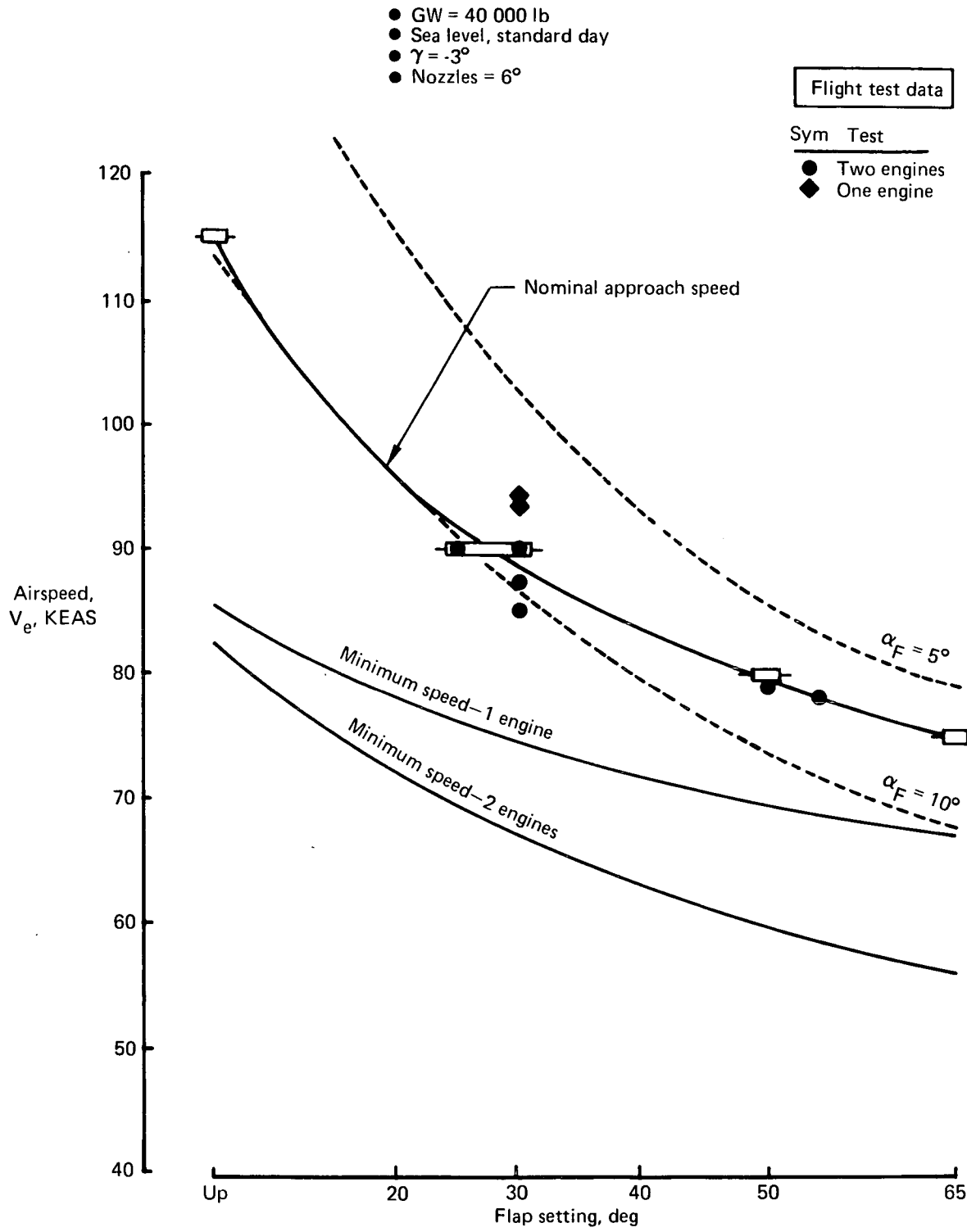

FIGURE 35.–APPROACH PERFORMANCE WITHOUT NOZZLE DEFLECTION–BASED ON FLIGHT TEST DATA

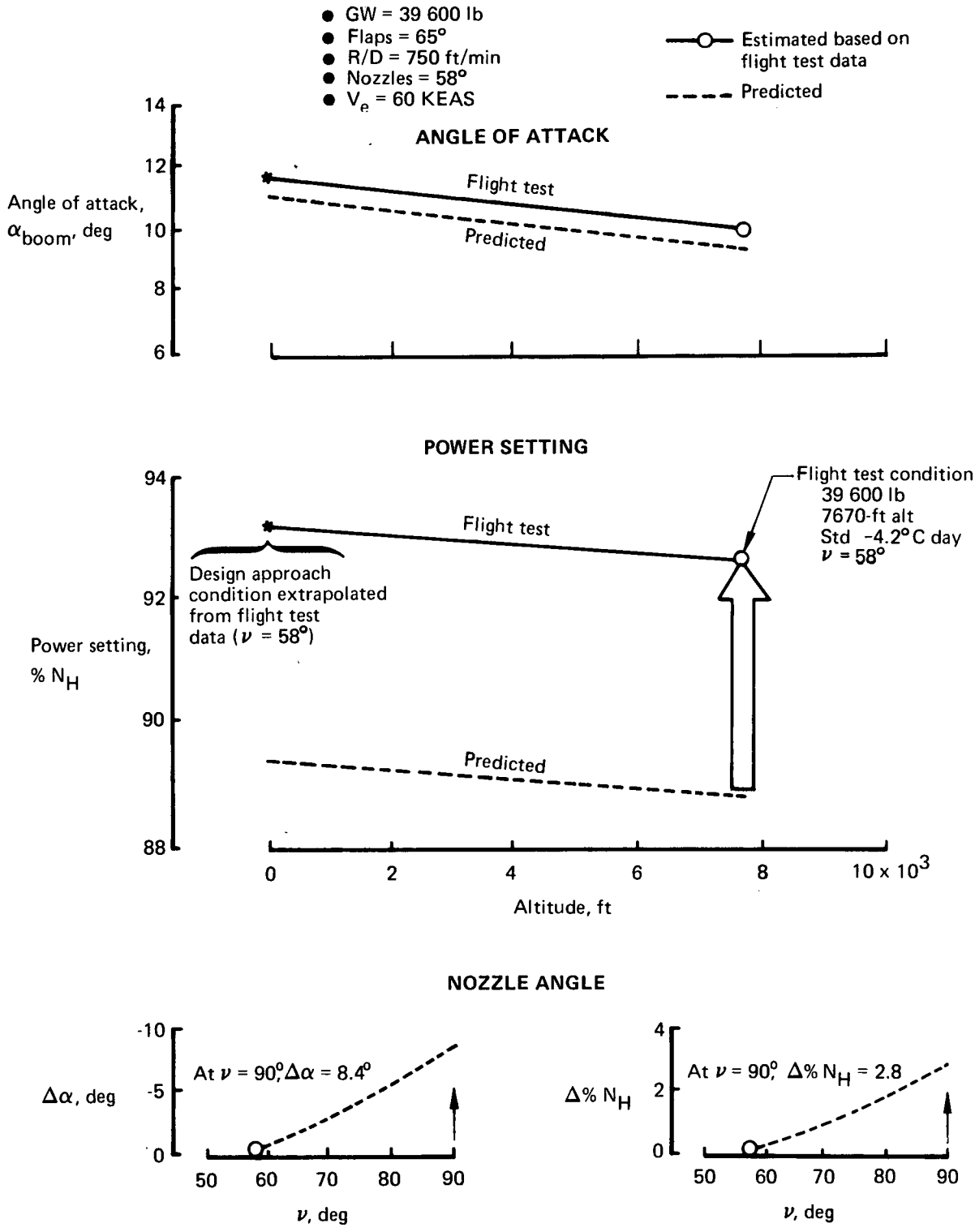

FIGURE 36.—STOL APPROACH COMPARISON

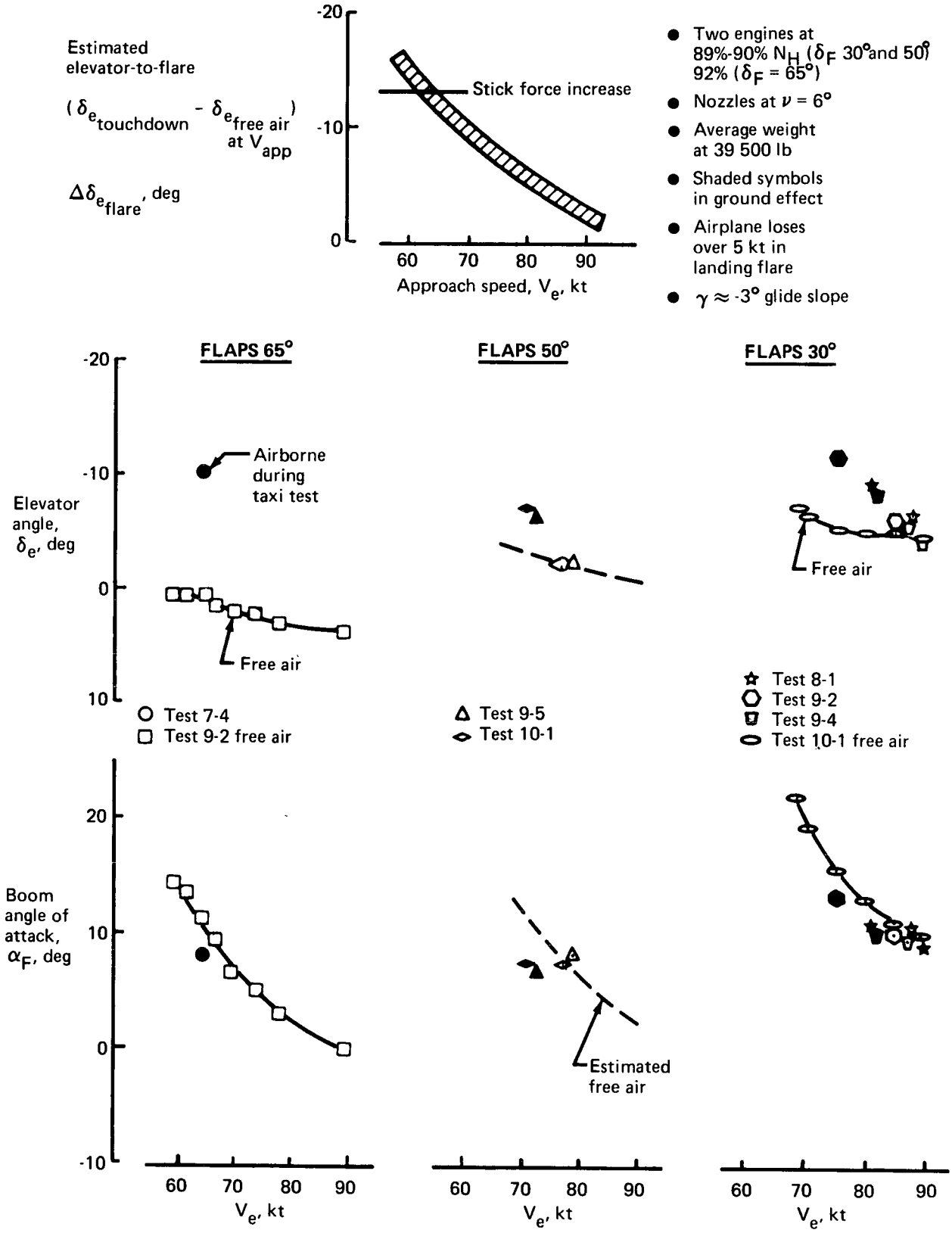

FIGURE 37.—ELEVATOR-TO-FLARE, NOZZLES AFT LANDING

TABLE V.–STOL APPROACH CONDITIONS

	Design point	Test condition
Gross weight, lb	40,000	39,600
Velocity, KEAS	60	60
Rate of descent, ft/min	800	750
Flaps, deg	65	65
Nozzles, deg	90	58
Altitude, ft	0	7,670
Temperature, std +°C	0	-4.2

N_H, and airspeed decreased about 5 kt in the flare. The elevator angle used at touchdown was more trailing edge up than corresponding trim data taken in free air. The pilot used $\Delta\delta_e \approx -5°$ to flare from approach speeds between 75 and 90 kt. The elevator required in ground effect at flaps 65°, 65 kt, was over $\Delta\delta_e \approx -10°$ above free air trim data. Angle of attack was always lower in ground effect than corresponding free air trim data. The pilot attempted a flaps 65° approach in test 10-1, but raised the flaps to 53° to improve handling characteristics. At 75 kt the pilot noted a slight nose-down pitching tendency near the runway. All data indicate that ground effect is perceptible.

Estimated elevator-to-flare is presented in figure 37 versus approach speed for nozzles aft and conventional approaches (3° glide slope). The tab stall limitation on the elevator control system is estimated to interfere with flare for approach speeds below 65 kt. Nozzles-down, steep-approach flare characteristics are unknown.

Landing Distance

The flare times and ground roll decelerations are presented in figure 38. The time to flare from 35 ft to touchdown was longer than would normally occur. Testing techniques artificially extended the flare so that ground effect could be evaluated.

Ground roll decelerations of 0.25 to 0.3 g were obtained during the flight test program. The lift dump was not used for any of the landings, and the aircraft does not have an antiskid braking system.

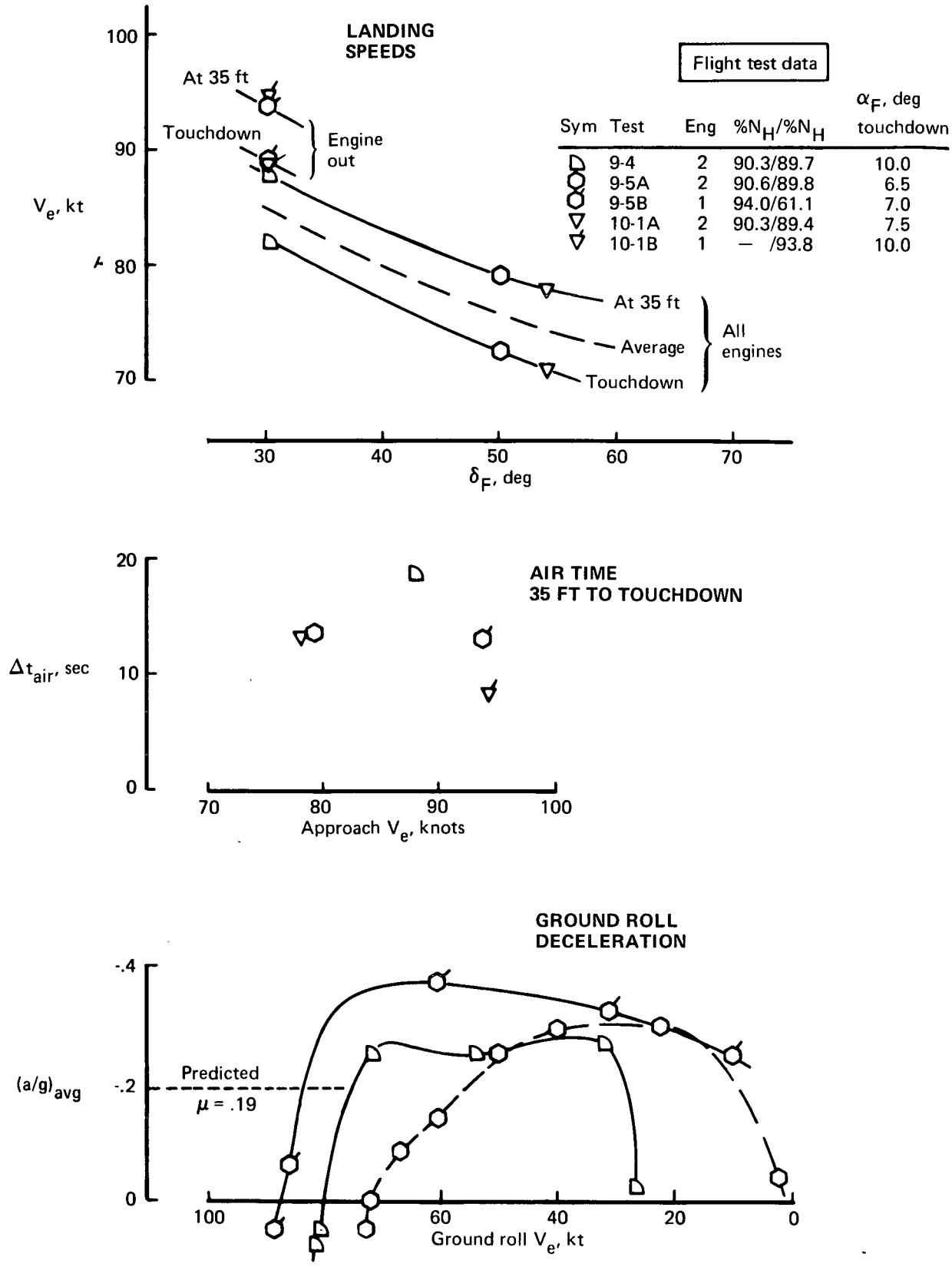

FIGURE 38.–LANDING PERFORMANCE DATA

Landing distances are shown in figure 39 for a conventional approach. Although the brake effectiveness was better, the demonstrated distances reflect larger flare times than predicted due to the test technique. A summary of all the landings made during the flight test program is given in table VI.

MINIMUM TEST SPEEDS

Several approaches to stall were made to obtain structural data at high angles of attack and to assess operating margins for later flight tests. Stalls were not scheduled and did not occur at any time during the test program. All approach-to-stall conditions were stopped when a predetermined angle of attack was reached.

A graphical summary of the two-engine conditions is presented in figure 40, where the minimum speeds demonstrated are compared to the predicted 1 g stall speeds. Single-engine minimum speeds are given in figure 41. Speeds were demonstrated for the flaps up setting which were equal to or slightly lower than the predicted stall speeds. At the 30° and 65° flap settings, the aircraft was operated within 5 to 7 kt of the predicted stall speeds. Position error corrections have not been applied to the airspeed or angle-of-attack data.

The velocity profiles of the stall approaches are compared with those predicted in figures 42 through 48 for the two-engine conditions and in figures 49 through 55 for single-engine operation. The predicted performance data were estimated for the same power setting as required for the flight condition. The flight test rate of climb indicated by the shaded area is only approximate since static trim checks were not made during the tests. Several of the conditions did have an initial trim point and are noted on the figures. The longitudinal stability and trim characteristics are indicated by the stick force and elevator angle.

The approaches to stall for flaps up and 30° with both engines operating were not continued up to the predicted maximum angle of attack. The remaining 3° before the predicted maximum is reached indicates that the stall speed could be several knots lower than the minimum speed demonstrated. Flaps 65° conditions were continued past the predicted maximum angle of attack, and a corresponding smaller margin would be expected between the minimum speed attained and actual stall. Angles of attack exceeding 20° were reached during the two-engine conditions. At and below the maximum alphas tested, no significant increase in buffet level was noted to indicate pending stall. All angles of attack quoted were as measured on the nose boom and are not corrected for any position error which may be present.

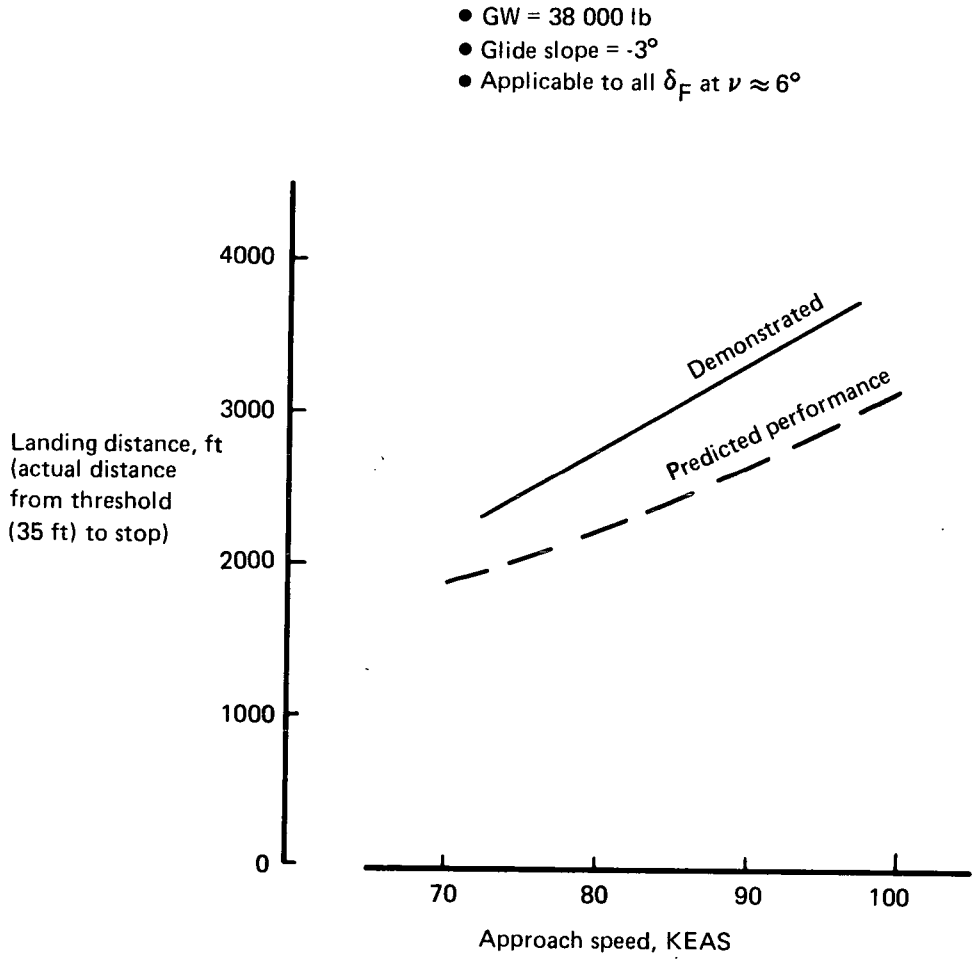

FIGURE 39.—LANDING FIELD LENGTH

TABLE VI.–FLIGHT TEST DATA–APPROACH AND LANDING CONDITIONS

Test Condition	8-1	9-2 1.00.003.009	9-3 4.08.001.010	9-4 1.00.003.009	9-5A 1.00.003.009	9-5B 1.00.002.002.1	10-1A 1.08.001.045	10-1B 1.00.003.009
Flap pos, $\delta_{F_{nom}}$, deg	25	30	30	30	50	30	54	30
Nozzle pos, ν, deg		8	8	11	11	11	10	12.5
Power setting, % N_H								
Engine 1	88	88		90.3	90.6	94.0	90.3	—
Engine 2	88	88		89.7	89.8	61.1	89.4	93.8
Gross weight, lb	39,100	37,200		40,000	37,900	39,100	38,900	42,600
Temperature, OAT °C, at approach		14.5		19.8	13.8	13.1	12.0	12.6
Approach, IRIG, hr-min-sec	11-11-10	13-08-10	16-06-34	16-13-0	15-25 00	17-21-00	14-39-10	16-16-30
Altitude, ft	330	1360			700	770	620	500
V_e, kt	90	85	~ 90	87.5	79	93.5	78	94.2
R/C, ft/min				-380.0	-380	-520	-520	-420
γ, deg				-2.45	2.7	-3.14	-3.76	-2.52
α_{boom}, deg	9	10.0		9.5	8.0	7.5	7.5	7.5
θ, deg	6.6	6.3		7.5		5.0	4.0	4.0
δ_e, deg	-4	-5.9		-5.5	-2.0	-3.5	-2.0	-4.0
35 ft, IRIG, hr-min-sec	11-11-29	13-10-45		16-13-10.5	15-25-10	17-21-23	14-39-30	16-16-37.5
Altitude, ft	242	595		335	682	675	480	450
V_e, kt	88	85			75	94.5	75.5	94.5
α_{boom}, deg	10.5	9.0		10.0		6.0		10.0
θ, deg	7.5	7.0		7.5		5.0		5.5
δ_e, deg	-6.5	-6.0		-5.0	-2.0		-3.5	-4.0

TABLE VI.—Concluded

Test Condition	8-1	9-2 1.00.003.009	9-3 4.08.001.010	9-4 1.00.003.009	9-5A 1.00.003.009	9-5B 1.00.002.002.1	10-1A 1.08.001.045	10-1B 1.00.003.009
Touchdown, IRIG, hr-min-sec	11-11-39	13-10-56		16-13-29	15-25-23.4	17-21-36	14-39-43.3	16-16-45.7
Altitude, ft	207	560		300	647	640	445	415
V_e, kt	81	75		82	72.5	89.0	71	88.7
α_{boom}, deg	11.0	13.0		10.0	6.5	7.0	7.5	10.0
θ, deg	9.5	10.0		8.5		6.0	6.5	7.0
δ_e, deg	-9.0	-11.5		-8.5	-6.0	-5.0	-7.0	-6.5
Ground run, a/g				-0.27	-0.10 to -0.30	-0.30 avg	-0.10 avg	-0.105 avg

Flight test data

Sym	Flap, deg	Test	ν, deg	$\%N_H/\%N_H$	Demonstrated α_{max}, deg	Predicted α_{max}, deg
○	Up	9-4	9	85.4/85.1	20	23.2
⊗	Up	10-1	8	60.6/61.4	22	21.5
□	30	10-1	8	80.0/80.4	22	24.8
⊠	30	10-1	8	89.7/89.9	22	24.6
△	65	9-5	9	89.8/88.6	23.5	22.8
▲	65	9-5	90	89.7/88.6	24	22.4
▼	65	10-1	58	92.8/92.4	21	19.8

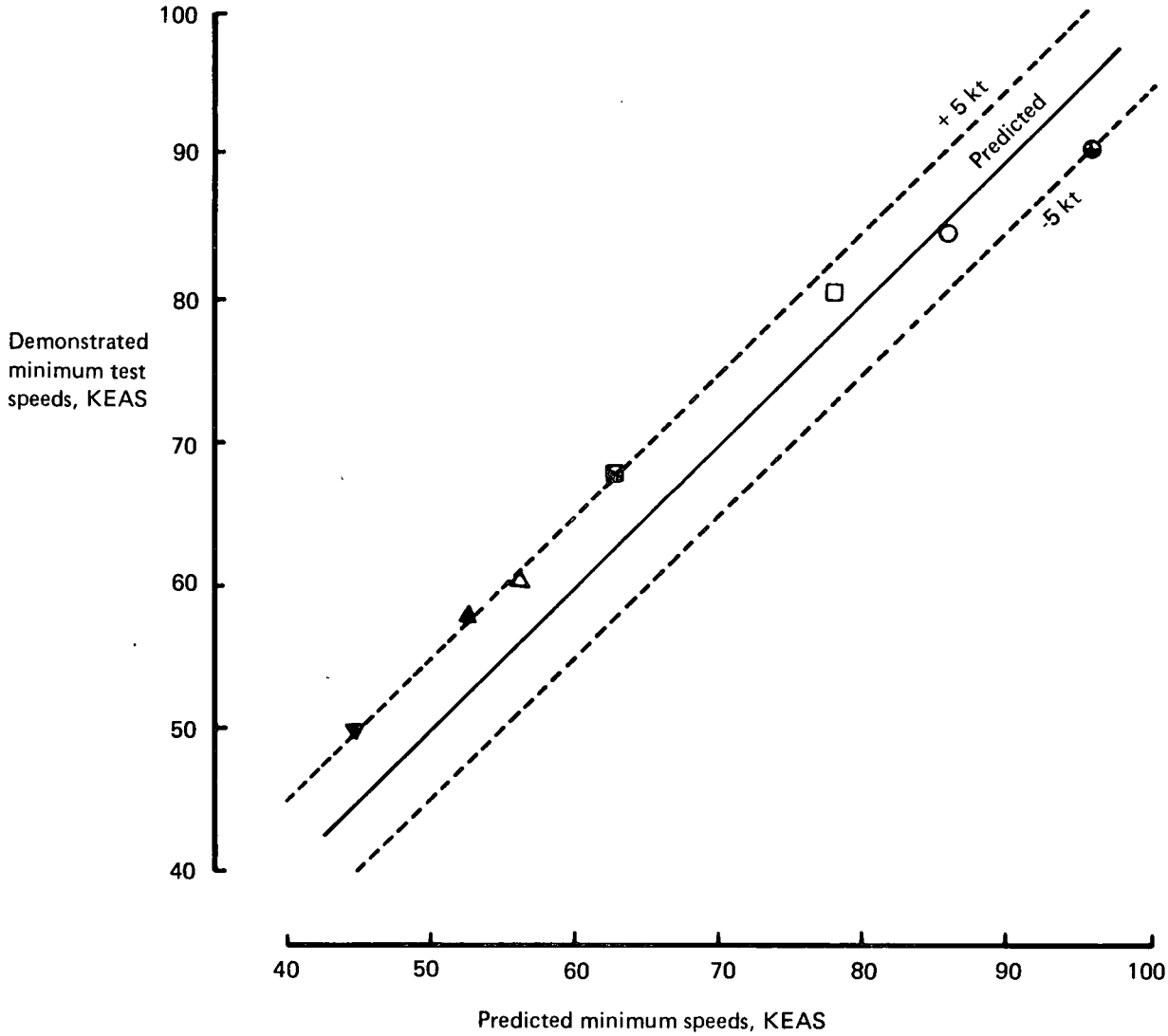

FIGURE 40.–MINIMUM SPEED CORRELATION–TWO ENGINES

Flight test data

Sym	Flap, deg	Test	ν, deg	$\%N_H/\%N_H$	α_{max}, deg
○	Up	9-5	7	60.9/99.9	19
□	30	9-5	9	60.6/101.7	19.2
⊠	30	9-5	8	60.7/96.5	19.8
▲	65	10-1	57	60.4/94.3	19
▶	65	10-1	57	60.6/92.6	21
▼	65	10-1	57	60.5/101.4	22
◀	65	10-1	56	60.6/101.4	20

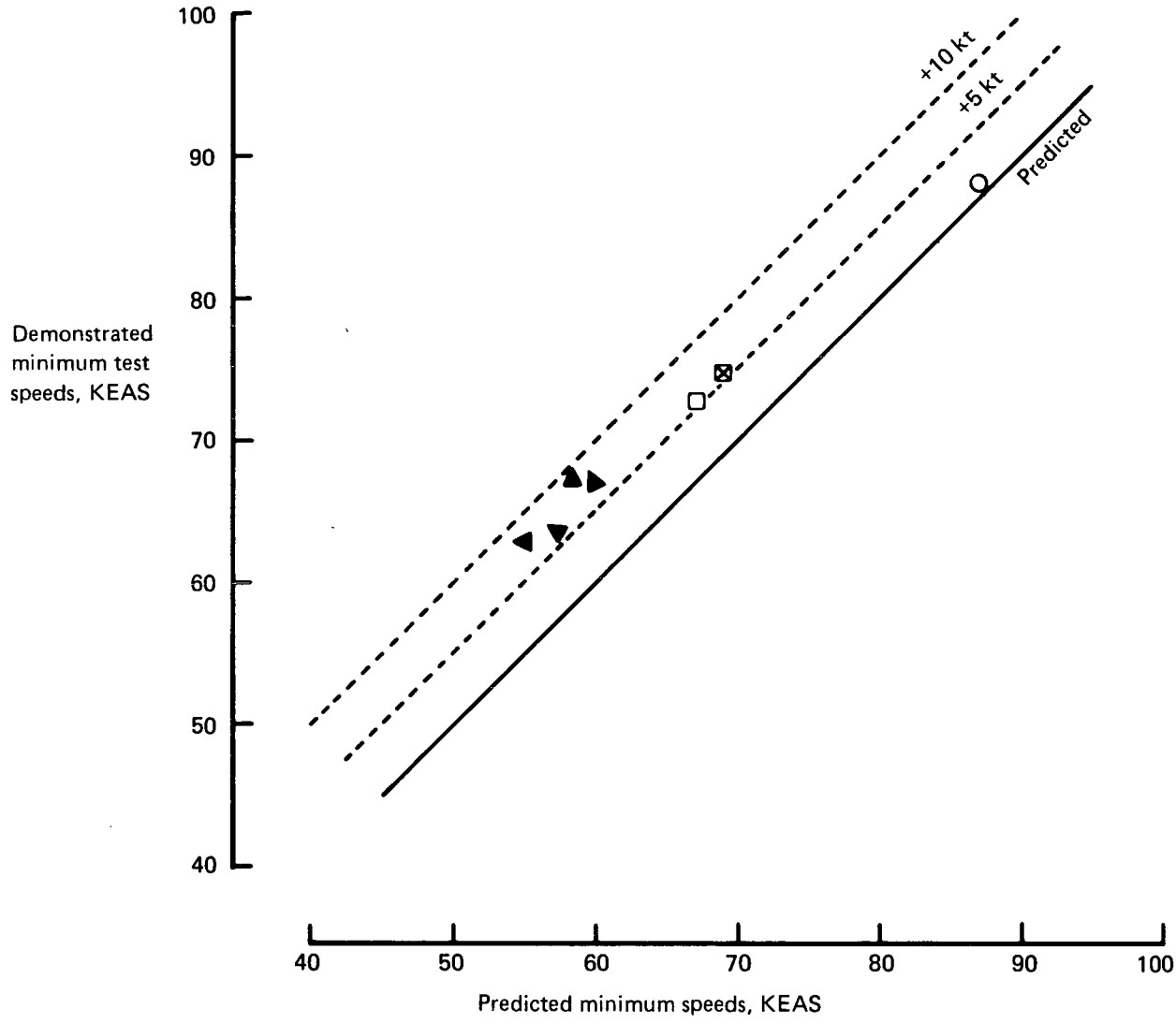

FIGURE 41.–MINIMUM SPEED CORRELATION–ONE ENGINE

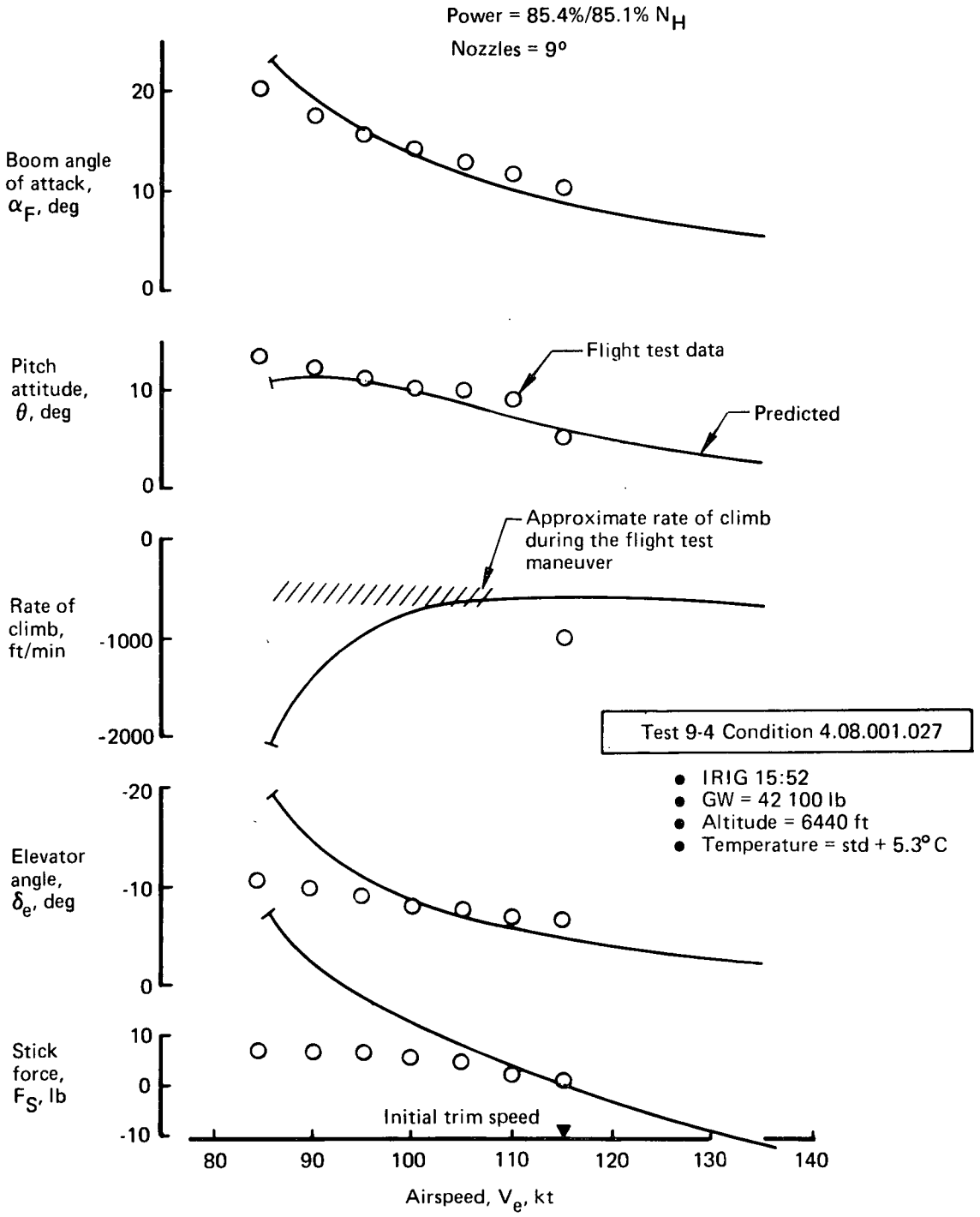

FIGURE 42.–APPROACH TO STALL–FLAPS UP, TWO ENGINES

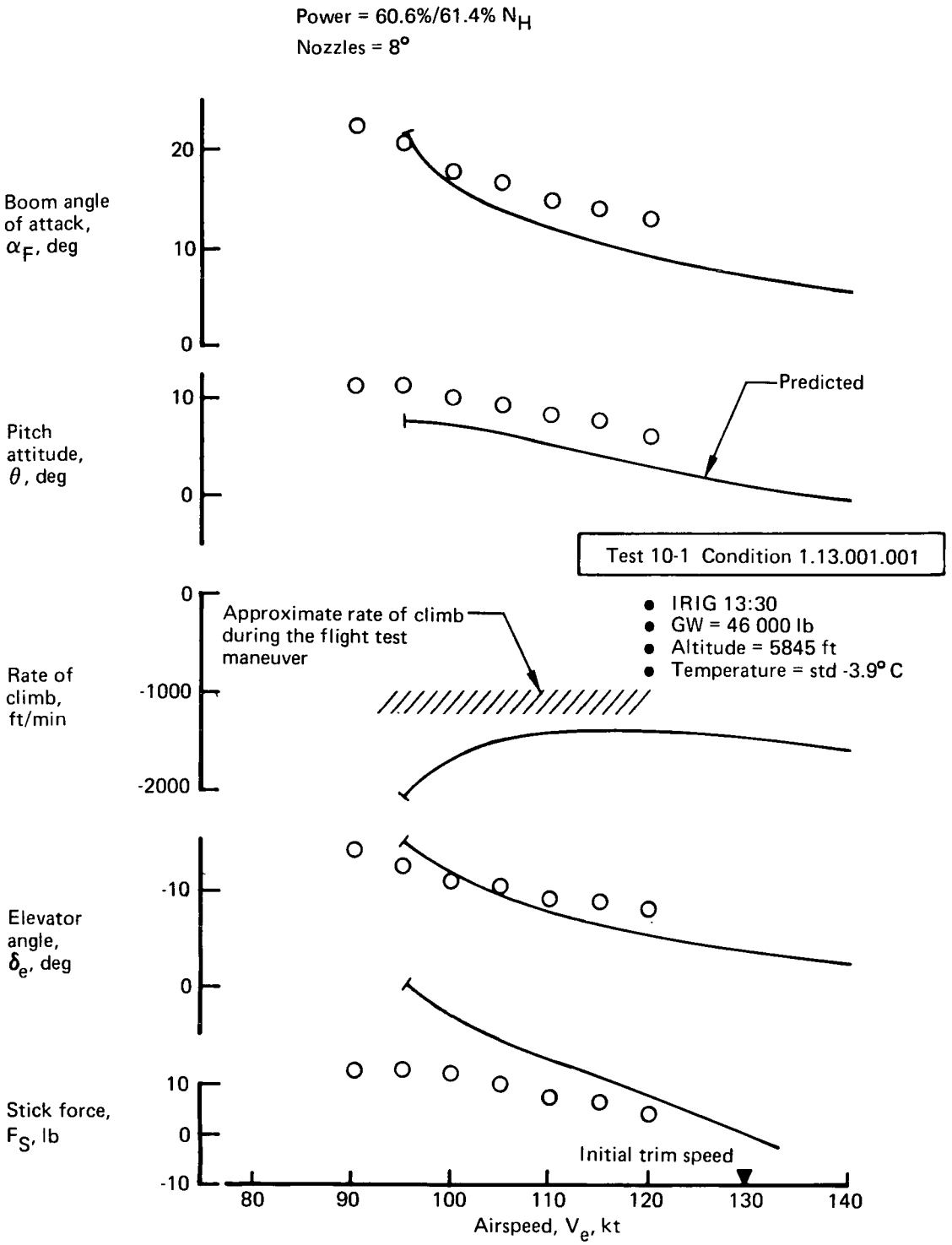

FIGURE 43.–APPROACH TO STALL–FLAPS UP, TWO ENGINES

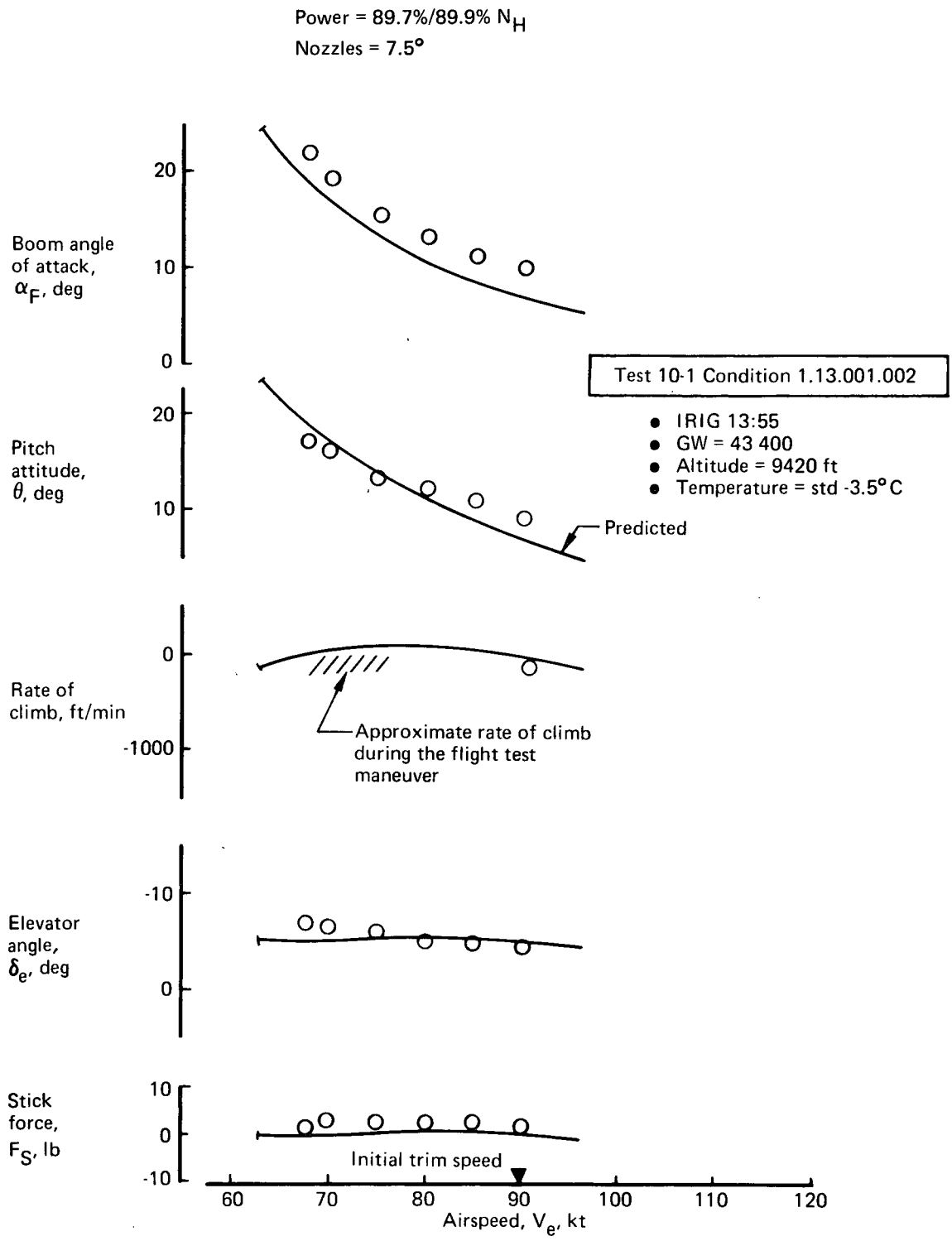

FIGURE 44.—APPROACH TO STALL—FLAPS 30°, TWO ENGINES

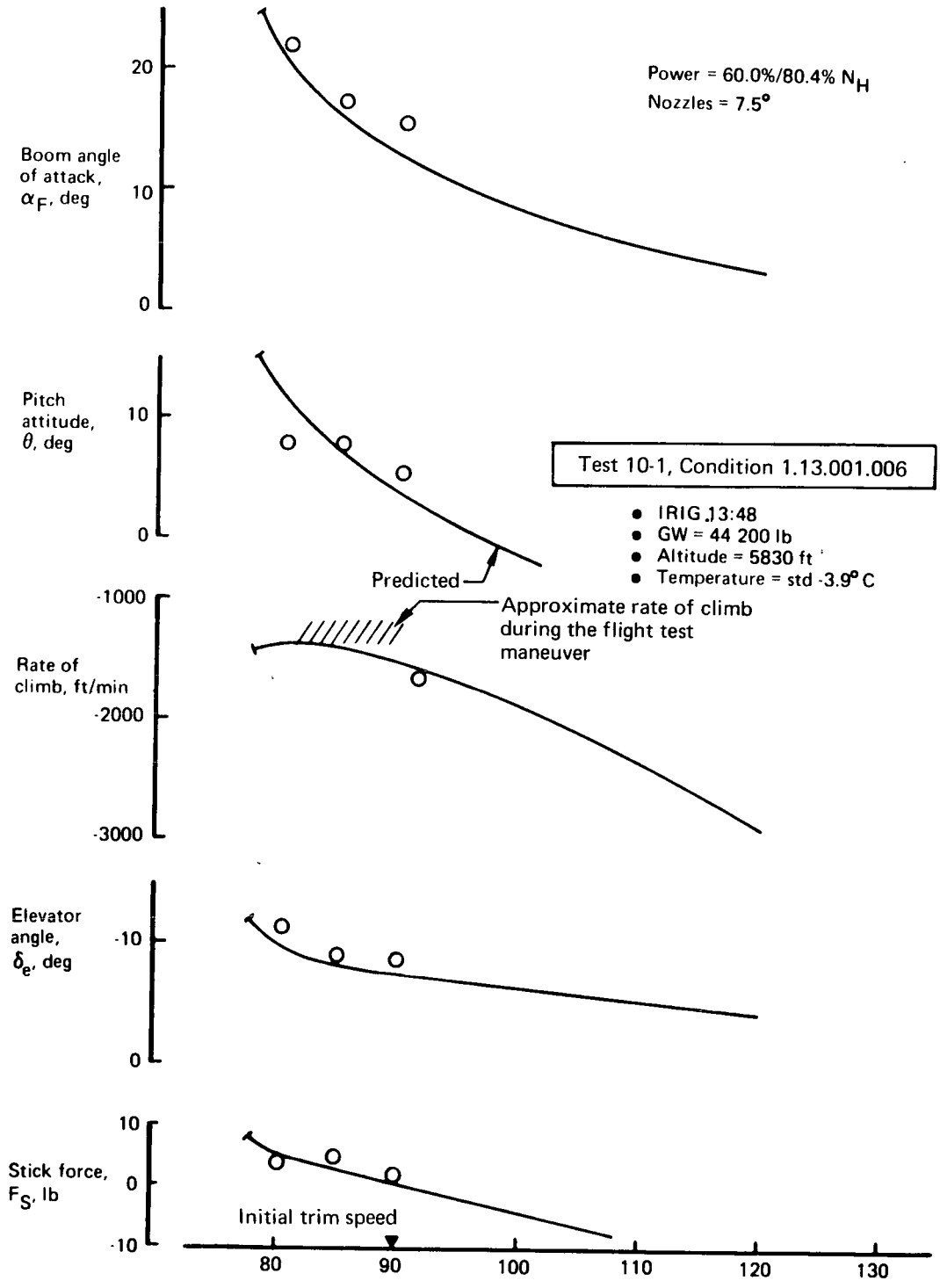

FIGURE 45.–APPROACH TO STALL–FLAPS 30°, TWO ENGINES

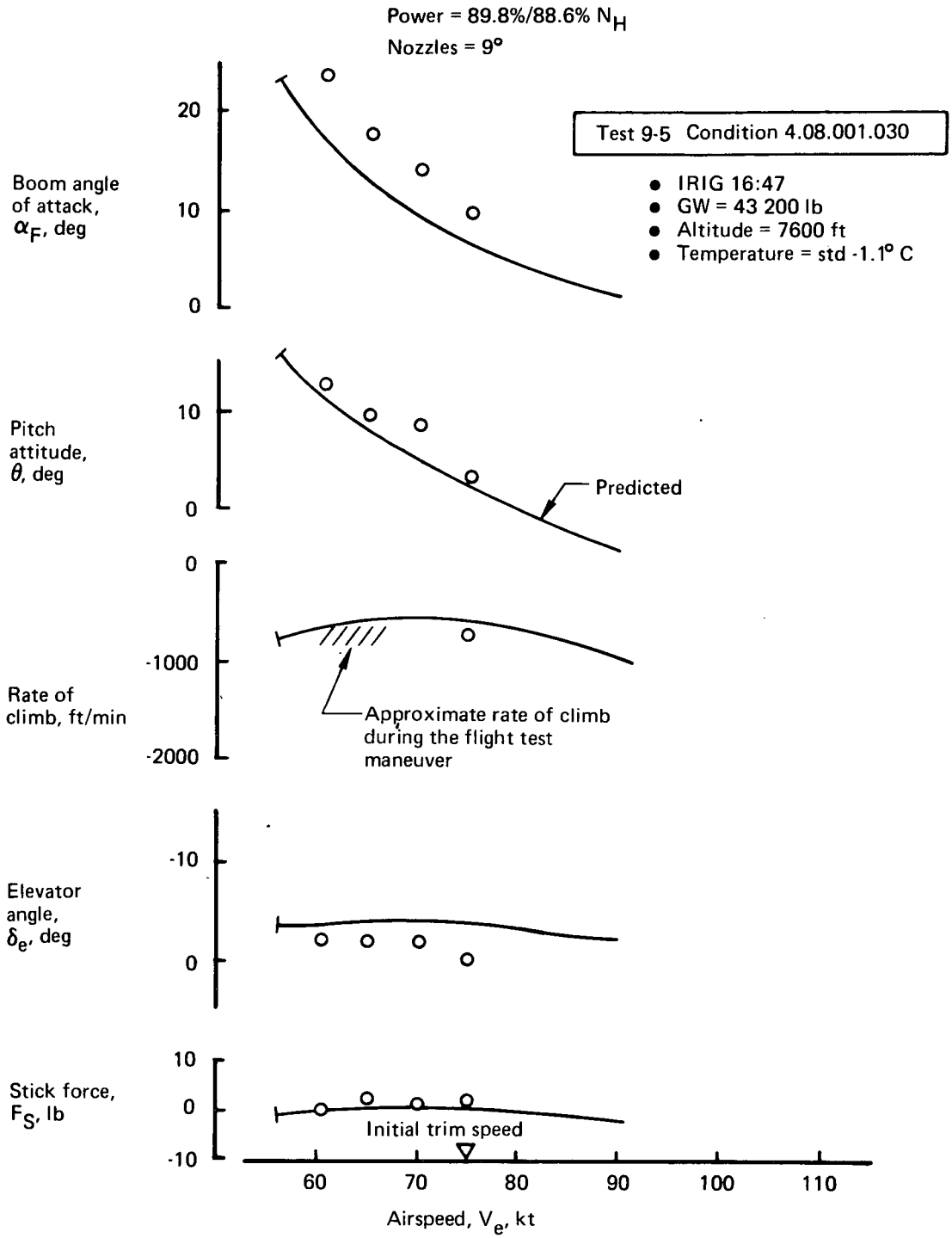

FIGURE 46.—APPROACH TO STALL—FLAPS 65°, TWO ENGINES

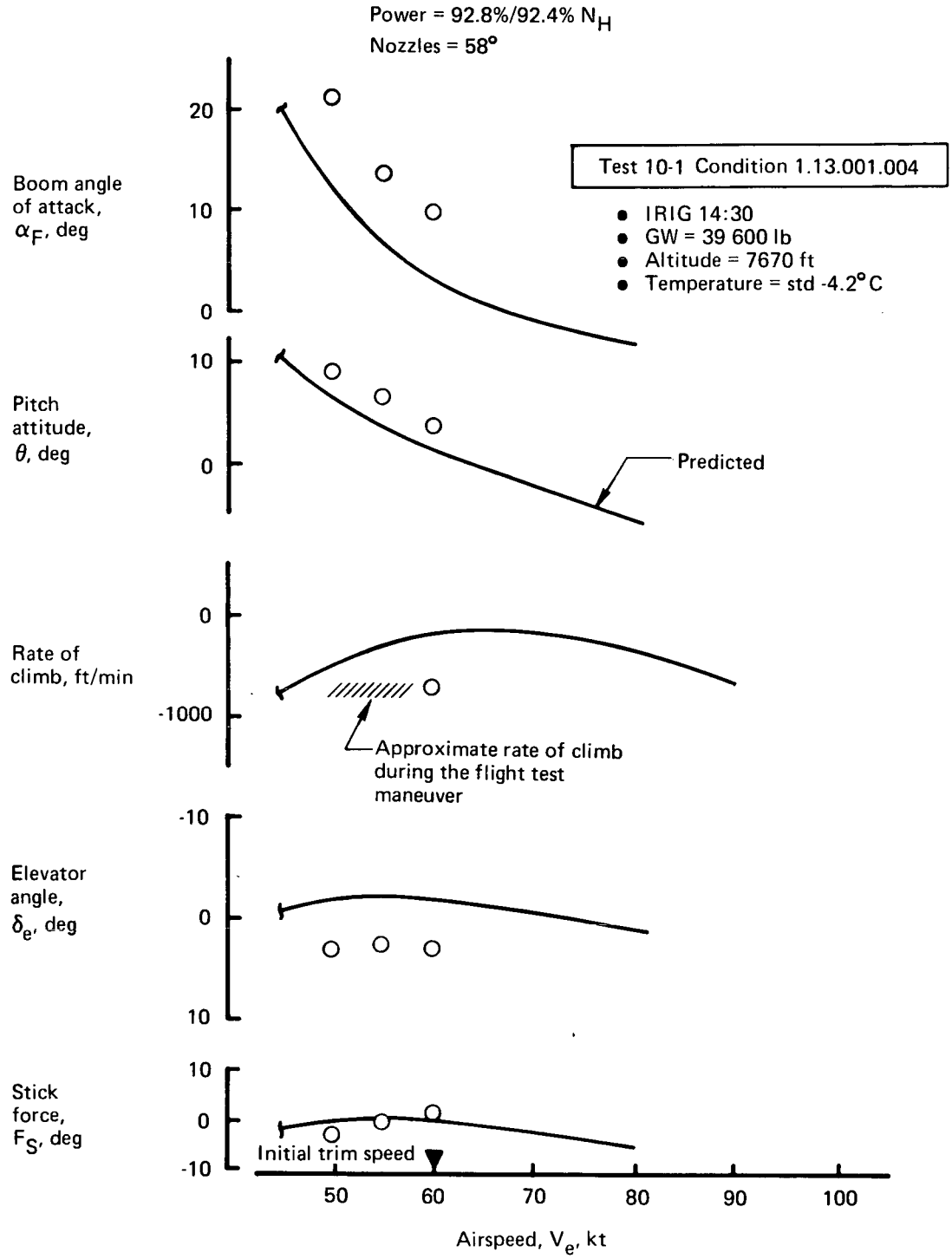

FIGURE 47.–APPROACH TO STALL–FLAPS 65°, TWO ENGINES

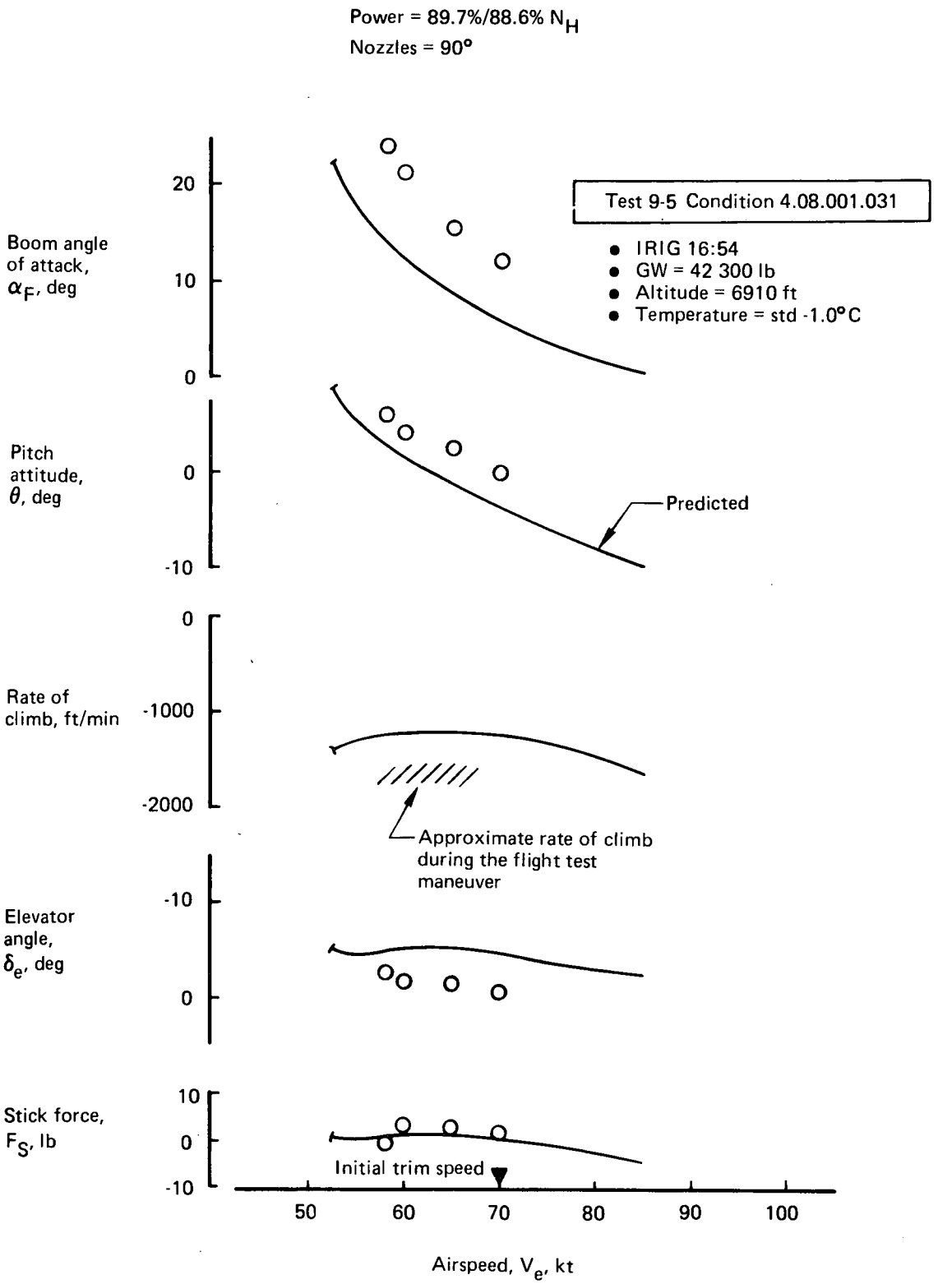

FIGURE 48.—APPROACH TO STALL—FLAPS 65°, TWO ENGINES

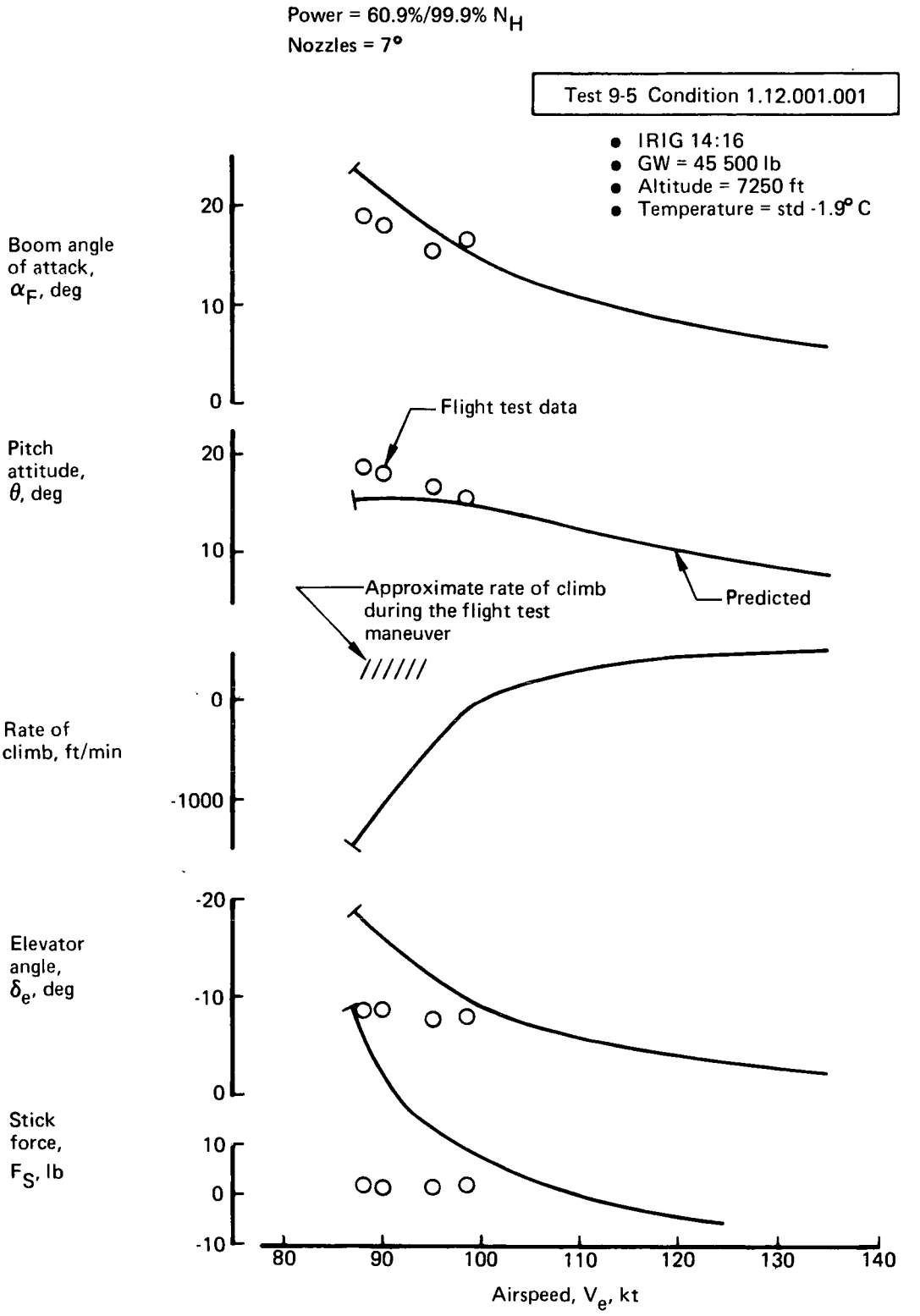

FIGURE 49.—APPROACH TO STALL—FLAPS UP, ONE ENGINE

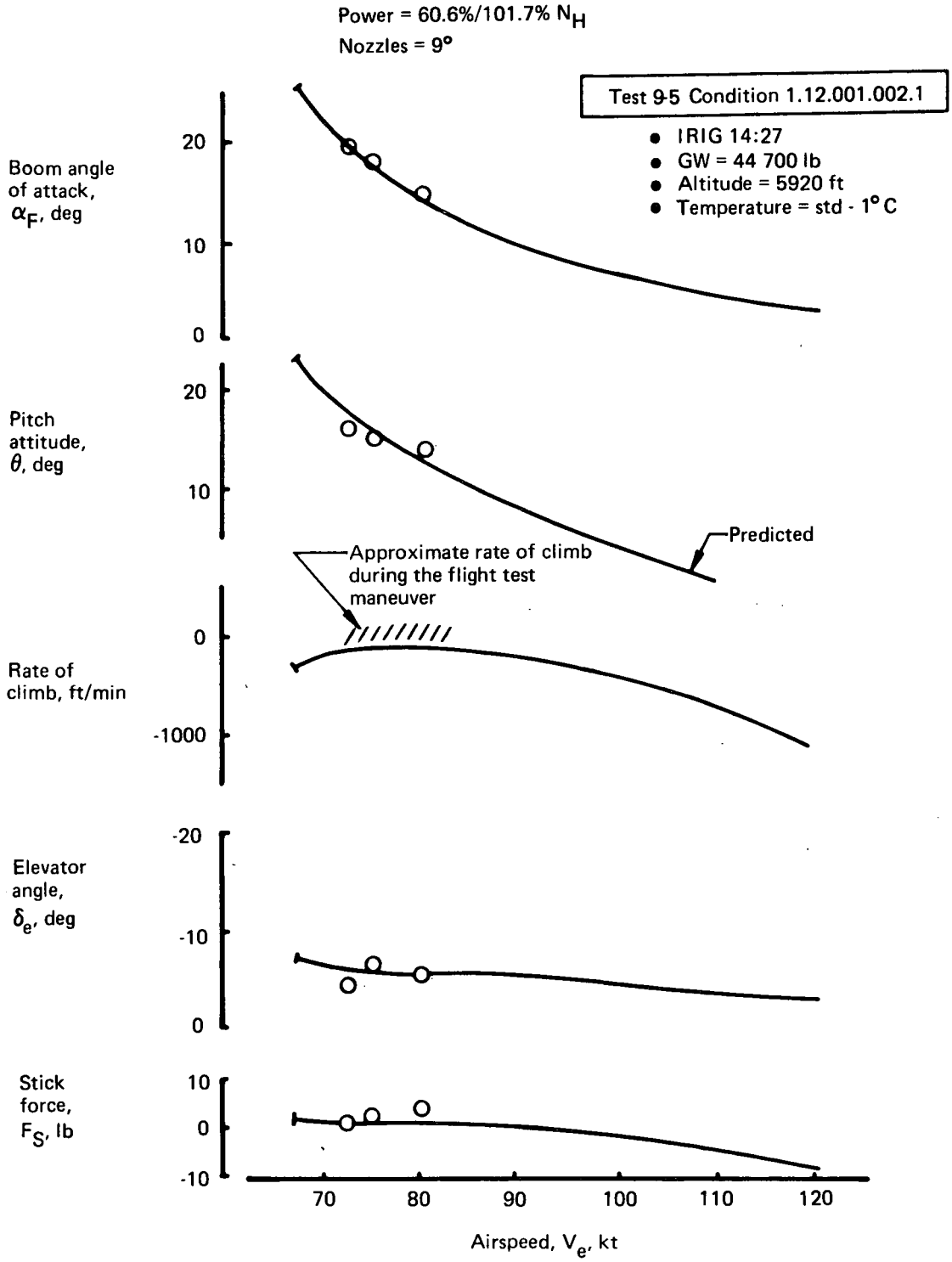

FIGURE 50.–APPROACH TO STALL–FLAPS 30°, ONE ENGINE

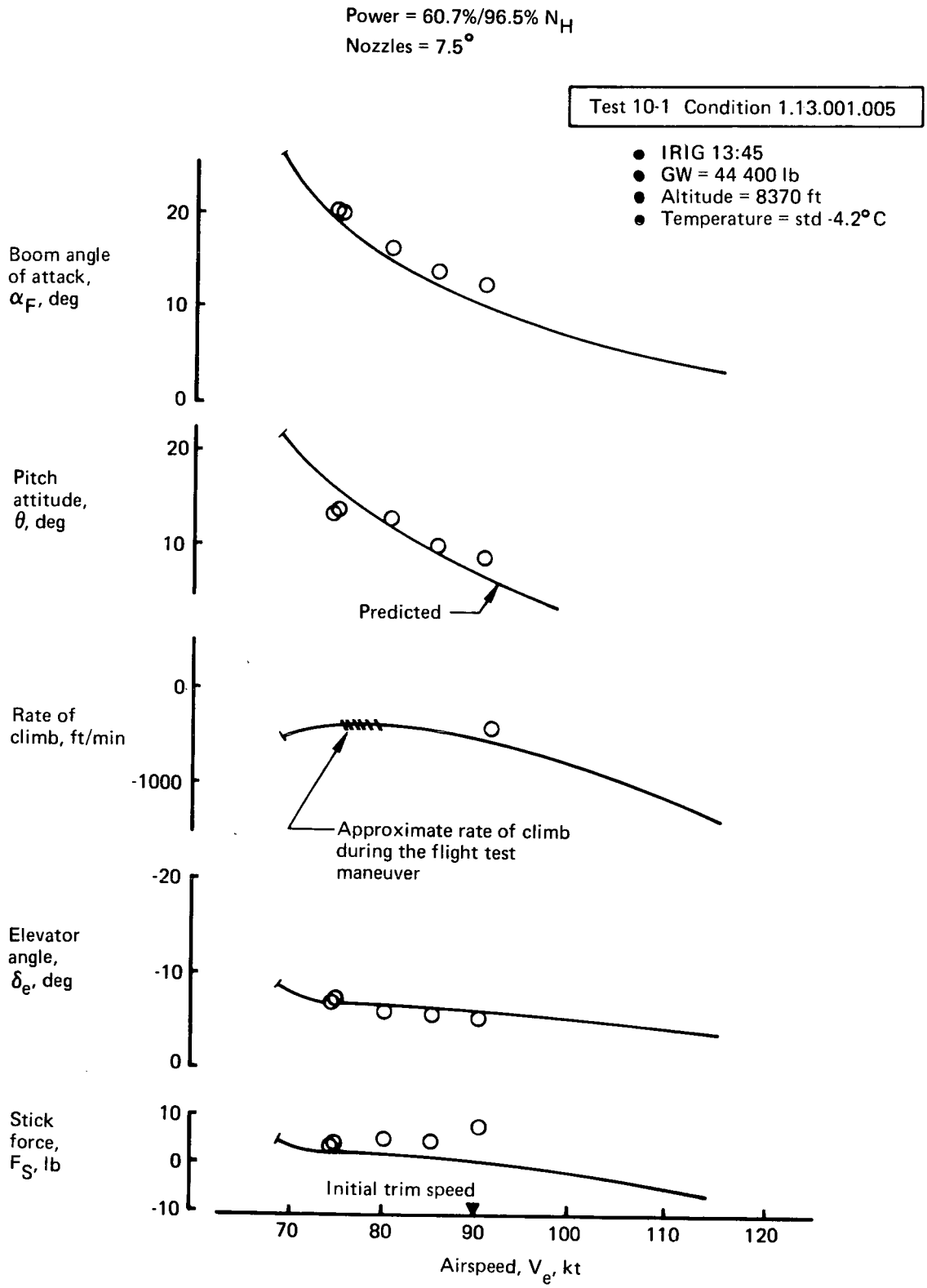

FIGURE 51.–APPROACH TO STALL–FLAPS 30°, ONE ENGINE

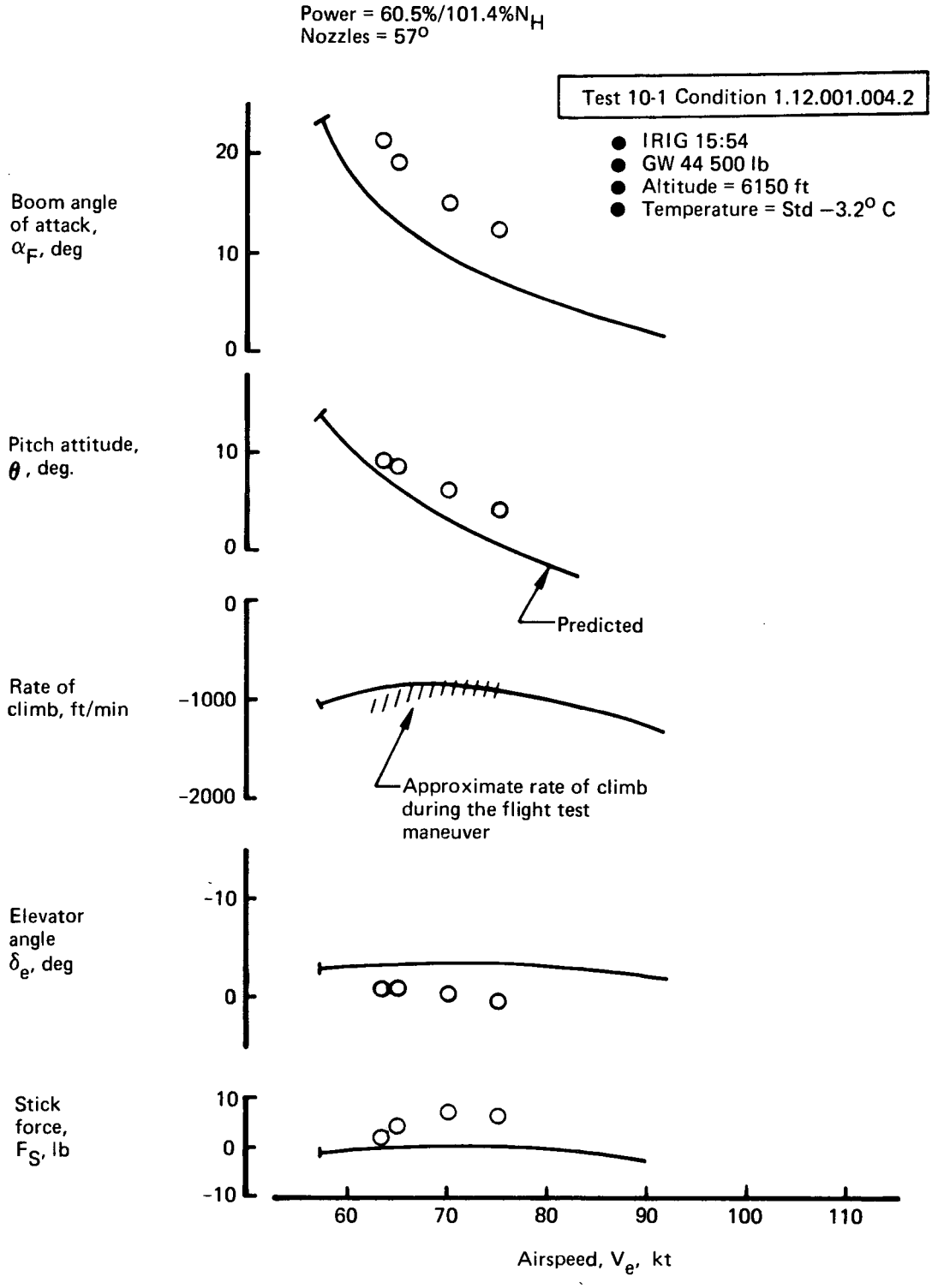

FIGURE 52.—APPROACH TO STALL—FLAPS 65°, ONE ENGINE

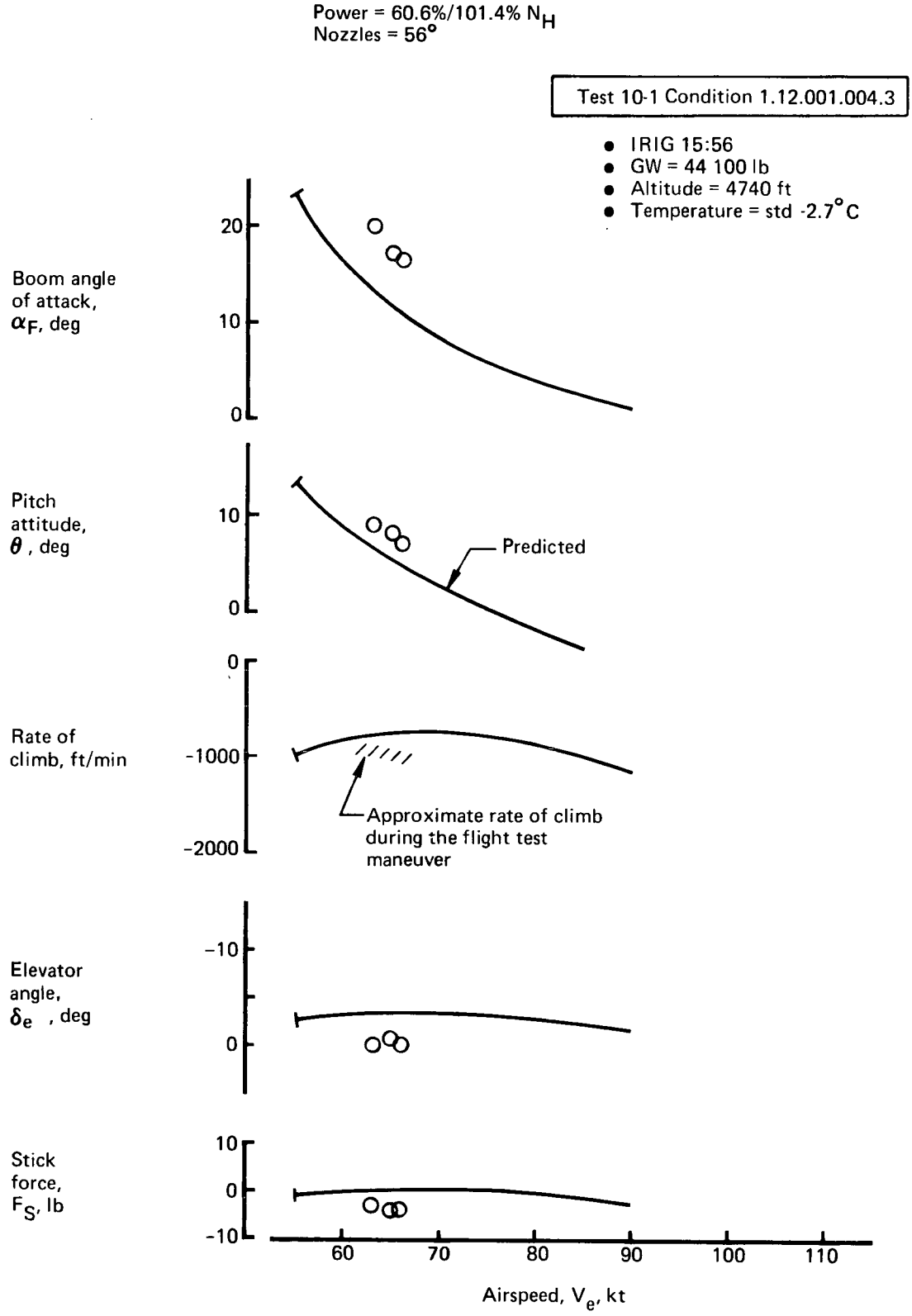

FIGURE 53.–APPROACH TO STALL–FLAPS 65°, ONE ENGINE

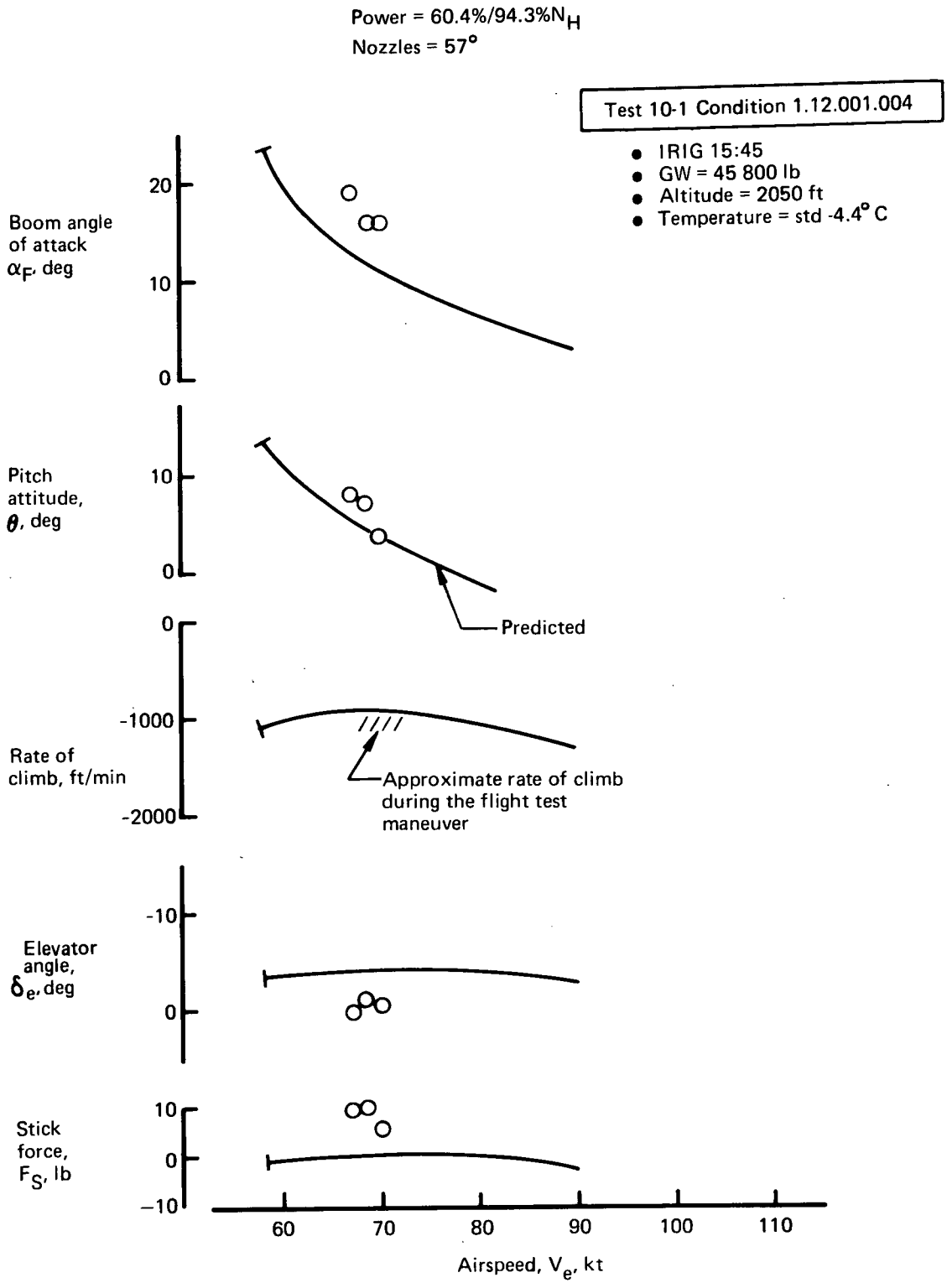

FIGURE 54.—APPROACH TO STALL—FLAPS 65°, ONE ENGINE

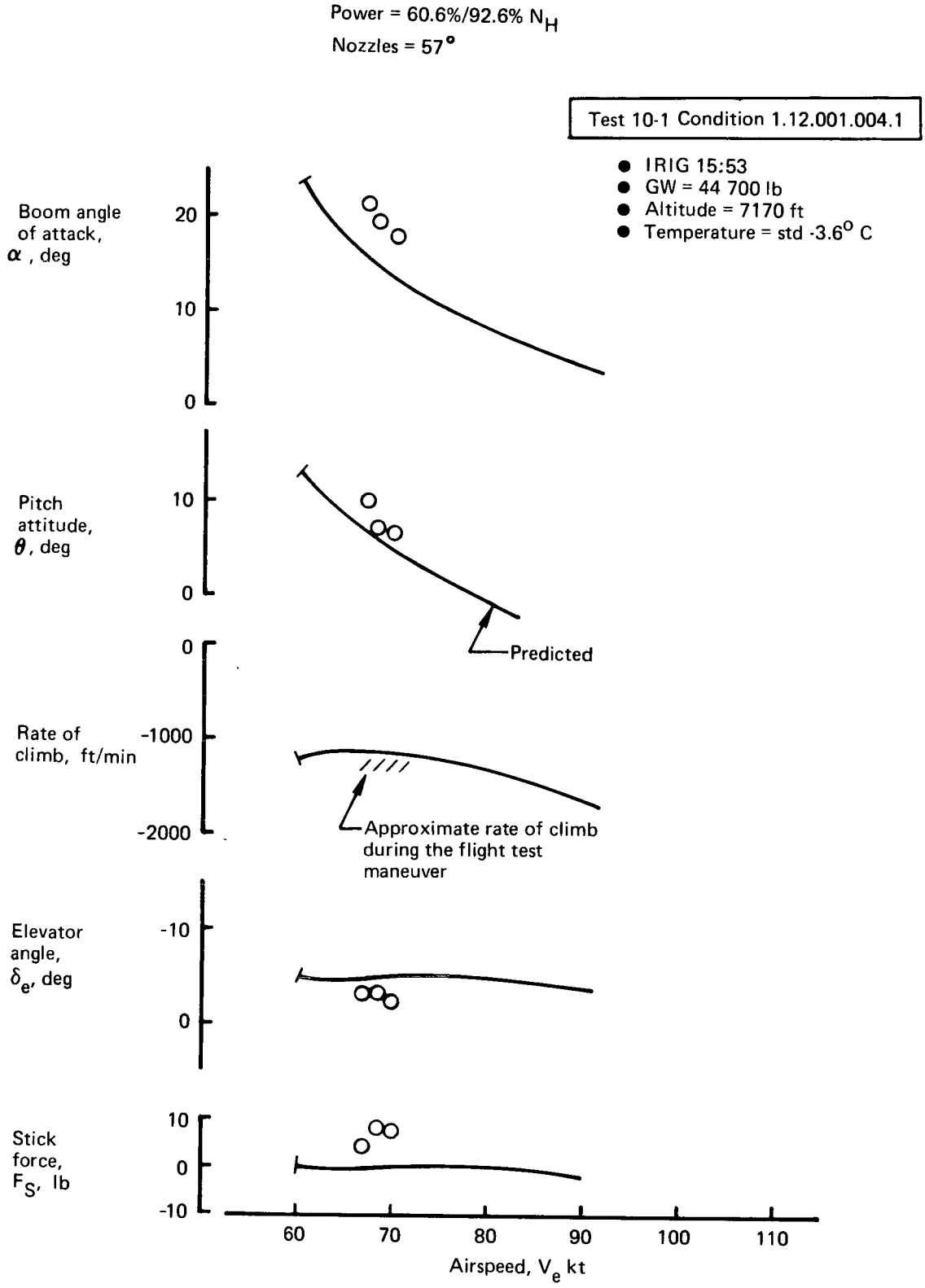

FIGURE 55.–APPROACH TO STALL–FLAPS 65°, ONE ENGINE

The majority of the single-engine cases were conducted for V_{MCA} evaluations. For all of the conditions tested, an alpha limit was reached before any apparent V_{MCA} limitation, and the tests were terminated at 4° to 5° less than the predicted stall angle of attack. This alpha margin may be an indication of the speed margin that exists before stall occurs.

The time histories for some of the approaches to stall are presented in figures 56 through 59 for the two-engine conditions and figures 60 through 62 for the single-engine conditions. The recoveries for the minimum speeds are also shown and indicate no problems for the cases tested.

A summary of the minimum speeds is given in figures 63 through 64 for operation with two and one engines, respectively. The actual test points were normalized to sea level, standard day, at a gross weight of 40 000 lb. The demonstrated speeds are compared to the predicted 1 g stall speeds as a function of power setting. A tabular summary of the flight test data is given in tables VII and VIII. The actual test conditions are listed in addition to the uncorrected airspeeds and attitudes that were attained.

LONGITUDINAL STABILITY AND CONTROL

Static Stability and Control

Modified C-8A flight testing was conducted with the center of gravity at locations approximately 1% MAC aft of the "nominal" fuel loading line used for design as presented in figure 65. For test weights between 37 200 and 46 600 lb the CG varied between 29% and 31% MAC.

Steady trim points obtained in the test program are tabulated in tables I through VIII. Generally speaking, the flaps up elevator angle for trim required about -2 $\Delta\delta_e$ more trailing edge up than predicted. Flaps 30° trim was about +1° δ_e more trailing edge down. Trim at flaps 65° was between +4° and +5° δ_e more trailing edge down than corresponding predictions.

All of the steady "1 g" trim points, including approaches to stall and single-engine conditions, have been collected in figure 66. The airplane nominally maintained trim within ±5° δ_e from neutral for all takeoff, climb, cruise, descent, and landing conditions. Approaches to stall for flaps up and 30° were exceptions requiring elevator deflections over -13°. The largest elevator deflections seen in the test program are also shown in figure 66. These points represent nosewheel liftoff conditions reached during taxi tests and the recovery from the 50 kt, flaps 65° approach to stall. Existing data indicate that the stabilizer incidence setting and trim tab authority are adequate for the narrow CG range examined in the test program.

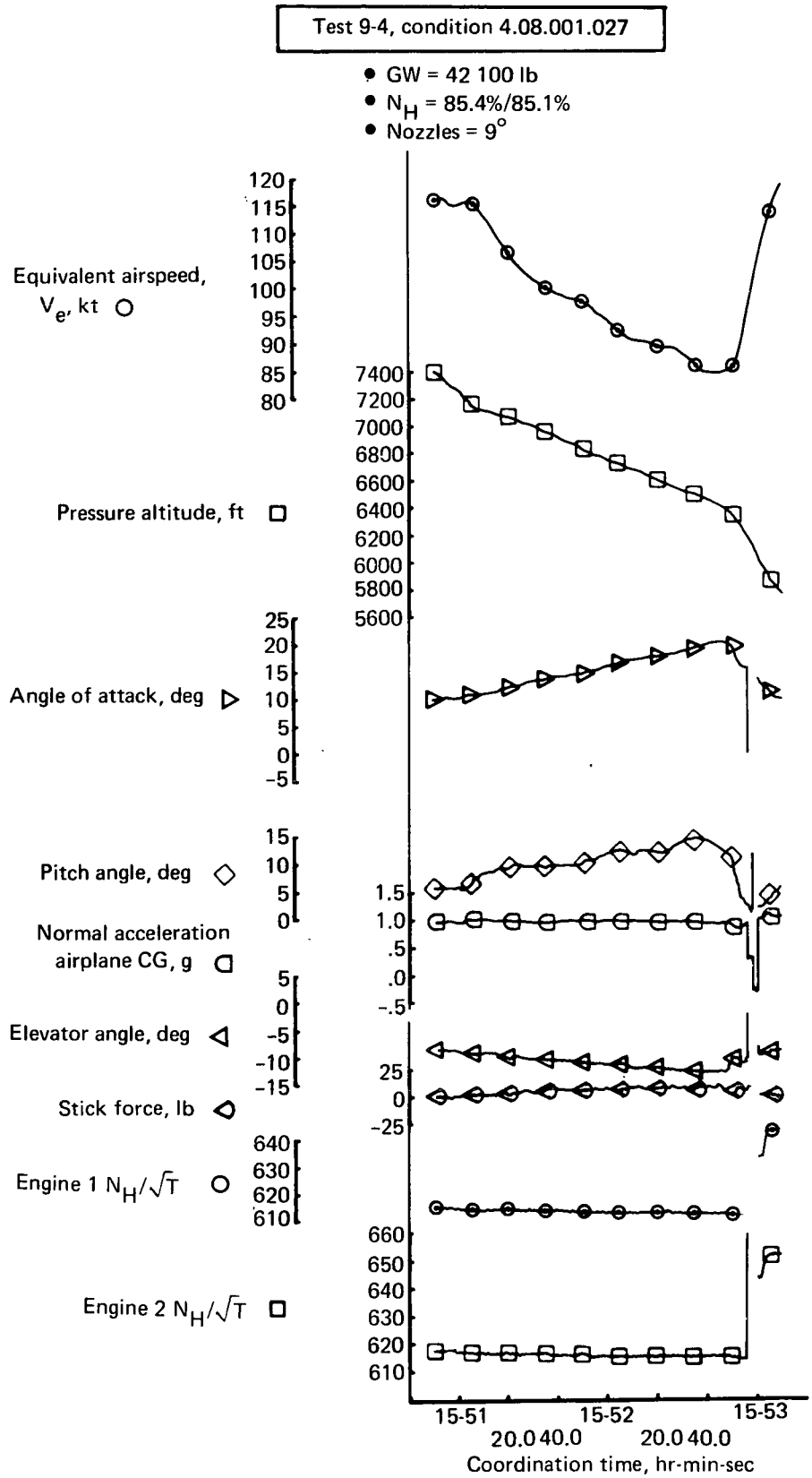

FIGURE 56.–APPROACH-TO-STALL TIME HISTORY–FLAPS UP, TWO ENGINES

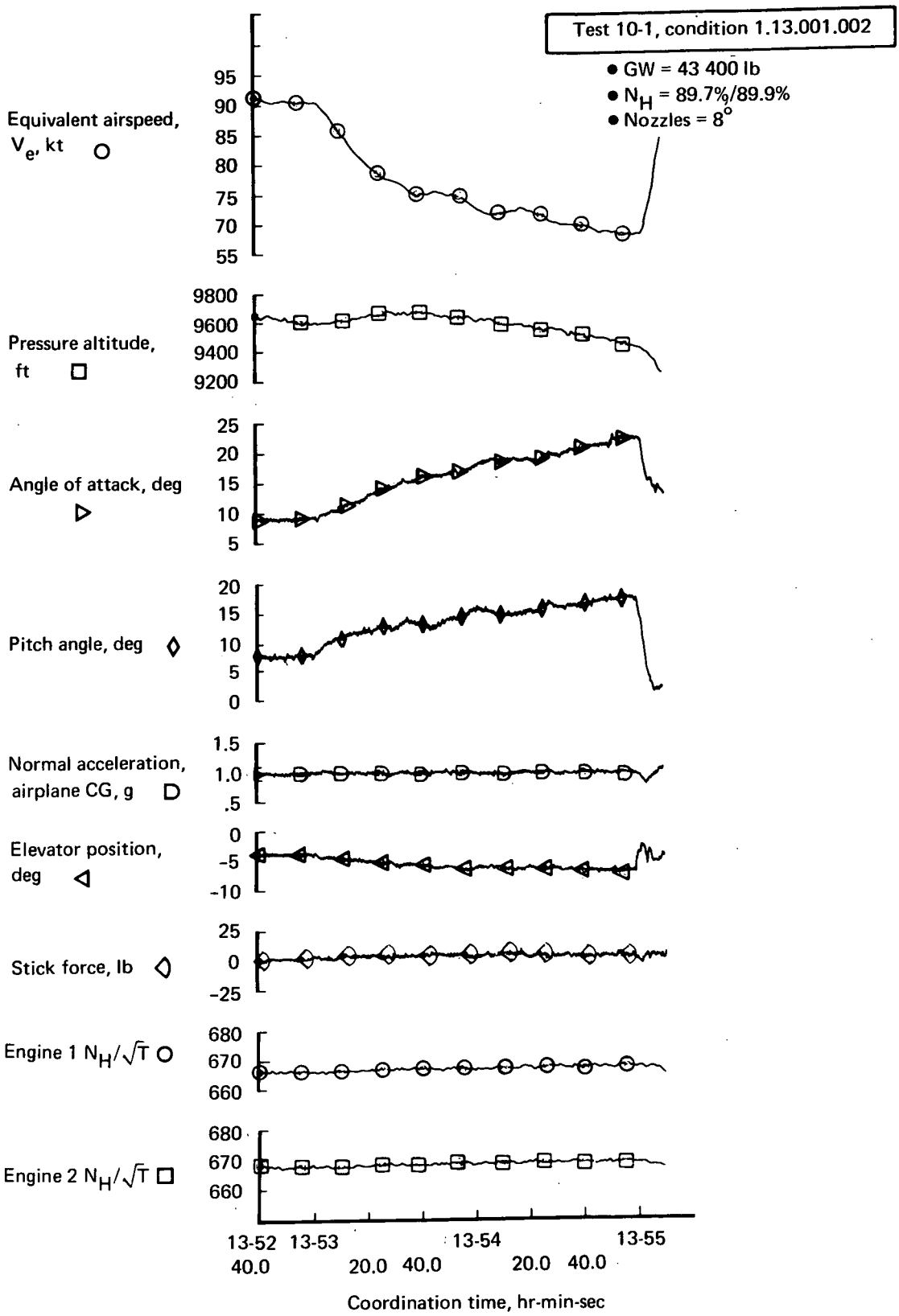

FIGURE 57.—APPROACH-TO-STALL TIME HISTORY—FLAPS 30°, TWO ENGINES

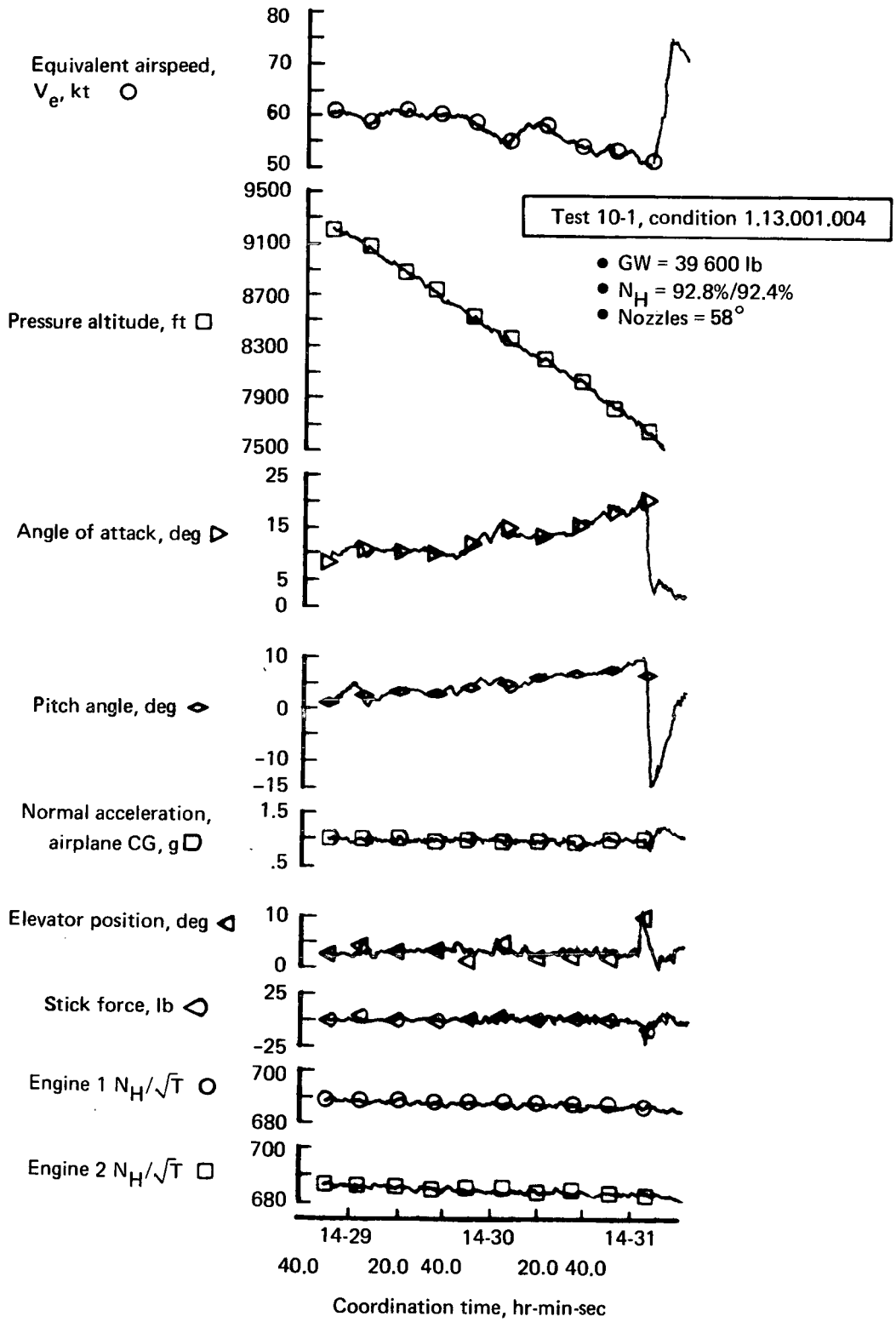

FIGURE 58.–APPROACH-TO-STALL TIME HISTORY–FLAPS 65°, TWO ENGINES

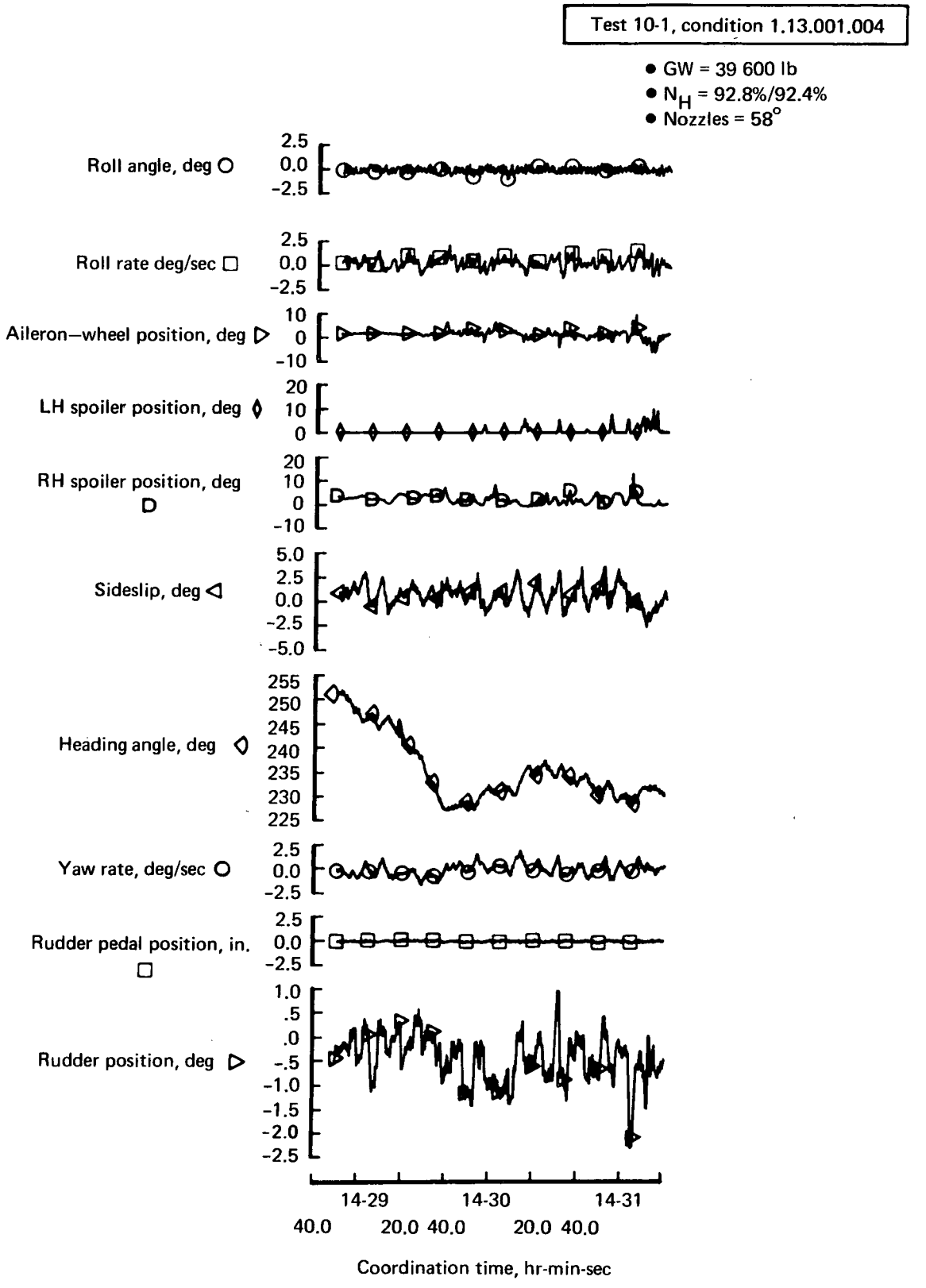

FIGURE 59.–APPROACH-TO-STALL TIME HISTORY–FLAPS 65°, TWO ENGINES

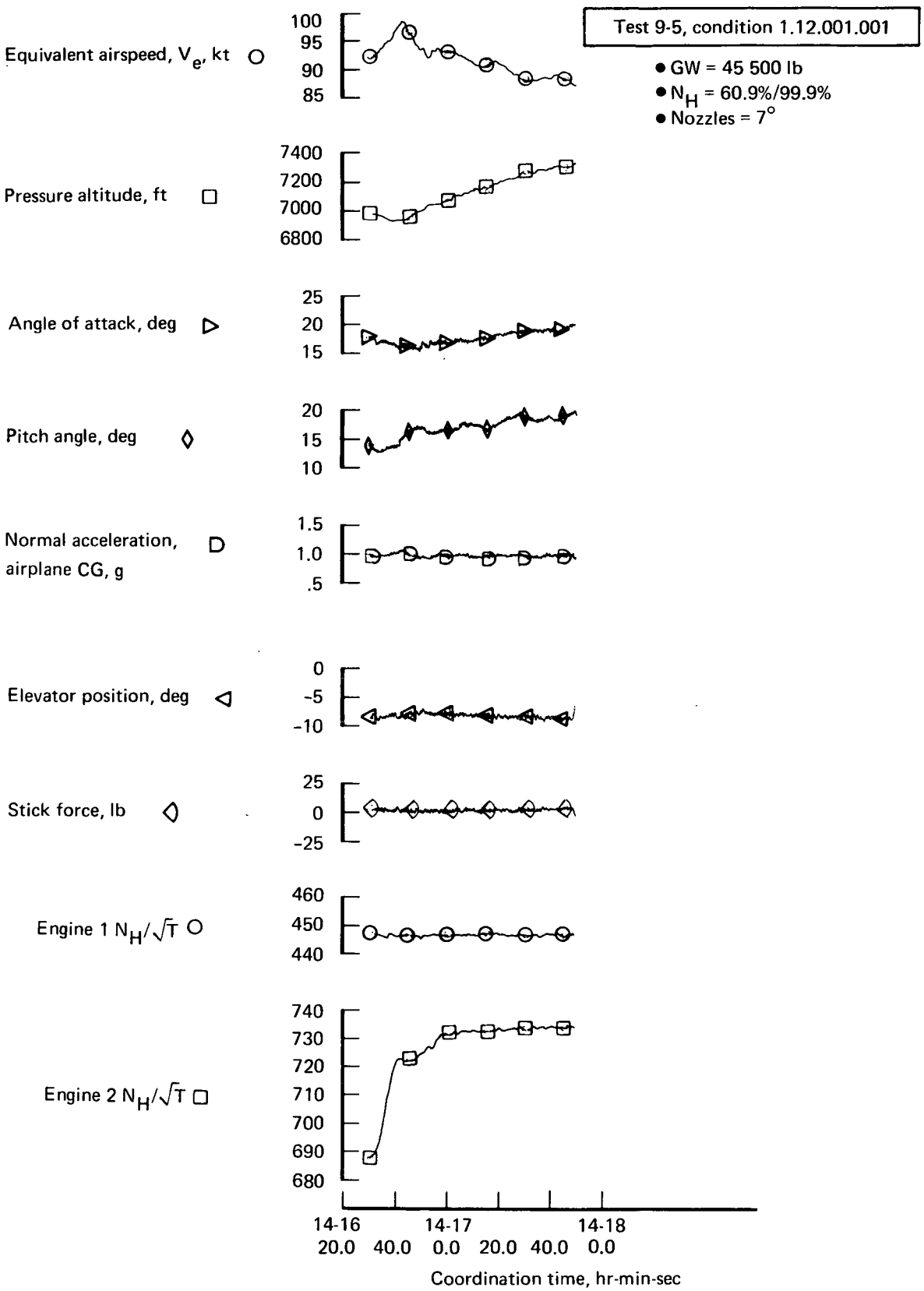

FIGURE 60.—APPROACH-TO-STALL TIME HISTORY—FLAPS UP, ONE ENGINE

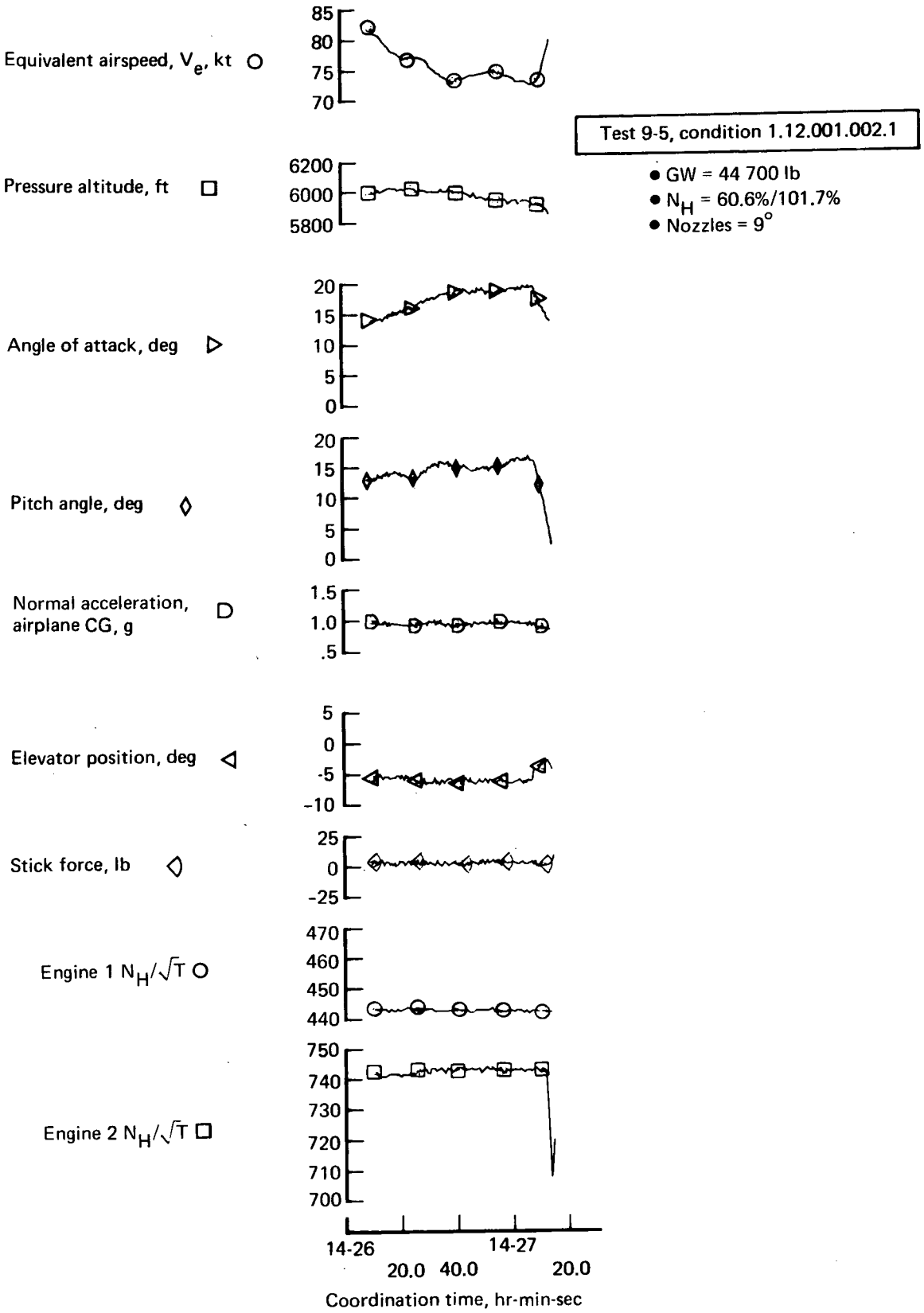

FIGURE 61.–APPROACH-TO-STALL TIME HISTORY–FLAPS 30°, ONE ENGINE

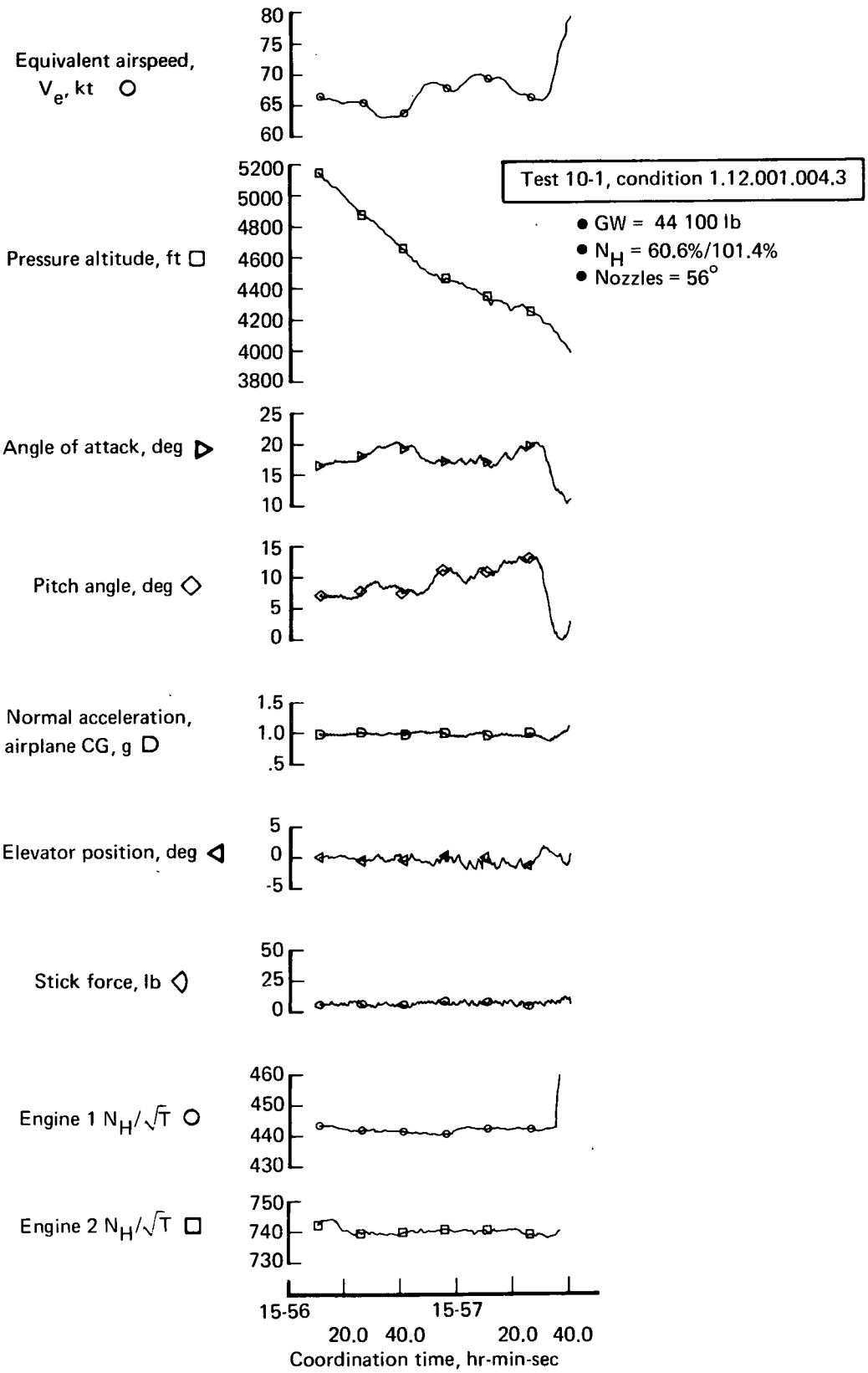

FIGURE 62.–APPROACH-TO-STALL TIME HISTORY–FLAPS 65°, ONE ENGINE

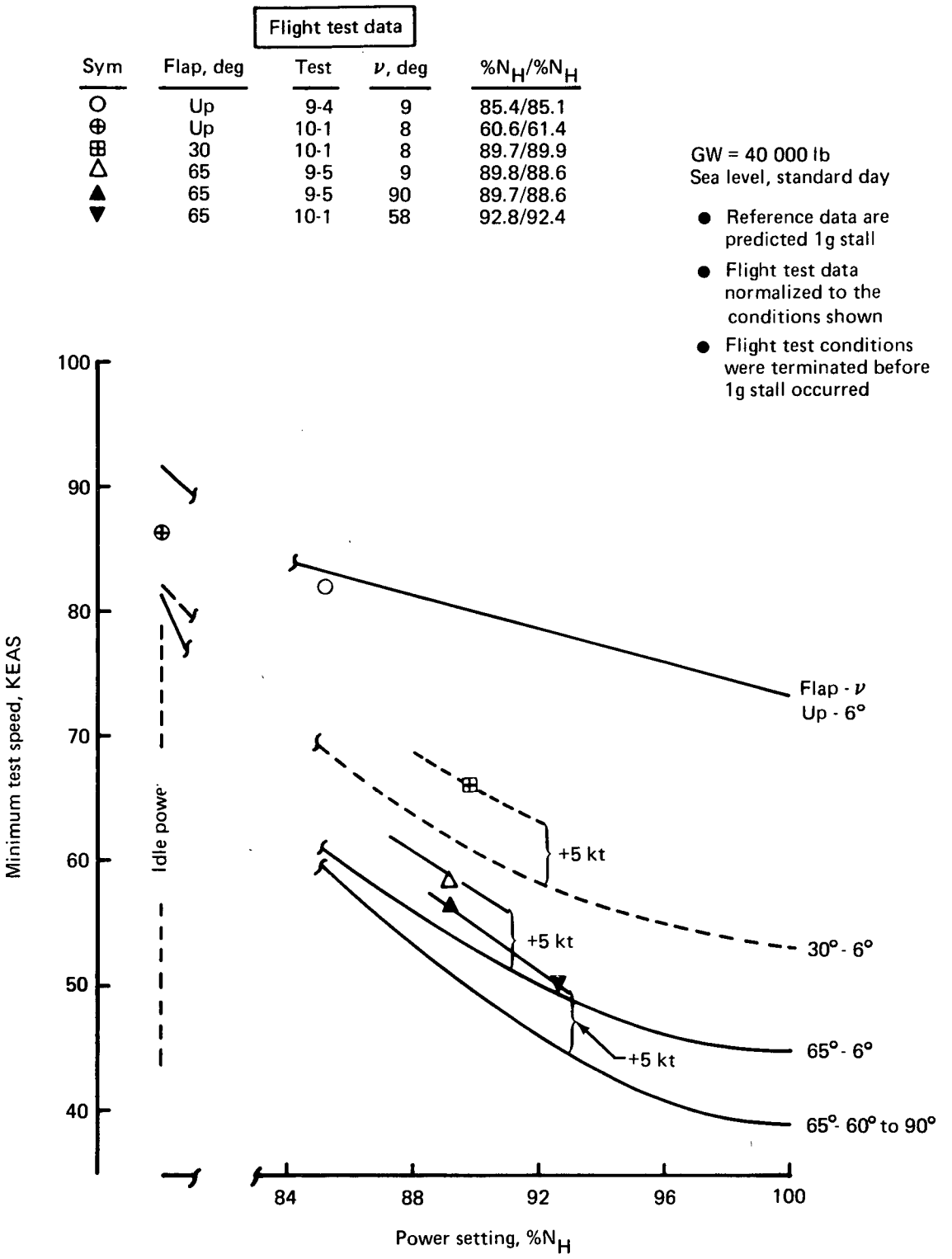

FIGURE 63.—MINIMUM TEST SPEEDS—TWO ENGINES

Flight test data

Sym	Flap, deg	Test	ν, deg	$\%N_H/\%N_H$
○	Up	9-5	7	60.9/99.9
□	30	9-5	9	60.6/101.7
⊠	30	9-5	8	60.7/96.5
▲	65	10-1	57	60.4/94.3
▶	65	10-1	57	60.6/92.6
▼	65	10-1	57	60.5/101.4
◀	65	10-1	56	60.6/101.4

GW = 40 000 lb
Sea level, standard day

- Reference data are predicted 1g stall
- Flight test data normalized to the conditions shown
- Flight test conditions were terminated before 1g stall occurred

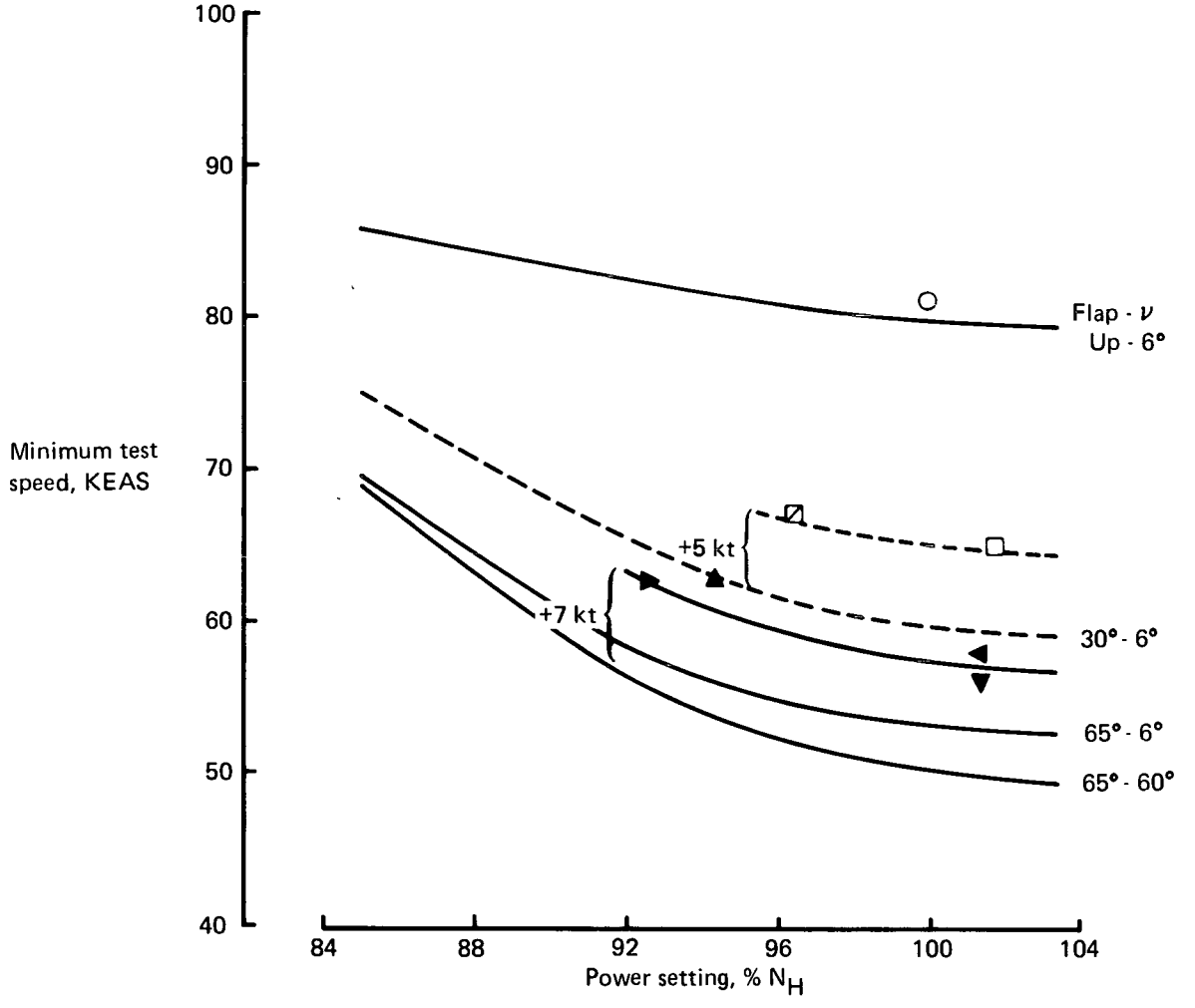

FIGURE 64.–MINIMUM TEST SPEEDS–ONE ENGINE

TABLE VII.–FLIGHT TEST DATA–TWO ENGINES

APPROACH TO STALL CONDITIONS

Test Condition	9-3 4.08.001.028	9-4 4.08.001.026	9-4 4.08.001.027	9-5 4.08.001.030	9-5 4.08.001.031	10-1 1.13.001.001	10-1 1.13.001.006	10-1 1.13.001.002	10-1 1.13.001.004
IRIG time, hr-min-sec	15-50-35 to 15-52-15	15-43-40 to 15-46-15	15-50-50 to 15-53-10	16-45-40 to 16-47-40	16-53-00 to 16-54-20	13-28-45 to 13-30-30	13-47-00 to 13-48-00	13-52-40 to 13-55-10	14-28-50 to 14-31-20
Flap pos, $\delta_{F_{nom}}$, deg	30	Up	Up	65	65	Up	30	30	65
Nozzle pos, ν, deg	11	8	9	9	90	7	8	8	58
Power setting, % N_H									
Engine 1	90.1	61.2	85.4	89.8	89.7	60.6	80.0	89.7	92.8
Engine 2	89.5	61.8	85.1	88.6	88.6	61.4	80.4	89.9	92.4
Gross weight, lb	40,200	42,700	42,100	43,200	42,300	46,000	44,200	43,400	39,600
Altitude, ft	6,050	6,440	6,400	7,600	6,910	5,845	5,830	9,420	7,670
Temperature, std + °C	1.2	5.1	5.3	-1.1	-1.0	-3.9	-3.9	-3.5	-4.2
V_{min}, KEAS	69.5	89	84.5	60.5	58.0	90.4	80.4	67.8	50
$\alpha_{max\ boom}$, deg	18	20.4	20	23.5	24	22	22	22	21
Pitch angle, θ, deg	13.5	11.5	13.5	12.6	6	11	8	17	9
W/qS	2.84	1.84	2.01	4.02	4.28	1.92	2.33	3.22	5.41
Elevator pos, δ_e, deg	-7	-12.7	-10.8	-2	-2.5	-13.7	-11.5	-7	2
Elevator spring tab, deg	2.5	6.8	4.5			8	4	1.5	-3
Elevator trim tab, deg	1.7	5.5	4.0			6	6.4	1.8	-2.8

TABLE VIII.–FLIGHT TEST DATA–ONE ENGINE–APPROACH TO STALL CONDITIONS

Test Condition	9-5 1-12-001-001	9-5 1.12-001.002.1	10-1 1.13.001.005	10-1 1.12.001.004	10-1 1.12.001.004.1	10-1 1.12.001.004.2	10-1 1.12.001.004.3
IRIG time, hr-min-sec	14-16-30 to 14-17-50	14-26-10 to 14-27-15	13-44-05 to 13-46-25	15-43-40 to 15-45-40	15-52-20 to 15-53-50	15-54-0 to 15-55-0	15-56-0 to 15-57-0
Flap pos, $\delta_{F_{nom}}$, deg	Up	30	30	65	65	65	65
Nozzle pos, ν, deg	7	9	8	57	57	57	56
Power setting, % N_H							
Engine 1	60.9	60.6	60.7	60.4	60.6	60.5	60.6
Engine 2	-99.9	101.7	96.5	94.3	92.6	101.4	101.4
Gross weight, lb	45,500	44,700	44,400	45,800	44,700	44,500	44,100
Altitude, ft	7,250	5,920	8,370	2,050	7,170	6,150	4,740
Temperature, std + °C	-1.9	-0.1	-4.2	-4.4	-3.6	-3.2	-2.7
V_{min}, KEAS	88	72.6	74.5	67.3	67.0	63.5	63.0
$\alpha_{max, boom}$, deg	19	19.2	19.8	19	21	22	20
Pitch angle, θ, deg	18.7	16.0	13.4	8.0	9.8		9.0
W/qS							
Elevator pos, δ_e, deg	-8.7	-4.5	-7.0				0
Elevator spring tab, deg	2.0	1.3	1.5				1
Elevator trim tab, deg	4.5	1.0	2.5				-3.8

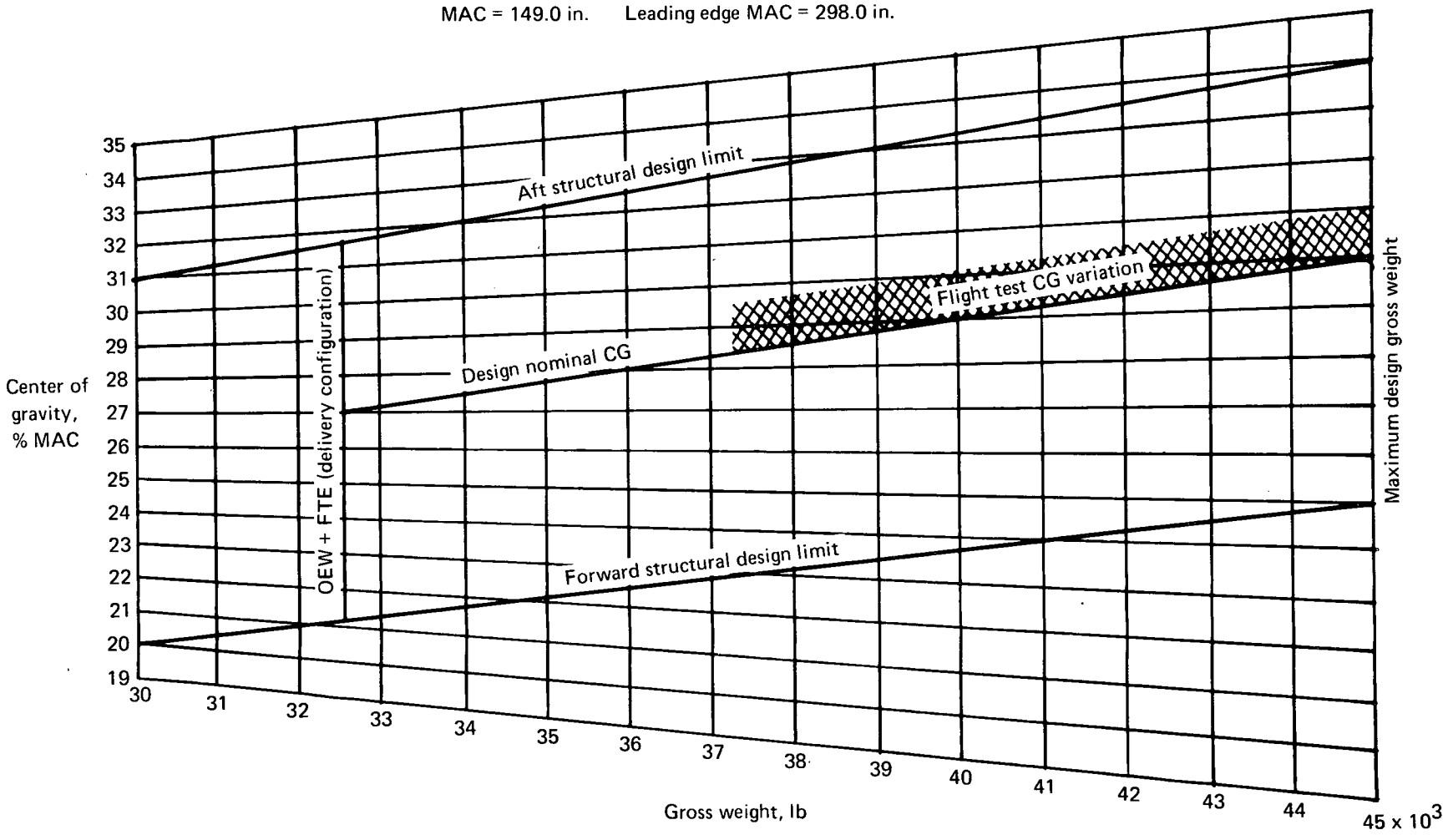

FIGURE 65.—CENTER-OF-GRAVITY LIMITS

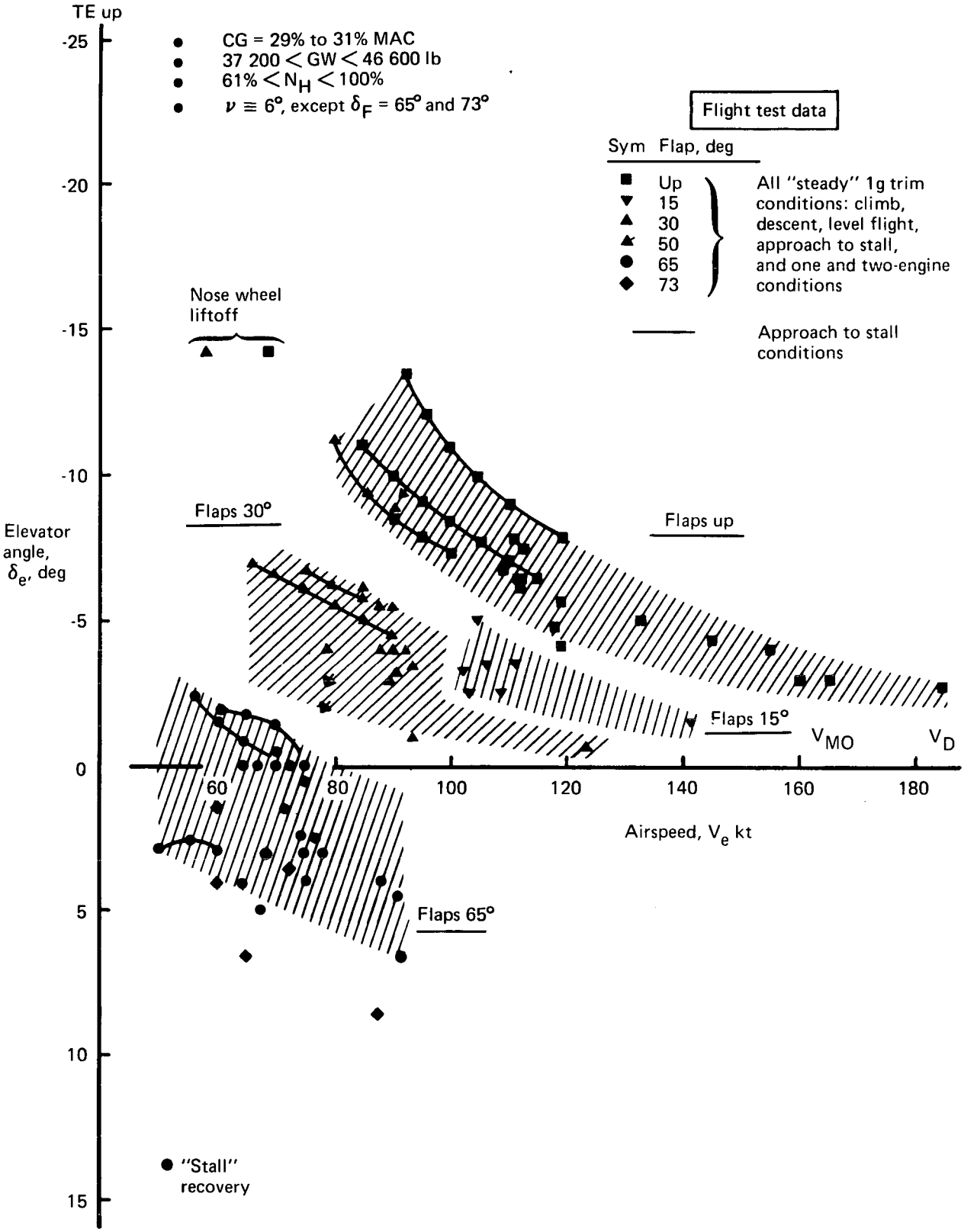

FIGURE 66.–FLIGHT TEST TRIM ELEVATOR SUMMARY

No attempt was made to examine forward and aft CG characteristics. Ballast would be required to shift the CG away from its normal fuel loading location. Aerodynamic limitations on CG location have not been established.

Minimum test speed conditions were achieved at angles of attack greater than $20°\alpha_F$. Stall entries at flaps up and 30° were predicted to reach tail stall. In the flight testing the pilot found no evidence of adverse control or stall characteristics; however, fully developed stalls were not scheduled. It appears that tail lift capability is adequate for all normal flight conditions.

Static longitudinal stability levels were low, as predicted. The stall entry data shown in "Minimum Speeds" indicate the elevator and stick force required to change speed. The airplane exhibited positive static longitudinal stability at the flaps up setting, although the level was less than that predicted. Stability at flaps 30° and 65° was virtually nonexistent, as predicted. The stick force required to change airspeed was zero. The pilots commented that very close attention was required to maintain trim condition at flaps 65°. The airplane acted as if it would diverge into a fully stalled conditon. Conditions at flaps 73° were similar. The pilots stated that the airplane felt somewhat better at flaps 65° than at flaps 73°.

The 50-kt minimum speed condition from a 60-kt approach point (figs. 58 and 59, condition 1.13.001.004, test 10-1) was accomplished by very small stick force inputs of less than ±5 lb. Even airplane nose-down elevator pulses resulted in airspeed reduction. In this speed regime, pitch attitude and airspeed drifted constantly for all trim conditions. When coupled with the constant buffet and the lateral-directional "snaking," the pilots pointed out that the STOL approach condition was not very "solid."

Dynamic and Maneuvering Characteristics

Even though static stability was quoted as "nil," the airplane exhibited stable characteristics for maneuvering at constant speed. Figure 67 summarizes the elevator-per-g data from pushovers/pull-ups and wind-up turns. Specific wind-up turn data points are presented in figures 68 through 71. Elevator-per-g and stick force-per-g are close to the predicted values. Some degradation in maneuvering stability is evident at the flaps 65° condition.

The spring tab modification to the elevator accomplished its objective. Stick-force-per-g came out near to 40 lb/g for acceptable, one-hand maneuvering characteristics.

Load factor produced by unit change in nose boom angle of attack, n_{z_α}, came out better than predicted at lower speeds. The total angle of attack required to achieve $n_z = 1.5$ at 77 kt was on the order of 10° to $11°\alpha_F$. Since maximum angle of attack exceeding 20° was demonstrated,

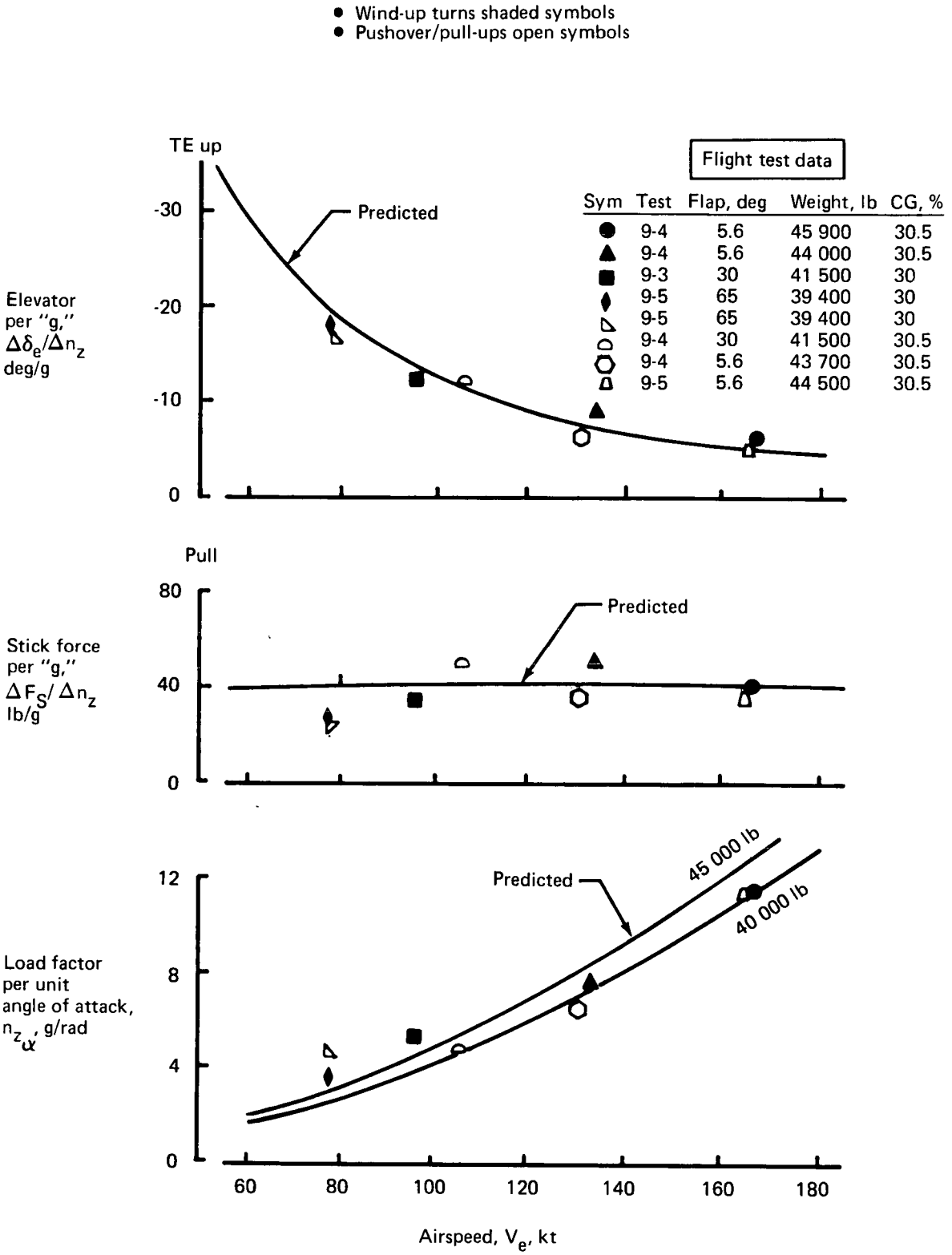

FIGURE 67.–MANEUVERING STABILITY SUMMARY

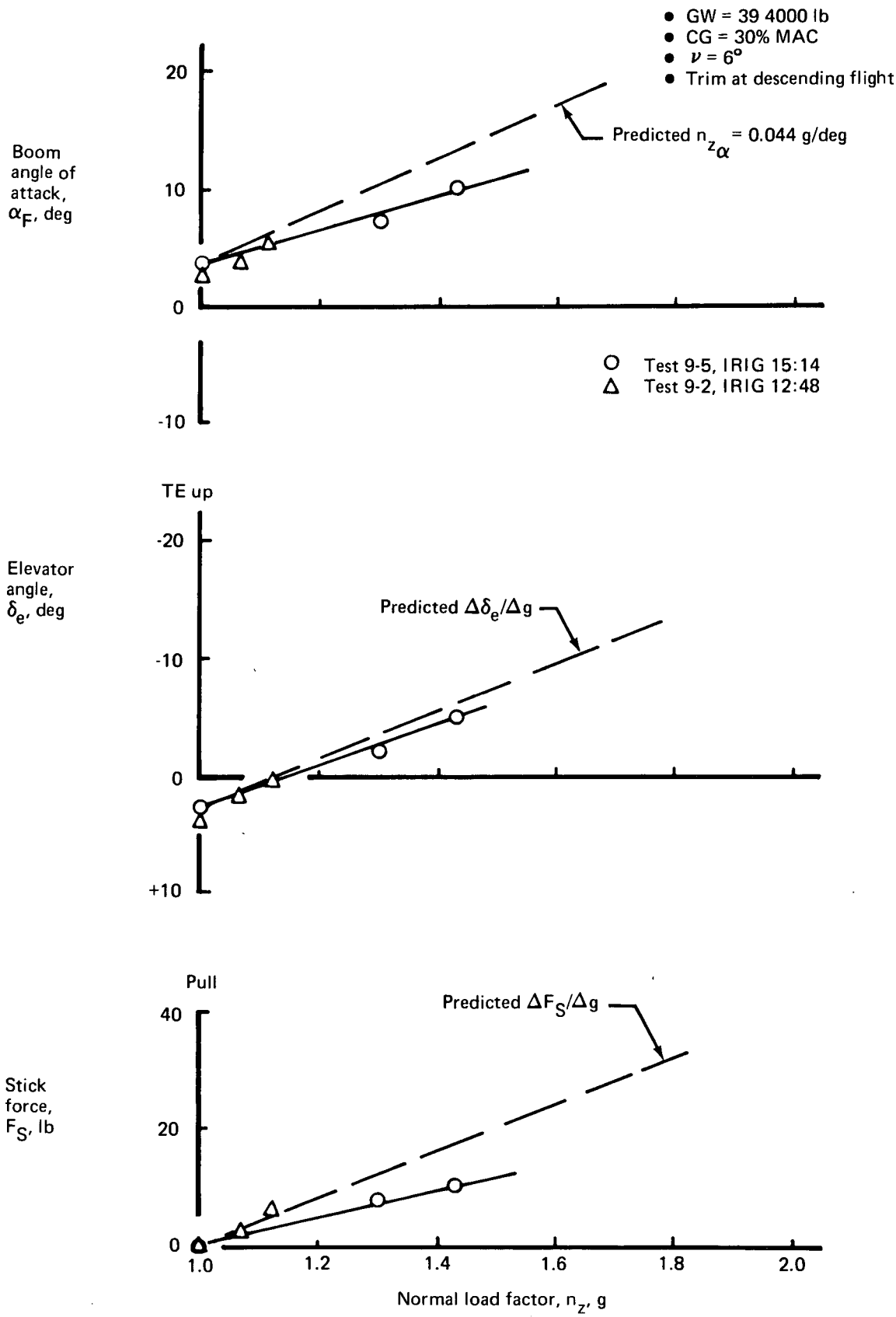

FIGURE 68.—WIND-UP TURN MANEUVER—FLAPS 65°, 77 KT

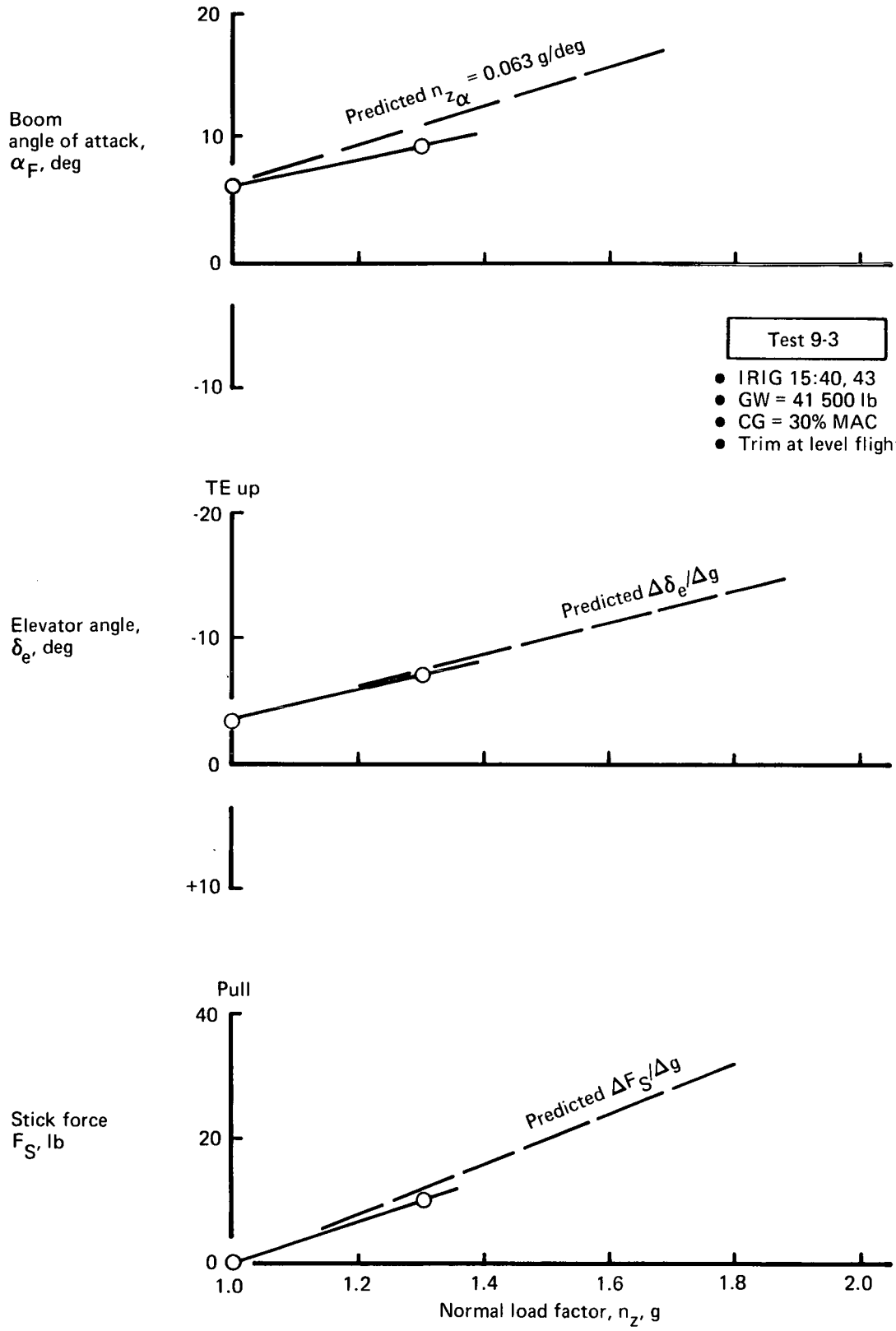

FIGURE 69.—WIND-UP TURN MANEUVER—FLAPS 30°, 95 KT

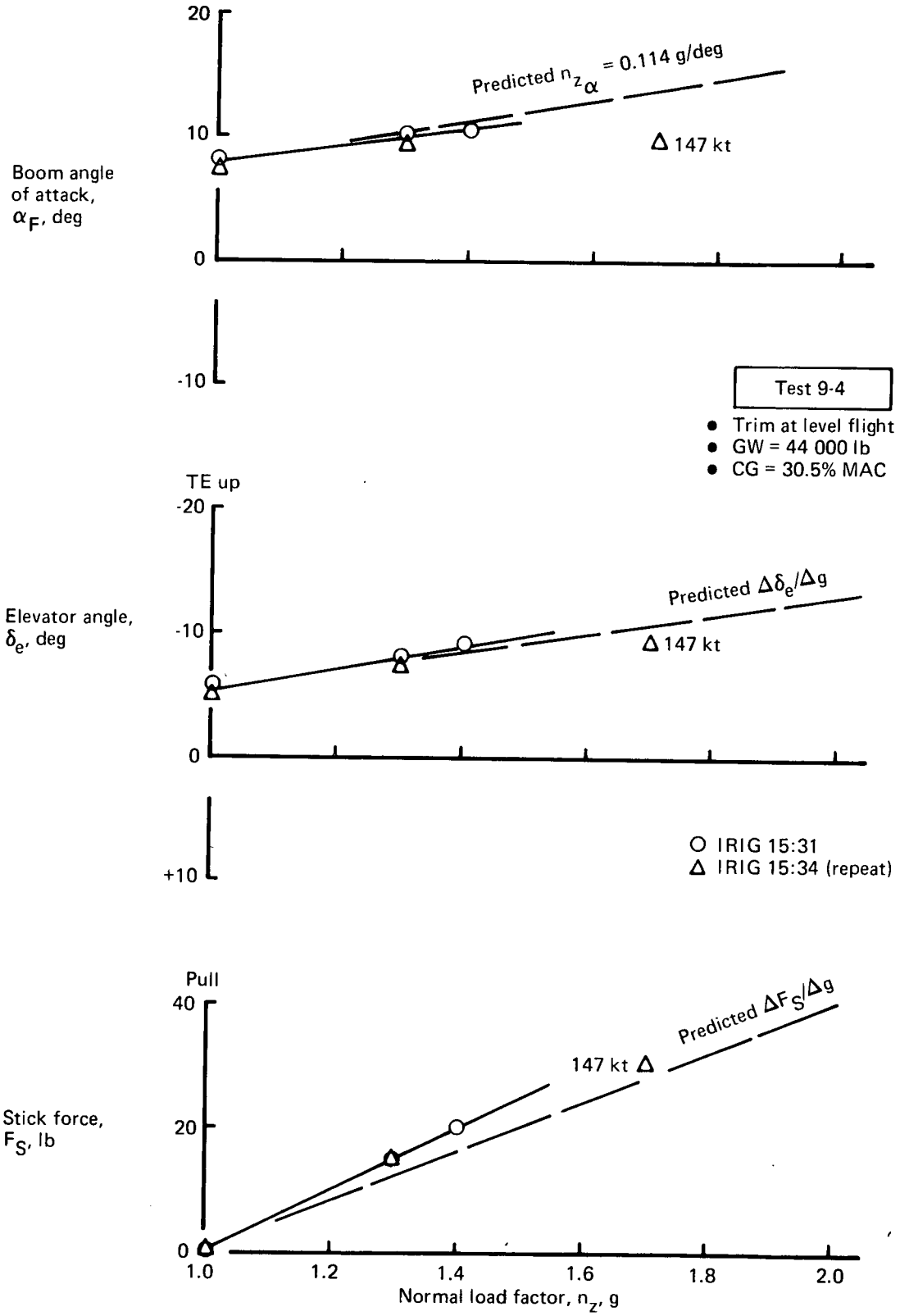

FIGURE 70.—WIND-UP TURN MANEUVER—FLAPS UP, 133 KT

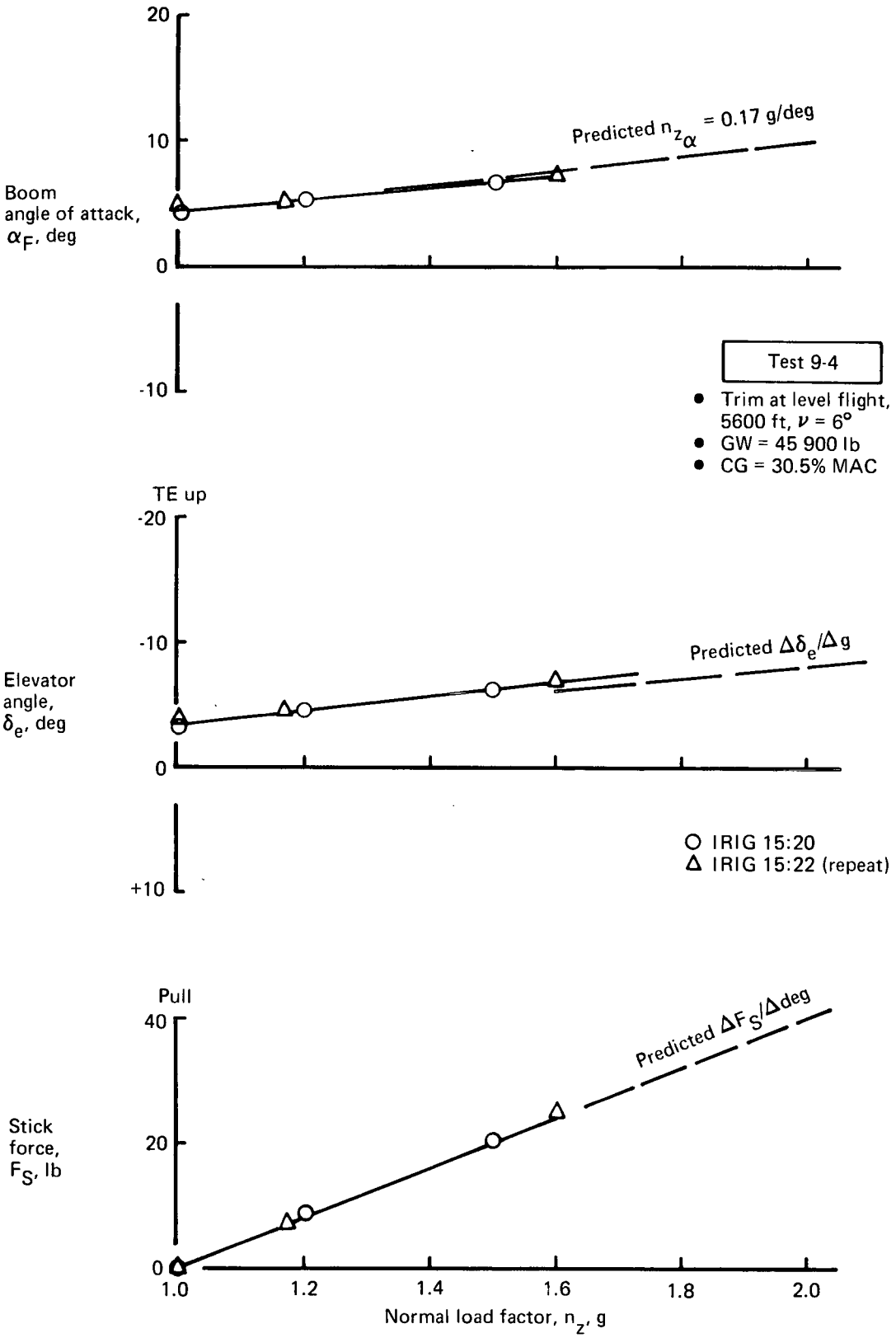

FIGURE 71.–WIND-UP TURN MANEUVER–FLAPS UP, 166 KT

considerably more load factor capability should be available in the airplane. Figure 72 presents the estimated maneuvering capability of the airplane. Load factor will be limited both by wing lift and elevator control system. Stick force increases abruptly at the θ_1 stops (see section on "Longitudinal Control System"). Maneuvering margin at 60 kt should be adequate ($\Delta n_z \approx 0.3$ g) provided that trim angle of attack is at $\alpha_F \leqslant 10°$. Actually, the pilots commented that turns of 30° bank angle ($\Delta n_z = 0.16$) below 75 kt were already three times beyond normal pattern maneuvers, owing to rapid turn rate.

Elevator control power was sufficient for the flight maneuvers performed in the test program. Elevator used for nosewheel liftoff at takeoff rotation has been presented in the section "Takeoff." Moderate elevator ($\delta_e \approx -10°$) was used for the conventional takeoffs; thus, tab stalling problems did not interfere with airplane operation. There was sufficient elevator to flare the airplane for the landings ($V_{app} \geqslant 75$ kt) accomplished in the program. Also, elevator to reach miminum speed was not a problem, owing to neutral static stability. At the lower airspeeds ($V_e \approx 50$ to 60 kt) the pilot commented that the elevator system felt "spongy" and the column tended to come back in his hand. These characteristics were presumably due to low q and elevator mass overbalance effects. (Taxi tests showed low natural frequency and significant elevator upfloat, to full trailing edge up at 25 kt.) The extent to which the elevator control system will limit STOL performance was not determined in the test program. STOL takeoffs, landings, and fully developed stall demonstrations were not scheduled.

Flap extension and retraction maneuvers were performed. Figure 73 presents the endpoints compared with prediction. The elevator required for trim more closely followed the flap-trim interconnect programming. Full flap extension and/or retraction can be made with virtually no change in trim by the pilot.

The effects of thrust changes are presented in figure 74 from both transient and steady-state conditions. Elevator authority is adequate for full power application from idle (61% N_H) to takeoff power (100% N_H), which causes nose-up pitching. The maximum required push force would not exceed $F_S \approx -25$ lb. (Transient flight conditions were flown from the right-hand seat without stick force instrumentation.) Transient points at 65 to 70 kt required very little stick force, since power setting was already high for the trim condition. At these STOL conditions with flaps down, speed decreased unconventionally as power was increased, as predicted. Angle of attack decreased as the airplane "heaved" upward beginning a climb. The airplane pulled positive load factor at $\Delta n_z \approx 0.05$ to 0.10 g in the initial transient.

Trim changes due to conical nozzle vectoring are presented in figure 75. Both slow cycling and rapid transient characteristics were evaluated. Significant changes in rate of climb were accomplished with very little trim change. Angle of attack was reduced with nozzles down. Raising

- GW ≈ 40 000 lb
- Based on flight test n_{z_α} and $\Delta\delta_e/\Delta g$
- θ_1 stops based on taxi test data
- Free air
- Flaps 30° and up, α_{trim} at level flight (test data)
- Flaps 65°, α_{trim} at nozzles-down approach (test data

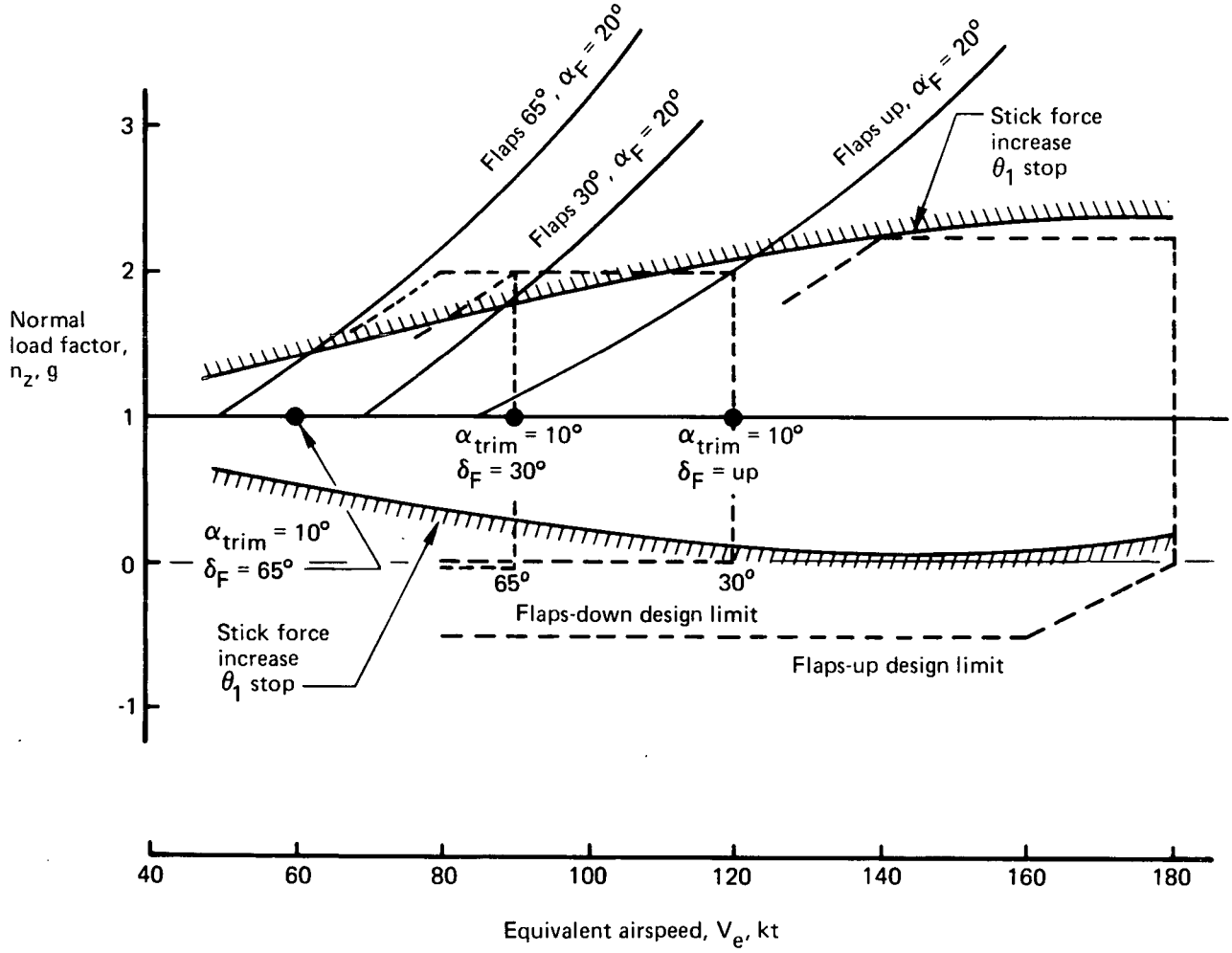

FIGURE 72.–ESTIMATED MANEUVERING CAPABILITY BASED ON FLIGHT TEST DATA

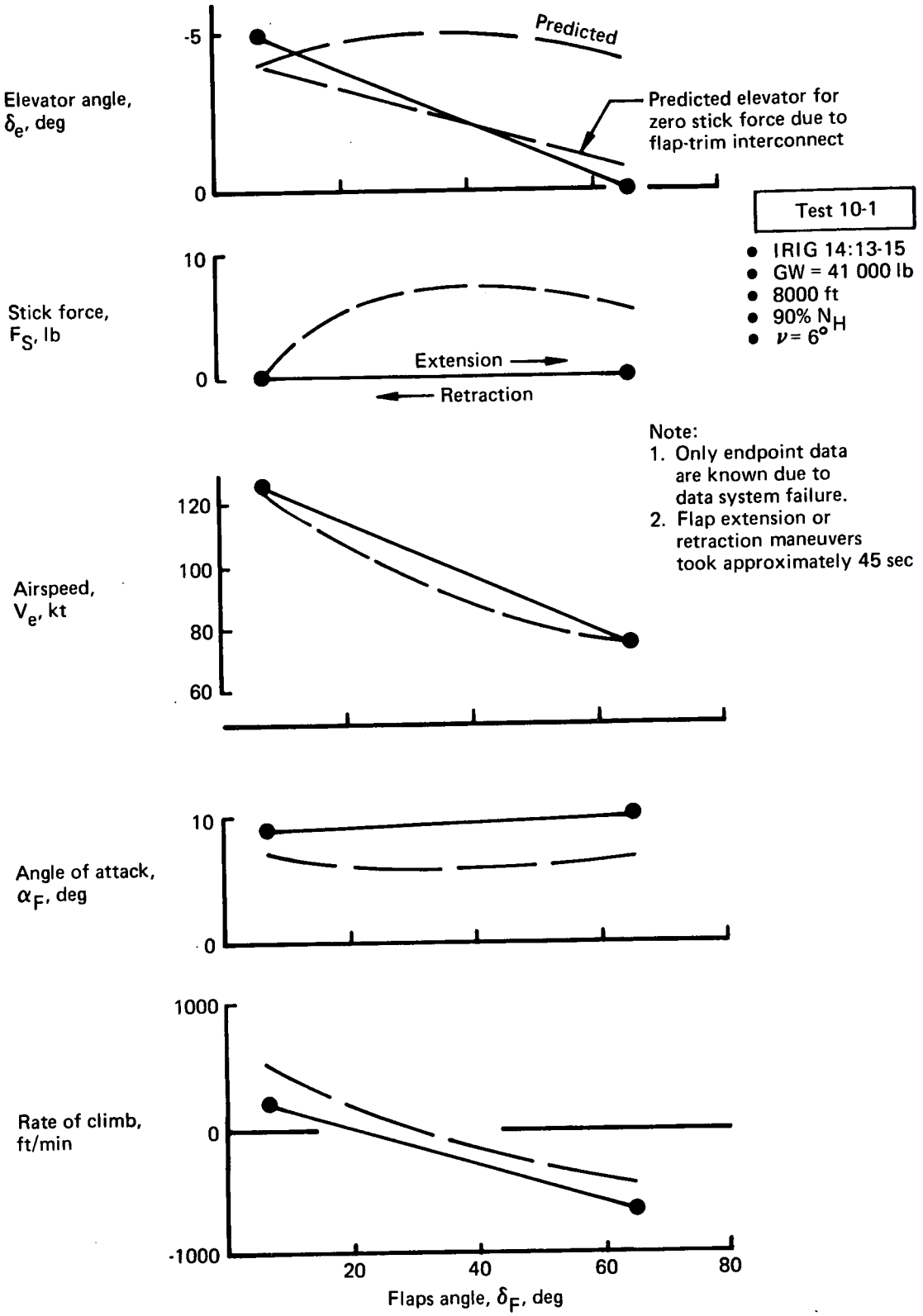

FIGURE 73.–FLAP EXTENSION AND RETRACTION TRIM CHANGE

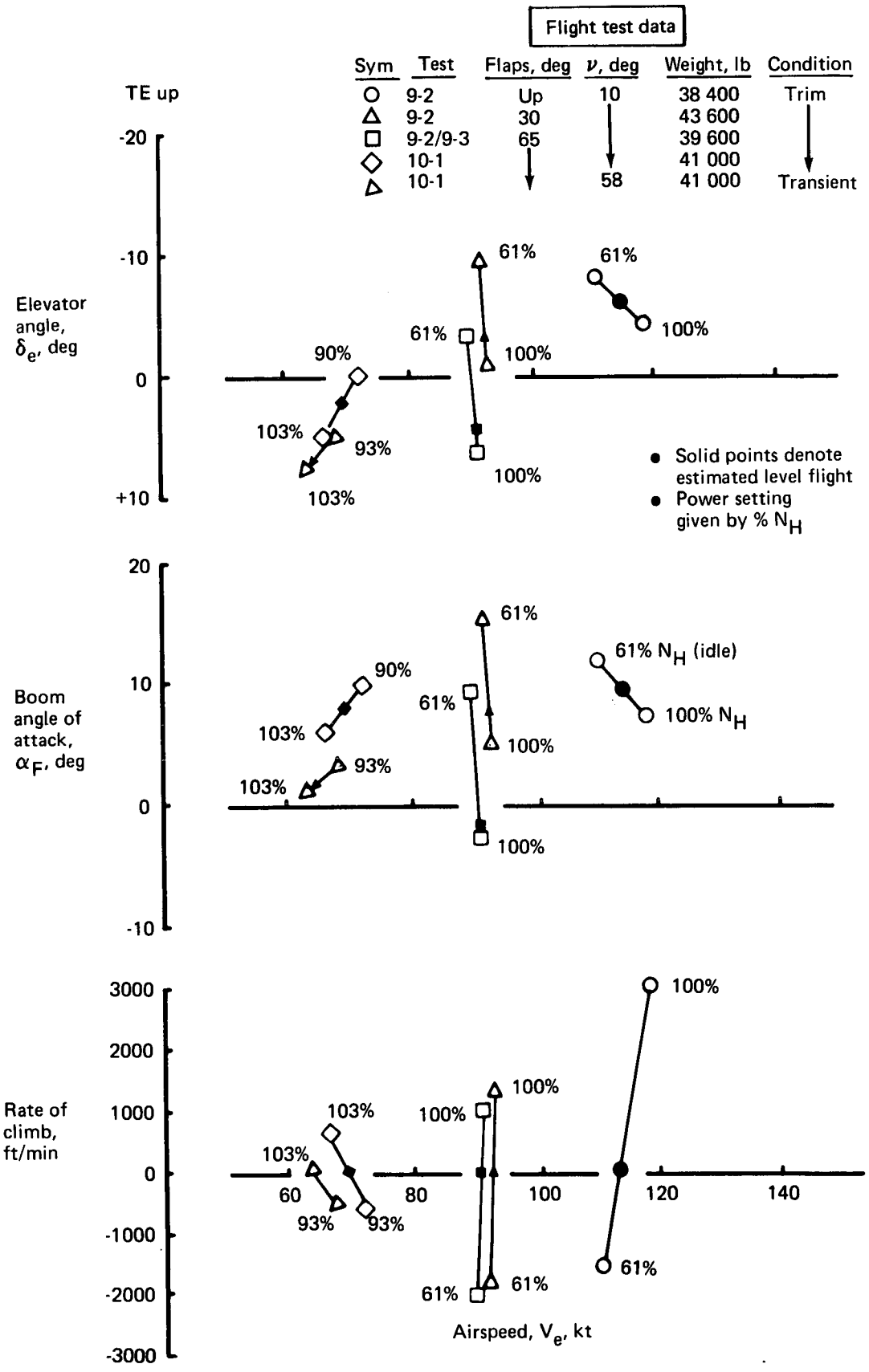

FIGURE 74.–TRIM CHANGE DUE TO THRUST (THROTTLES)

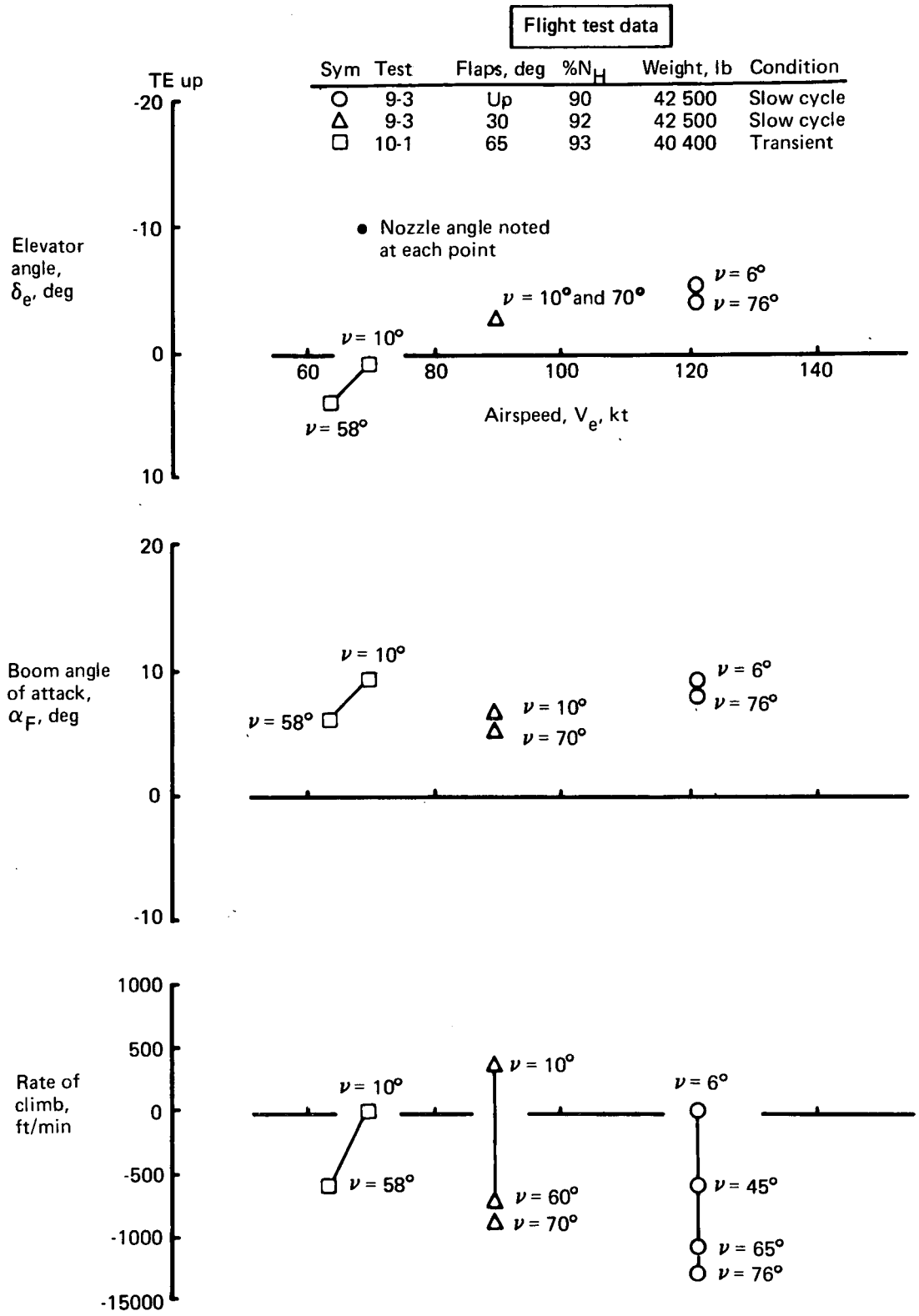

FIGURE 75.–TRIM CHANGE DUE TO CONICAL NOZZLE VECTORING

nozzles quickly at 64 kt produced a speed increase, as predicted. Nozzle modulations produced the same effect as power change on a conventional airplane.

Pitch response to elevator input was very good. In the pushover/pull-up maneuvers, pitch rate tracked elevator very well with small time delay. The 75-kt pushover (test 9-5, IRIG 15:15) was characterized by the time lags from elevator input listed in table IX. Stick force and spring tab angle led elevator by 1/2 sec.

TABLE IX.—TIME LAGS FROM ELEVATOR INPUT

	Time lag, Δt
Pitch rate, $\dot{\theta}$	1/2 sec
Normal acceleration, n_z	1 sec
Angle of attack, α_F	1 sec
Pitch attitude, θ	1-1/2 sec

Airplane response to elevator was good down to 50 kt. Figure 76 presents steady pitch rate developed by elevator input. Recovery from the approach-to-stall high angle-of-attack conditions was prompt. In the 50-kt recovery, pitch attitude was changed from $\theta = +9°$ to $\theta = -15°$ in 4 seconds using an elevator pulse of about +12° (see figs. 58 and 59 for time history. Pitch rate response agrees with prediction at STOL airspeeds.

Short period and phugoid characteristics were not determined in the flight test program. There was nothing objectionable noted about the longitudinal dynamics outside the STOL regime. Low static stability produced constant wandering in speed and attitude at speeds below 75 kt.

LATERAL-DIRECTIONAL STABILITY AND CONTROL

Lateral-Directional Static Stability

Lateral-directional static stability characteristics were assessed in the flight test program by performing steady sideslip maneuvers. Figures 77 through 81 present the data, which cover the entire airspeed envelope. The Modified C-8A is statically stable about both the lateral and

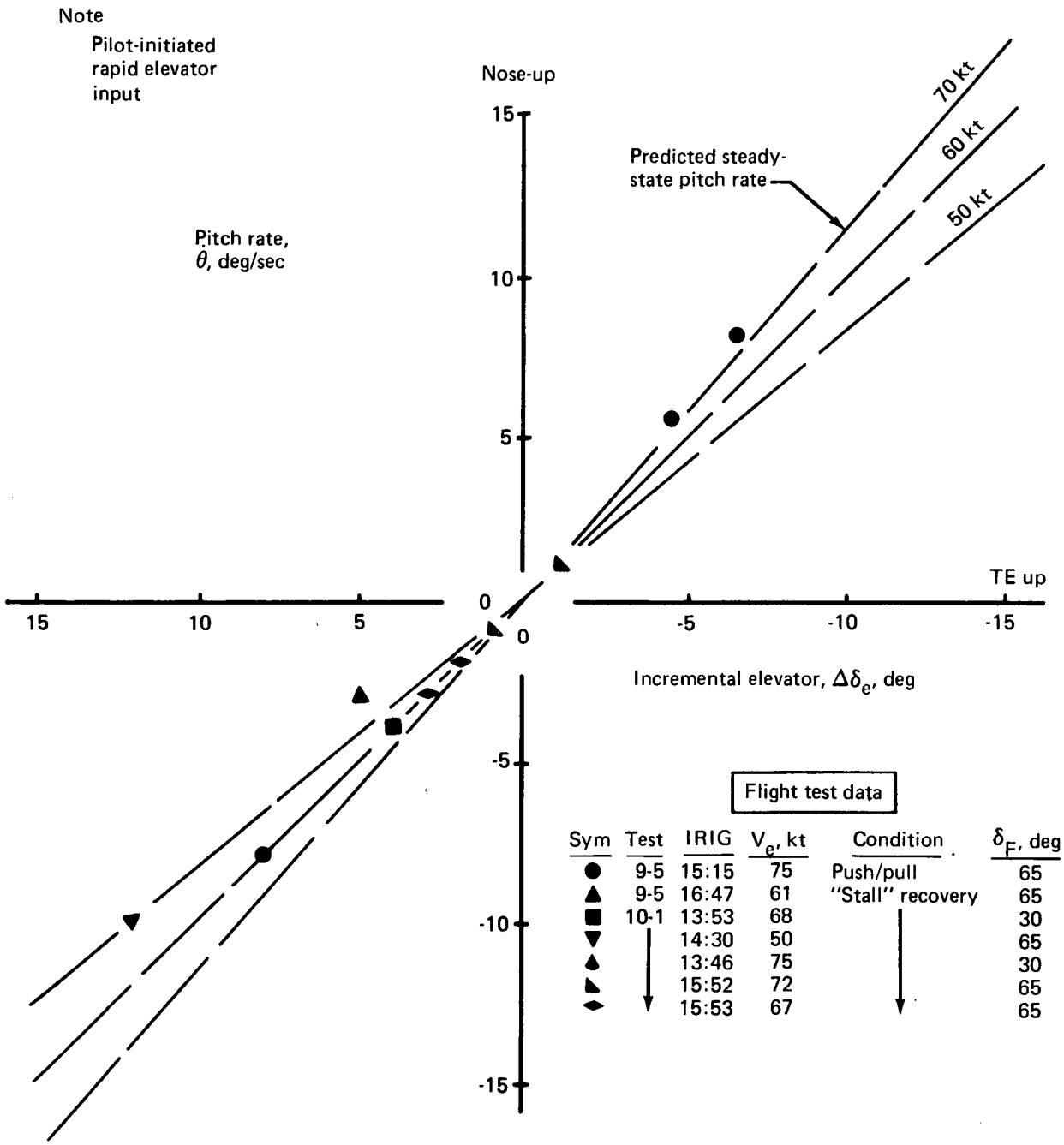

FIGURE 76.–PITCH RATE DEVELOPED BY RAPID ELEVATOR INPUT DURING FLIGHT TESTING

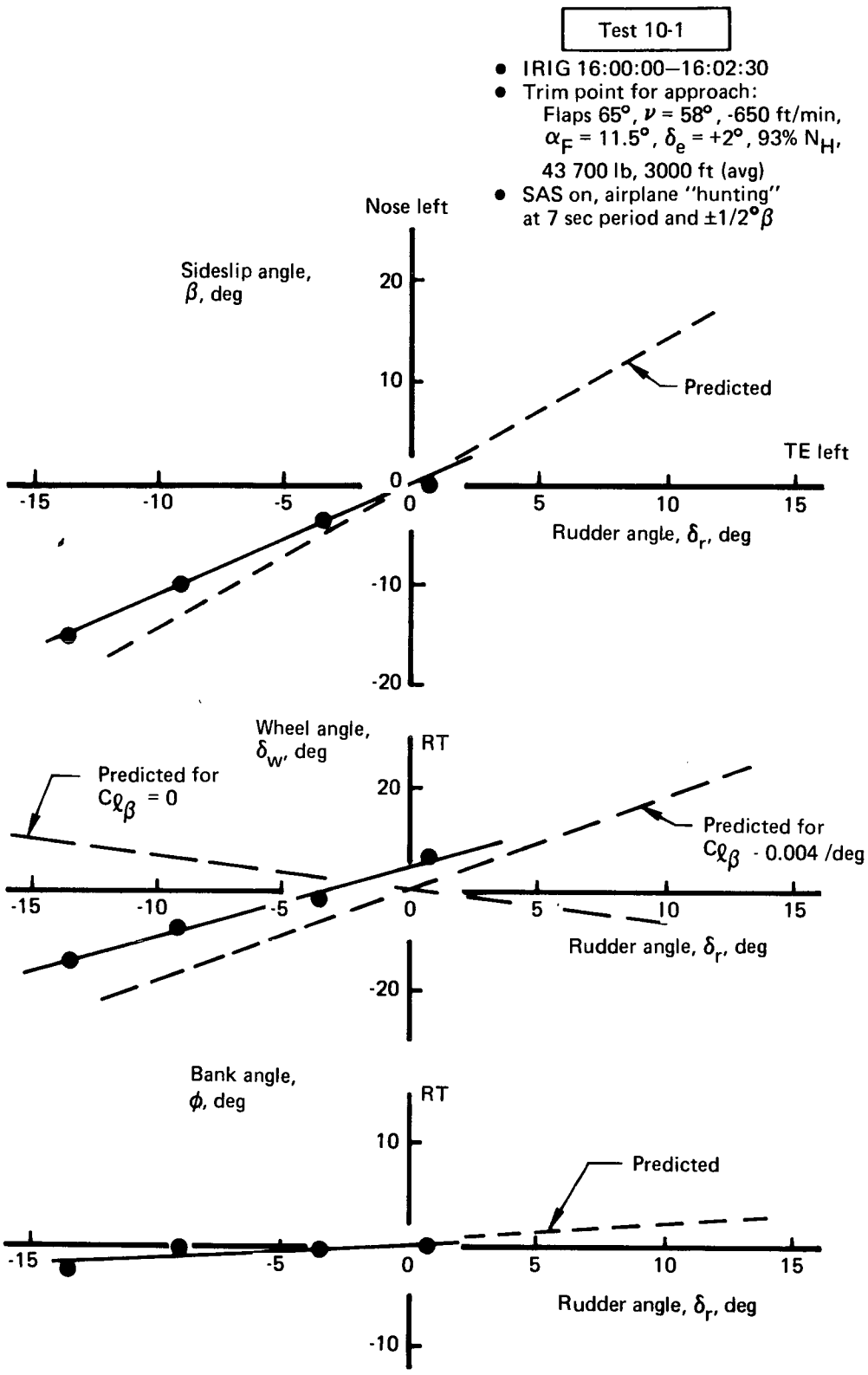

FIGURE 77.–STEADY SIDESLIP–FLAPS 65°, 65 KT

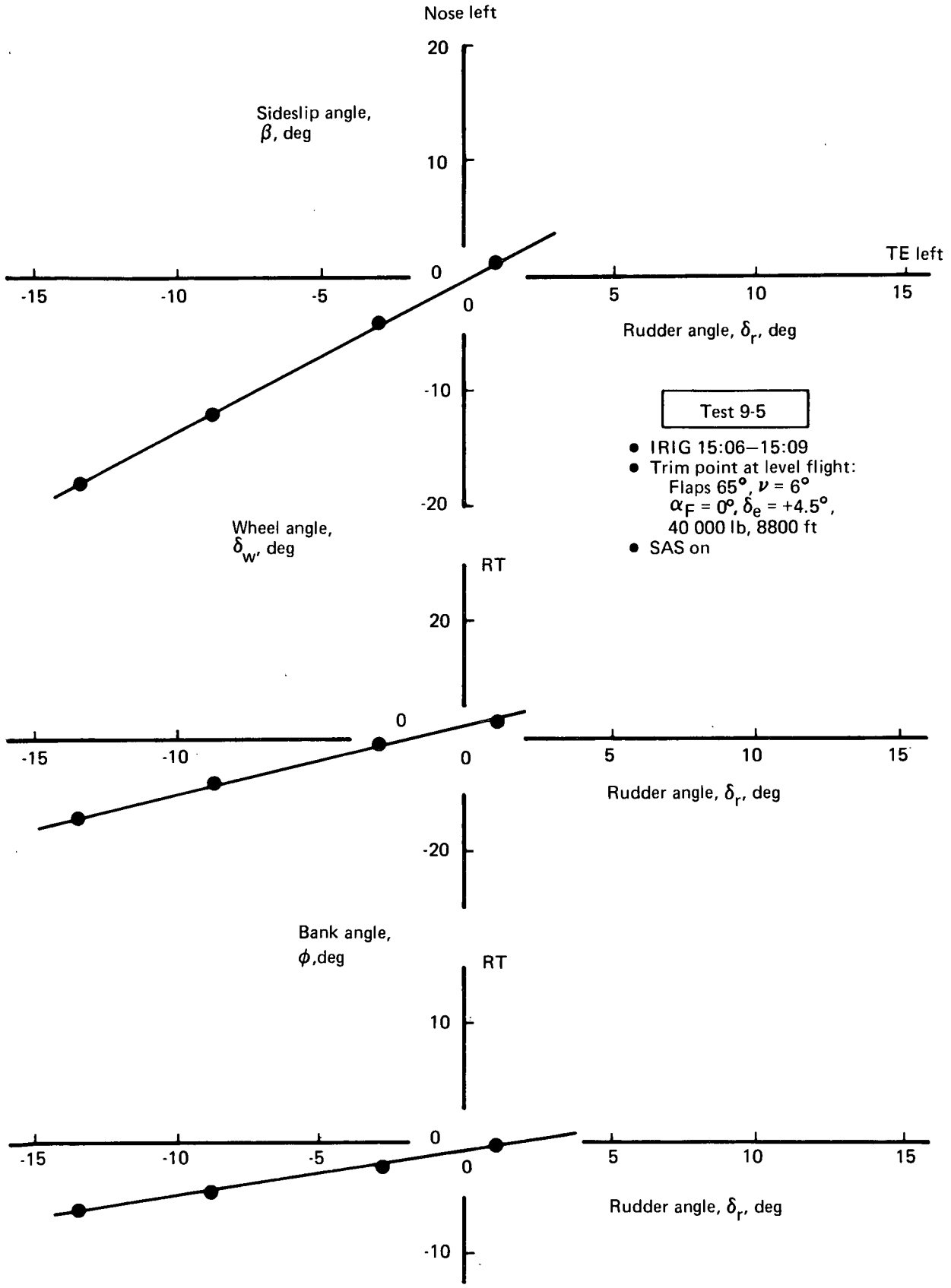

FIGURE 78.–STEADY SIDESLIP–FLAPS 65°, 90 KT

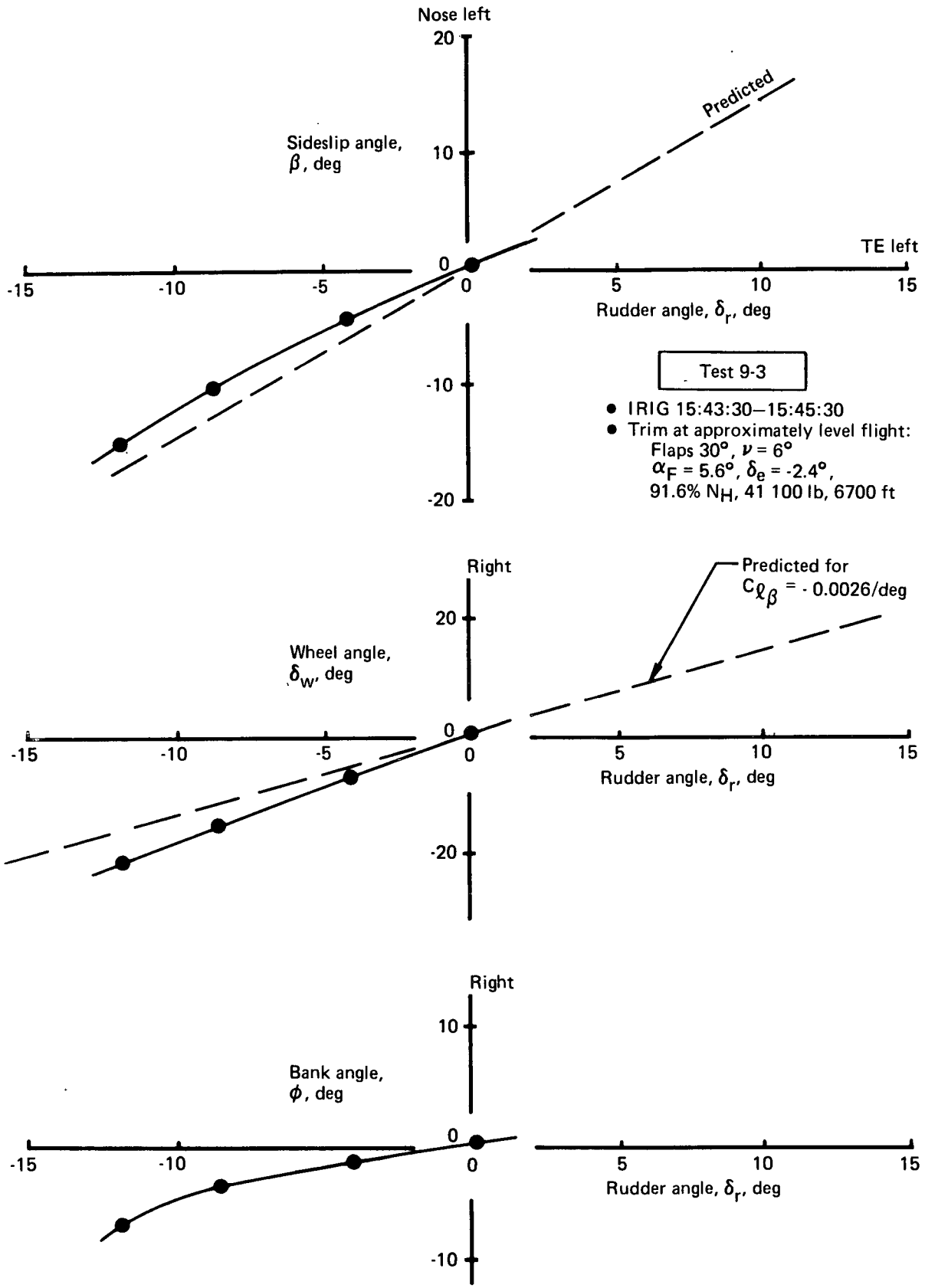

FIGURE 79.–STEADY SIDESLIP–FLAPS 30°, 90 KT

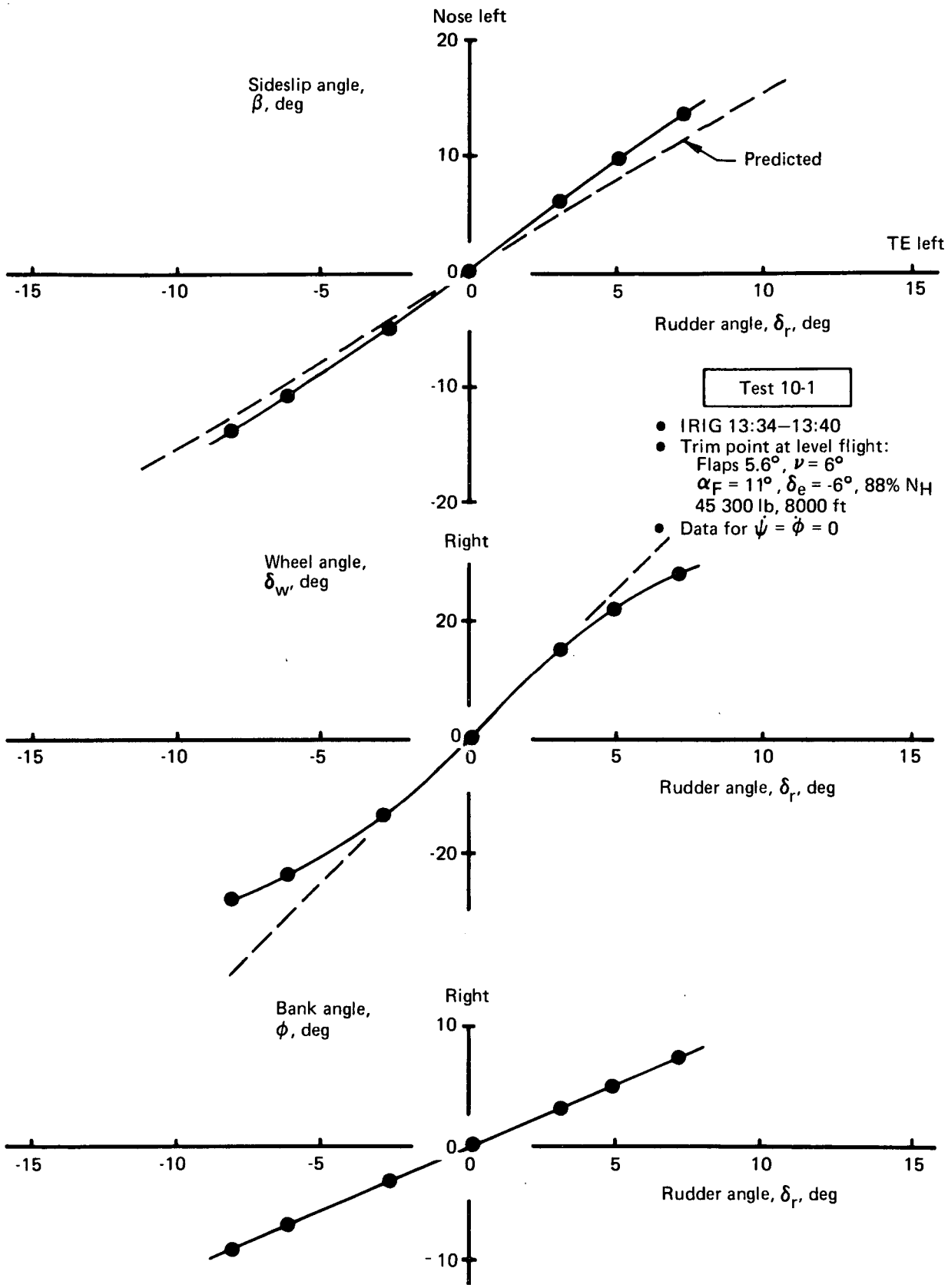

FIGURE 80.–STEADY SIDESLIP–FLAPS UP, 120 KT

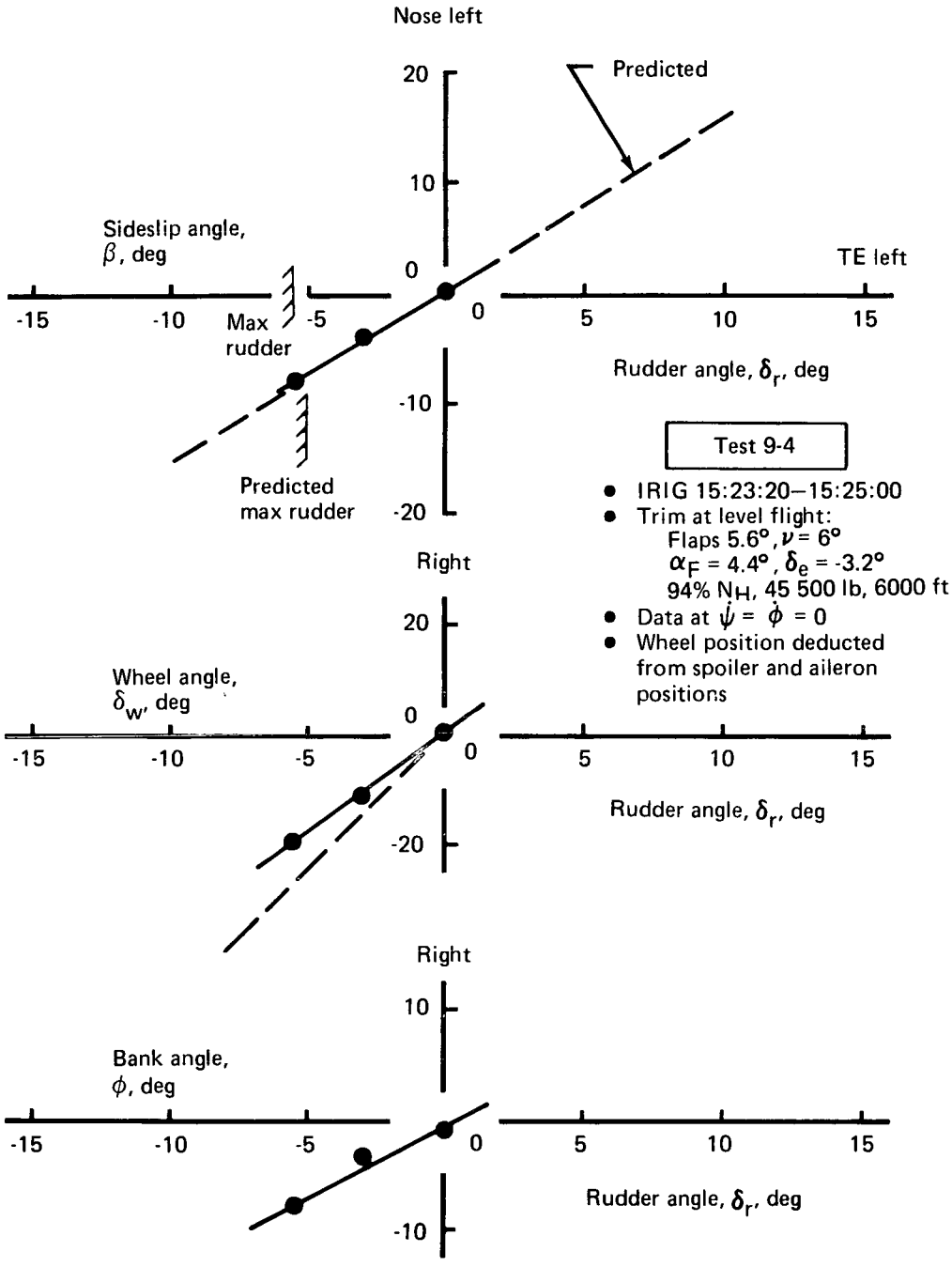

FIGURE 81.–STEADY SIDESLIP–FLAPS UP, 166 KT

directional axes out to 15°β demonstrated in flight. Lateral stability (dihedral effect) does exist at STOL conditions, and the data correlate better with C_{ℓ_β} = -0.004/deg predictions than with C_{ℓ_β} = 0. Wind tunnel data indicated C_{ℓ_β} to be between -0.004 and 0. The pilot also demonstrated that the airplane rolled into a turn in the conventional direction using only rudder. Stable dihedral effect is an encouraging result of the test program.

Directional stiffness, C_{n_β}, appears to be slightly higher than predicted at flaps 65° and 65 kt for large sideslip angles. (Rudder power is estimated to be near that predicted based on engine-out control.) The airplane exhibited a directional "snaking" tendency below 90 kt for $\beta \approx \pm 1°$ to 2° indicating very low directional stiffness about β = 0°. Net sideforce is low, as predicted. Only about half the available rudder deflection was used to attain 15°β. The airplane should be capable of reaching considerably larger sideslip angles. At the flaps up, 166-kt condition sideslip was limited by rudder blowdown, as predicted (only single hydraulic system to rudder above 100 kt). Lateral-directional stability at flaps up is near to the prediction.

Lateral-Directional Control

Directional control power on the Modified C-8A was found to be adequate for engine-out control in addition to the preceding sideslip conditions. Figure 82 presents the "engine-out" control data obtained in flight test. These data represent high-power/idle-power conditions. Rudder required is near to the prediction (nozzles aft) for the average test altitudes. Wheel, bank angle, and sideslip are generally conventional (favorable direction). Nozzle-down (ν = 57°) engine-out checks took only 20° δ_W or about two-thirds of that predicted for the flight condition. Lift and angle-of-attack limitations prevented flight below 63 kt. Lightweight (lower speeds), sea-level (more thrust), engine-out conditions will require more control input; however, it appears that the airplane will not be limited by lack of control capability at any flap setting.

Lateral control surface gearing was measured in the test program. Lateral control system characteristics were found to be satisfactory. Wheel forces were light (12 lb maximum) and centering was positive, after increasing the centering detent breakout force. Lateral trim was maintained within a few degrees of neutral wheel for all combinations of flaps, speed, and power tested.

Lateral control power was evaluated by conducting full wheel roll reversal maneuvers. This maneuver yields maximum roll acceleration at zero roll rate. Figures 83 and 84 show a roll reversal at flaps 30°, 90 kt. The pilot applied wheel to the left and then rapidly reversed direction. Maximum rate of change of roll rate occurs at full wheel as the roll rate itself passes through zero. The maneuver also demonstrates maximum surface rates. From the condition in figures 83 and 84, the following rates were achieved:

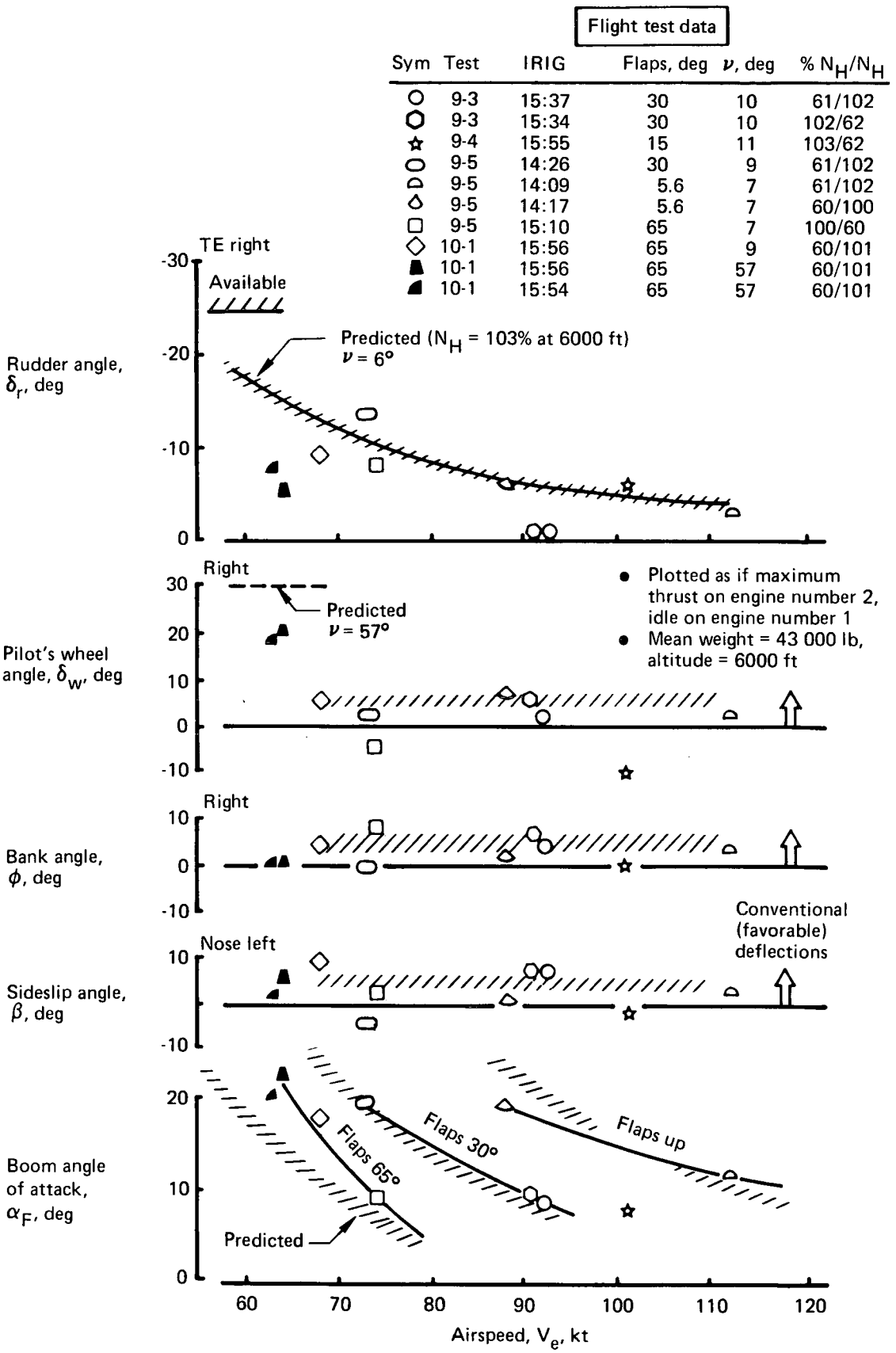

FIGURE 82.—ENGINE-OUT CONTROL SUMMARY

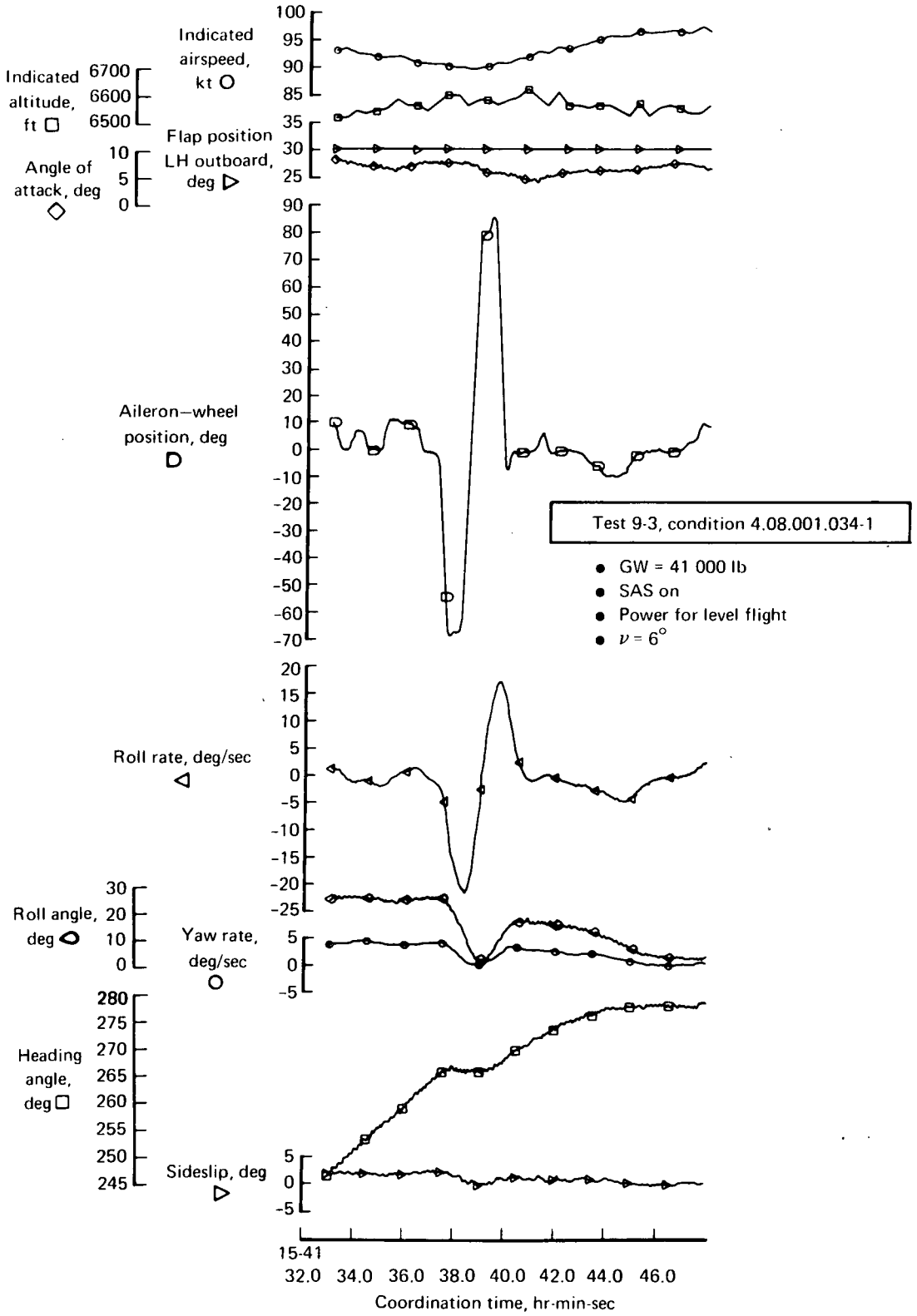

FIGURE 83.–ROLL REVERSAL–FLAPS 30°, 90 KT

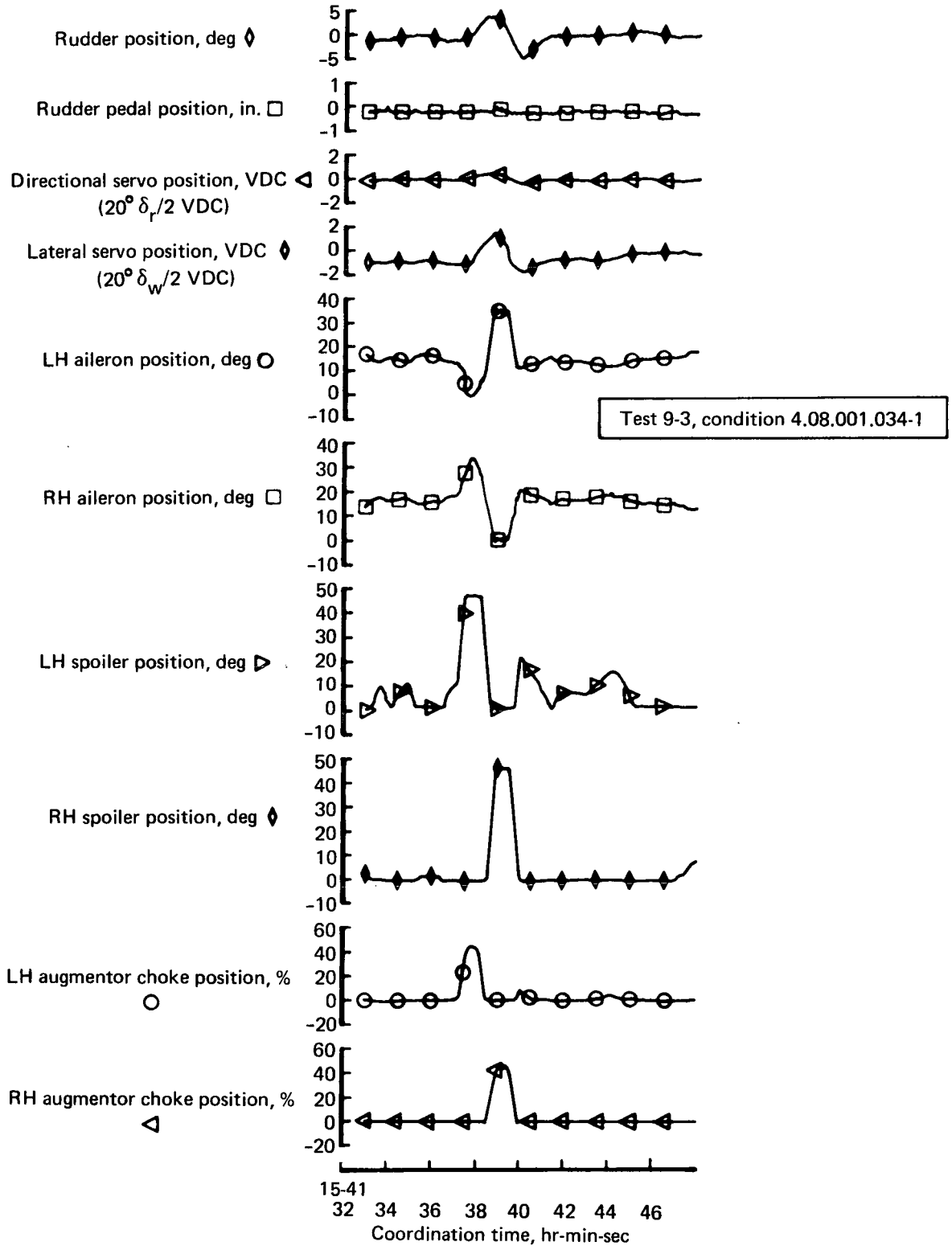

FIGURE 84.–ROLL REVERSAL–FLAPS 30°, 90 KT

$\dot{\delta}_W \geq 200$ deg/sec (1/2 sec stop-to-stop)

$\dot{\delta}_a \geq 50$ deg/sec

$\dot{\delta}_{SP} \geq 120$ deg/sec

$\dot{\delta}_{CH} \geq 90\%$/sec

Full lateral control from neutral wheel can be achieved in less than 1/2 second.

The maximum roll acceleration demonstrated in the flight test program is summarized in figure 85. The airplane has considerable roll power, particularly at flaps up. Flaps up rolling moment coefficient is apparently $C_\ell \approx 0.06$ instead of the $C_\ell = 0.035$-0.040 predicted. The high value is due partially to the 6° flap deflection at flaps up and the chokes acting as ailerons. At flaps down, the airplane exceeds the design criterion of $\ddot{\phi} = 0.4$ rad/sec^2 at 60 kt. Figures 86 and 87 show the roll reversal at 60 kt. Rolling moment coefficients at landing flaps and 60 kt should be on the order of $C_\ell \approx 0.16$.

Control power and characteristics for various hydraulic system failures were not explicitly tested. In the flutter testing, hydraulic power was turned off to the augmentor chokes and aileron power control unit but not to spoilers at flaps up, 110 kt (test 9-2). The pilot could then only command the spoilers by manually driving the ailerons. Friction forces were found to be very high ($F_W \approx 28$ lb). Application of up to 50 lb of wheel force generated only $\pm 1° \delta_a$ and $5° \delta_{SP}$, producing a roll rate of $\dot{\phi} \approx 1$ deg/sec. Because of the high friction forces, the pilot had to apply almost the same wheel force in the opposite direction to center the system. Lateral control in this "semi-manual" mode was very poor. It appears quite likely that a manual reversion landing (flaps 30°, 90 kt) may not be possible.

Lateral control and airplane transient characteristics were evaluated in more than a dozen turn entries. The lateral control system was described as "sensitive" and "responsive" by the pilot. Normal turn entries to 10° to 20° bank angles required less than $20° \delta_W$. In the 60 to 75 kt regime (flaps 65° and 72°) an input of $15° \delta_W$ would produce a 10° bank angle in about 3 sec with a peak roll rate of 5 deg/sec. The initial slope of the roll rate trace showed $\ddot{\phi} \approx 0.1$ rad/sec^2. Further testing is required to quantitatively determine lateral control sensitivity.

Adverse sideslip excursions occurred in the turn entry. Figure 88 summarizes the turn entry coordination characteristics, $\Delta\beta/\Delta\theta$, with airspeed. Values of $\Delta\beta/\Delta\theta$ below 0.3 are generally considered acceptable. The lateral-directional SAS turn coordination augmentation produces acceptable turn entry down to 60 kt. With SAS off the airplane has degraded turn entry characteristics, as expected.

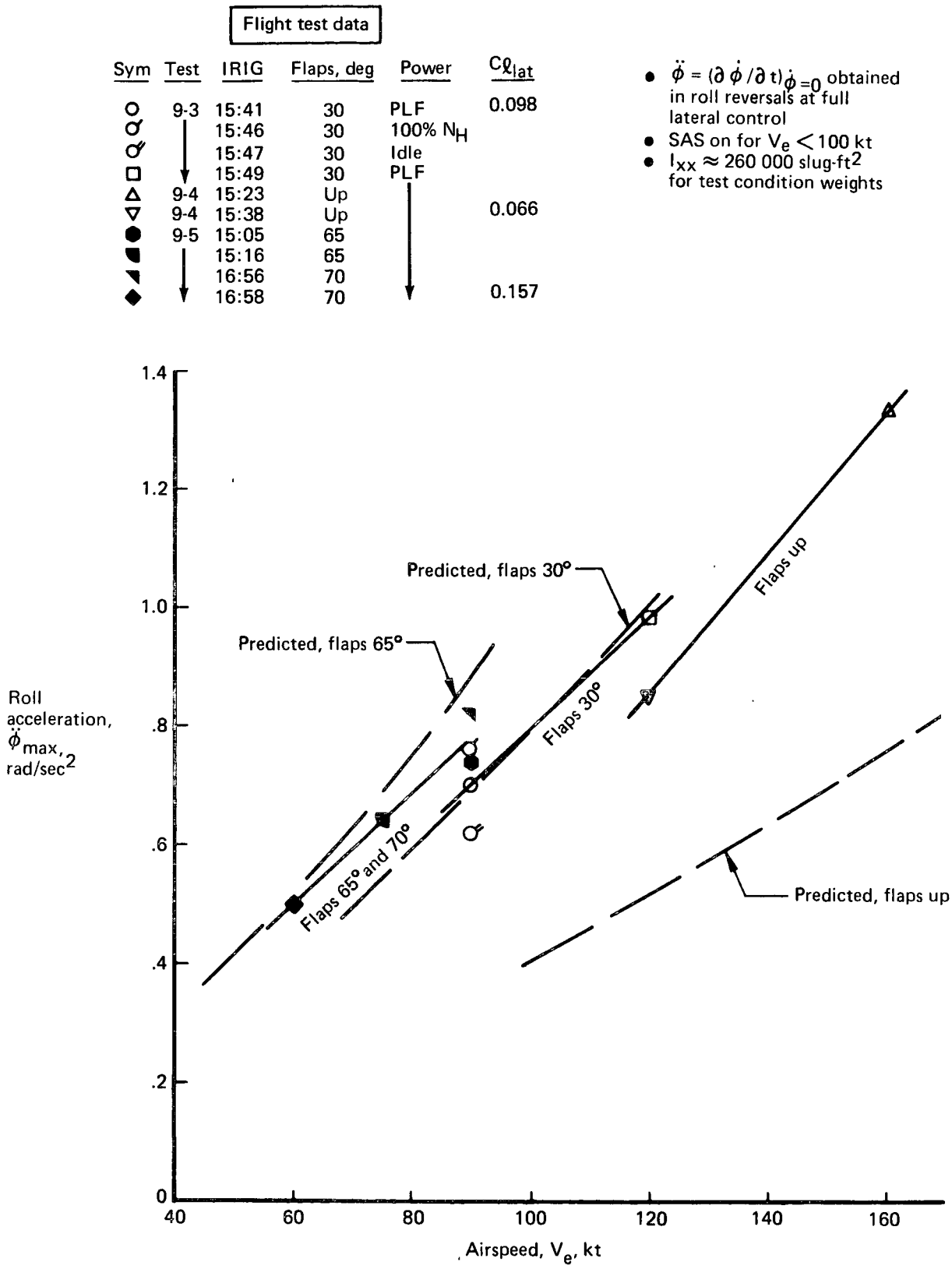

FIGURE 85.–MAXIMUM ROLL ACCELERATION FROM ROLL REVERSAL MANEUVERS

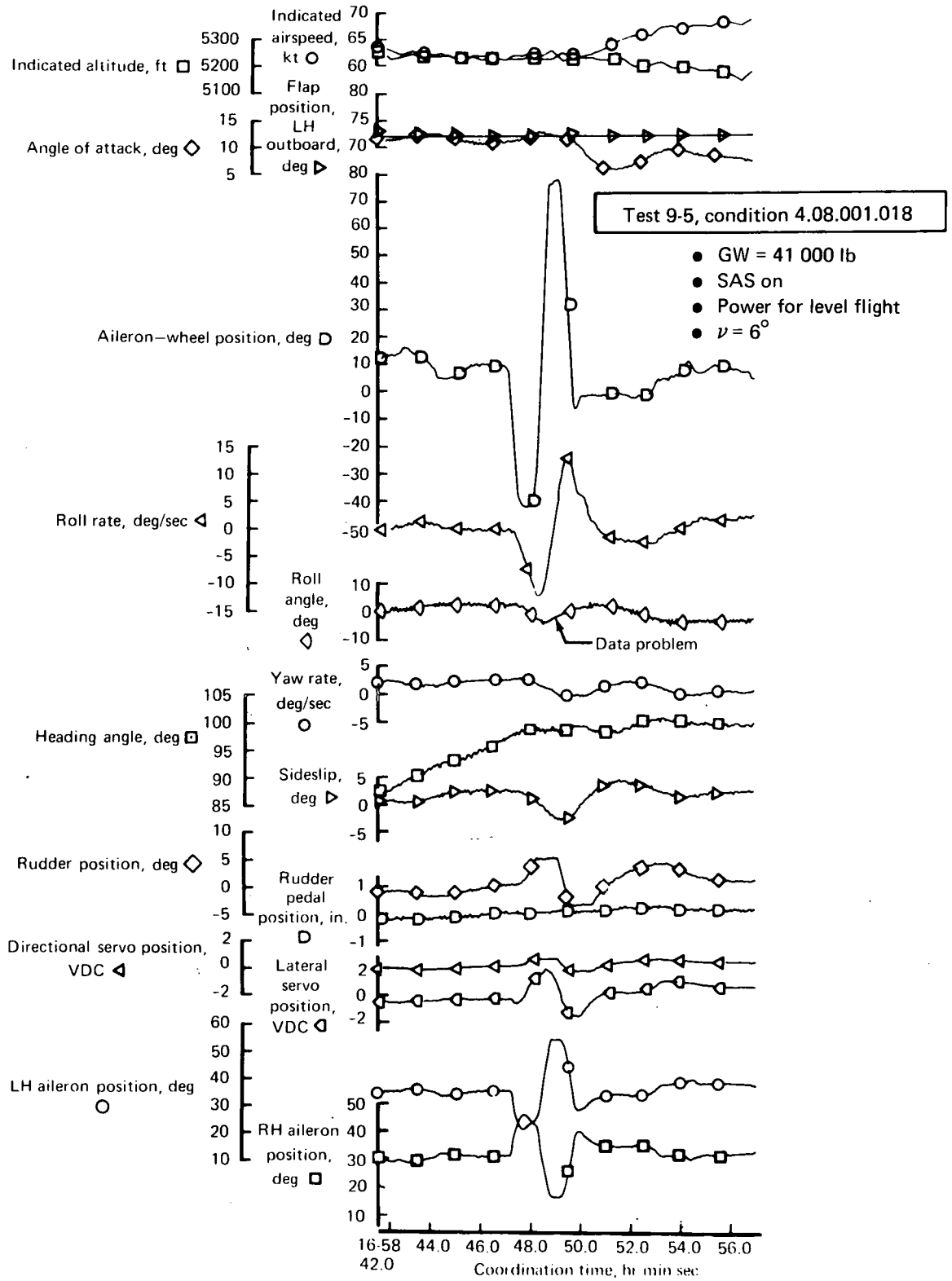

FIGURE 86.–ROLL REVERSAL–FLAPS 70°, 60 KT

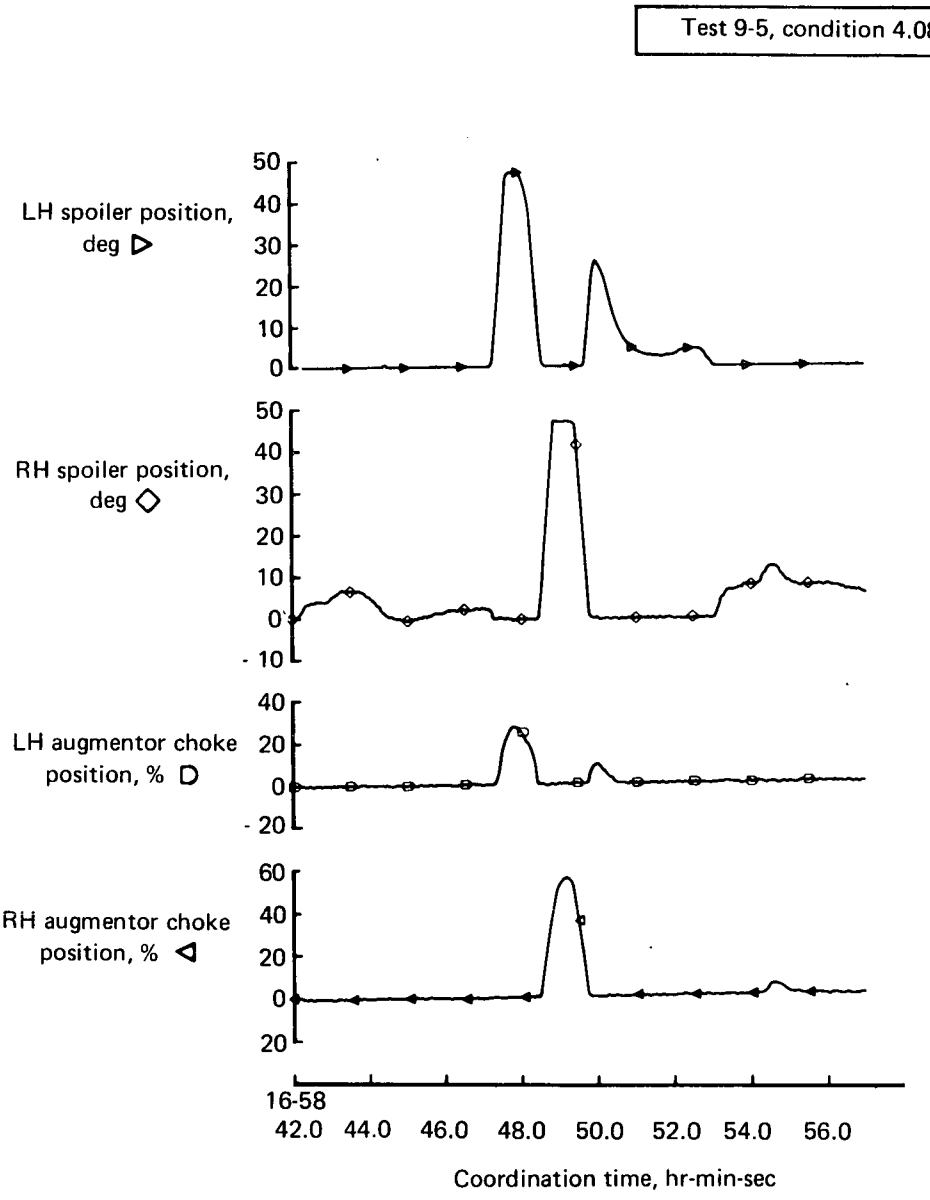

FIGURE 87.–ROLL REVERSAL–FLAPS 70°, 60 KT

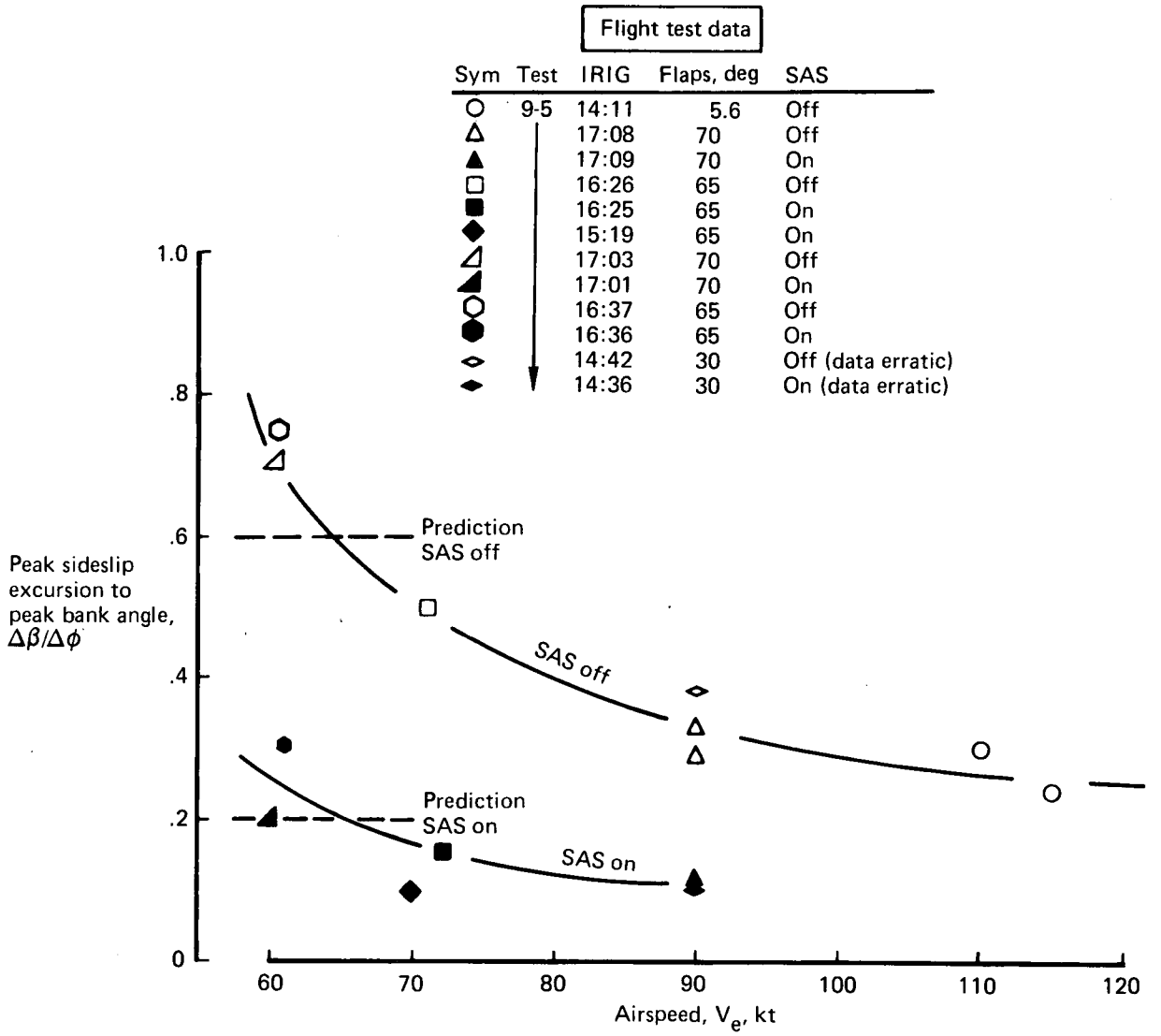

FIGURE 88.—TURN ENTRY COORDINATION DATA SUMMARY

Selected turn entry time histories are presented in figures 89 through 93. The flaps up turn entry in figures 89 and 90 shows good roll rate and bank angle response. Roll mode time constant, τ_R is estimated at about 1 sec. Turn rate was almost immediate indicating "favorable" yawing moment from the lateral control. Steady-state turn rate was established within a second of achieving steady-state bank angle. Sideslip excursion was small compared to the bank angle.

An SAS-off turn entry at flaps 72° and 62 kt is shown in figures 91 and 92 at a STOL approach condition set up by the pilot. Considerable adverse sideslip was generated, and change in heading lagged initial wheel input by over 3 sec. Yaw rate did not reverse in this instance. (There was virtually no yaw rate reversal for any of the SAS-off turn entries.) The airplane was judged controllable to a landing with SAS off.

An SAS-on turn entry at flaps 65° and 62 kt is shown in figure 93 at a STOL approach condition. The sideslip excursion is greatly reduced by the SAS. Even with a slight initial opposing yaw rate, the heading changed to the proper direction within 2 sec. The lack of adverse yaw rate in a turn entry is indicative of the low yawing moment due to lateral control.

Lateral-Directional Dynamic Stability

The pilots evaluated lateral-directional dynamic characteristics at a limited number of flight conditions. Figure 94 presents the Dutch roll summary. Both the SAS-off and SAS-on period came out shorter than predicted, indicating greater directional stiffness. Unaugmented Dutch roll damping tends to be low at reduced airspeed. This characteristic follows the trend toward greater dihedral effect, as also seen in the static stability data. The airplane exhibited mostly yawing in the Dutch roll with $|\phi/\beta|$ amplitude ratio at about unity. SAS-on Dutch roll damping was quite good at flaps 65° and acceptable at flaps 30° for large-amplitude disturbances. A low-amplitude "snaking" characteristic was found at speeds below 90 kt. The amplitude on yaw rate seen in this limit cycling (about a 6 to 8 sec period) would only generate on the order of $\pm 0.2°\ \delta_r$ from the SAS. At 60-kt conditions the pilot described the airplane as "snaking" and "wallowing" ±2° in bank angle and ±3° in sideslip, even with the SAS on. An example of this tendency is seen in the stall entry maneuver at 60 kt shown in figures 58 and 59. This characteristic, when added to the airplane's poor static longitudinal stability, made flight at 60 kt very unpleasant. The SAS gains were originally selected to offset low dihedral effect. Improvement to the SAS yaw damping characteristics is warranted.

Spiral stability was evaluated throughout the flight envelope down to the 60-kt STOL condition. SAS-off spiral stability was found to be nearly neutral in all cases and often masked by small lateral trim offsets. This characteristic again indicates positive dihedral effect. With the SAS on, the pilots noted definite spiral stability at all conditions.

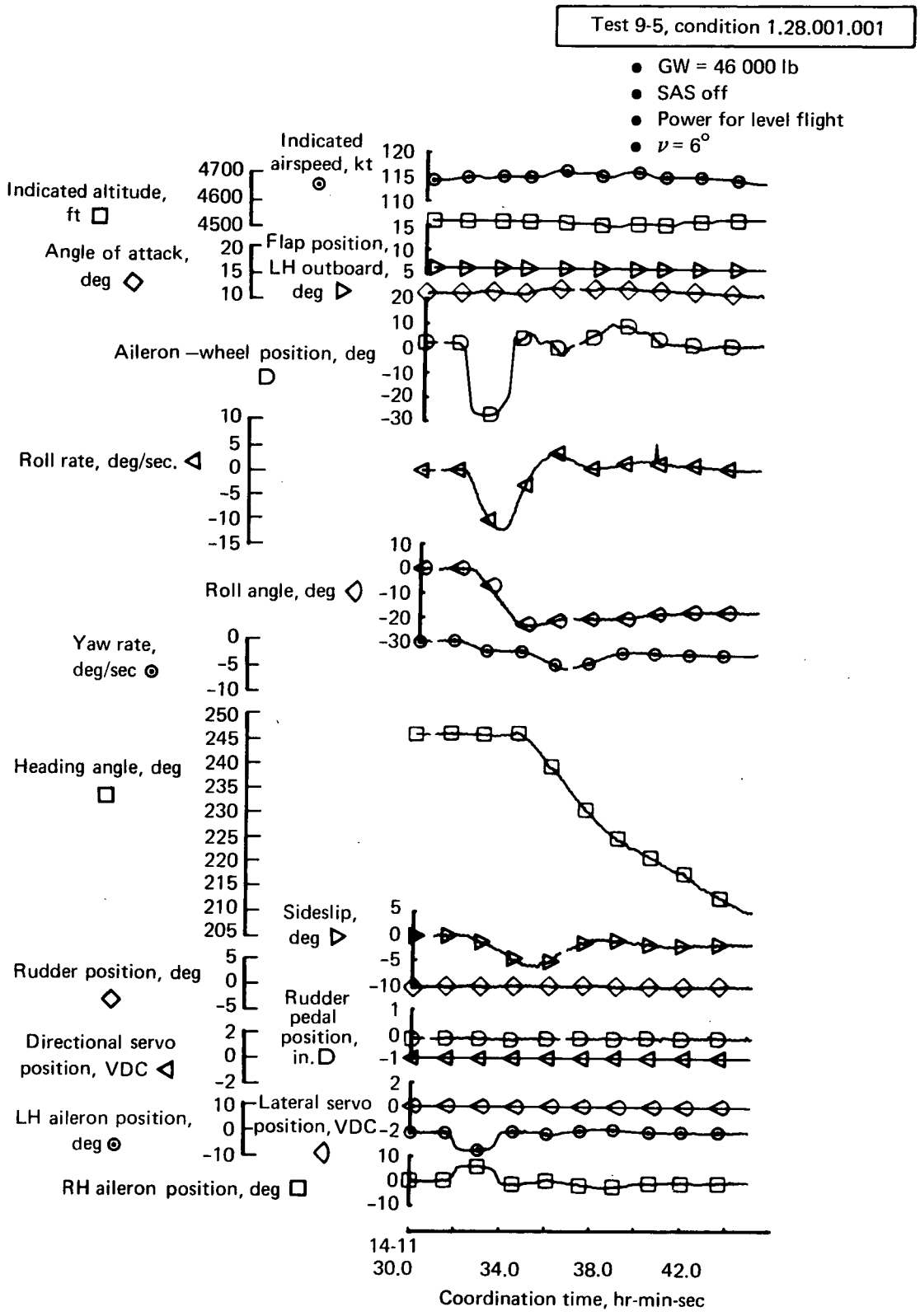

FIGURE 89.—TURN ENTRY— FLAPS UP, 115 KT

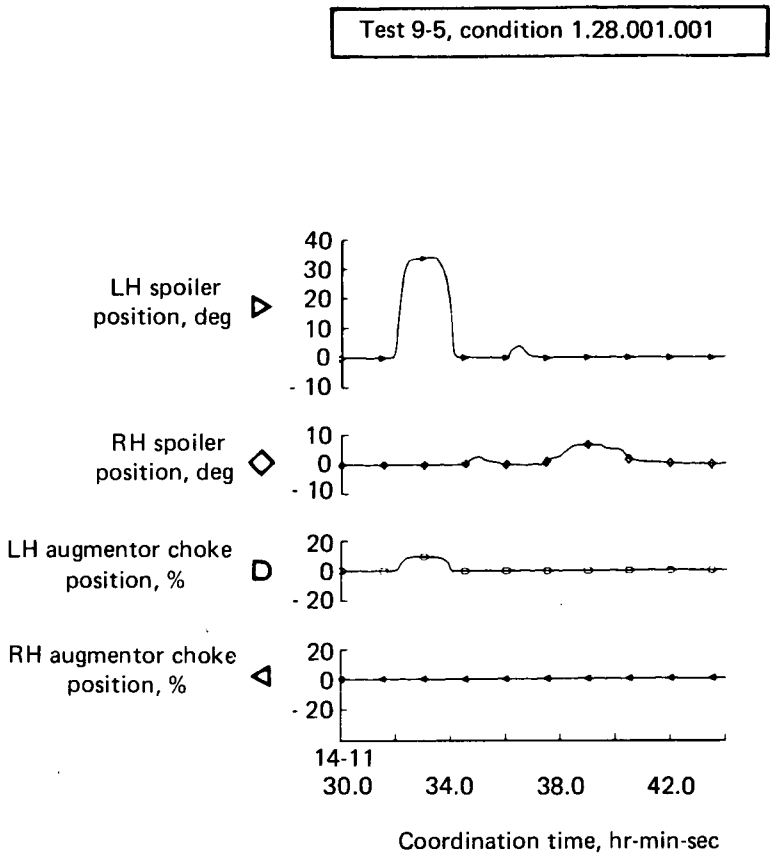

FIGURE 90.—TURN ENTRY—FLAPS UP, 115 KT

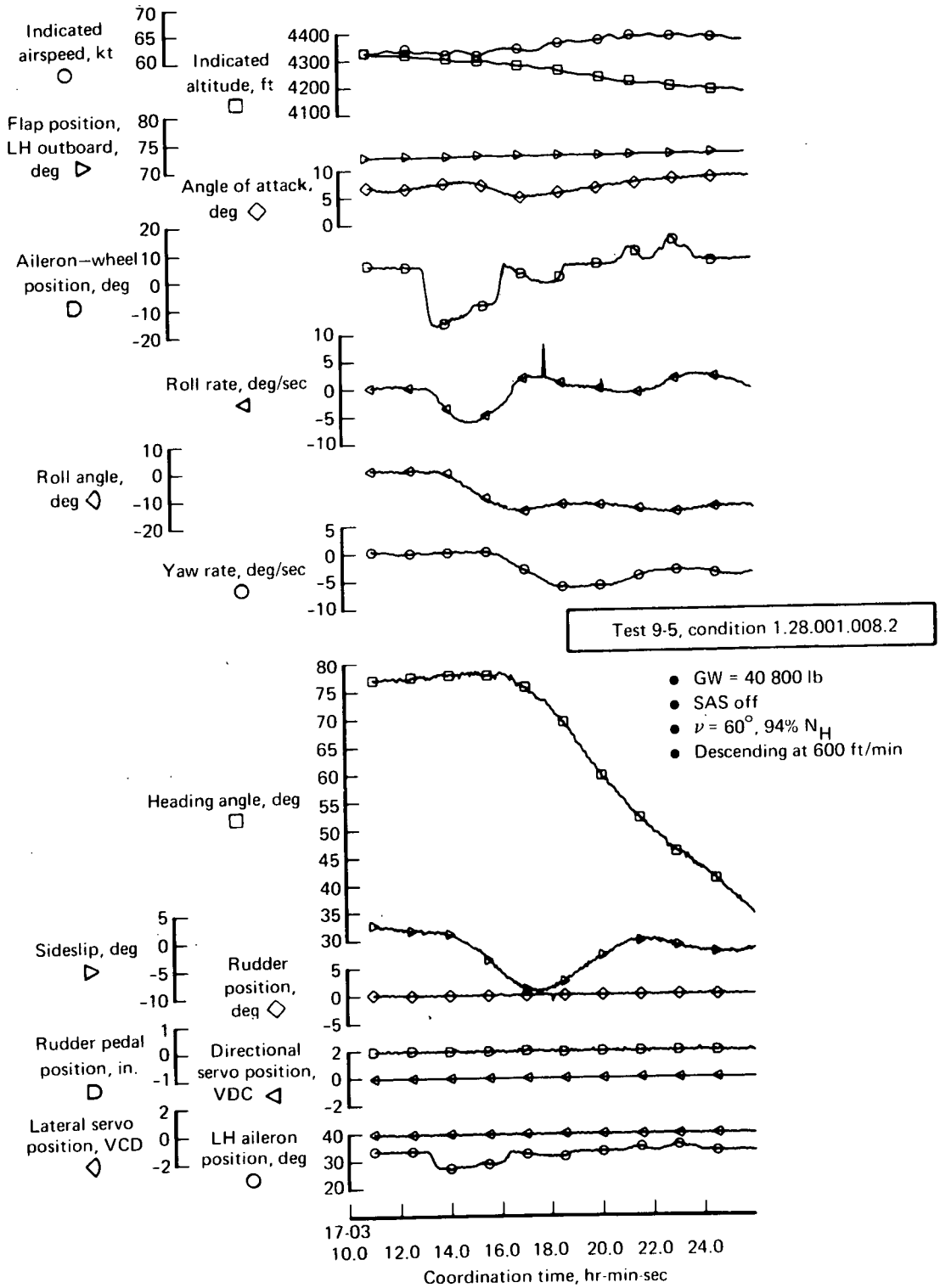

FIGURE 91.–TURN ENTRY–FLAPS 72°, 62 KT

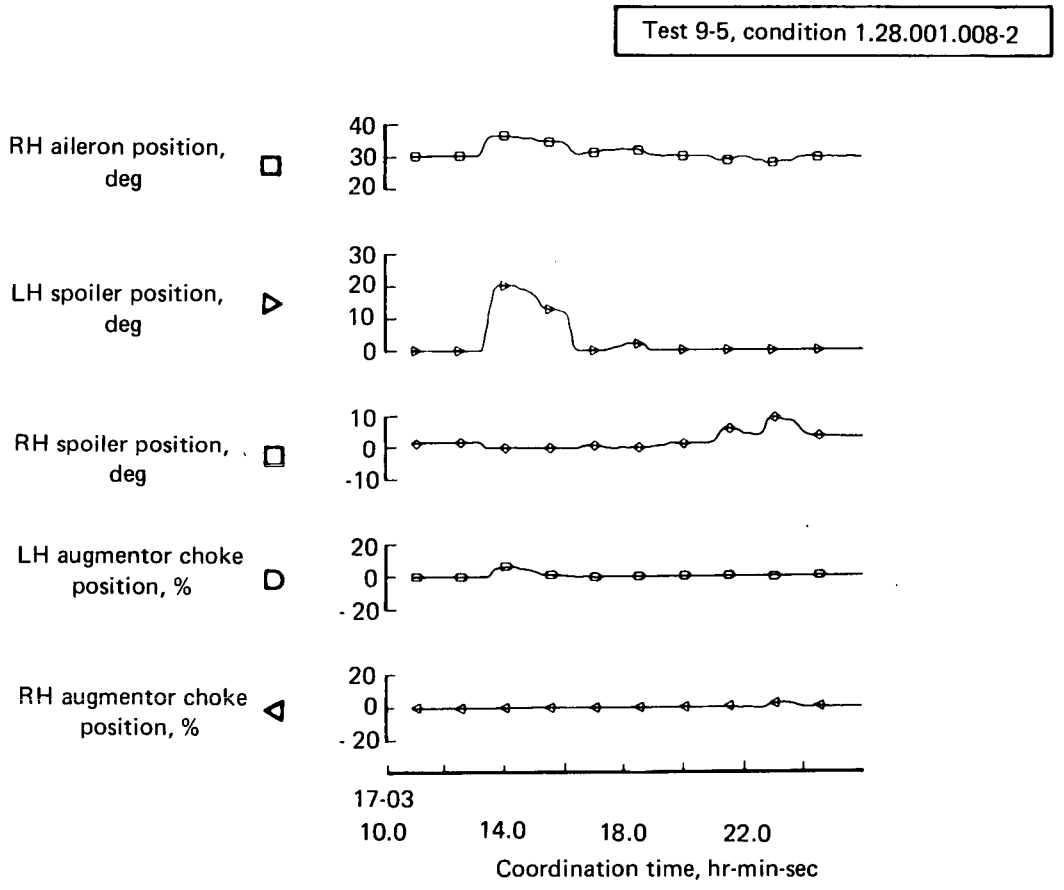

FIGURE 92.–TURN ENTRY–FLAPS 72°, 62 KT

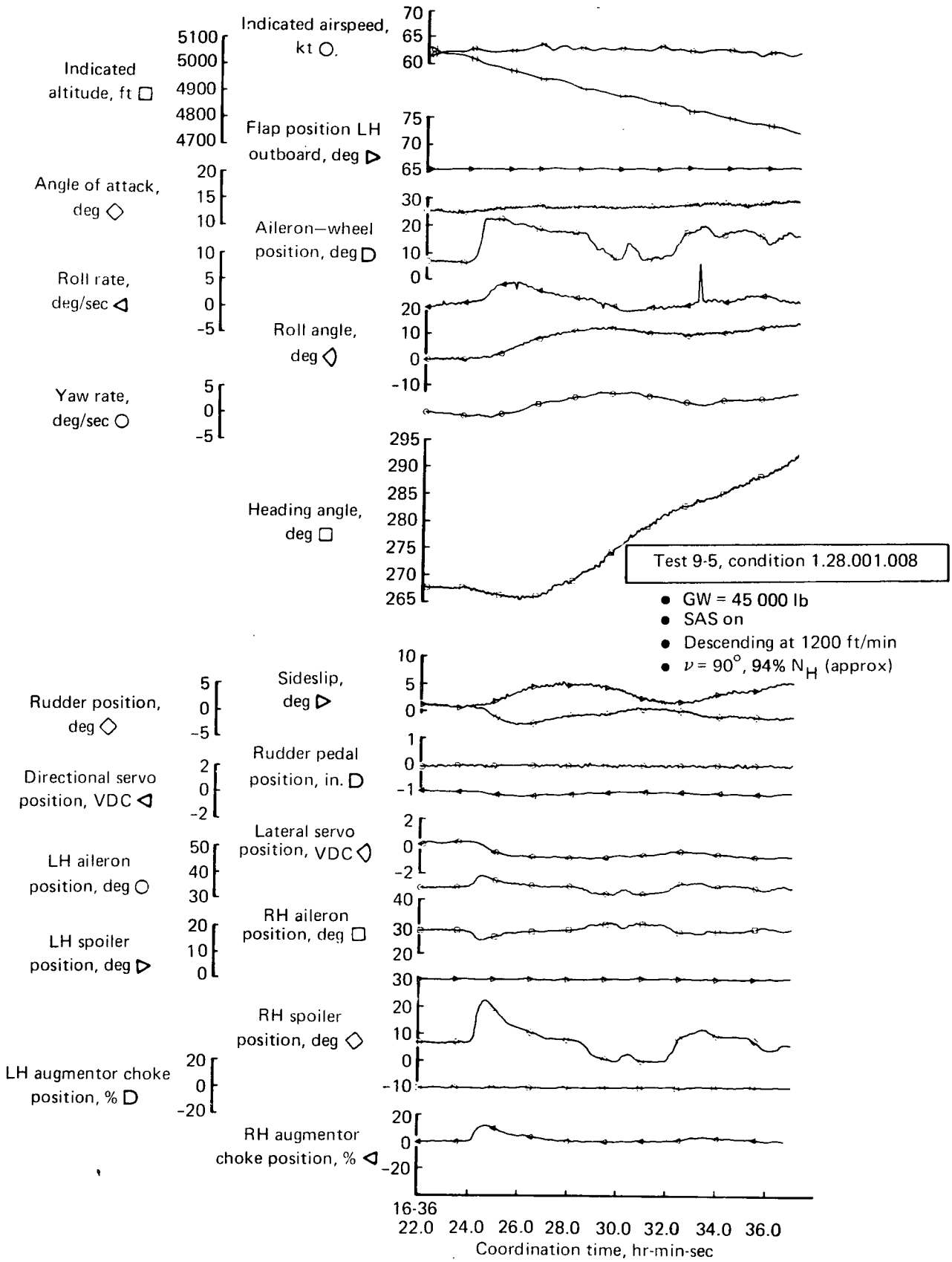

FIGURE 93.–TURN ENTRY–FLAPS 65°, 62 KT

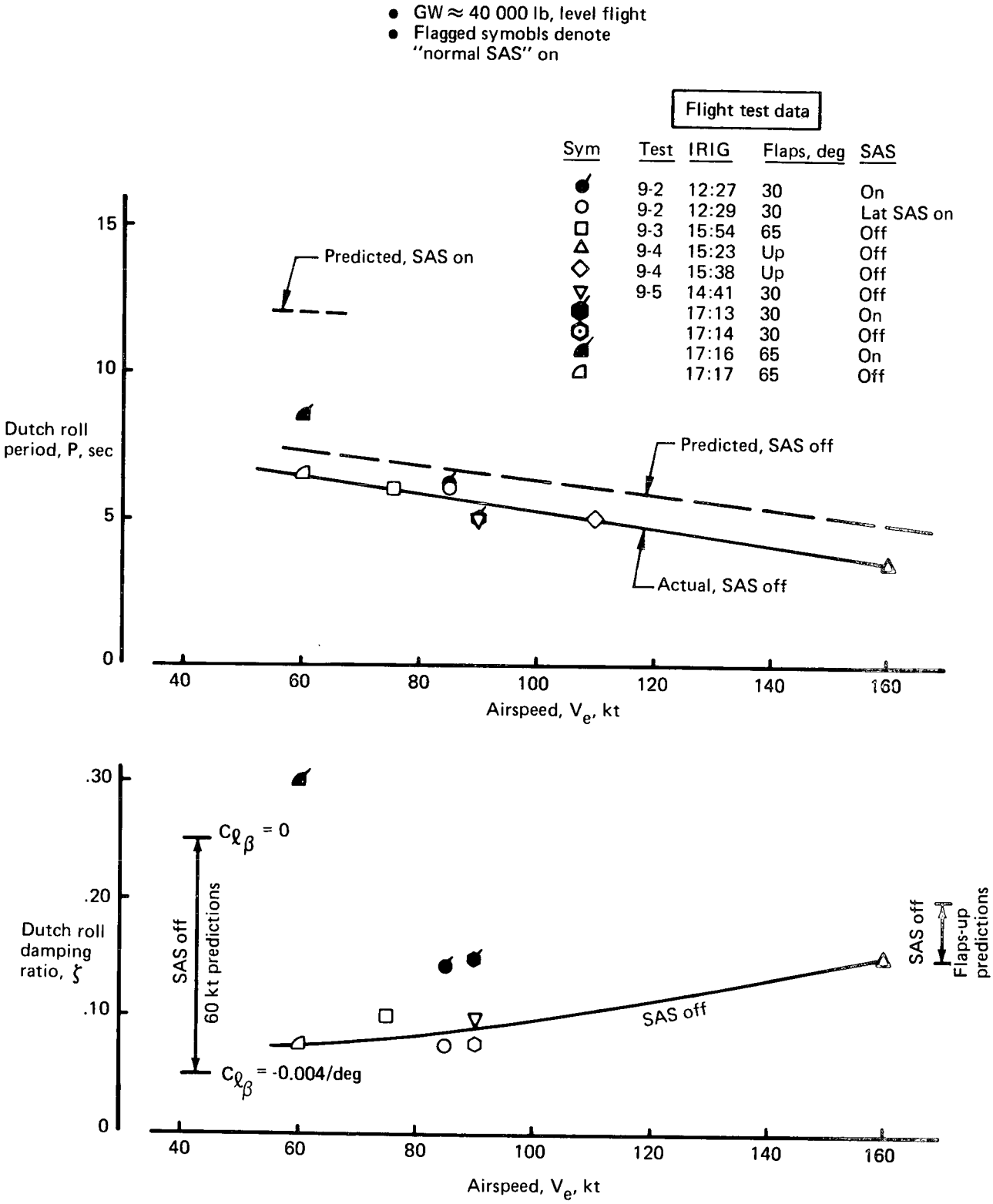

FIGURE 94.–DUTCH ROLL DATA SUMMARY

PROPULSION SYSTEMS TESTS AND OPERATION

ENGINE OPERATION

The engines are installed as during the ground testing, that is, with serial number 8745 in No. 1 position and 8746 in No. 2 position. Their performance and operation have been satisfactory during the flight test program. An incident occurred during an in-flight restart of engine 1 on May 18, damaging the nacelle but not the engine.

The following conclusions relate to topics which are written up more fully in subsequent sections.

- The engine performance is the same in flight as was determined during the ground testing.
- The deceleration time is longer in flight than on the ground because of a control system characteristic.
- Apart from slow decelerations below 90% N_H, the engines responded satisfactorily to throttle movement in any flight condition.
- Forward thrust or idle speed should be selected at 60 kt after landing to avoid reingestion.
- The vibration level of engine 1 was still satisfactory after the repair of foreign object damage.

Some minor additional observations are:

- Engine oil usage and leakage have required some attention. The usage is not excessive, but the leakage is scheduled for attention before aircraft delivery.
- The original conical primary exhaust nozzles cracked at their sheet metal outlet stiffener after about 12 hr of ground testing. Nozzles with the replacement machined outlet stiffener showed no cracking after 25 hr.
- The airflow control regulator of engine 2 was suspected to have a drifting calibration during the ground testing. It has caused no further trouble since then.

Performance

Sample points were checked from all flights at conditions which involved at least 1 min of stable running. Using nondimensional ratios based on the stagnation pressure and temperature at engine inlet, the flight performance was as determined during the ground testing. This is demonstrated by the representative flight test points plotted over the curves from the ground test report, as shown in figures 95 through 98.

The points plotted were taken from the Boeing PCM data system. Most parameters were unchanged, and the instrumentation appeared reliable. One parameter which apparently shifted was P_{S8} for engine 2, which now lines up better with the test bed results. The only other parameter in trouble was T_6 for engine 1, the computer printout showing about ±10° C scatter due to noise.

The fuel consumption points from the PCM system are believed to be too high. During the ground testing on April 11, the cockpit indicators were read as the performance points were run. Both sets of results are shown in figures 96 and 98, and it can be seen that the PCM system reads up to 7% higher than the cockpit gages. As the cockpit readings plot close to the test bed curves, which were obtained using calibrated flow meters, and as other flight and ground test measurements line up well with their respective test bed curves, it is believed that the cockpit gages give a more accurate indication than the PCM system.

Although the basic parameter of primary thrust is specified in terms of exhaust pressure level, N_H was found to be a more convenient operating parameter. The difference in thrust level is not apparent to the pilot.

Acceleration Characteristics

It was found during the second flight (May 5) that engine 1 took a very long time to decelerate past 89% N_H at 5000 ft, although it later decelerated satisfactorily at 7000 ft. The problem recurred on the third flight (May 11), when it was slow to decelerate past 86% N_H at 4000 ft, but was satisfactory at 6500 ft.

The deceleration time was checked before flight on May 12, and found to be 14 sec from 600° C EGT to 71% N_H. (The required time is 13 to 14 sec.) No adjustment was made, therefore, but the engine was very slow to decelerate at 9000 ft in the next flight. The deceleration adjuster was screwed out one sixteenth of a turn on May 15, which would reduce the deceleration time to 13 sec. In flight on May 16, the engine was found to accelerate and decelerate satisfactorily at the same rate as engine 2, so was acceptable.

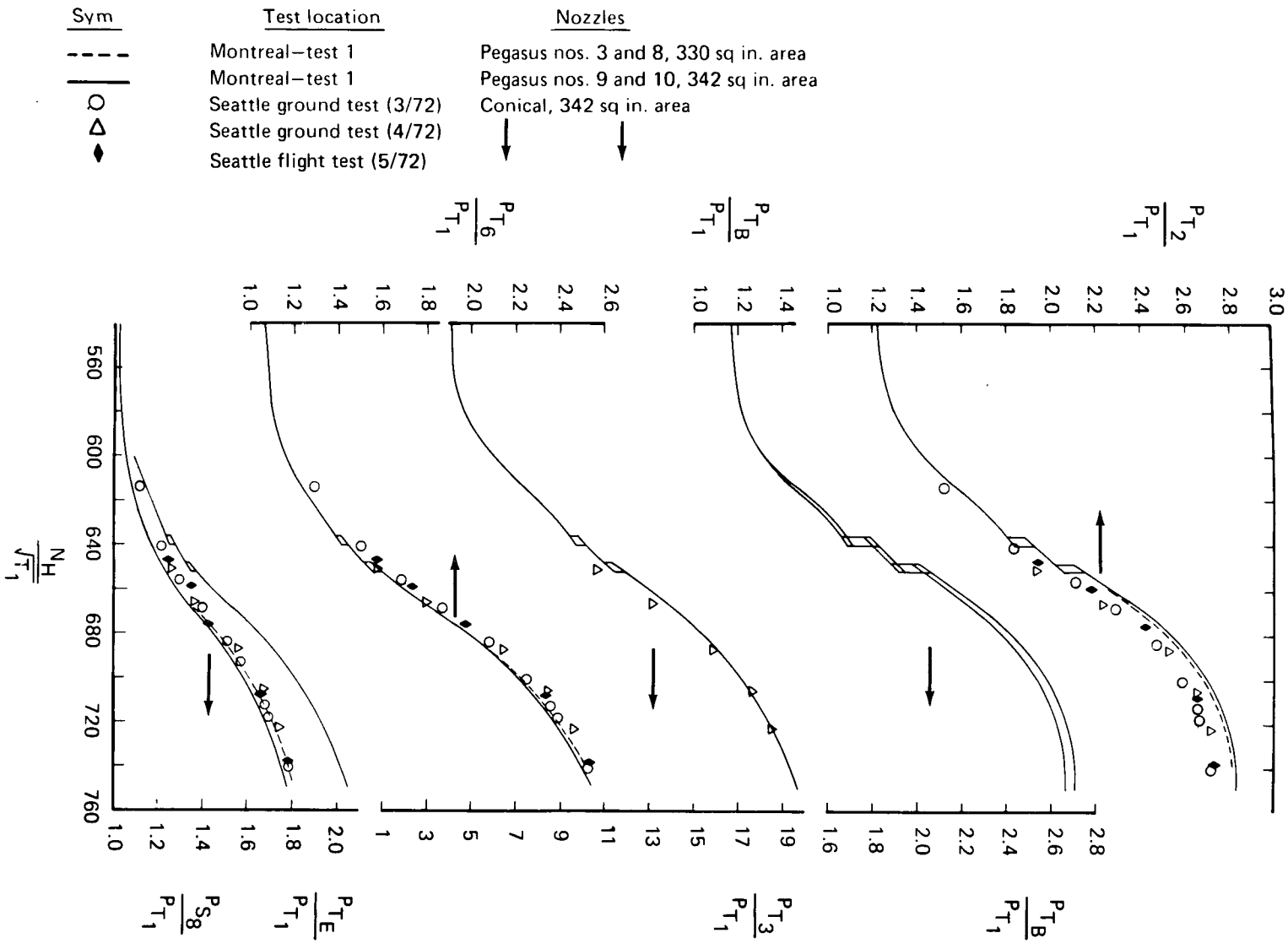

FIGURE 95.–PRESSURE RATIOS, ENGINE 1 (8745) TEST

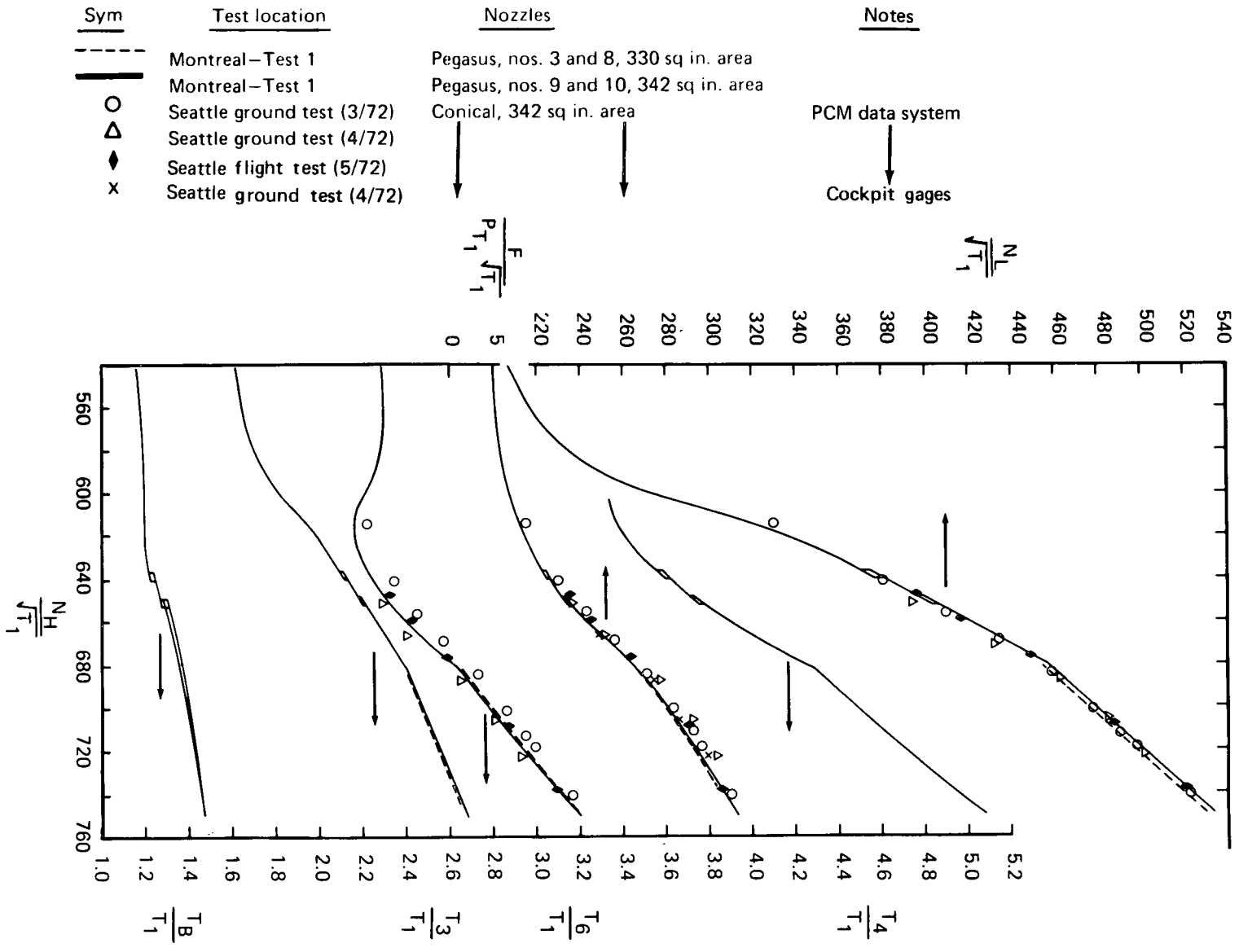

FIGURE 96.–TEMPERATURE RATIOS, ENGINE 1 (8745) TEST

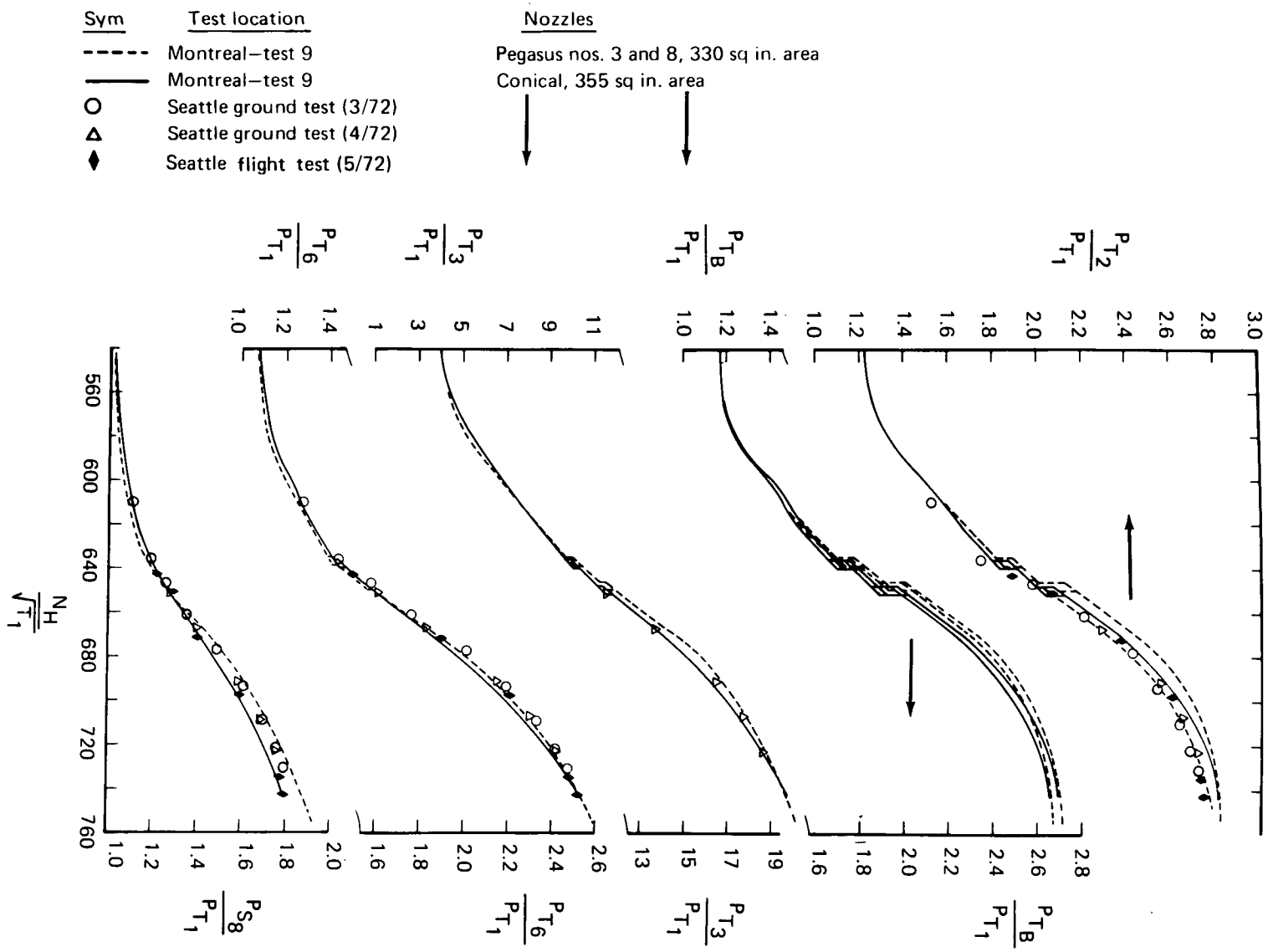

FIGURE 97.—PRESSURE RATIOS, ENGINE 2 (8746) TEST

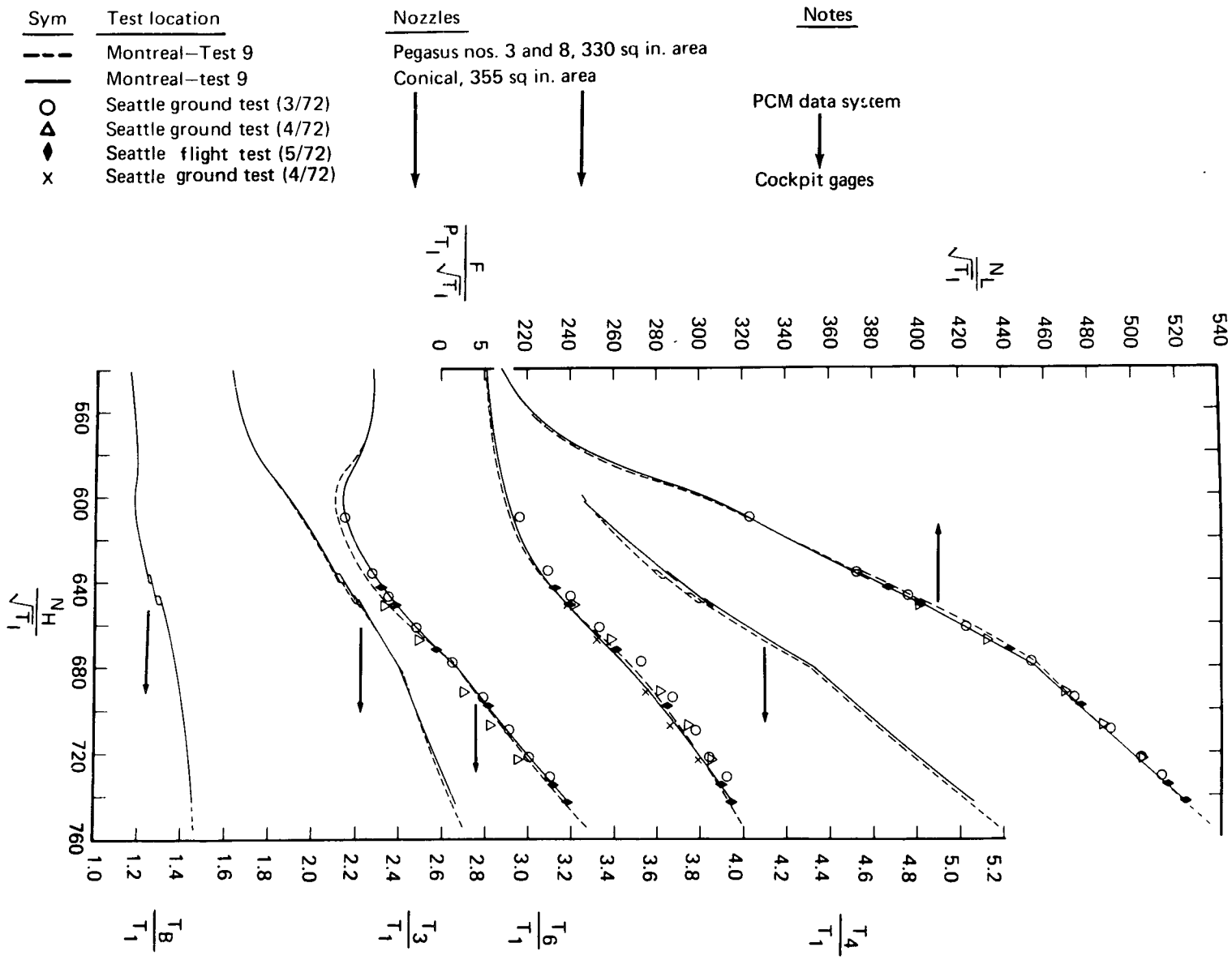

FIGURE 98.—TEMPERATURE RATIOS, ENGINE 2 (8746) TEST

This phenomenon is likely to recur, and is a function of the very slow deceleration through the 90% to 80% N_H range. The deceleration "plateau" is the result of using a longer than standard deceleration time, to isolate the engine from the effect of the large wing duct volume which could cause engine surge during a fast deceleration. However, the "plateau" makes the deceleration very sensitive to minor adjustment, and therefore also to the different inputs experienced at altitude. Because the acceleration time is not affected, it is not considered a hazard.

Engine Response in Flight

A rapid handling check was done for each engine on May 18. The altitude was 8000 ft, airspeed 95 kt, and angle of attack 15°. The sequence used was:

1) Rapid deceleration from 89% N_H to idle

2) Immediate acceleration to emergency power

3) Immediate deceleration to 88% N_H

4) Immediate acceleration back to emergency power

5) Return to 89% N_H

The engines followed these maneuvers without trouble. Item 1 took a long time, but the sequence of 2, 3, and 4 was not delayed by the long deceleration characteristics.

Reverse Thrust Limitations During Taxi

Taxi testing was carried out on May 4 to test the operation of the primary nozzle control mechanism when loaded by high power settings. This was done with sufficient speed to protect the tires from the hot gas. However, during some lower speed runs, there was sufficient exhaust gas reingestion to cause surging (see table X).

Surging is not a regular occurrence on Spey engines, and conditions causing surge should be avoided. Extensive investigation after these occurrences revealed no internal damage and only a very slight FOD mark on one stage 2 compressor blade on engine 2, which was polished in place.

It is recommended that forward thrust or idle power should be selected when the speed falls below 60 kt after landing, to prevent reingestion.

TABLE X. –TAXI TESTING

Engine	N_H, %	IAS, kt	Nozzle angle	Type of surge
Both	96	43	108	Bang
1	92	47	108	Rumble
1	92	50	108	Rumble
Both	92	53	108	None

Foreign Object Damage–Engine 1

Some minor FOD was observed on a stage 2 rotor blade of engine 1 after a flight on May 5. It had not been present after the surge incidents on May 4, and the nozzles were not vectored during or after the landing on May 5. It is therefore not known how the material was picked up, and the object itself was not found or identified. It left no thread imprint, so a nut or stone is suspected.

The blade damage was inaccessible and at the limit for dressing in place. Therefore, the top half of the compressor casing was removed to gain access and look for damage farther back. Some LP stage 4 blades were found damaged at the trailing edge, beyond normal repair limits. Inspection visually and by borescopes revealed no damage to the HP compressor. The LP compressor rotor was therefore removed by a Rolls-Royce (Canada) repair party, new blades fitted, and the engine reassembled. Damaged blades were replaced with new blades of the same weight as follows: stage 2–4 blades; stage 3–1 blade; stage 4–4 blades. Some other blades and damaged stator vanes were dressed smooth.

During the subsequent engine run, no vibration was apparent, and the engine was cleared for flight on May 11. However, the opportunity did arise to record vibration levels during an engine ground run on June 5, which demonstrated that the vibration level was unchanged. The reference vibration levels, against which any future tests should be checked, are shown in table XI with the original test results in mils.

TABLE XI.–REFERENCE VIBRATION LEVELS (MILS)

Speed, N_L, %	Idle	40	50	60	70	80	90	100	105
Speed, N_H, %	Idle	73	80	84	87	90	94	100	102
Engine 1, June 5,	0.1	0.25	0.35	0.35	0.4	0.6	0.8	0.9	–
(Feb 24)	(0.1)	(0.4)	(0.3)	(0.3)	(0.4)	(0.5)	(0.7)	(1.0)	(1.1)
Engine 2, Feb 24	0.1	0.1	0.3	0.4	0.5	0.6	0.8	1.1	1.2

ENGINE AND NACELLE ENVIRONMENT

Temperatures at various engine accessories (and at other points of interest) in nacelle zones 1 and 2 have been measured during flight to check whether the operating temperature limitations for these accessories are being exceeded. In addition, the differential pressure between zone 2 and zone 1 for each engine has also been recorded. The zones and instrumentation locations are shown in figure 99.

The following paragraphs discuss each of these measurements. Comments are made on the values recorded during a typical flight, namely test 9-5.

Zone 1 Ambient Temperature

This is a thermocouple attached to some electrical wiring at a point which is close to a high-pressure bleed pipe. There was some concern that the HP bleed pipe may heat the wiring at this point. The highest temperature recorded was 148° C at the following flight conditions:

Freestream total temperature = 5.6° C
IAS = 69.5 kt
Altitude = 4558 ft
RPM (N_H) = 11 618

The limiting temperature for the wire insulation is 200° C (or 392° F).

Flight test data

Sym	Meas. no.	Instrumentation
⊕	685	Zone 1 ambient temperature
⊕	687	Zone 2 firewall temperature
⊕	692	Exhaust temperature controller
⊕	693	Inlet temperature sensing capsule
⊕	695	Exhaust thermocouple head temperature
⊕	698	Zone 2 ambient temperature firewall
△—△		pressure differential

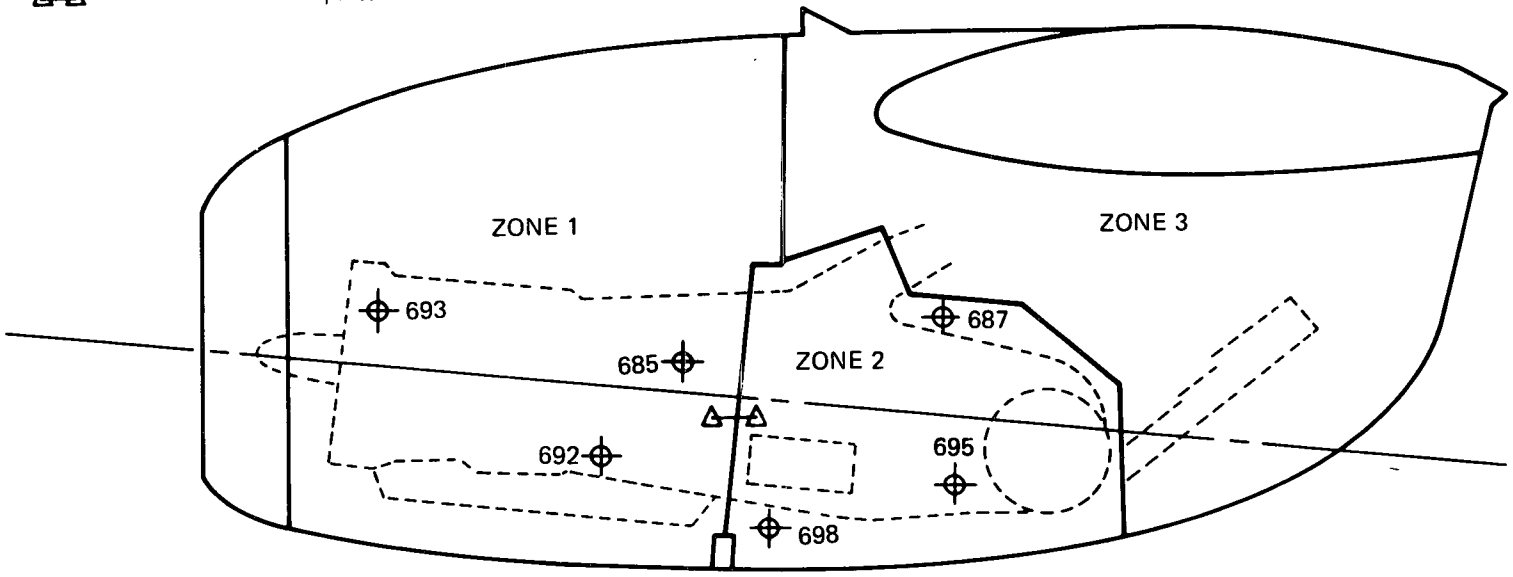

FIGURE 99.—NACELLE INSTRUMENTATION LOCATIONS

Zone 2 Firewall Temperature

This thermocouple was situated at the top of zone 2 near the rear engine mount. This would be expected to be the hottest region in zone 2 since, in addition to being a high point in the zone, it is also near the support plate which is one of the "hot" parts of the engine not covered by a Refrasil insulating blanket. The highest temperature recorded was 179° C, which occurred at the following conditions:

Freestream total temperature	= -14.7° C
IAS	= 74.8 kt
Altitude	= 9118 ft
RPM (N_H)	= 7446
EGT	= 373° C

It is of interest to note that the highest temperature occurred when the engine was operating at approximately idle RPM. This may be due to the fact that the amount of air the cooling injectors pump into the zone depends on the primary nozzle supply pressure, which in turn is a function of engine RPM. A temperature of 175° was reached shortly after the engine was stopped after landing. In comparison, at 12 147 RPM (98.4% normal takeoff RPM) the temperature recorded was 158° C when the EGT was 577° C. The only structural member in this area is the rear engine support link, which is made of stainless steel.

Zone 2 Ambient Temperature

This is a thermocouple situated in the lower part of zone 2. The highest temperature recorded was 88° C. The flight conditions were:

Freestream total temperature	= 14.6° C
IAS	= 73.1 kt
Altitude	= 659 ft
RPM (N_H)	= 10 948
EGT	= 400° C

Exhaust Temperature Controller

This temperature was measured at the exhaust temperature control actuator. The highest temperature recorded was 55° C. Conditions were as follows:

Freestream total temperature	= 7.6° C
IAS	= 105.6 kt
Altitude	= 3354 ft
RPM (N_H)	= 10 701

The temperature limit for this component is 110° C.

Exhaust Thermocouple Head Temperature

This thermocouple is located on the turbine exhaust terminal block. The highest value recorded was 236° C. Conditions were:

Freestream total temperature	= 1.9° C
IAS	= 74.4 kt
Altitude	= 6385 ft
RPM (N_H)	= 11 253
EGT	= 437° C

The limiting temperature for this component, as given in the engine specification, is 130° C. Rolls-Royce (Canada) are aware that the limit is being exceeded but are satisfied that this component will still function properly.

Inlet Temperature Sensing Capsule

This is a thermocouple located on the inlet total temperature sensing capillary carcase. The highest temperature recorded was 35° C. Conditions were:

Freestream total temperature	= 6.5° C
IAS	= 73.9 kt
Altitude	= 3900 ft
RPM (N_H)	= 11 606

The limiting temperature for this component is 110° C.

Firewall Pressure Differential–Engine 1

This is a measurement of the differential pressure between zone 2 and zone 1 (differential pressure, ΔP, recorded as positive when zone 2 pressure is higher than that of zone 1). The specification requires that ΔP should be positive at all times, when the engine is operating, to ensure

that no fuel vapor leaks past the firewall from zone 1 into zone 2 where it may ignite in contact with hot parts of the engine. The results are somewhat erratic, but at lower speeds ΔP is essentially positive for most of the time. However, it is noted that ΔP registered a small negative value during the period at which the aircraft was flying at approximately 160 kt. Recent calculations, in which the flow into and out of zone 1 was studied, indicated that the pressure in this zone will increase with forward speed, which may explain the reversal of ΔP at the higher speeds.

To improve the situation, a further ventilation exit has now been added to zone 1. In addition, the performance of the ventilation ejector at the top of zone 1 (which pumps air out of the zone) has been improved by increasing the size of the supply pipe to the primary nozzle, thereby reducing pressure losses, and the seal between the jet pipes and the nacelle skin has been made more effective to increase the pressure in zone 2.

Firewall Pressure Differential–Engine 2

Essentially the same remarks apply with regard to the ΔP measurements made for engine 2 as for engine 1, except that at 160 kt the values recorded were even more negative. The modifications and improvements described in the previous section to remedy this situation have also been carried out on the engine 2 nacelle.

CONICAL NOZZLE OPERATION

Early experience gained during ground running of the engine suggested that some modifications to the control system and nozzle position indicators were required. The first flight took place with the nozzle control system locked in the "forward thrust" position. The nozzle control system was modified, and then checked out during taxi trials which took place between the first and second flights.

Operation of the vectoring nozzles was quite smooth, although slight "bounce back" occurred following rapid movement of the nozzle control levers. However, the manufacturers warn against sudden movement of the levers. The nozzles were set at a given angle at low power setting and then power was applied. Under these circumstances the nozzle position would drift slightly but then remain steady.

Additional discussion of nozzle operation relative to engine operation is given under "Engine Operation."

FUEL SYSTEM

The fuel system tests consisted of vent spillage and operational evaluation.

Vent System Evaluation

The vent system was evaluated for possible spillage by making two figure eight turns on the taxi strip with outboard tanks full. Washable white paint had been applied at the vent locations. No fuel spillage was observed during the figure eight turns, and no indication of spillage was evident on the painted surface.

Operational Evaluation

Fuel system evaluation in flight was accomplished concurrently with other testing. All systems functioned correctly.

During flight 9-2, the fuel was intentionally used to a low quantity. During a right-hand turn on the taxi strip the lights for low fuel pressure and low boost pump pressure illuminated with 780 lb fuel remaining in the right-hand inboard tank. However, the engine continued to feed from the suction line as expected. Fuel continued to be used from the right-hand inboard tank to 600 lb.

All components of the fuel system operated normally throughout the flight envelope tested.

AIR DISTRIBUTION SYSTEM PERFORMANCE

The air distribution system collects the engine bypass air and distributes it to the appropriate blowing nozzles, as shown in figure 100. The ground operation data are presented in figure 100 for a fixed operating condition (flaps 6°, engine nozzles 30°). The in-flight data points are also shown. These indicate that airspeed, flap position, engine nozzle angle, and engine speeds do not have a significant effect on the airflow distribution. A detailed summary of data for the in-flight conditions is shown in table XII.

The system pressure losses are shown in figure 101 and are essentially as predicted. The overall duct system losses are relatively low. Therefore, a relatively high percentage change in a particular pressure loss difference would have little effect on the overall system losses.

The bypass airflow thrust distribution for approach and medium engine power settings for static conditions are shown in figures 102 and 103, respectively. The nozzle velocity coefficient used for the body and aileron nozzles is 0.98. The augmentor nozzle coefficients were based on the 0.7-scale model tests but required adjustment to account for internal augmentor duct roughness due to fasteners and the difference in reference station location.

Acceptable operation of the duct failure warning system which operates from augmentor nozzle duct pressure difference was established by using differential power settings on the engines.

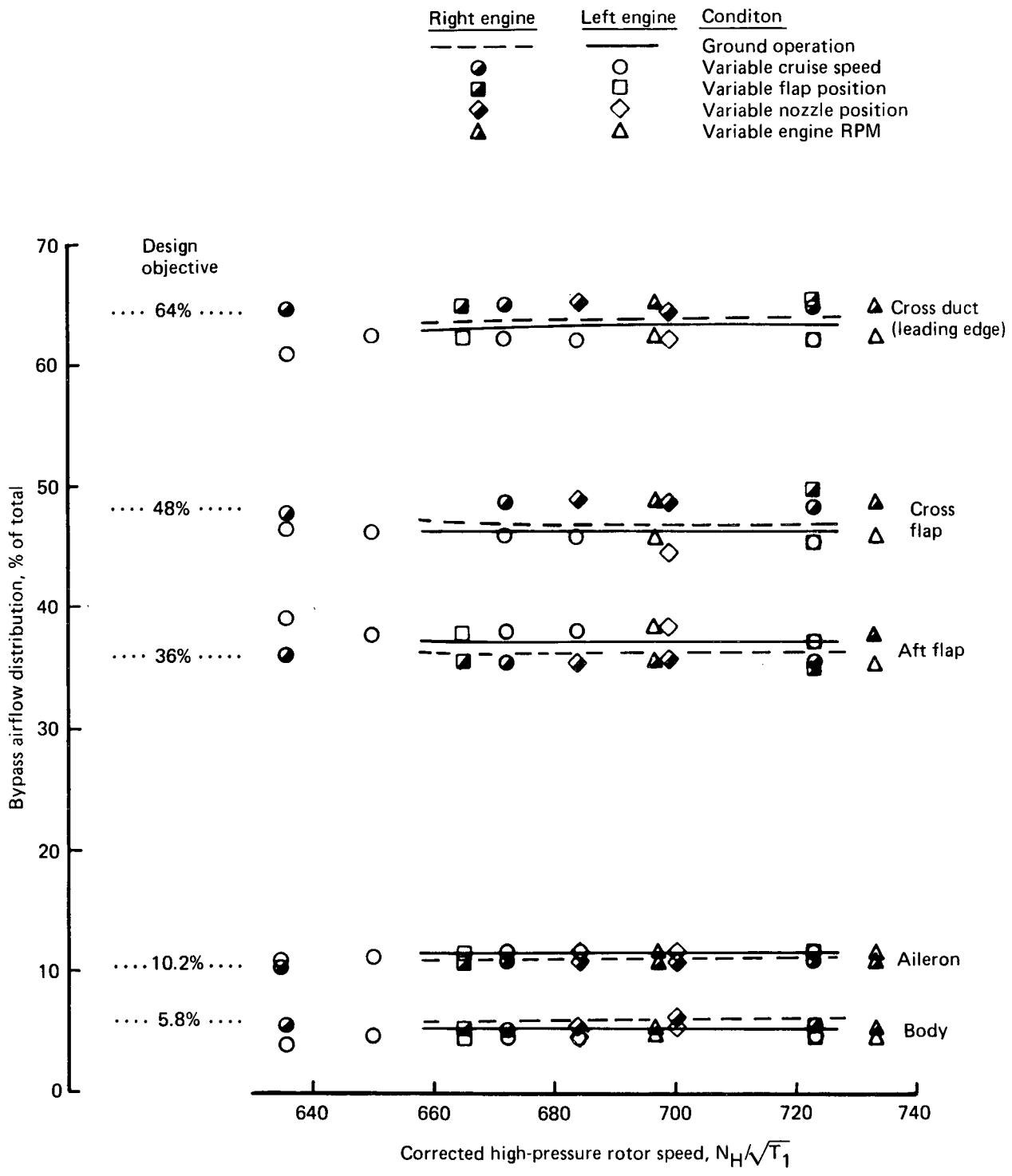

FIGURE 100.—ENGINE BYPASS AIRFLOW DISTRIBUTION FOR GROUND AND FLIGHT OPERATION

TABLE XII.–IN-FLIGHT AIRFLOW DISTRIBUTION

	Condition						Duct airflow as percentage of engine bleed								Flight test data source
							LH engine duct number				RH engine duct number				
	Airspeed, knots	LH flap, deg	Nozzle LH, deg	Nozzle RH, deg	$N_H/\sqrt{T_1}$*	$\%N_H$	(Cross) 2, %	(Aft) 4, %	(Body) 5, %	(Aileron) 8, %	(Cross) 1, %	(Aft) 3, %	(Body) 6, %	(Aileron) 7, %	Reference condition no.
Effect of airspeed	110	6.4	9.0	7.0	723		61.9	38.1	4.9	11.6	64.5	35.5	5.2	11.1	4.08.001.004
	110	6.8	9.0	9.0	651		62.3	37.7	4.8	11.2	64.2	35.8	5.0	10.9	4.06.002.010
	130	6.4	6.7	6.5	636		60.8	39.2	3.8	10.8	64.0	36.0	5.6	10.6	4.06.002.015
	160	7.0	9.0	0.01	672		62.0	38.0	4.7	11.6	64.7	35.3	5.2	10.9	4.06.002.027
	180	7.0	6.0	0.01	684		61.9	38.1	4.8	11.6	64.8	35.2	5.2	11.0	4.06.002.036
Effect of flap position	110	6.4	9.5	7.0	446		62.1	37.9	5.6	11.0	62.5	37.5	3.7	10.4	4.08.001.005
	90	30.0	6.0	6.0	665		62.2	37.8	4.3	11.6	64.7	35.3	5.5	10.8	1.00.002.001.1
	↓	66.0	10.5	9.0	723		61.9	38.1	4.9	11.5	65.0	35.0	5.2	11.0	4.08.001.010
		73.0	11.0	0.05	699		61.8	38.2	6.2	11.4	64.5	35.5	5.2	10.8	4.08.001.015
Effect of nozzle angle	180	7.0	6.0	0.01	684		61.9	38.1	4.8	11.6	64.8	35.2	5.2	11.0	4.06.002.036
	160	7.0	9.0	0.01	672		62.0	38.0	4.7	11.6	64.7	35.3	5.2	10.9	4.06.002.027
	90	73.0	11.0	0.05	699		61.8	38.2	6.2	11.4	64.5	35.5	5.2	10.8	4.08.001.015
	60	72.0	60.0	0.5	681		62.0	38.0	6.3	11.3	65.8	34.2	4.6	9.4	1.28.001.008
	75	64.0	90.0	0.8	692		61.8	38.2	4.7	11.5	64.6	35.4	4.4	10.7	4.08.001.014
Effect of engine rpm, N_H	110	6.0	9.0	7.0	723	100%	61.9	38.1	4.9	11.6	64.5	35.5	5.2	11.1	4.08.001.004
	110	6.0	9.0	7.0	446	Idle	62.1	37.9	5.6	11.0	62.5	37.5	3.7	10.4	4.08.001.005
	90	30.0	10.0	10.0	733	100%	62.1	37.9	4.9	11.5	64.7	35.3	5.2	11.0	4.08.001.008
	↓	30.0	10.0	10.0	444	Idle	62.8	37.2	5.5	11.3	63.2	36.8	3.8	10.9	4.08.001.007.1
		65.0	11.0	9.0	697	100%	61.9	38.1	4.9	11.5	65.0	35.0	5.2	11.0	4.08.001.010
			10.0	9.0	441	Idle	63.0	37.0	5.4	11.8	64.0	36.0	3.6	10.9	4.08.001.011

*LH engine reference

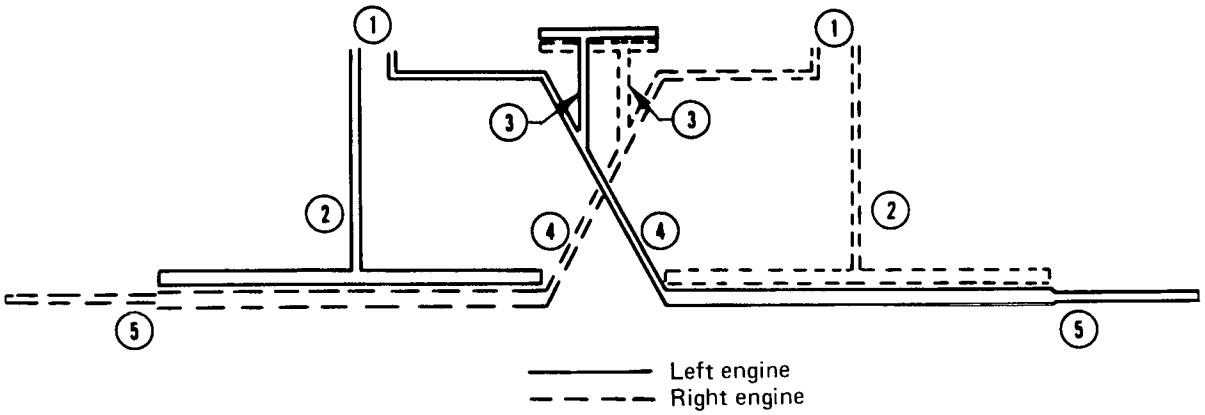

Test 4-11	
Condition 3.18.003.077 65° flap 6° nozzle	Condition 2.04.002.024 6° flap 6° nozzle
Airflow, lb/sec Left engine = 79.32 Right engine = 78.44 $P_{T_{2.5}}$, in. HgA Left engine = 79.6 Right engine = 79.2	Airflow, lb/sec Left engine = 81.19 Right engine = 80.15 $P_{T_{2.5}}$, in. HgA Left engine = 81.9 Right engine = 81.8

Location	Item	Pressure loss, in. Hg*			
		Left engine		Right engine	
		Estimated	Test	Estimated	Test
		Condition 3.18.003.077			
1	Port loss (aft)	–	2.40	–	2.40
	Port loss (cross)	–	2.80	–	2.80
1-2	To aft reference station	3.6	3.94	3.4	3.69
1-3	To body duct calibration station	10.9	9.43	9.9	9.27
1-4	To cross duct reference station	8.8	6.9	8.3	7.5
1-5	To aileron calibration station	11.3	10.12	11.0	10.2
		Condition 2.04.002.024			
1	Port loss (aft)	–	2.6	–	2.6
	Port loss (cross)	–	3.0	–	3.0
1-2	To aft reference station	3.5	4.2	3.5	4.0
1-3	To body duct calibration station	10.4	10.0	10.4	9.8
1-4	To cross duct reference station	9.0	7.5	9.0	7.8
1-5	To aileron duct calibration station	11.9	10.56	11.8	11.02

*Referenced to $P_{T_{2.5}}$

FIGURE 101.–AIR DISTRIBUTION SYSTEM PRESSURE LOSSES

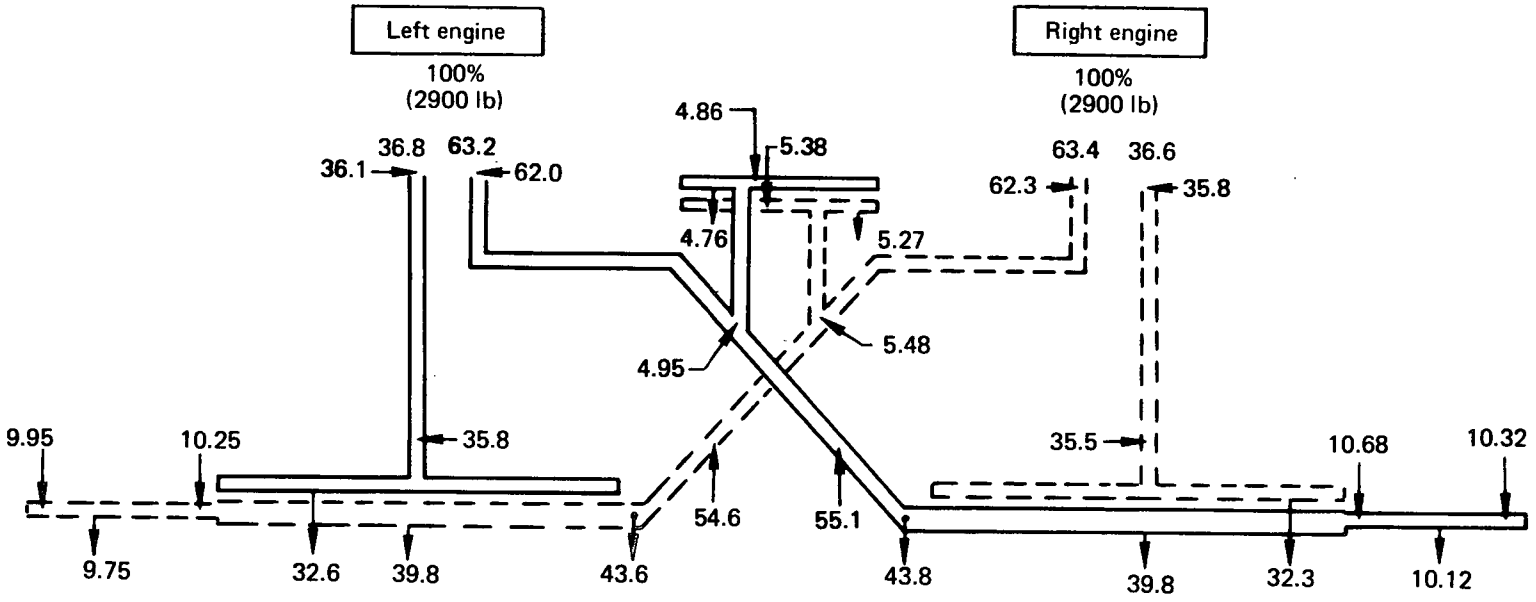

Loss summary, %*		
Item	Left engine	Right engine
Port	1.90	1.90
Duct	3.32	3.68
Nozzles	7.5	7.3
Total	12.72	12.88

Test 4-11

Condition 3.18.003.039
$N_H/\sqrt{T_1}$ = 669 (left and right engines)
Augmentor flap 30°
Conical nozzle 6°

↓ % of engine thrust availble

*Based on engine $P_{T_{2.5}}$

FIGURE 102.–AIR DISTRIBUTION SYSTEM THRUST LOSSES (APPROACH)

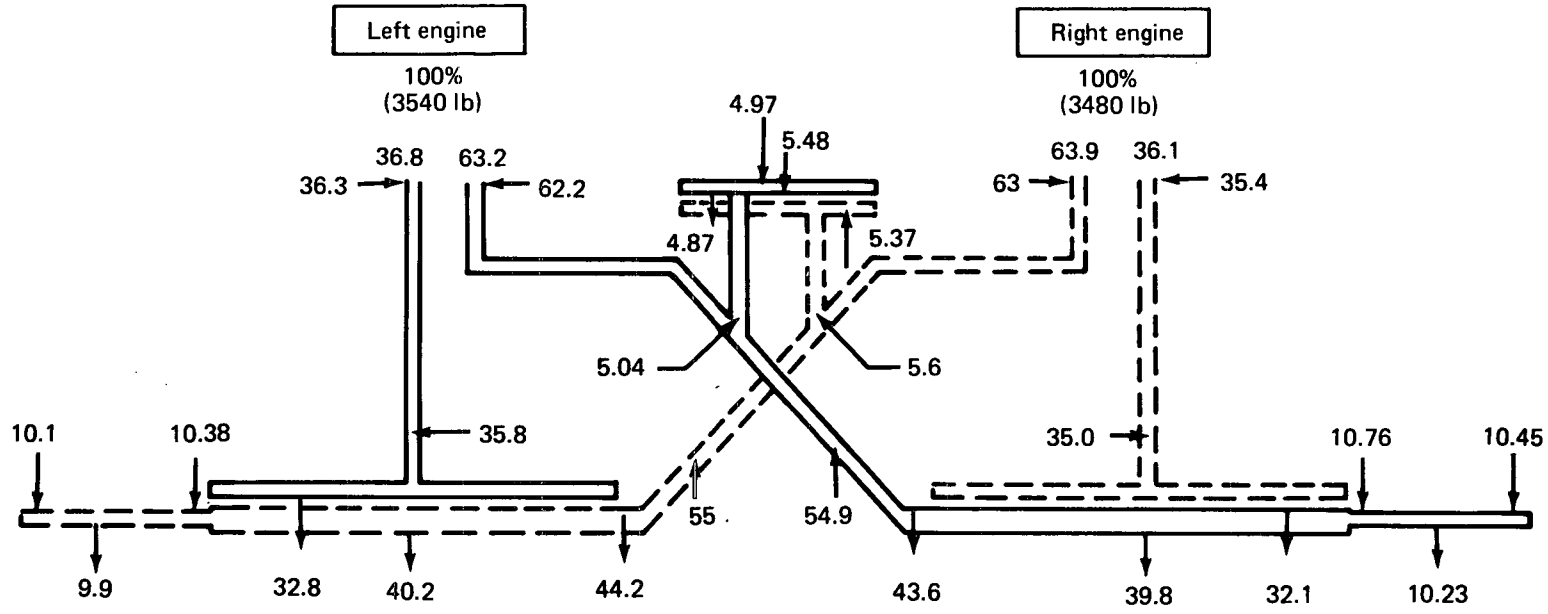

Loss summary, %*		
Item	Left engine	Right engine
Port	1.5	1.6
Duct	3.68	3.62
Nozzles	7.12	7.21
Total	12.3	12.43

*Based on engine $P_{T_{2.5}}$

Test 4-11

Condition 3.18.003.077
$N_H/\sqrt{T_1}$ = 706 left engine, 705 right engine
Augmentor flap 65°
Conical nozzle 6°

↓ % of engine thrust available

FIGURE 103.—AIR DISTRIBUTION SYSTEM THRUST LOSSES (MEDIUM POWER SETTING)

STRUCTURAL TESTING

A major purpose of the flight tests was to aid in verifying the airworthiness of the structural modifications. These tests consisted of measuring the dynamic response of the airframe to control pulses, and measuring the loads and stresses on modified components. Control surface position indicators and accelerometers were used to measure the airframe dynamic response. Actuator pressures were measured to obtain hinge moments, and strain gages were installed on the airplane to measure loads and stresses. The location of the instrumentation is illustrated in figure 104. The V-n envelope investigated during this flight testing is illustrated in figure 2. The following paragraphs discuss the test procedures and results.

FLUTTER

The flight flutter checks demonstrate that the Modified C-8A airplane is free from flutter and has adequate damping for all normal operating conditions within the aircraft design speed envelope, 180 KEAS. Further, the aircraft was shown to be free from flutter, with adequate damping up to 160 KEAS with the hydraulic systems off.

To carry out the checks, the pilot excited the airplane through sharp inputs to the elevator, rudder, and aileron at prescribed speed test points. The responses of the various airplane components were analyzed to determine damping characteristics. Figure 105 presents typical responses to aileron and elevator excitation at 180 KEAS. The effect of fuel variations was included by performing flutter checks at the beginning of a flight with nearly full fuel and then repeating the flutter checks at the end of the flight, at a partial fuel condition.

The instrumentation used for the flight flutter testing consisted of accelerometers mounted in the wing and nacelle. The accelerometer outputs were integrated to provide displacement. Position indicators were installed to measure the angular position of the control surfaces. A list of the instrumentation is presented in table XIII.

The output of the measurements was recorded on magnetic tape onboard the airplane. After each flight, the conditions of interest were recorded on strip charts for review. Instrumentation to record the altitudes and velocities of test points was also provided. A direct-write oscillograph was used for fast evaluation of flutter damping between flights on the same day.

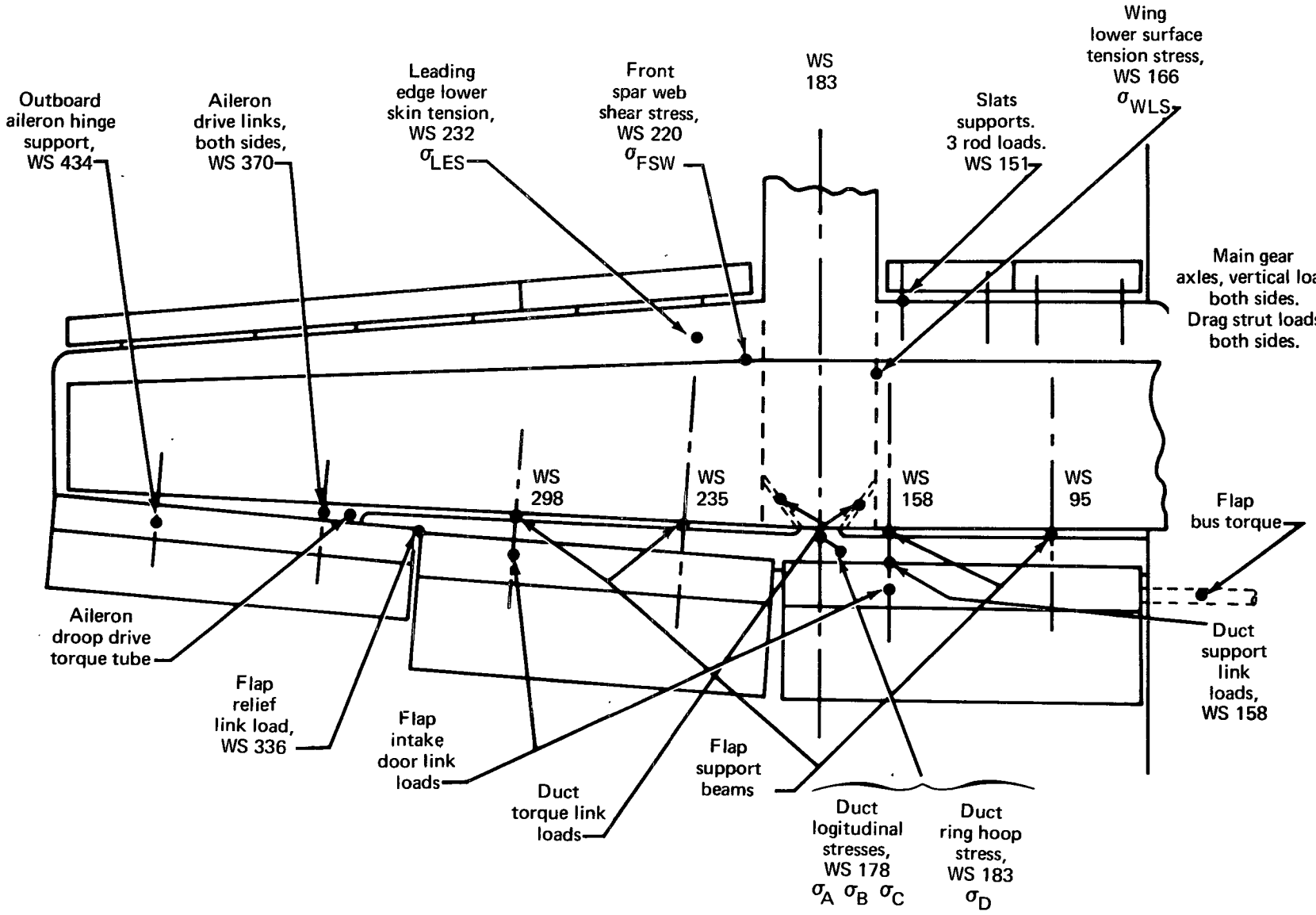

FIGURE 104.–STRUCTURES INSTRUMENTATION DIAGRAM

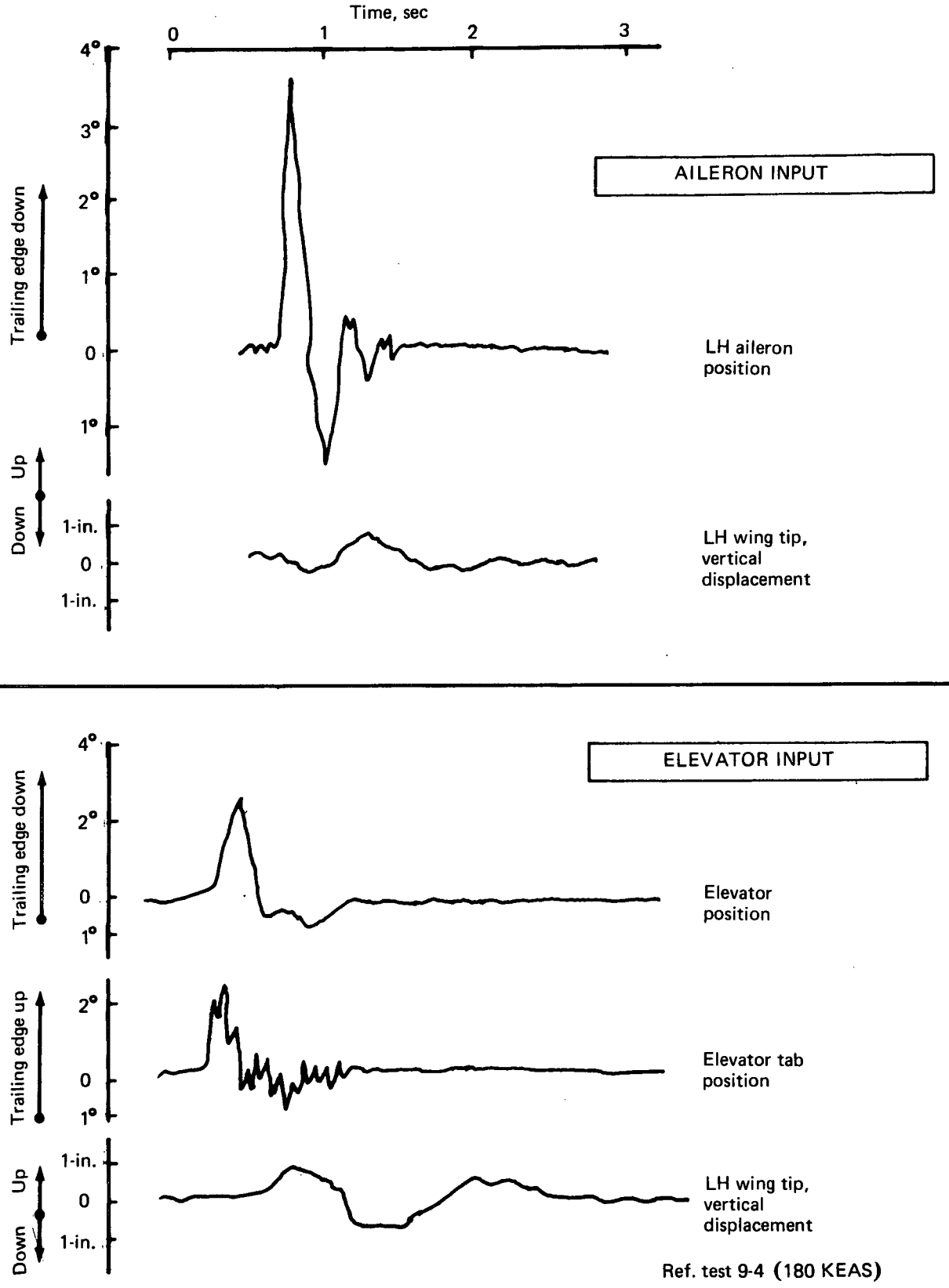

FIGURE 105.—AIRPLANE RESPONSE TO AILERON AND ELEVATOR INPUTS

TABLE XIII.–INSTRUMENTATION FOR FLIGHT FLUTTER TESTING

Measurement location	Direction
LH wingtip	Vertical
RH wingtip	Vertical
LH engine	Vertical
LH engine	Lateral
LH outboard flap choke	Rotation
RH outboard flap choke	Rotation
RH inboard flap	Rotation
LH aileron	Rotation
RH aileron	Rotation
Rudder	Rotation
Elevator	Rotation
Elevator spring tab	Rotation

LOADS

Leading Edge Slats

Flight test results were used to obtain loads comparable to the slat design loads. Figure 106 shows slat normal force coefficient, C_N, plotted against airplane angle of attack for various flap angles, δ_F. Figure 107 shows the chord force coefficient, C_c, plotted against C_N for various δ_F values.

Maximum slat loads occur at the airplane maximum lift coefficient. Loads calculated using slat coefficients obtained by extrapolating the test data fall within the design loads envelope as shown in figure 108.

Aileron

The flight test results for aileron hinge moments appear in figure 109. Aileron hinge moment coefficient, $C_{H_{ail}}$, is plotted against aileron deflection, δ_a, for various δ_F values. It is also noted on the plot whether the spoiler ahead of the aileron is up or down. If the spoiler is up, the effect is to change the slope of the curve. This results in the highest hinge moments occurring when the aileron is deflected from its droop position. The flight test hinge moments are substantially lower than design hinge moments, as shown by the table in figure 109.

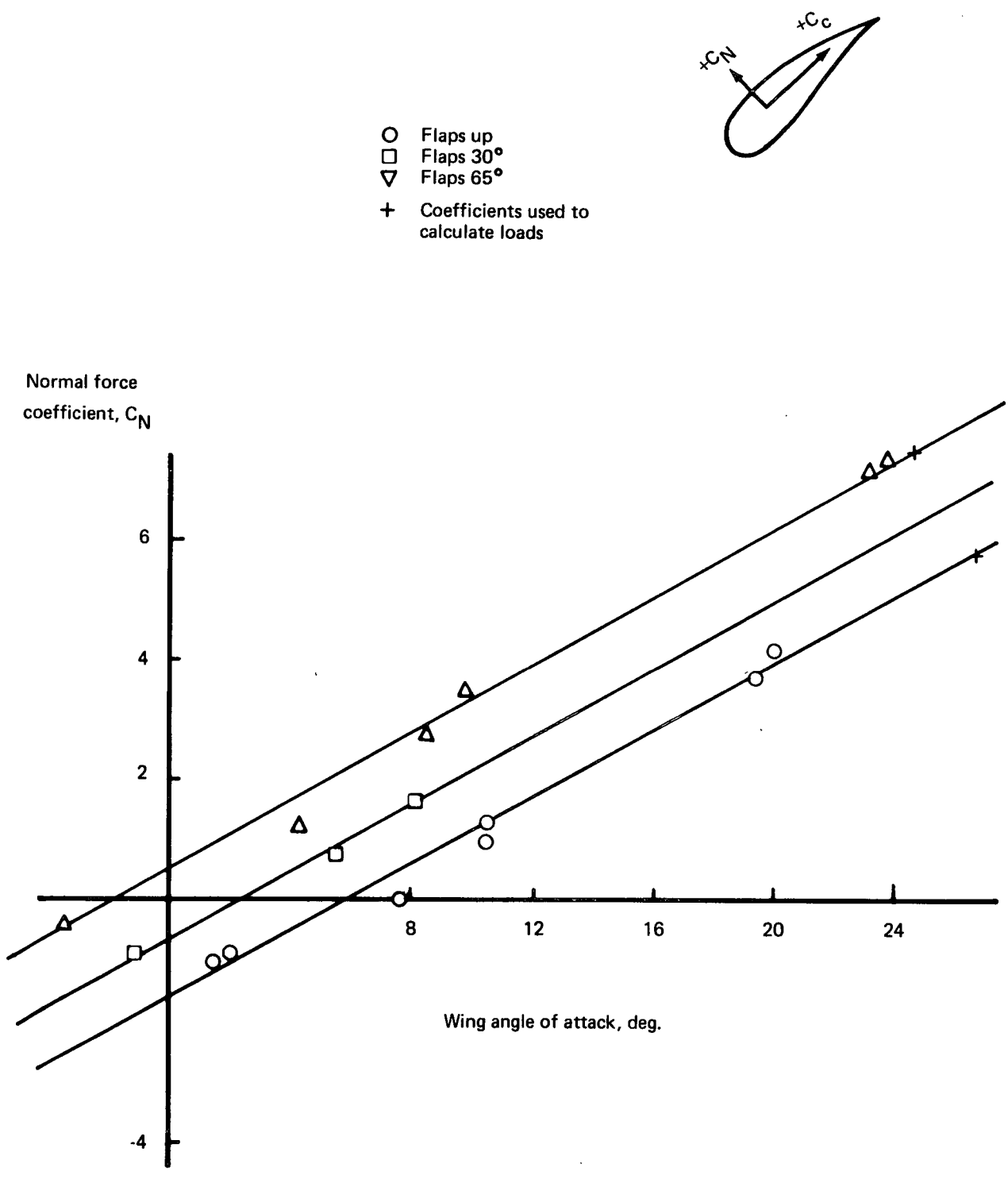

FIGURE 106.—SLAT NORMAL FORCE COEFFICIENT

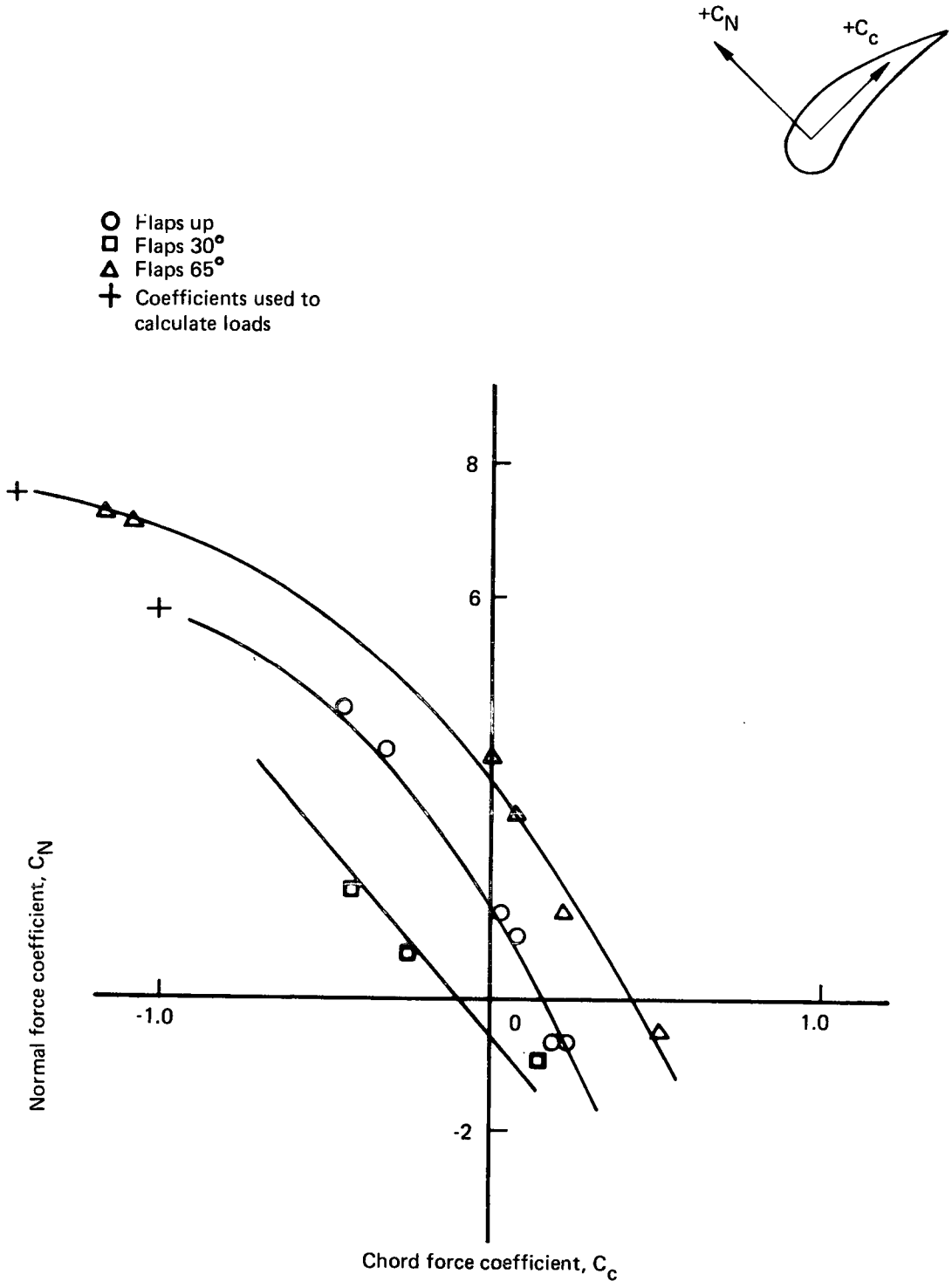

FIGURE 107.—SLAT CHORD FORCE COEFFICIENT

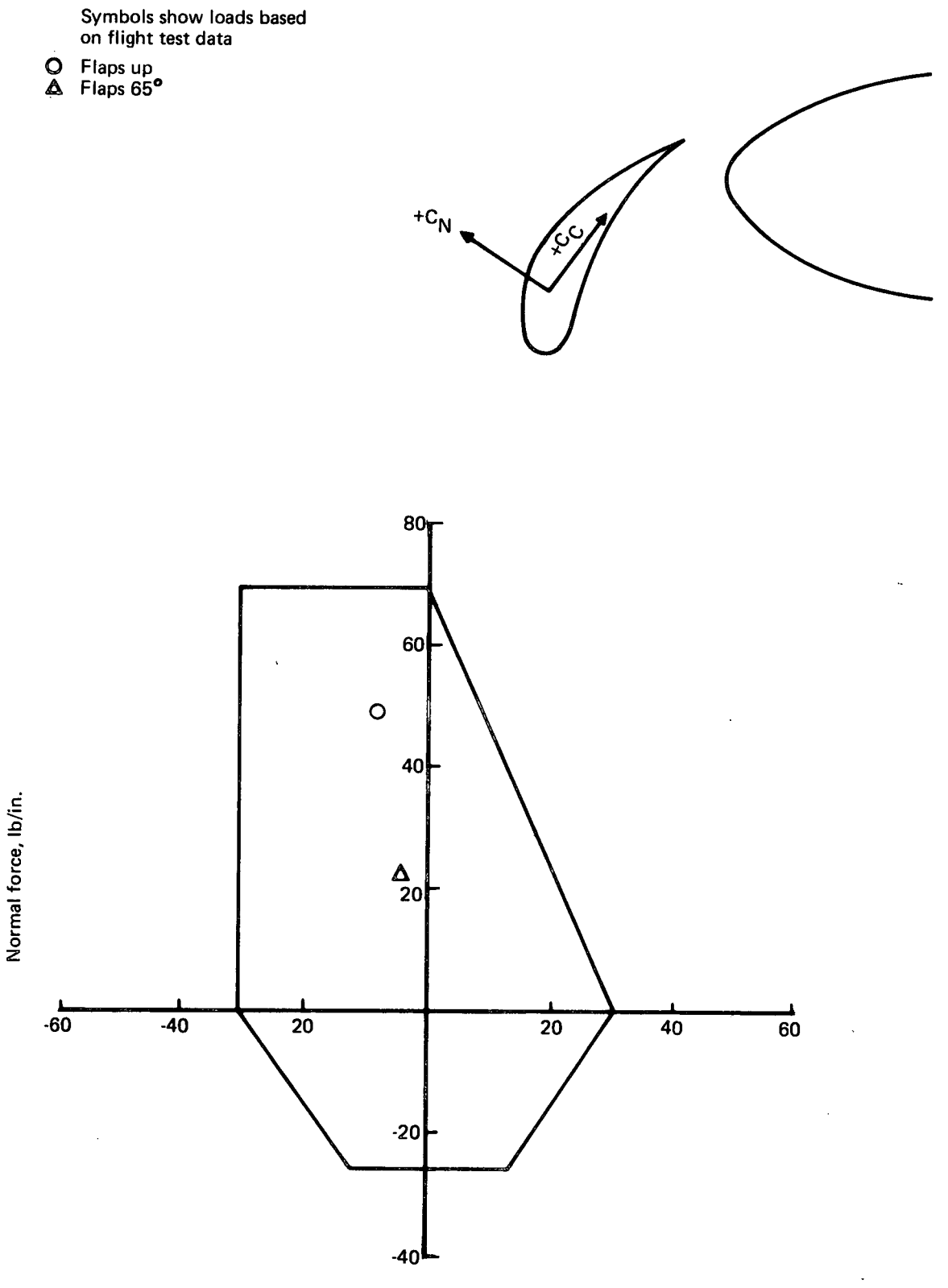

FIGURE 108.—LEADING EDGE SLAT DESIGN ENVELOPE

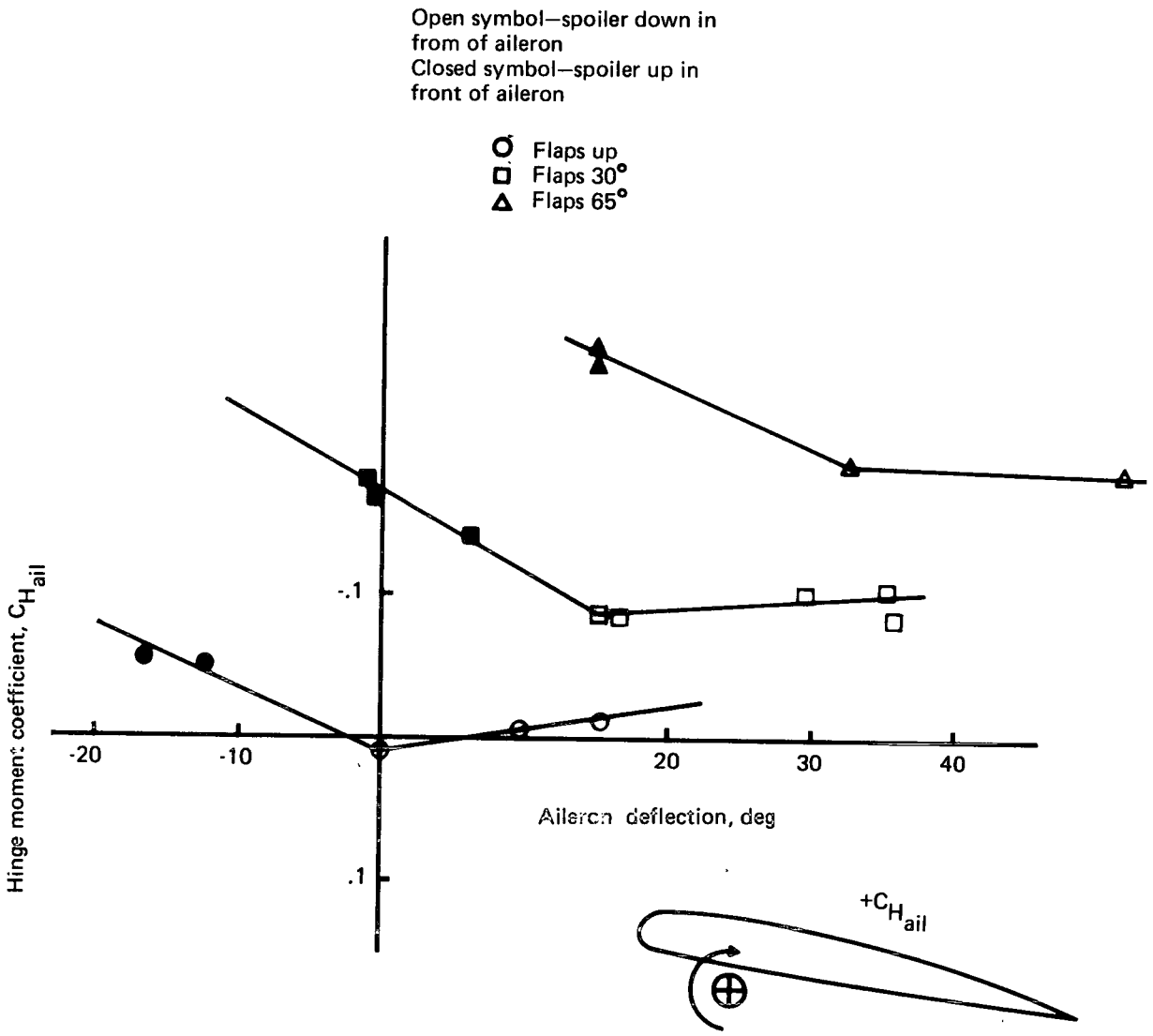

Flight test			Design
Flap angle, δ_F, deg	Aileron deflection, δ_a, deg	Aileron hinge moment, in.-lb	Aileron hinge moment, in.-lb
65	12.5	-5400	-26 500
30	-5	-6000	
0	-20	-3880	
0	0	615	13 500

FIGURE 109.—AILERON HINGE MOMENTS

Empennage

A plot comparing the sideslip angle obtained using the flight test β/δ_r relationship and the maximum available rudder angles for both one and two rudder systems appears on figure 110. Maximum rudder availability was confirmed during flight test.

At 120 kt, the maximum available rudder angle with both rudder systems functioning is 18.8°. Extrapolating the flight test condition to $\delta_r = 18.8°$ gives a sideslip $\beta = 31.4°$. This β would result in a load in excess of the design load. However, with only one system operating the maximum rudder angle is only 9.3°, which would give flight test $\beta = 15.5°$. This gives empennage loads well under design.

At 166 kt, similar comments are applicable. Based on these data, it is concluded that the system to disengage one rudder power system, flaps up, is required.

AUGMENTOR DUCT STRENGTH

The augmentor duct is a complex structure subjected to combinations of loads due to transient temperature differences, internal pressures, and wing bending.

Strain gage instrumentation was used to investigate:

- Support loads at WS 158.5
- Support loads in the torque links attaching the T junction leg to the nacelle about WS 183
- Longitudinal duct stresses just inboard of the T junction at WS 178
- Local stresses in the duct-reinforcing ring around the outer duct at WS 183

These areas are discussed individually on the following pages. Figure 104 shows the locations of the instrumentation.

Figures 111 through 114, discussed in the following paragraphs, show areas into which the majority of test points fall for the test condition, rather than showing the discrete points. This scatter results from the sensitivity of the loads and stresses to variables that were not well controlled during the test. For instance, minor changes of engine RPM produced noticeable changes in some cases and are largely responsible for the scatter of results.

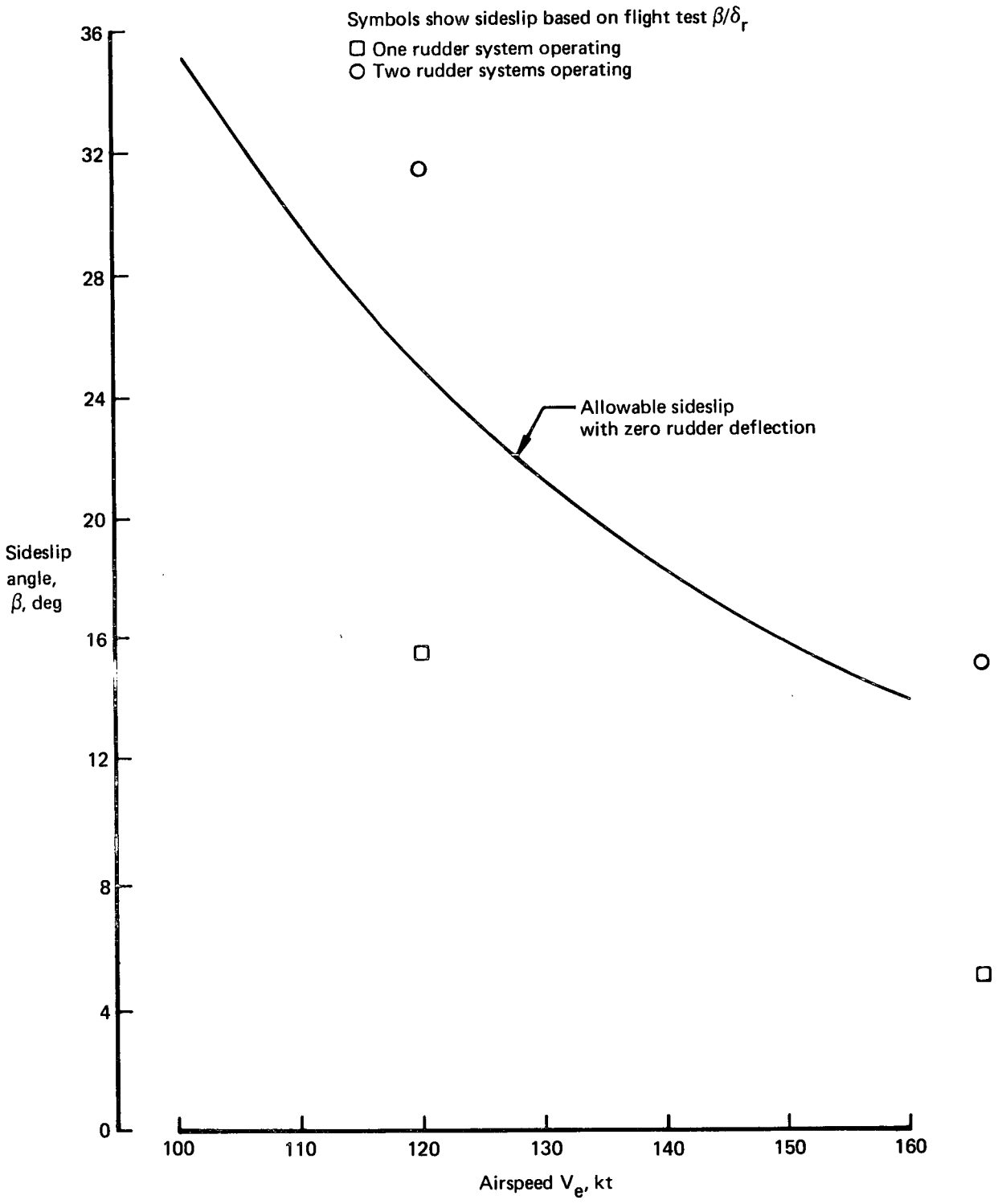

FIGURE 110.—BETA ALLOWABLE FOR LIMIT LOAD BASED ON SHEAR

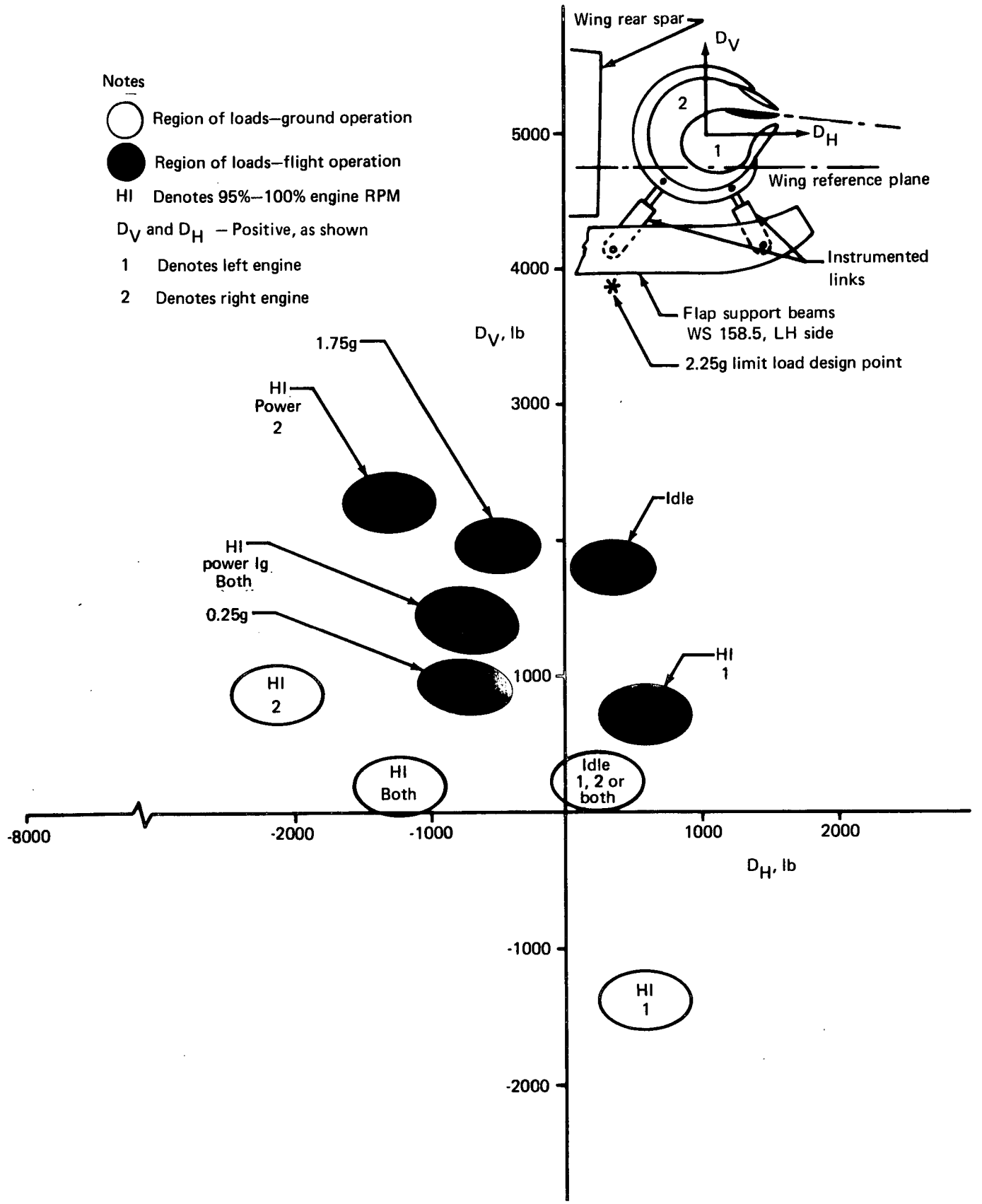

FIGURE 111.—AUGMENTOR DUCT SUPPORT LOADS – WING STATION 158.5

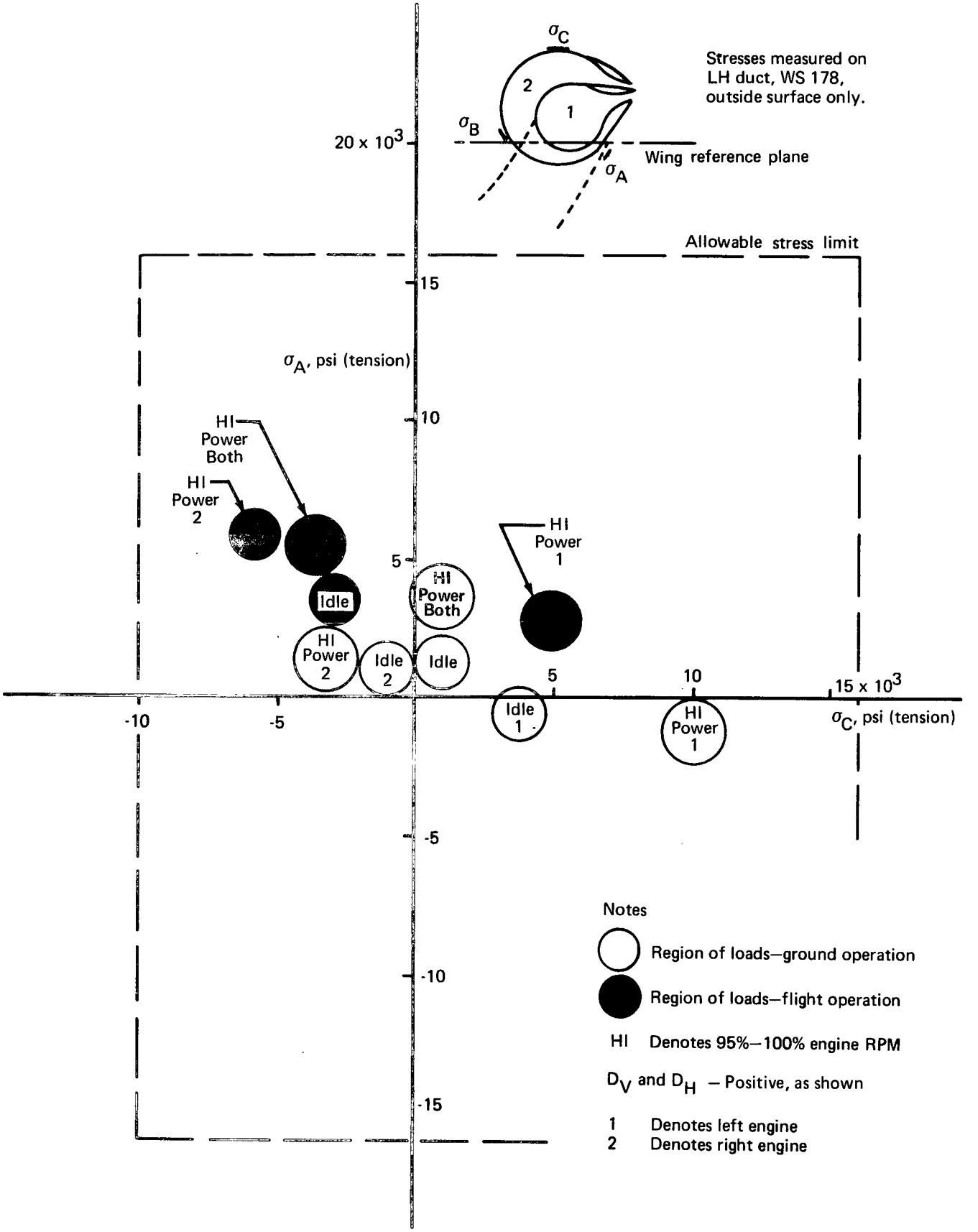

FIGURE 112.—AUGMENTOR DUCT LONGITUDINAL STRESSES—σ_A VS σ_C

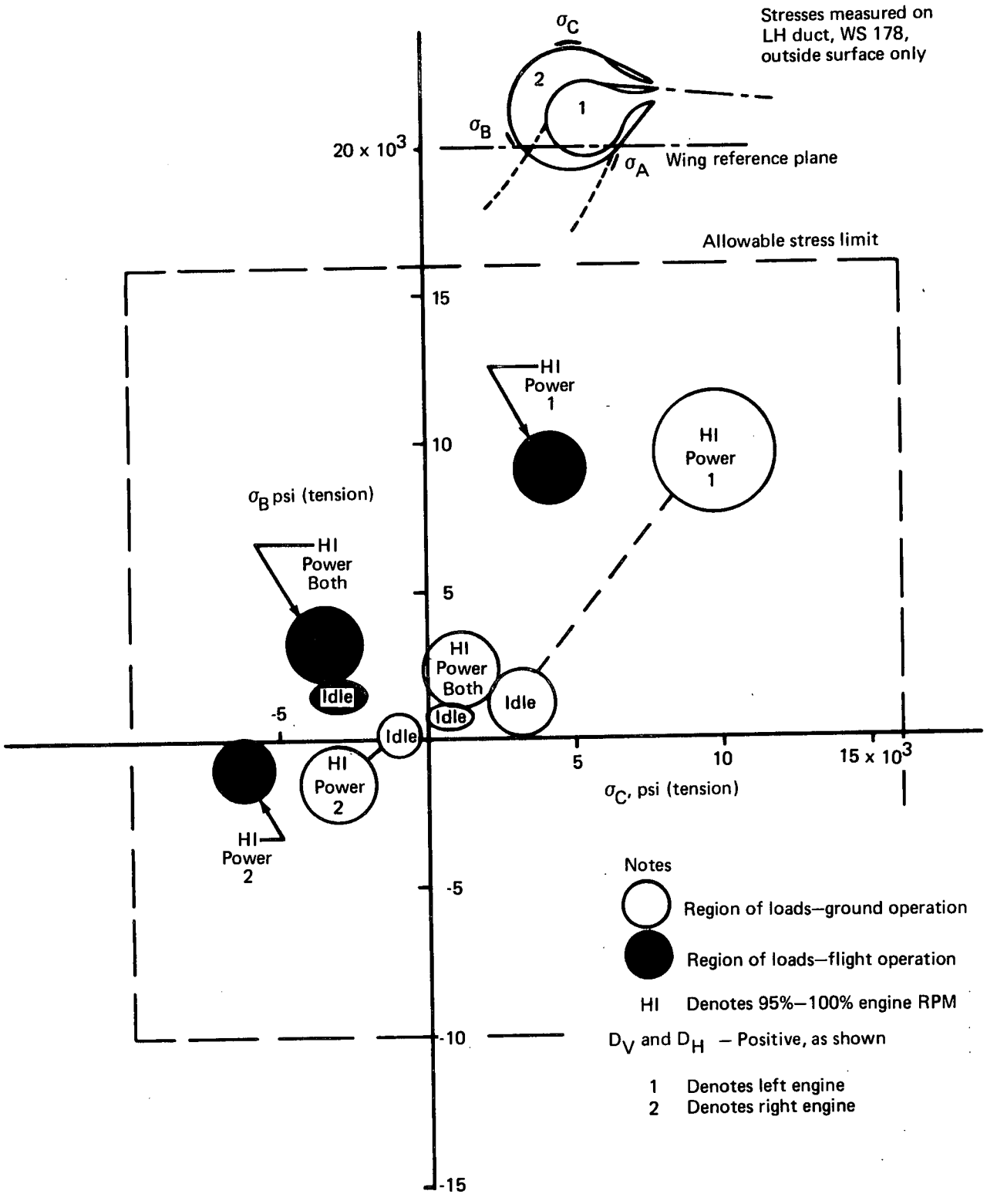

FIGURE 113.—AUGMENTOR DUCT LONGITUDINAL STRESSES—σ_B VS σ_C

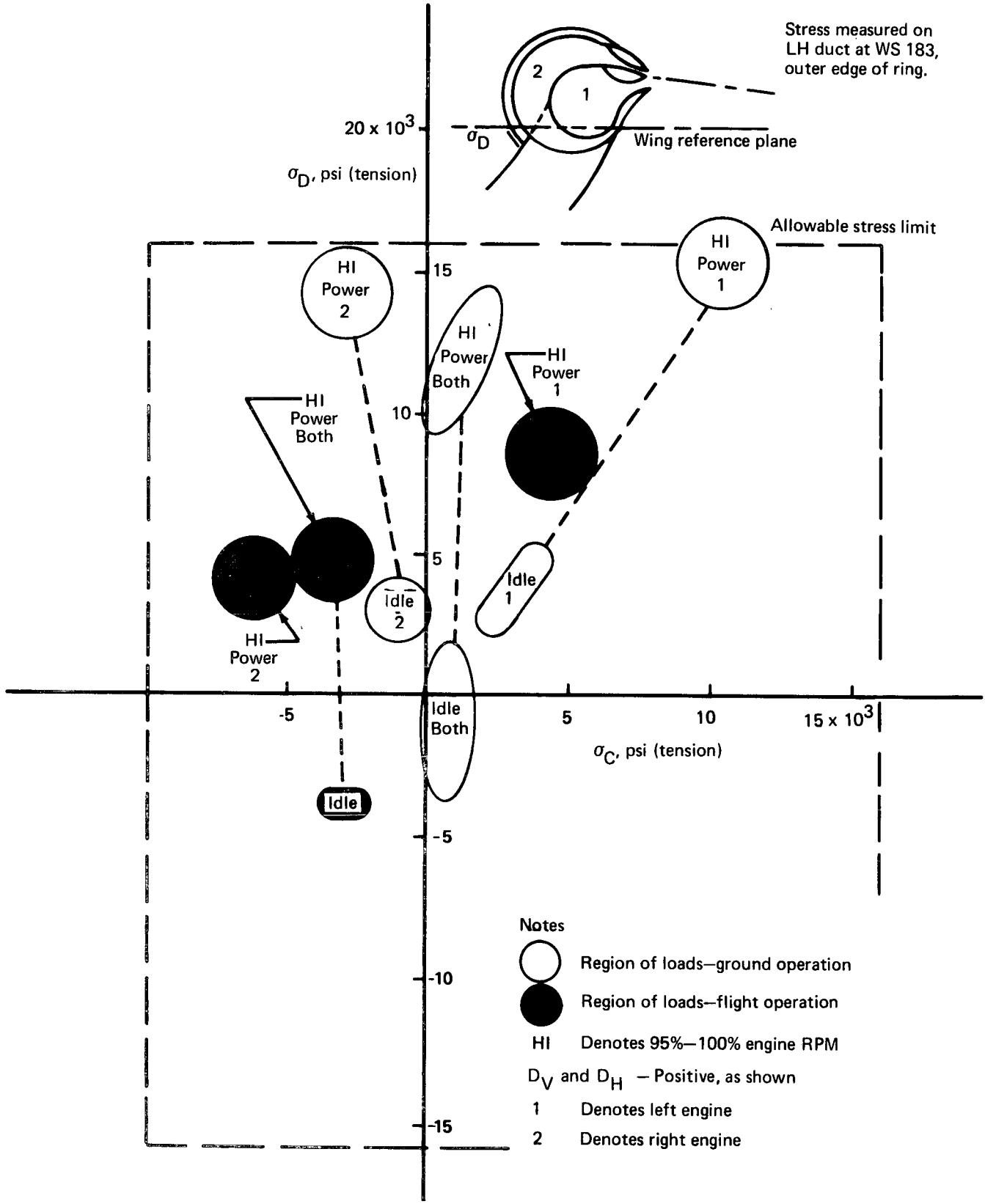

FIGURE 114.–AUGMENTOR DUCT–HOOP STRESS IN REINFORCING RING

Support Links at WS 158.5

Figure 111 presents the measured duct loads at the WS 158.5 support links. Difficulty was experienced in estimating duct support loads, particularly those due to initial transient conditions during engine starting. As shown by the test results, the transient starting conditions and the effect of duct bending due to load factor were overestimated.

Generally, analysis predicts the loads at the other three support locations. WS 95, 235, and 298, to be appreciably less than those at WS 158.5, whereas the available strengths are essentially the same.

Torque Links at WS 183 (Approximately)

The augmentor duct torque links perform two functions:

1. They jointly provide spanwise restraint on the duct, thus reacting the "plug" load imposed on the duct by the aileron duct which is "plugged" into its outboard end.

2. They jointly provide redundancy to react duct torque, each being sized to react all of the torque.

Both ground and flight tests indicate loads, not exceeding 25% of limit design load with relatively large scatter due to the small magnitude. These loads show the expected spanwise effect described in item 1 above, but show very little of the torque loads described in item 2.

Because of the generally small magnitudes, it is not considered necessary to show a plot of these loads.

Longitudinal Stresses at WS 178

The stresses in the augmentor duct result from engine bypass air temperature and pressure, which are functions of engine RPM, time, and airplane normal acceleration, with minor perturbations due to flap and aileron loads. It should be noted that both engines affect each duct due to the crossover interconnection.

Three strain gages were installed as illustrated in figure 112 to confirm that the stresses were not exceeding the design limits.

To show the general stress pattern in different conditions, σ_A and σ_B are separately plotted versus σ_C in figures 112 and 113, respectively.

The effect of load factor on duct longitudinal stress is not shown since measurements indicate small changes from the corresponding 1 g condition in the expected direction. This may be due to the transient nature of the available data, and the concurrent engine RPM changes, which themselves lead to transient effects that may mask or partially cancel g effects.

The allowable stresses shown are based on the allowable tensile yield stress of 16 200 psi for a class A weld in 5456 material at room temperature. At a typical mean metal temperature of 200° F there is virtually no reduction; hence, a value of 16 000 psi was used. The estimated buckling stress for the cylindrical duct shell was estimated conservatively to be about 10 000 psi. Again, no reduction for a temperature of 200° F is used.

It should be noted that longitudinal stresses due to bending would be expected to be as much as 35% higher at WS 158.5 than at this station, WS 178. However, a large fraction of the total stress measured at A, B, and C is due not to bending but to temperature differences causing restrained differential longitudinal expansions.

Hoop Stress in Reinforcing Ring

Stress analysis indicated the possibility of attaining high stresses on the forward edge of the reinforcing ring around the outer duct on the centerline of the T joint at WS 183. Previous ground tests showed that stresses close to yield could occur at this location during single-engine running at high power.

Figure 114 presents the results of ground and flight test measurements. In-flight results show reduced stresses, this reduction being attributed to wing/duct bending effects. The high stresses, such as those found during earlier ground tests, occur during the takeoff run.

An additional strain gage added to the base of the reinforcing ring showed the hoop stress dropping to approximately zero at the duct wall. Also, an added strain gage measuring circumferential stress showed a reduction in the reinforcing ring hoop stress in moving away from point D. The high stresses occurring in the reinforcing ring appear to be a local problem only at point D.

General Conclusions–Augmentor Duct

The magnitudes of the measured support loads confirm that the design conditions for the attachments to the wing are adequate and conservative. However, stresses very close to yield values have been measured in the duct. Since the critical engine starting condition cannot be avoided they will continue to occur.

Continued application of stresses of this magnitude appears to cause small permanent changes in duct dimensions. Measurements of the horizontal distance between the nozzle and a reference point on the flap at several spanwise locations have appeared to increase with time. This was not detected early enough to institute a systematic investigation.

WING, FLAP, AND CONTROL SYSTEM MEASUREMENTS

Wing

The effects of higher airplane weights and an adverse fuel management routine that tend to increase wing stresses are offset by the large reduction in wing span and the specification of lower maneuver acceleration factors.

The detail design of the modified airplane showed three potentially critical areas in the wing: the lower leading edge skin at WS 232, the front spar web at WS 220, and the lower skin at WS 166.

Wing Leading Edge Lower Skin Stress–σ_{LES} at WS 232

Analysis indicated that the outboard leading edge, to be left essentially unchanged, might encounter higher than anticipated local loads. As a result of this analysis, some local strengthening was incorporated and a strain gage on the lower leading edge skin at WS 232 was installed, identified as σ_{LES}.

The flight test results show very low stresses. The 1 g level flight stress varies from zero to about 1000 psi depending primarily on airplane angle of attack. The highest stress recorded was about 2500 psi during a 1.75 g pull-up maneuver at 160 kt.

Since these stresses are less than 10% of limit stress, they are not critical.

Wing Front Spar Web Stress—σ_{FSW} at WS 220

Strength calculations based on wing data from de Havilland documents, together with vertical shears and torques estimated by Boeing, indicated the possibility of high stresses being developed in the front spar web outboard of the nacelle. This measurement was included to ascertain the situation at this location.

The flight test results, shown on figure 115, confirm that the stresses are within the design envelope for the original structure. Subsequent modifications by Boeing in this region, for the purpose of attaching slat and flap support fittings to the web, also have the desirable effect of adding strength to the web.

Wing Lower Surface Stress—σ_{WLS} at WS 166

At this wing station just inboard of the nacelle, the lower surface is penetrated by a number of holes for fuel pipes, hydraulic pipes, and fire extinguisher lines. The predicted stresses were low enough to render reinforcement unnecessary. The strain gage was installed to confirm the stress level.

The flight test results are presented in figure 116, confirming the adequacy of the design.

Aileron

Flap Relief Link Load at WS 336

During the design phase it was predicted that critical loads would be imposed by the aileron droop drive mechanism on the outboard end of the outboard flap, approximately at WS 336. As a safeguard, therefore, a fail-safe link was incorporated to react the load imposed by aileron hinge moment. This link also acts as a redundant restraint on the flap.

Flight test results show that the load due to aileron moment is approximately as predicted, whereas that due to flap restraint is much less than predicted. Since they are normally additive, total loads are significantly lower.

Outboard Aileron Hinge Support at WS 434 (Approximately)

A brief examination of flight test data indicates that the support loads are of the expected order of magnitude and are not critical.

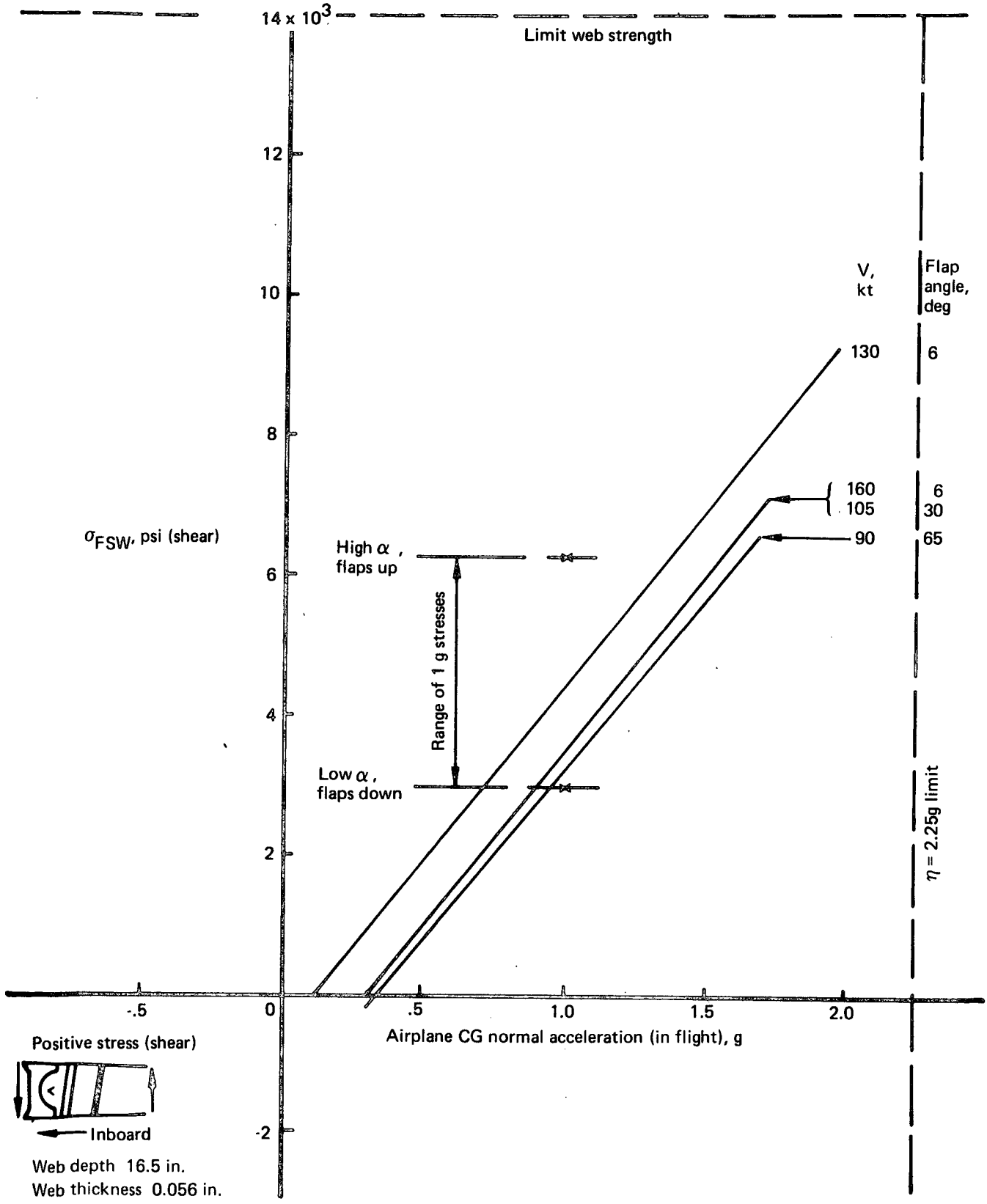

FIGURE 115.—WING FRONT SPAR WEB STRESSES—WING STATION 220

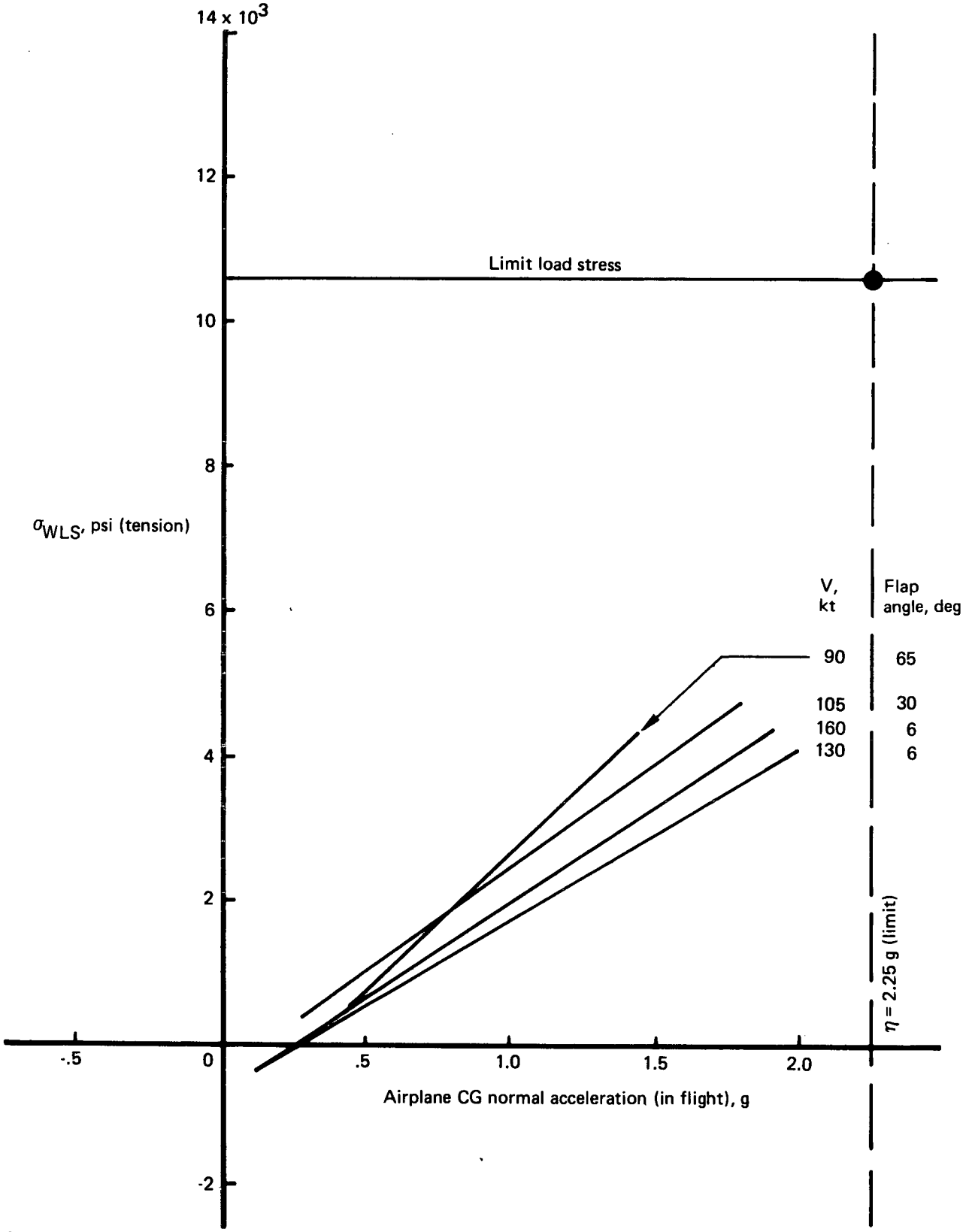

FIGURE 116.–WING LOWER SURFACE STRESS–WING STATION 166 BETWEEN S1 AND S2

FIG 11 C

Trailing Edge Flaps

Torque in Main Flap Bus Torque Tube

Accidental failure of both flap interconnections on separate occasions during final assembly led to a requirement to measure the torque in the "across-the-body" flap interconnection tube during both ground and flight testing.

Ground and flight test data indicate the following general behavior:

- A "flap selection" would cause a torque of no greater than 1000 in.-lb to be developed
- Flaps reaching either full-up or full-down position cause a torque of about 2000 in.-lb consistent in sense with any rigging difference between sides
- During ground testing only, with maximum engine RPM, flaps at 65° full asymmetric aileron, and augmentor choke operation, a torque of about 5000 in.-lb was developed
- During asymmetric flight, torques of less than 2000 in.-lb were developed

For comparison with these observations the design limit torque for the interconnect is greater than 40 000 in.-lb. It is concluded that the torque developed in the "across-the-body" interconnection during normal operation with no system or structural failures present is within the design loads.

Flap Intake Door Links

The flap intake door link loads measured during flight are presented in figure 117. These loads show much less deflection angle effect than was anticipated. The maximum measured load is about 39% of limit design load on the link.

Flap Supports

The stress levels measured on the flap support beams were less than 10% of the limit stress for the members and are considered to be adequate. It should be pointed out, however, that the sign of the measured stress is opposite to that calculated. The reason for this discrepancy is not known.

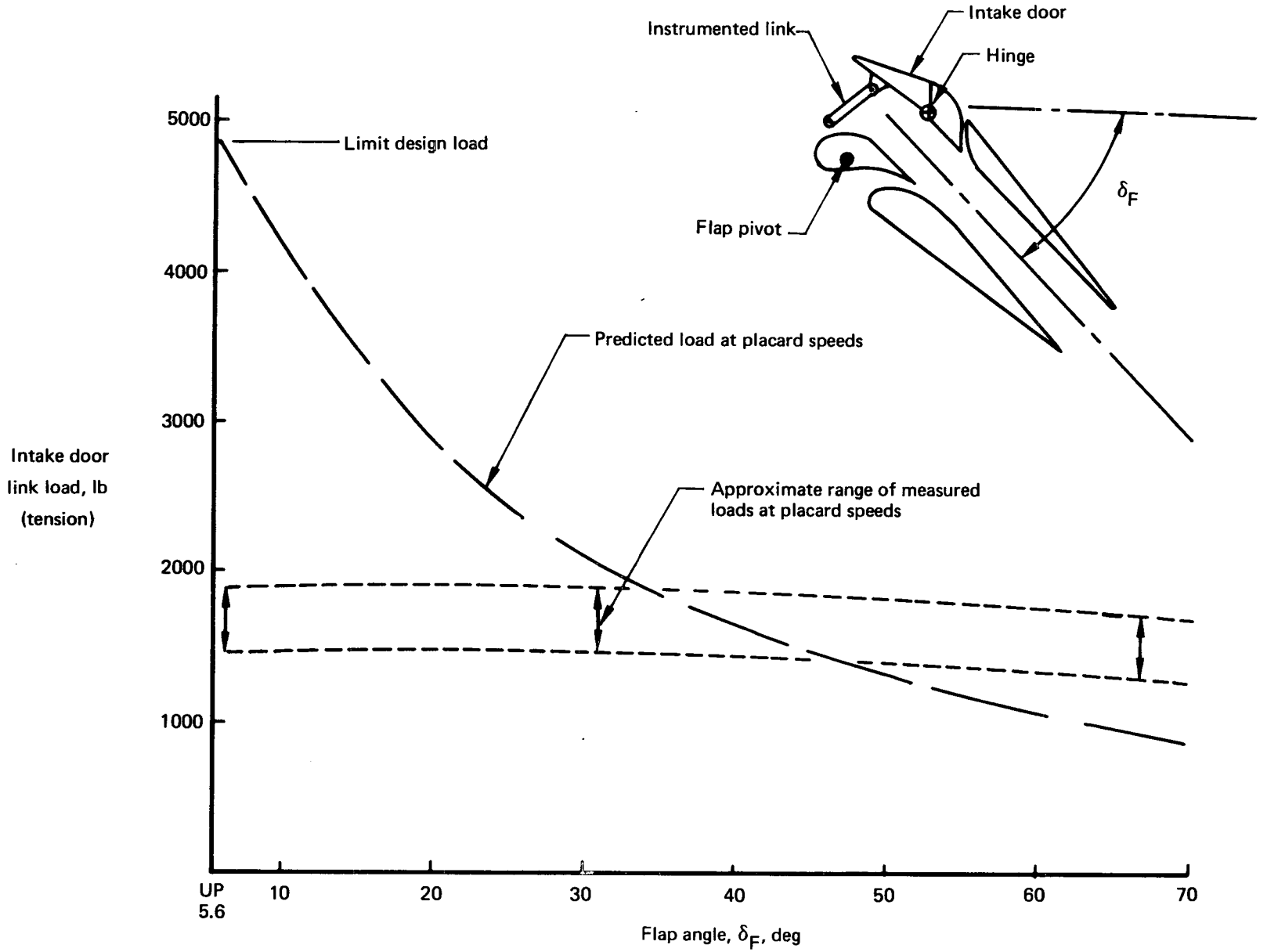

FIGURE 117.—AUGMENTOR FLAP INTAKE DOOR LINK LOADS

MAIN GEAR LOADS

Initial landing impact loads for the right-hand gear are presented in figure 118. Since all landings were at low descent velocities, in the range of 1 to 4 ft/sec, these loads are mainly for information.

The initial impact vertical load was always less than the final static value. Maximum loads during the entire landing ranged up to about 20% over the static value due to runway roughness. Although the LH gear was also instrumented, the installation was unserviceable during these initial flights.

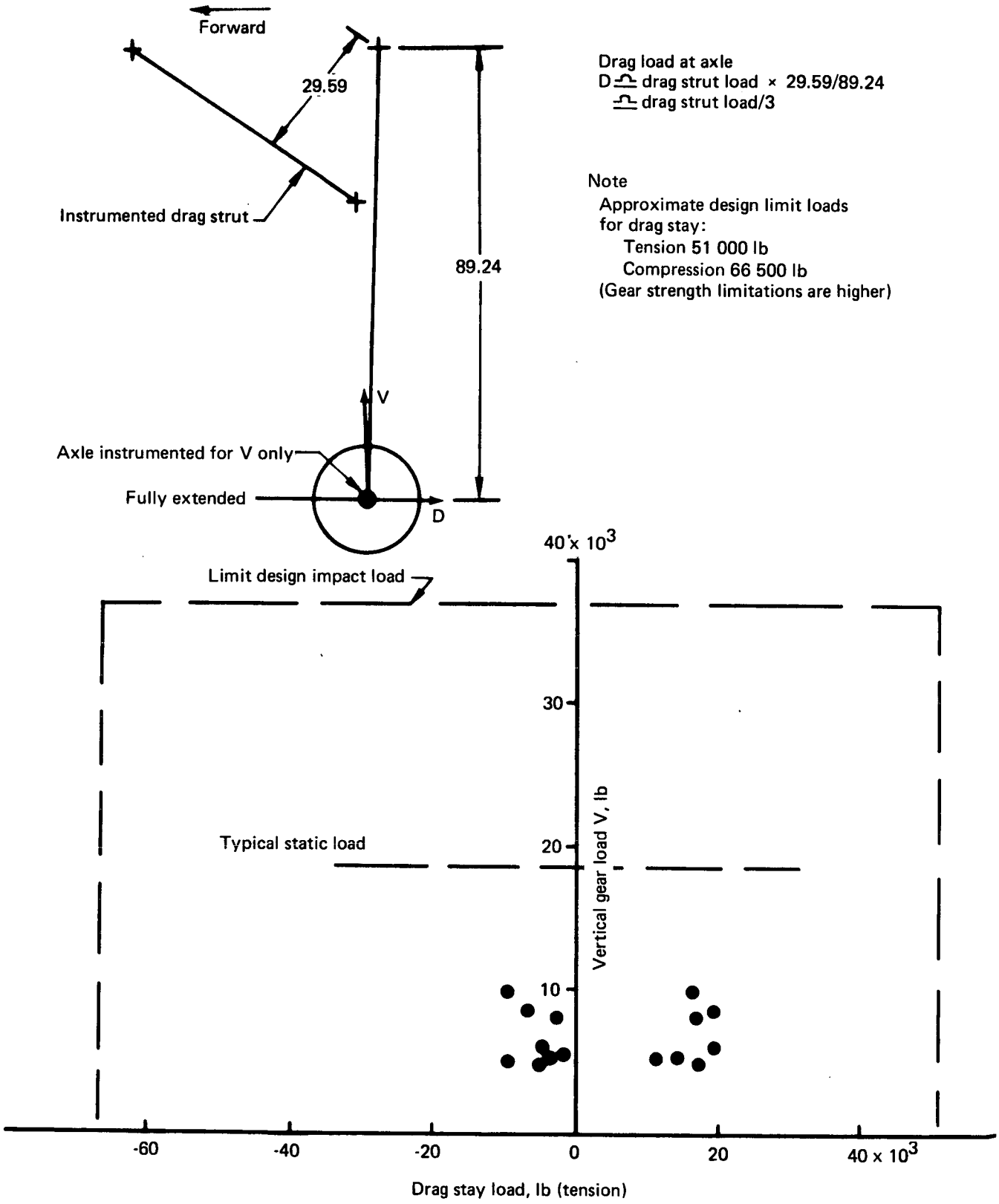

FIGURE 118.—RH MAIN GEAR LOADS (INITIAL LANDING IMPACT)

SYSTEM TESTS AND OPERATION

HYDRAULIC SYSTEMS

The purpose of the testing was to verify that hydraulic system operation is proper and within prescribed limits.

Test Conditions and Procedures

The tests were run concurrently with other flight tests and consisted of a continuous time survey of the hydraulic pump case drain fluid temperatures of system A on the left engine and of system B on the right engine and of lateral actuator and flap actuator hydraulic pressures. In addition, instrument panel hydraulic pressure gages were monitored for correct system pressures. No special flight conditions were included in this test.

Results

Hydraulic system operation was evaluated simultaneously with specific airplane and systems operation and flying qualities testing. Results of the temperature and pressure survey are shown in figure 119 for one complete, typical flight. The temperatures shown are of the pump case drain fluid temperature, which is considered one of the hottest areas within the hydraulic system.

The temperature and pressure profiles are shown for an entire flight from engine start to engine shutdown. This particular flight (9-3, May 11, 1972) was conducted to continue expansion of the flight envelope. Flutter checks were made at 130 to 150 kt with normal hydraulic systems and with aileron and augmentor choke hydraulics off. Extensive flight load survey conditions were accomplished at the 30° flap setting. The maximum hydraulic fluid temperatures indicated are 110° F for system B and 140° F for system A.

Flap actuator pressures for both systems and lateral actuator pressures for system A were recorded throughout the flight. Evaluation of these data plus monitoring of the cockpit gages show that both systems are operating at a nominal 3000-psi supply and the flap control pressure regulators in both systems are supplying a nominal 1400 psi to the flap control system.

Conclusions

The maximum temperatures experienced during flight testing were within the criteria for hydraulic system design, i.e., the fluid bulk temperature did not exceed 180° F and the hydraulic fluid temperature at any localized hot spot did not exceed 225° F. The pump case drain

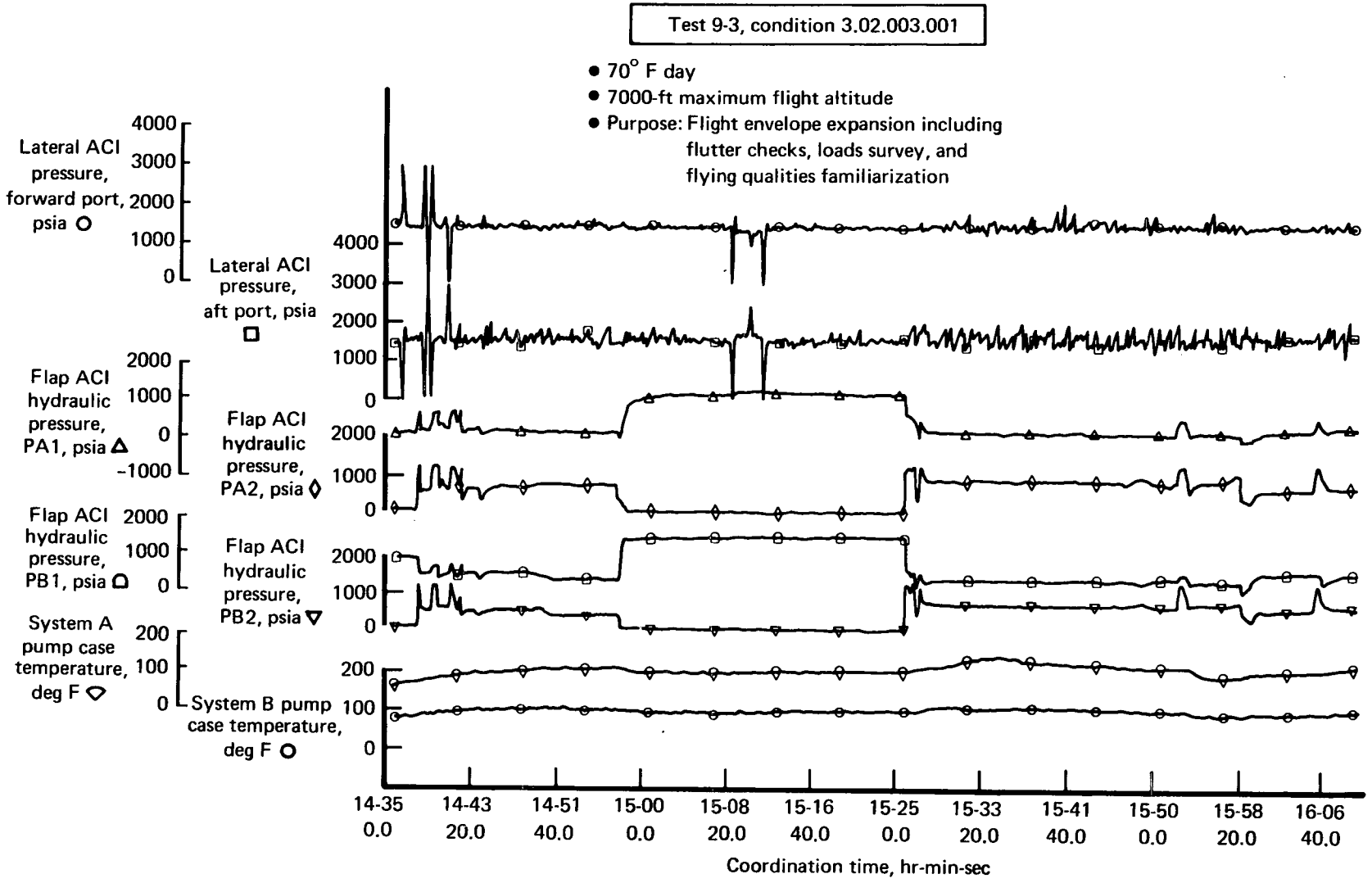

FIGURE 119.–HYDRAULIC TEMPERATURE SURVEY

temperature, considered one of the hottest areas in the system, was less than 140° F for both systems. As predicted during early system design thermal analyses, system A would run hotter than system B because of its greater steady-state power requirements. The greater power requirement, and the equivalent thermal energy added to system A, thus result in a higher fluid temperature. The test results are consistent with the analytical predictions. Although the airplane flight tests were conducted on days closer to standard day +10° F conditions, it is anticipated that even for a hot day condition and normal airplane operation the hydraulic system fluid temperatures will not exceed the design limits stated above.

System operation with regard to hydraulic pressures is completely satisfactory and within design limits.

BRAKE SYSTEM

The purpose of the testing was to evaluate brake system operating characteristics, develop braking techniques, and functionally check the brake systems.

Test Conditions and Procedures

The tests were run during initial ground taxi testing and consisted of evaluating brake operating characteristics during low-speed taxi operations and at speeds progressively increasing to approximately 100 kt. Braking temperatures were monitored during all braking tests. A functional check of the system using brake accumulator pressure only (i.e., hydraulic system A selected off) was conducted. Similarly, a check of the system using the emergency braking system (air bottle) was conducted.

Results

During initial ground taxi testing of the brake system, the pilot commented on brakes being "grabby." This is attributed to lateral asymmetrical braking causing difficulty in airplane directional control during initial braking. The brake system does not incorporate any automatic antiskid system. The geometry of the main gear with the relatively large separation between the left and right gear, coupled with the pedal-to-brake pressure characteristic of the Buffalo system, produces a highly sensitive braking configuration. A pilot familiarization period was required to develop a braking technique that was not disturbing. The technique of pumping the brake pedals rather than applying a constant pressure to the pedals at the initiation of braking appears to be a satisfactory means of reducing the disturbing effects of the lateral asymmetric braking and "grabby" feel. There was no further criticism of the brake system once the pilot became accustomed to the system operation.

The predicted brake operating temperatures shown in figure 120 were confirmed by monitoring brake temperature indicators in the cockpit. The highest brake stator temperature noted was 1000° F. There were no incidents of wheel thermal relief plug release. The predicted stator temperature when the thermal relief plugs release is 1200° F (288° F thermal relief plugs installed in wheel).

A functional check of the emergency braking system was made. The airplane was brought to a full stop from about 40 kt using the brake accumulator only (i.e., hydraulic system A selected off). Similarly, the airplane was brought to a full stop from about 30 kt using the emergency (air bottle) braking system. System operation was completely satisfactory.

Conclusions

Following initial pilot familiarization of the lateral asymmetrical braking sensitivity of the Buffalo airplane during initial braking, the brake system operating characteristics were satisfactory and within design limits.

System performance under normal (no failures) conditions as well as during emergency operations was demonstrated with success. Stops were made using the brake accumulator only and the air bottle only.

Predicted brake operating temperatures were verified to be within design limits (see fig. 120).

Based on these test results, it is expected that the brake system will satisfy all the design conditions required of the Modified C-8A airplane.

ENVIRONMENTAL CONTROL SYSTEM

The environmental control system was unmodified except for local rerouting of supply air ducts in the fuselage and an extension that was required on the ram air inlet because of the extended airplane nose boom. Therefore, the flight tests were strictly functional. The system was monitored during the flight testing period to verify its operational status.

STABILITY AUGMENTATION SYSTEM

The lateral-directional stability augmentation system was flight tested throughout its normal operating envelope with no major problems encountered. The system has adequate performance, with authority limited to a safe value. The airplane can be safely flown to a landing without stability augmentation.

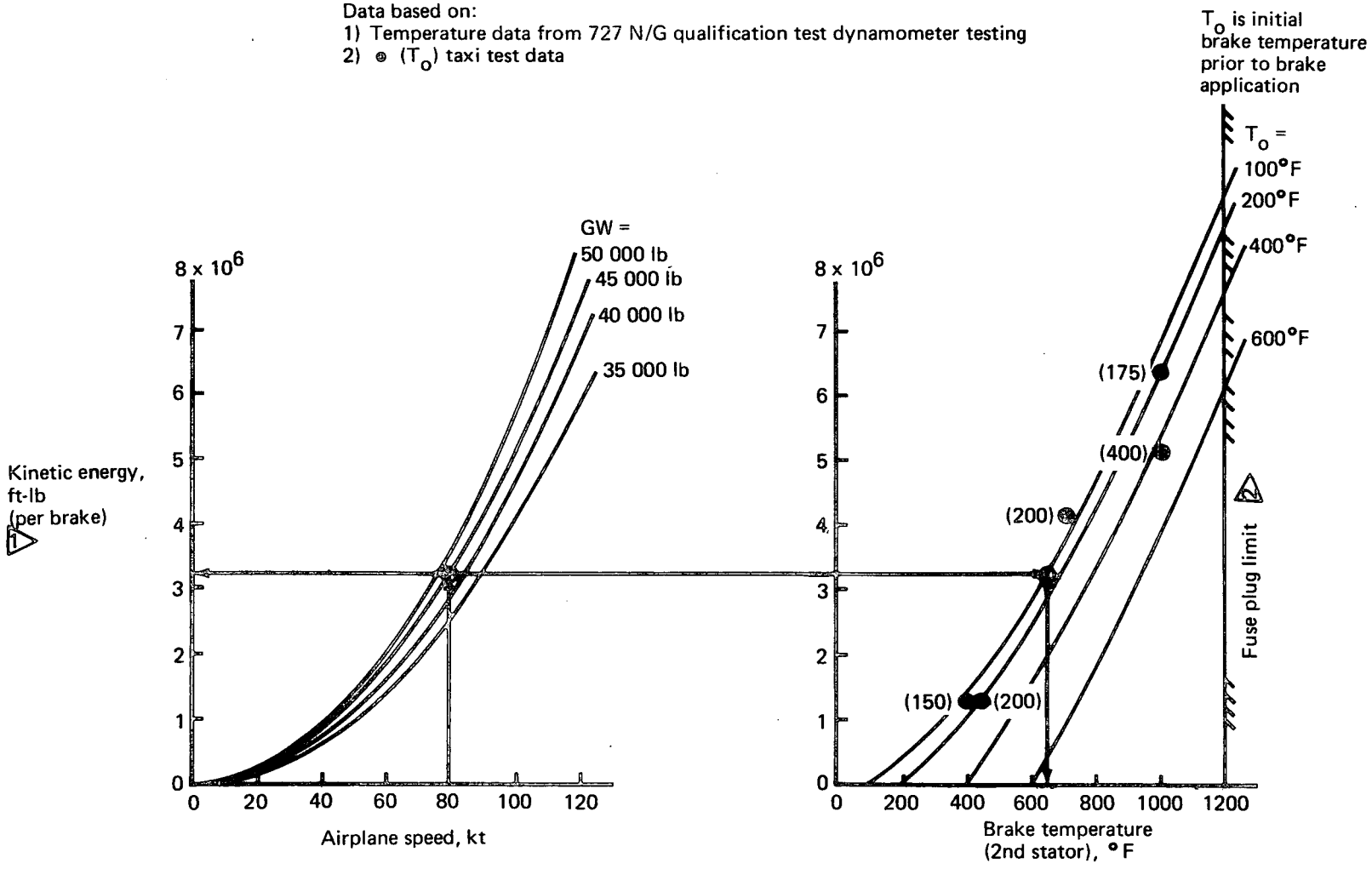

1 Includes 5% factor for unequal braking
2 288° F thermal relief plugs installed in wheels

FIGURE 120.–BRAKE TEMPERATURE

System Installation

Early during the taxi testing of the Modified C-8A airplane it was found that the yaw rate gyros for the roll axis SAS and yaw axis SAS caused oscillations at 10.7 and 8.0 Hz, respectively, at amplitudes as high as ±15 deg/sec. The oscillations occurred only when the aircraft was moving, and were therefore not detected during the ground test. The amplitude was sufficiently high to result in a noticeable aileron and rudder surface oscillation.

The yaw rate gyros are located within the roll axis and yaw axis SAS computers. These computers are mounted on vibration isolators to make them compatible with the 10 g vibration design requirement. The present vibration mount has a resonance close to a structural mode, which is sufficiently amplified by the vibration mount to cause the oscillation.

The oscillation was eliminated prior to first flight by "stiffening" the vibration mounts. Stiffening was temporarily accomplished by placing a wooden spacer between the vibration mount and aircraft structure. However, this has the undesirable side effect of increasing the vibration transmissibility to the computers by an unknown amount. This could possibly result in the premature failure of some component of the SAS computers. The yaw rate gyros should therefore be removed from the computers and hardmounted to the airplane structure.

SAS Performance

Flight test results indicate that the Modified C-8A airplane has considerably more positive dihedral effect than that for which the stability augmentation system was optimized. Dutch roll damping rather than spiral divergence is the dominant cause of instability in the lateral-directional axis. Although SAS performance appears adequate, further improvements in handling qualities are possible through gain optimization.

Spiral Mode Augmentation

The free airplane appears to have a spiral mode with time to double amplitude greater than 15 sec for all flight conditions tested. The present SAS configuration results in a convergent spiral mode, which requires the pilot to hold the wheel into the turn. Typically, at flaps 30°, V_e = 85 kt, and level flight, +10° right wheel is required to hold a +20° bank angle (flight test 9-2, IRIG 12:04:42). A reduction in $\delta_w/\dot{\psi}$ gain is required if this is considered objectionable.

Roll Mode Augmentation

No specific tests were made to determine the roll mode time constant. Performance appears to be satisfactory, however, with an estimated time constant of 1.0 sec or less.

Control Wheel Feed Forward

The effect of the control wheel feed forward signal was not specifically evaluated. The signal does, however, cause a lateral trim shift between SAS on and SAS off, and thus could be a nuisance for SAS on-off tests by continually forcing the pilot to retrim laterally.

Dutch Roll Damping

Dutch roll damping for the augmented airplane appears to be dependent on the amplitude of the oscillation. For large amplitudes, the airplane has a damping ratio, ζ, approximately equal to 0.30, which is acceptable.

The airplane also exhibits a low-amplitude residual oscillation with SAS both on and off. The oscillation is not like the classical Dutch roll, but rather is very nonlinear with questionable periodicity. Figure 121 shows a typical example with the SAS on. The airplane has a 0.75 deg/sec (peak to peak) yaw rate oscillation. This commands 0.3° (peak to peak) rudder deflection, a command that the rudder PCU does not follow.

The residual oscillation was noticeable to a greater or lesser degree at all flight conditions below approximately 100 kt. An increased yaw rate to rudder feedback gain should reduce the magnitude of this oscillation.

Turn Coordination

Turn coordination appears to be satisfactory, with the airplane exhibiting a $\Delta\beta/\Delta\phi$ ratio less than 0.3 at the flight conditions tested.

SAS Authority

The stability augmentation system has satisfactory rate and position authority for normal maneuvering within the flight envelope tested. Typical maneuvers and peak authorities as determined from flight test 9-5 are shown in table XIV.

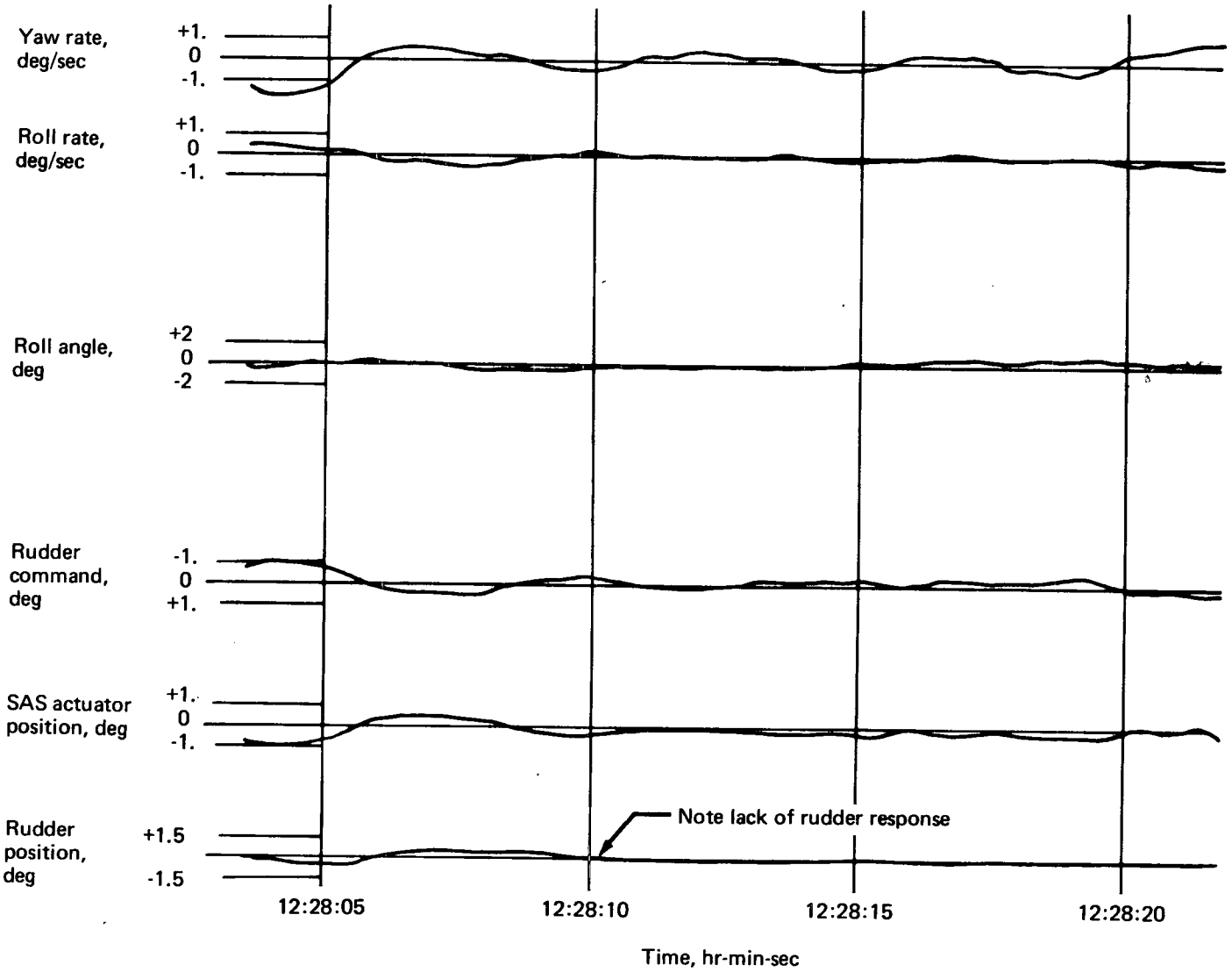

FIGURE 121.—RESIDUAL DUTCH ROLL—FLAPS 30°, 80 KT, TEST 9-2

TABLE XIV.—TYPICAL MANEUVERS AND PEAK AUTHORITIES FROM FLIGHT TEST 9-5

IRIG	V_e, kt	Flaps, deg	$\dot{\phi}_{max}$, deg/sec	$\dot{\psi}_{max}$, deg/sec	$\delta_{w_{max}}$ SAS, deg	$\dot{\delta}_w$ SAS, deg/sec	δ_R SAS, deg	$\dot{\delta}_R$ SAS, deg/sec
14:36:05	90	30	7.0	3.0	15.5	16	3.0	3.8
14:36:45	90	30	9.0	4.0	12.5	22	3.8	4.4
14:47:34	75	30	5.0	3.5	11.0	13	2.2	2.8
14:48:06	75	30	5.75	4.8	8.5	12	2.8	2.6
17:01:45	60	73	4.0	5.0	16.5	19	3.2	5.0

No instances of roll SAS servo saturation were noted; however, the yaw SAS servo was position limited on several occasions while flying at 45° bank angles with flap settings greater than 40°.

Hardover failures and loss of servo actuator position feedback were evaluated for the roll axis and yaw axis SAS at 65 and 95 kt. The failures were detectable and resulted in no airplane control problem. Hardovers could be overridden or disconnected. Loss of servo actuator position feedback resulted in an oscillatory failure that required SAS disconnect.

Typical failure characteristics are as shown in table XV.

Variable Stability System

No in-flight testing of the variable stability system was done.

SAS Automatic Shutoff

SAS failure warnings were incurred frequently during the flight test program. All warnings were triggered by the airspeed switch monitor, which trips when the two airspeed switches used to automatically disengage or engage the SAS at 100 kt (nominal) are in different states for longer than 5 sec.

TABLE XV.–TYPICAL FAILURE CHARACTERISTICS

Flight condition	Failure	Characteristics
95 kt, $\delta_F = 30°$	Roll hardover	$\phi_{max} = 6°$
95 kt, $\delta_F = 30°$	Roll servo open feedback	Oscillation, 2.1 sec period, $\phi = \pm 2°$
95 kt, $\delta_F = 30°$	Yaw hardover	$\beta_{max} = 4.5°$
95 kt, $\delta_F = 30°$	Yaw servo open feedback	Oscillation, 2.0 sec period, $\beta = \pm 1.5°$
65 kt, $\delta_F = 65°$	Roll hardover	$\phi_{max} = 6°$
65 kt, $\delta_F = 65°$	Roll servo open feedback	Oscillation, 2.1 sec period, $\phi = \pm 1°$
65 kt, $\delta_F = 65°$	Yaw hardover	$\beta_{max} = 90°$
65 kt, $\delta_F = 65°$	Yaw servo open feedback	$\beta = \pm 1.5°$ with β offset Oscillation, 3.5 sec period

For test flights 9-5 and 10-1 a 15-sec monitor time delay was flown. This appears to have helped considerably. The frequency of nuisance failure warnings may be further reduced by changing the airspeed switch trip speed from 100 to 110 kt.

LONGITUDINAL CONTROL SYSTEM

The elevator control system was modified to reduce stick forces to "one-hand" levels. Spring tab follow-up ratio and elevator centering spring stiffness were changed. Control checks were made prior to each taxi and flight test to verify rigging and static gearing. Figures 122 and 123 present elevator characteristics with gust lock on and off. The gust lock "on" data show the stick force produced by the elevator spring. The data with the gust lock "off" show the combined effect of elevator spring and elevator mass overbalance. The mass overbalance causes the elevator to rest at full trailing-edge-up deflection. Approximately 40 lb of push force are required to center the elevator at zero forward speed.

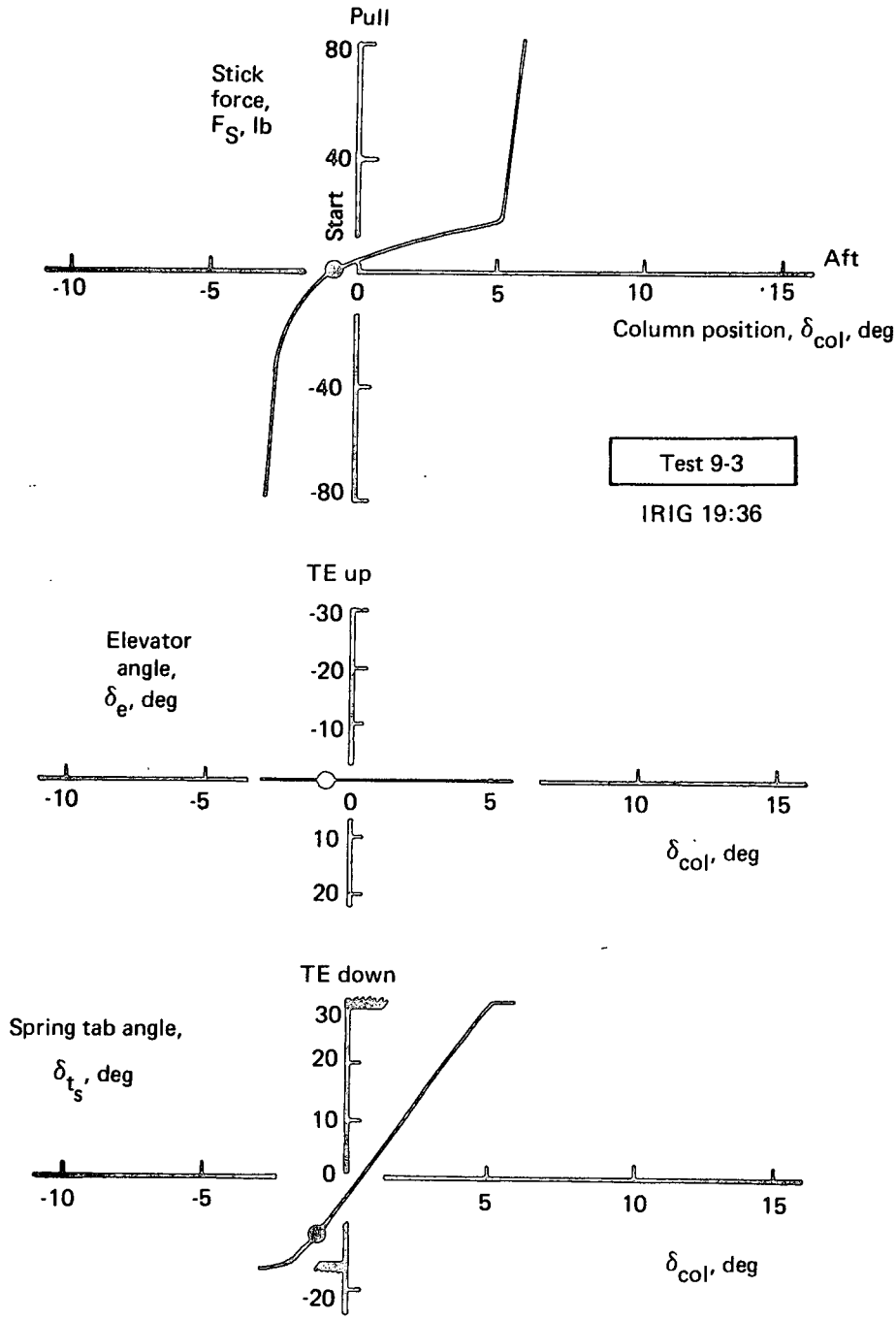

FIGURE 122.–ELEVATOR CHARACTERISTICS–ZERO AIRSPEED, GUST LOCK ON

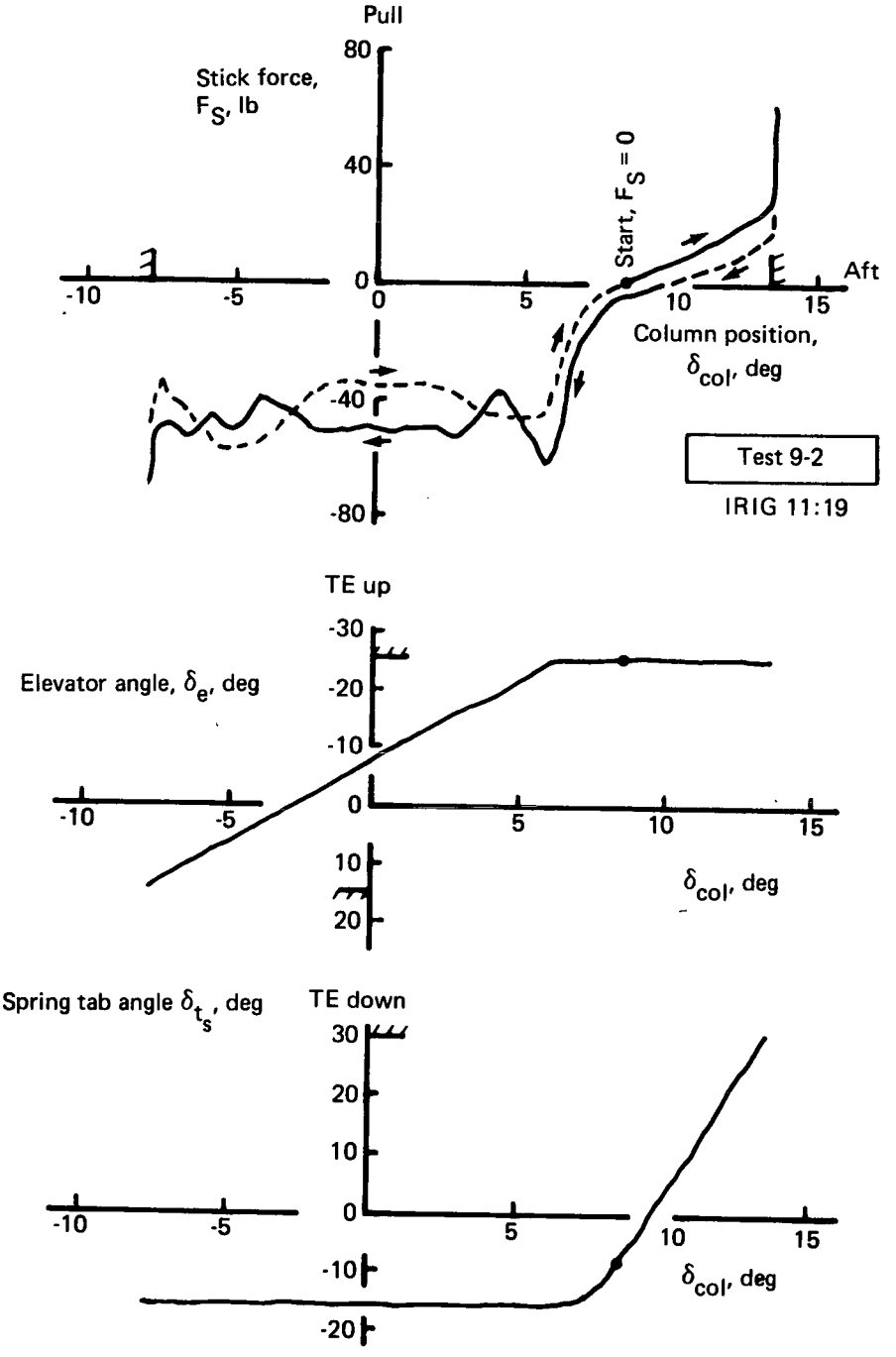

FIGURE 123.–ELEVATOR CHARACTERISTICS–ZERO AIRSPEED, GUST LOCK OFF

During the initial taxi tests the airplane failed to achieve maximum trailing-edge-up elevator without extremely high stick forces. After a thorough inspection and extension of the spring tab and column deflection limits, a special taxi test was conducted to determine elevator characteristics. Stick force and spring tab gearing with elevator for zero trim tab angle are presented in figures 124 through 126 from test 7-5. Several characteristics are evident:

- Elevator up float angle changes considerably from 40 to 80 kt, due presumably to mass and aerodynamic overbalance effects. This effect was quite pronounced during the taxi tests, as shown in figure 127.

- Stick force gradient is low and near to the predicted value at lower elevator angles. Stick force stiffens considerably as large elevator deflections are called for.

- The ability of the spring tab to drive the elevator is less than predicted, and the tab apparently stalls beyond $\delta_{t_{spring}} = 15°$. The pilot then drives the elevator directly at greater than tenfold stick force gradient. Data also indicate that the basic elevator hinge moment gradient is much stiffer than predicted at large deflection angles (beyond $\delta_e \approx -15°$).

Figure 128 presents the elevator-to-column gearing at the 60-kt taxi condition. Column gearing is close to the prediction up to tab stall, at which point several degrees of column travel are expended with no elevator output. Large elevator deflections are produced by direct pilot effort to the elevator. When this characteristic was discovered in the taxi testing, the original Buffalo flight test data were reviewed. It was determined that the original airplane had achieved $\delta_e = -18°$ to $-19°$ at 60 kt with $F_S = 75$ lb and that 150 lb of pull force was required to reach $\delta_e = -25°$. Large elevator deflection achieved with low stick force is not possible with the present elevator system.

Trim-tab setting affects elevator float position but not stick force characteristics, as shown in figures 129 and 130. The trim tab is almost identical to the spring tab in size and shape. Trim tab effectiveness is virtually the same as the spring tab as shown in figure 131. Trim rate on the tab was checked and confirmed at $\dot{\delta}_t = \pm 2$ deg/sec.

Stick force and spring tab characteristics for full airplane speed range are shown in figure 132 based on taxi test and in-flight maneuvering. The θ_1 stops are based on taxi data at low speeds and estimated for higher speeds, as the stops were not reached in flight. Elevator-to-column gearing is presented in figure 133 showing good agreement with the prediction below tab stall deflections.

Premature tab stall has a detrimental effect on low-speed control capability. Conventional flight characteristics are not hindered for the weight/CG/load factor regime of the Modified C-8A.

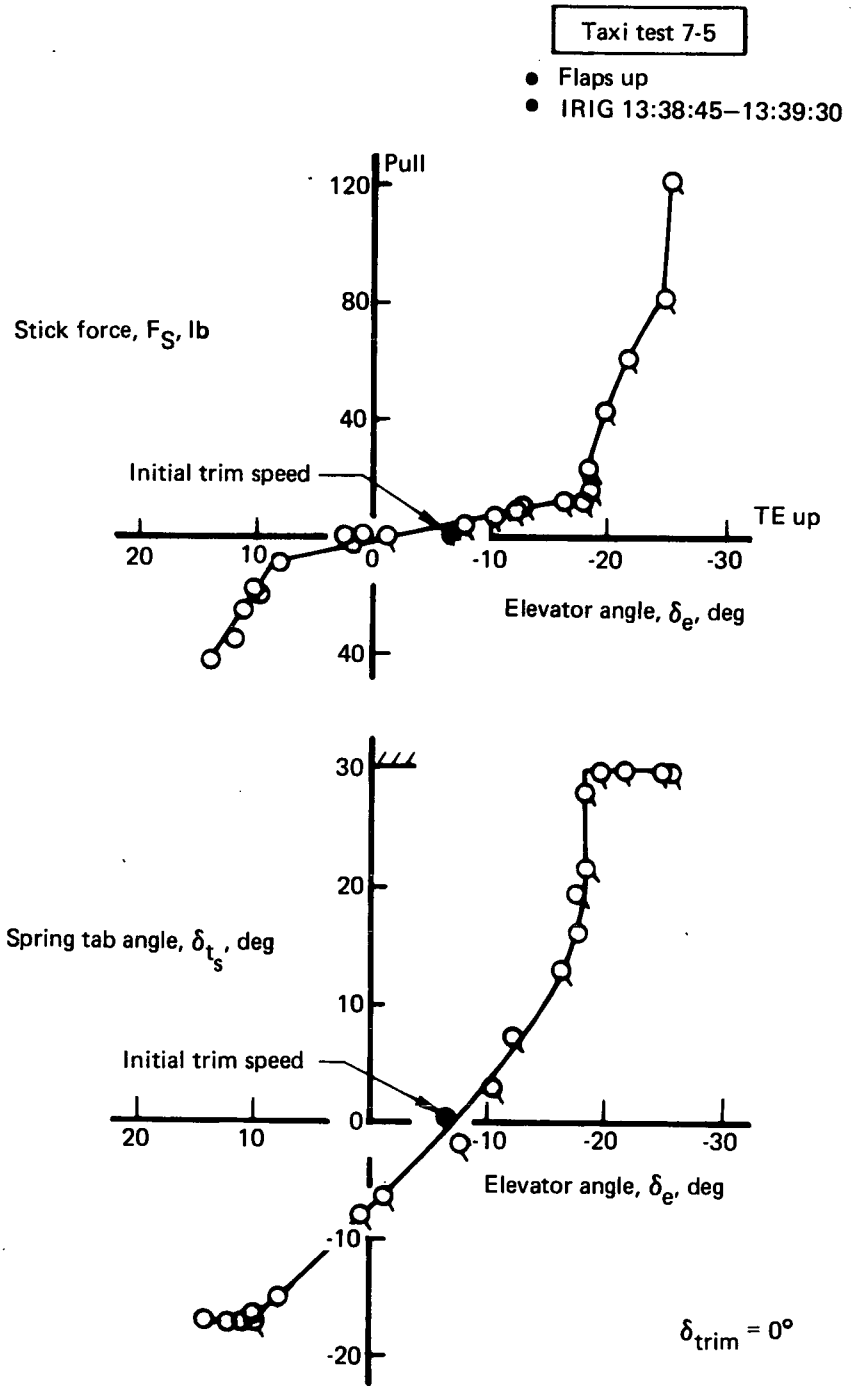

FIGURE 124.–STICK FORCE AND SPRING TAB CHARACTERISTICS AT 40 KT TAXI, $\delta_{t_{trim}} = 0°$

FIG 12
Pg 237

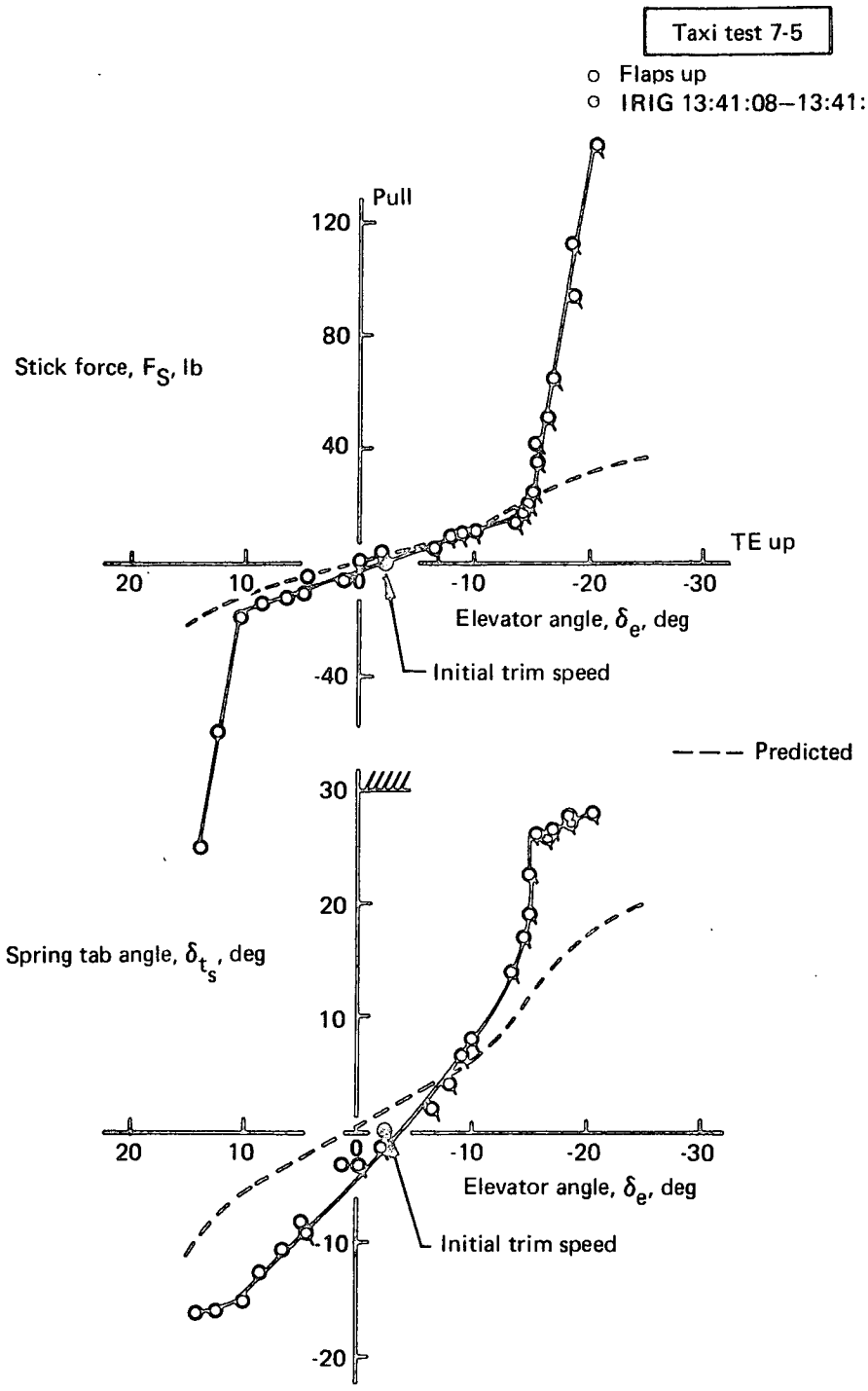

FIGURE 125.–STICK FORCE AND SPRING TAB CHARACTERISTICS AT 60 KT TAXI, $\delta_{t_{trim}} = 0°$

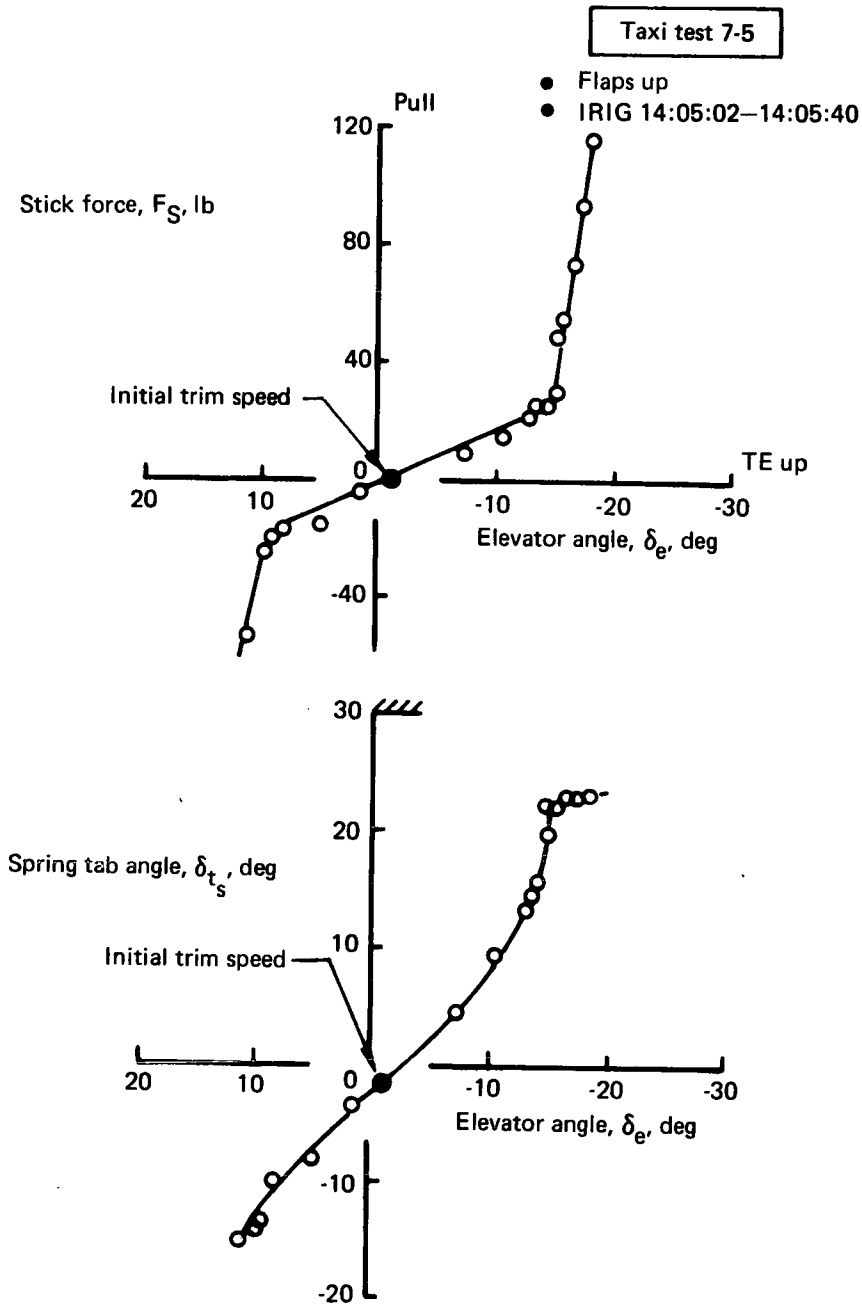

FIGURE 126.–STICK FORCE AND SPRING TAB CHARACTERISTICS AT 80 KT TAXI, $\delta_{t_{trim}} = 0°$

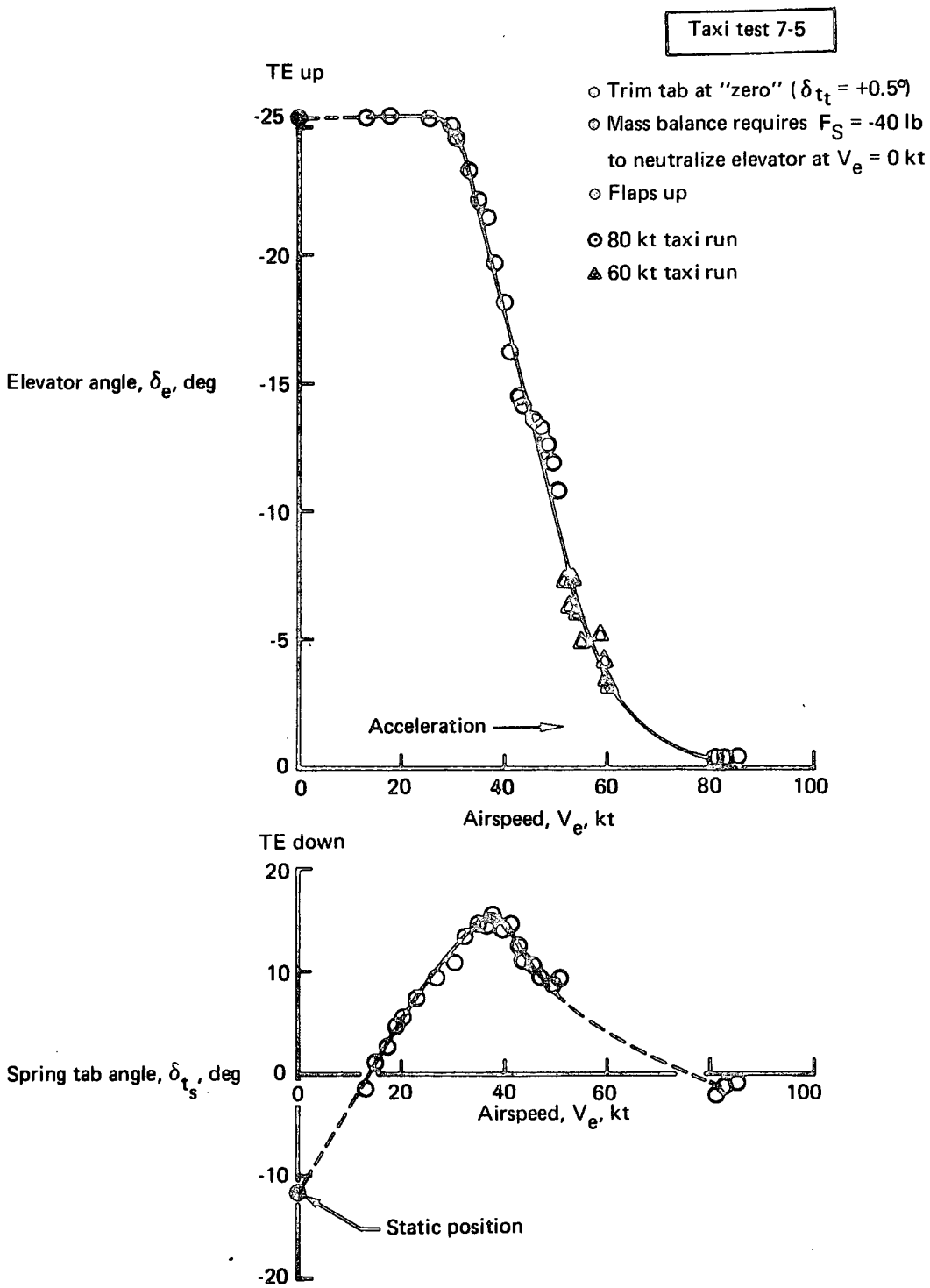

FIGURE 127.—ELEVATOR FLOAT AT ZERO STICK FORCE DURING TAXI

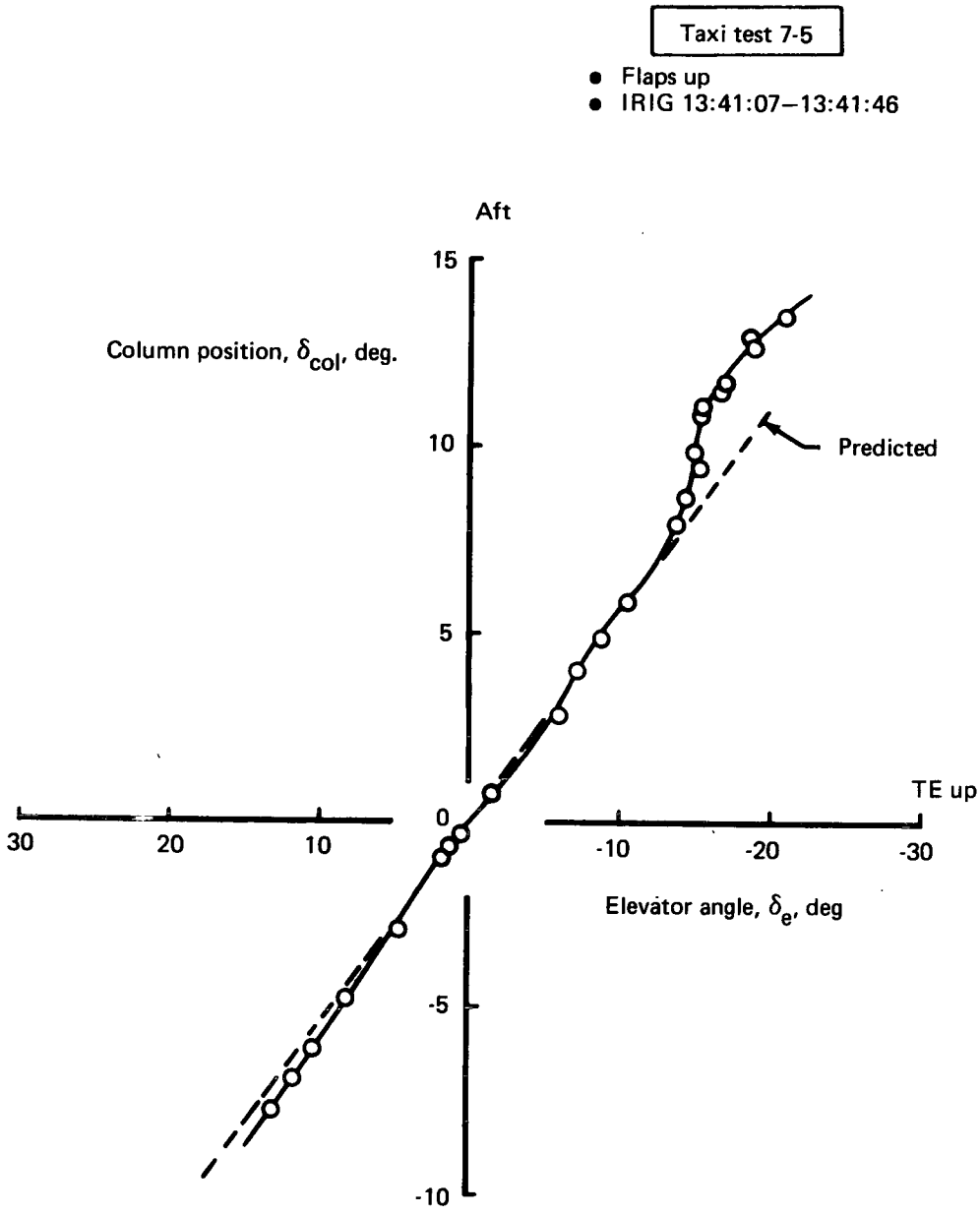

FIGURE 128.–ELEVATOR-TO-COLUMN GEARING AT 60 KT TAXI

C3

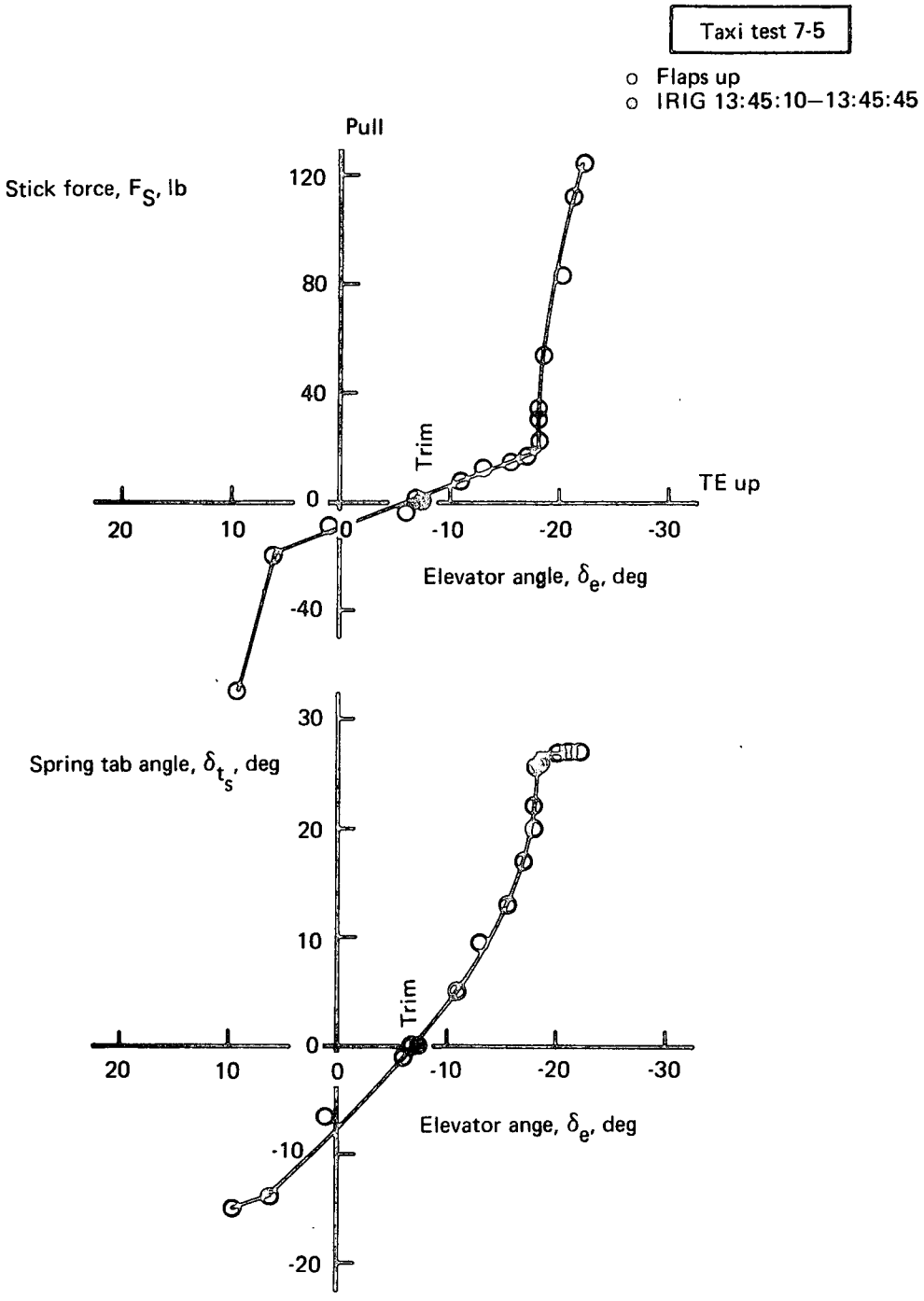

FIGURE 129.–STICK FORCE AND SPRING TAB CHARACTERISTICS AT 60 KT TAXI, $\delta_{t_{trim}} = 5°$

FIG 131
P. 242

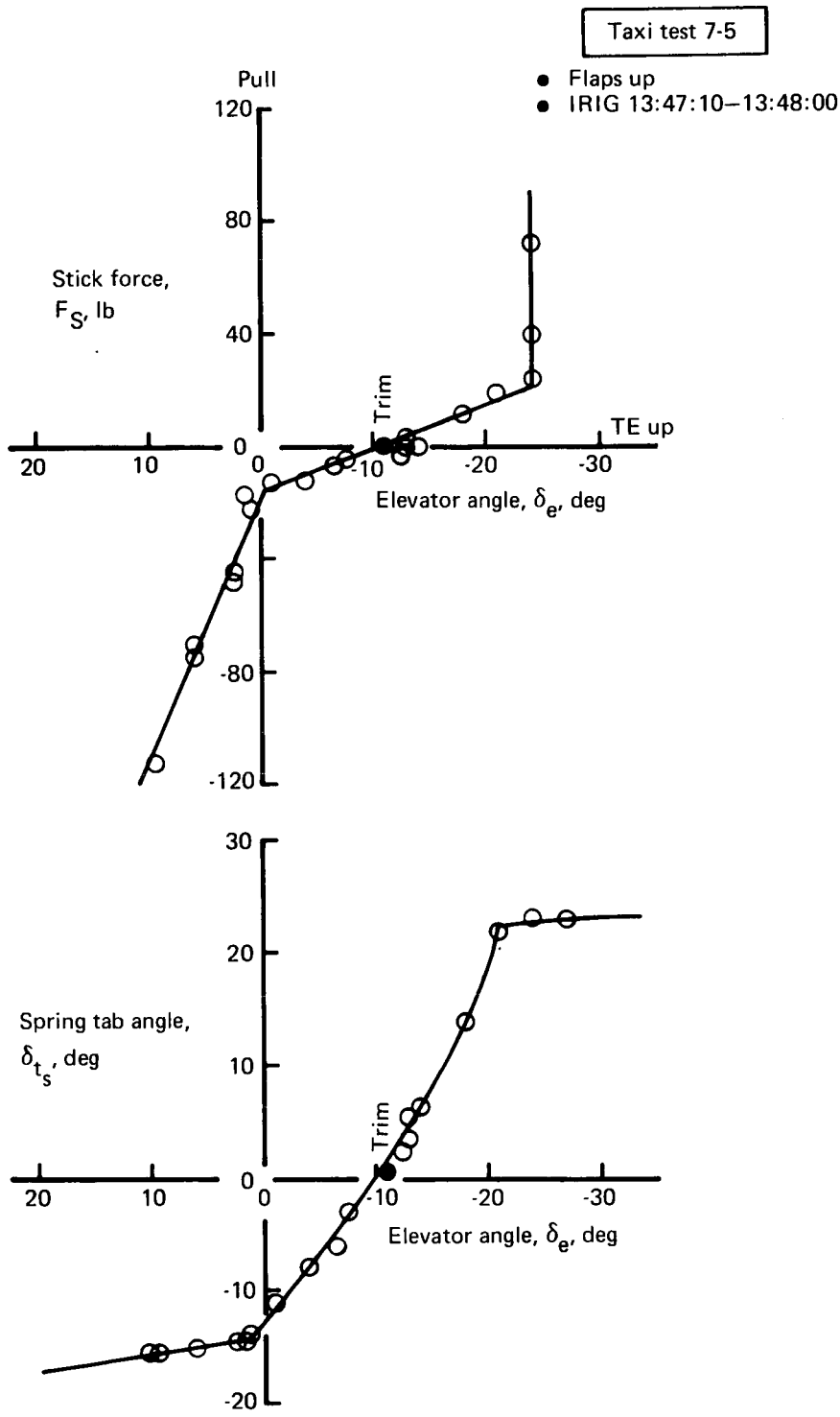

FIGURE 130.–STICK FORCE AND SPRING TAB CHARACTERISTICS AT 60 KT TAXI, $\delta_{t_{trim}} = 10°$

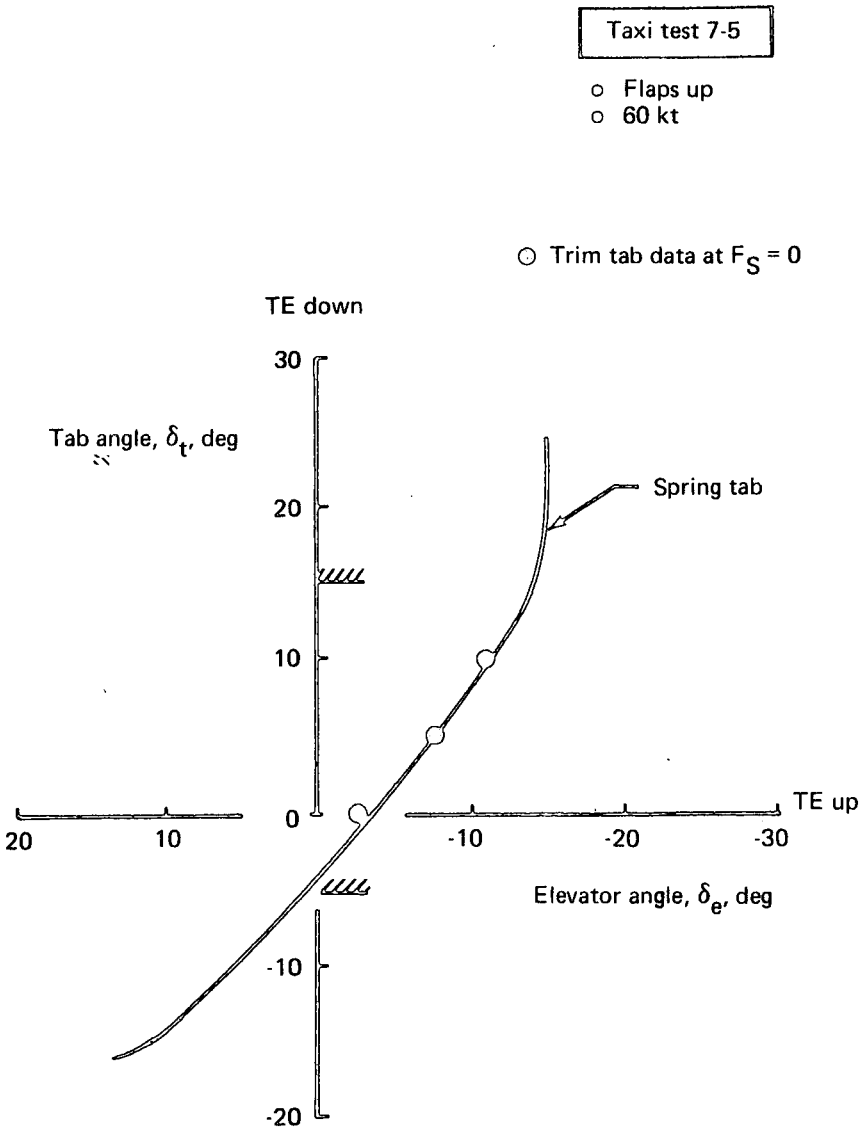

FIGURE 131.—TRIM TAB EFFECTIVENESS

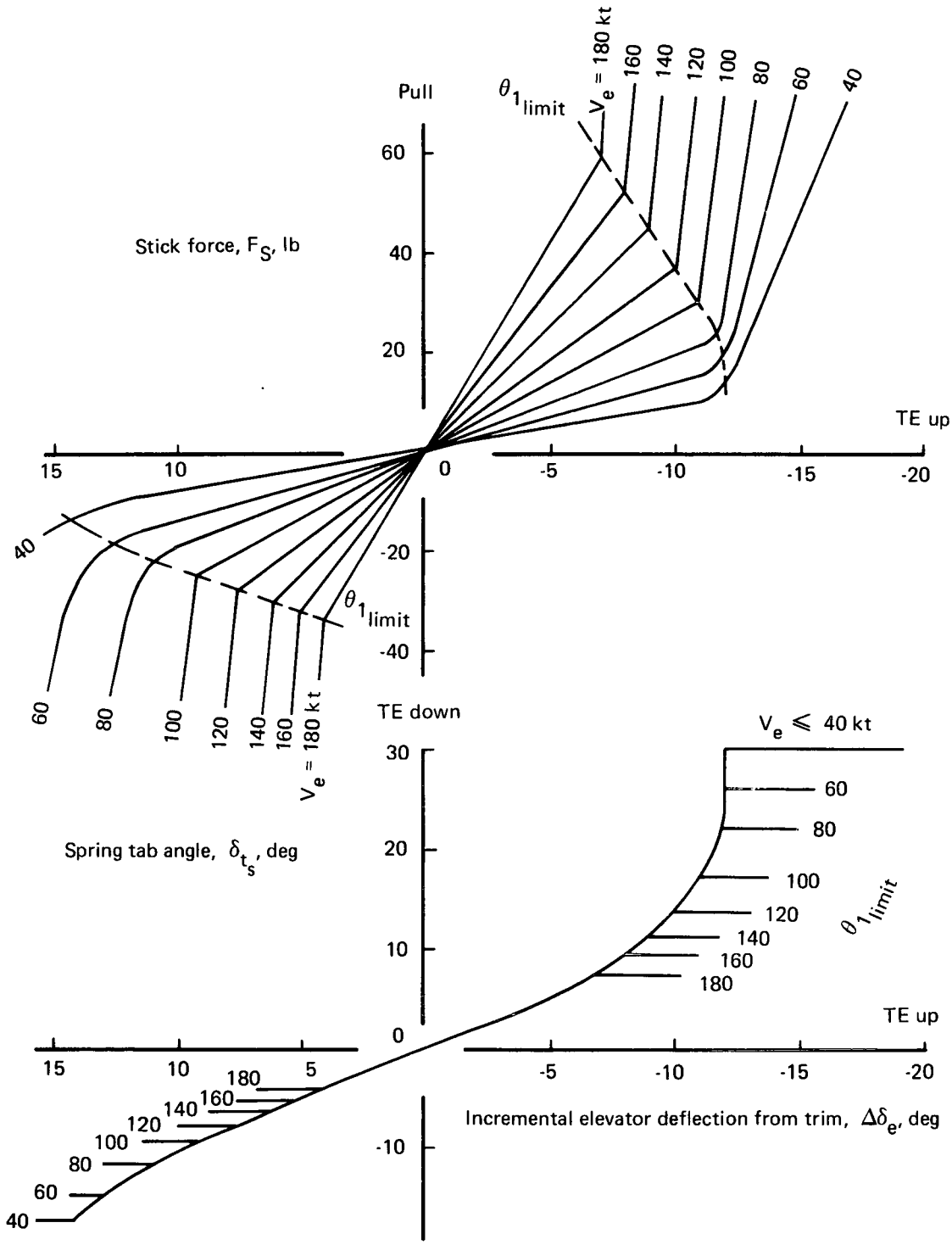

FIGURE 132.–STICK FORCE AND TAB EFFECTIVENESS BASED ON TAXI AND FLIGHT TESTING

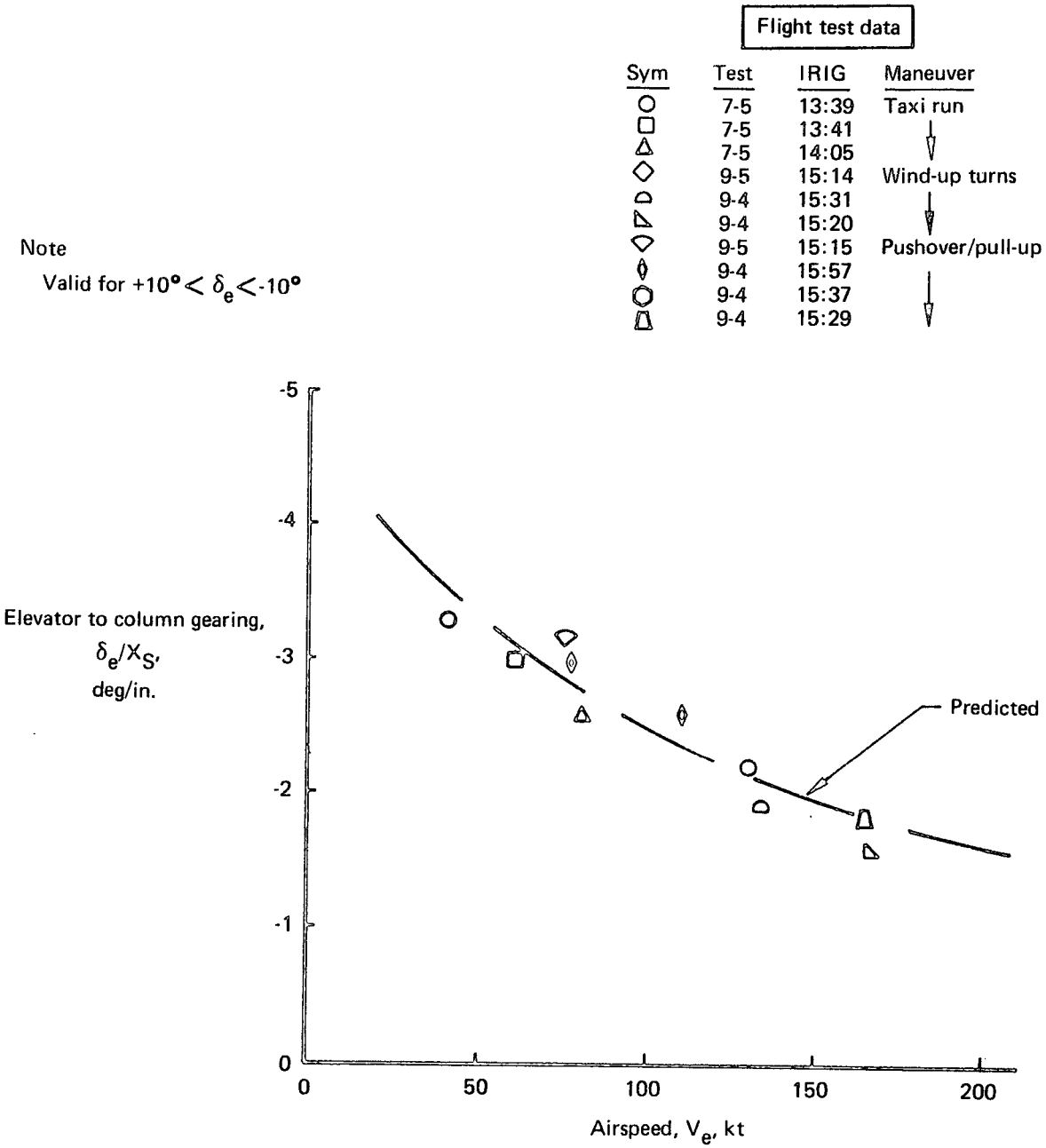

FIGURE 133.–ELEVATOR-TO-COLUMN GEARING SUMMARY

STOL takeoff rotation, landing flare, and stall recovery capability are jeopardized. STOL takeoffs, full stalls, and STOL landings were not scheduled in the flight test program.

Figure 134 presents elevator dynamic characteristics at 60 kt. The pilot put in two step-column pulses while taxiing in test 7-4. The first pulse represents a 50% control authority input. The elevator oscillates at a rather sluggish 1-sec period. The second pulse achieved full column and maximum spring tab deflection ($\delta_{t_{spring}} = 26°$ was the limit for this test). Again the elevator oscillated at about 1-sec period or $\omega = 6$ rad/sec. The predicted frequency was 10 rad/sec.

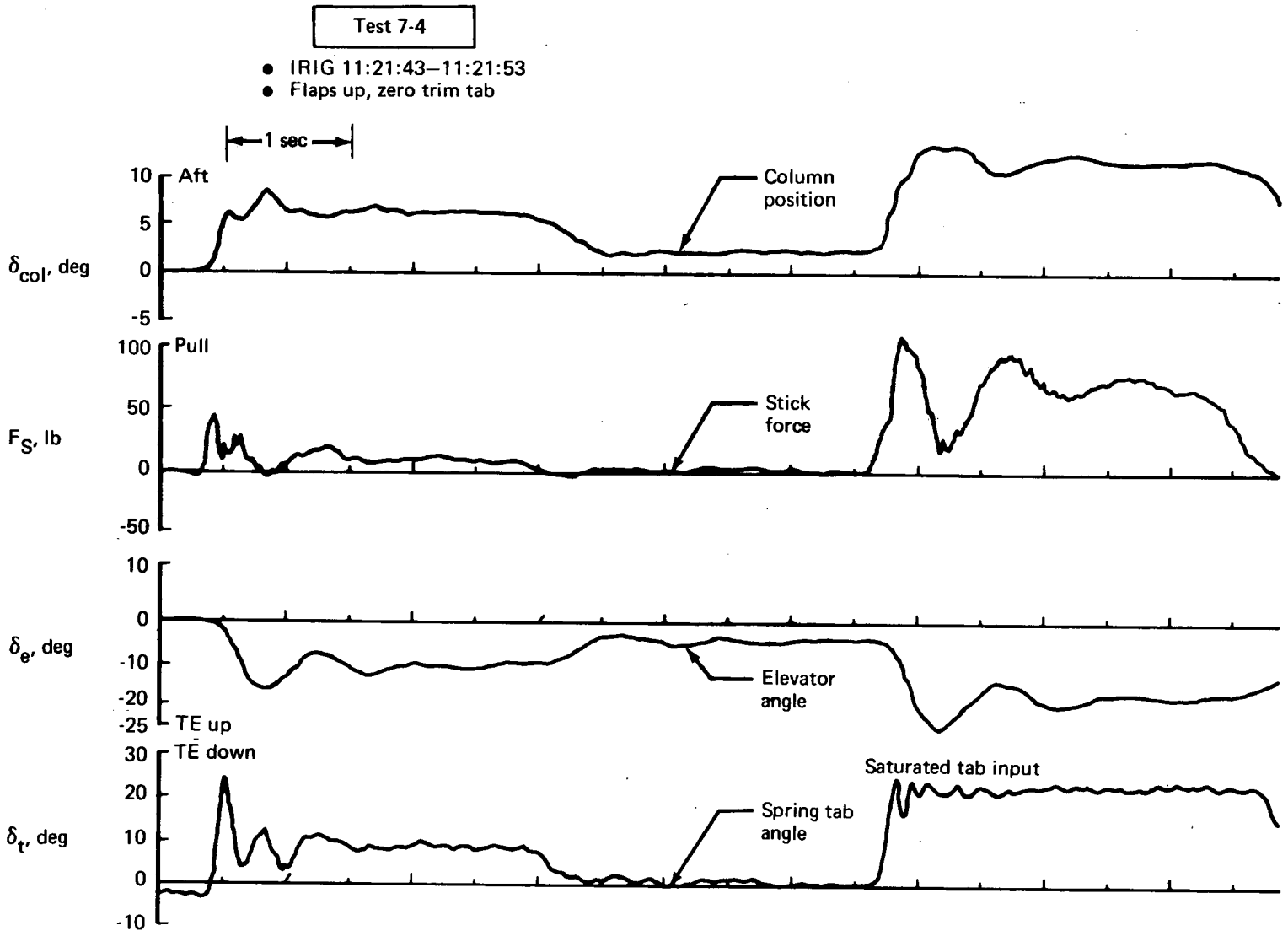

FIGURE 134.–ELEVATOR DYNAMICS AT 60 KT TAXI

CONCLUSIONS AND RECOMMENDATIONS

The contractor's flight test program achieved its primary objective; the airplane was demonstrated to be airworthy. All systems were operated in the test program. A flight envelope was explored from 50 KEAS to the dive speed of 180 KEAS. At the minimum test speed condition, the equivalent lift coefficient was W/qS = 5.4. The full ranges of flap setting, conical nozzle deflection, and power setting were evaluated. Angles of attack above 22° and sideslip angles to 15° were achieved. Full stalls and STOL takeoffs and landings were not scheduled. Sufficient flight testing was performed to clear the airplane for the augmentor wing research flight test program. The stresses measured on various structural members were within design stress levels.

Airplane flying qualities were examined to some extent in the contractor's test program. In summary, the airplane exhibited positive static lateral and directional stability throughout the flight envelope. Satisfactory lateral control power was demonstrated down to the 60 KEAS condition where full wheel produced a roll acceleration of $\ddot{\phi}$ = 0.5 rad/sec^2. Directional control power was adequate for sideslips and engine-out control. The airplane's minimum engine-out speed appears to be limited by wing stall, not control power. With the lateral-directional SAS the airplane exhibited good turn entry characteristics, positive spiral stability, and well-damped Dutch roll for large-amplitude disturbances. With SAS turned off the airplane characteristics were judged acceptable for safe flight to a landing. The one undesirable lateral-directional characteristic found in the test program was a low-amplitude directional "snaking" tendency at speeds below 90 KEAS.

Longitudinal trim was maintained for most flight conditions at elevator deflections within ±5° of neutral. Contractor flight tests showed that the existing, fixed stabilizer incidence was adequate. Trim changes for changes in speed, flaps, nozzle, and power were small. The airplane exhibited positive static longitudinal stability at speeds above 80 KEAS. Static longitudinal stability was neutral or negative at lower speeds. Stable maneuvering characteristics were demonstrated throughout the flight envelope. Taxi tests revealed that tab stall limited trailing-edge-up elevator to two-thirds of maximum using one-hand stick force. Existing data indicate that minimum distance takeoffs and landing flare from the 60 KEAS STOL approach will be restricted. Stall recovery may also be hindered. Significant airplane performance results from the flight test program are as follows:

- The maximum operating speed of 160 KEAS can be maintained in level flight with a power setting of 92% N_H (approximately 75% of the maximum thrust available).
- Minimum test speeds were demonstrated within 0 to 7 kt of the predicted stall speeds. However, full stalls were not scheduled to determine actual minimum airspeeds.

- Minimum control speeds are lower than the minimum test speeds for all flap settings and, therefore, are not limiting.

- Emergency climb capability with a failed engine is nominally as predicted, which will permit takeoffs over a reasonable range of airplane weight and ambient conditions.

- A 1% to 2% higher power setting than predicted is required to maintain a given rate of climb for two-engine operation with the conical nozzles aft.

- The uncorrected angle of attack as measured on the nose boom is 1° to 2° higher than predicted for the same airspeed and rate of climb.

- Vectoring the conical nozzles down ($\nu \geqslant 60°$) requires an additional 2% to 3% higher power setting than predicted.

The thrust required to maintain a given flight condition was 10% to 20% higher than predicted. Because of the limited amount of performance flight testing accomplished, it was not possible to determine the reasons for the higher thrust required. Possible explanations are local separation, loss of augmentation ratio, and inability to resolve the drag and/or thrust to the necessary accuracies.

Since the original objectives of the Modified C-8A program were to prove the augmentor wing concept with respect to aerodynamics, performance, and handling qualities and to contribute to the development of jet STOL transport design and operating criteria, it is recommended that NASA extend the flight test program into the following areas:

- Conduct a test program exploring the STOL flight regime in further depth. Particular emphasis should be placed on landing maneuvers, including the following specific items:

  - Steep approach flare techniques related to simulator findings

  - Evaluation and, possibly, measurement of ground effects

  - Simulation of engine failure at critical conditions

  Caution is urged in approaching flight conditions having low margins. Give particular attention to the type of longitudinal stability augmentation needed on the airplane.

- Conduct a flight test investigation to determine accurate performance characteristics including a ground test to measure static thrust. With accurate data in hand, conduct an analysis of airplane performance. Static thrust data, flaps on and off, will allow identification of static augmentation. Tuft studies of suspected areas of poor flow during both flight and static tests will allow qualitative assessment of drag sources and will guide corrective action to improve performance. This work is recommended as essential to the proof of the augmentor wing concept.

- Install a powered elevator system on the airplane to permit full and safe exploration of the airplane's high lift and STOL operation capabilities.

- Use the variable-gain SAS to find the optimum lateral-directional handling qualities and reduce the "snaking" tendency, then modify the fixed-gain SAS to this configuration.